



A University of Sussex PhD thesis

Available online via Sussex Research Online:

<http://sro.sussex.ac.uk/>

This thesis is protected by copyright which belongs to the author.

This thesis cannot be reproduced or quoted extensively from without first obtaining permission in writing from the Author

The content must not be changed in any way or sold commercially in any format or medium without the formal permission of the Author

When referring to this work, full bibliographic details including the author, title, awarding institution and date of the thesis must be given

Please visit Sussex Research Online for more information and further details

Cytocidal activity of Cry41Aa, an anticancer
toxin from *Bacillus thuringiensis*

Wided Souissi

Submitted for the award of Degree of Doctor of Philosophy

Department of Biochemistry

School of Life Sciences

University of Sussex

July 2018

Work not submitted elsewhere for examination

I hereby declare that this thesis has not been submitted in whole or in part to this or any other University for the award of a degree.

Wided Souissi

Acknowledgements

I would like to express my deepest gratitude to my supervisor Dr Neil Crickmore for his excellent guidance, encouragement and support throughout my PhD research study. I have been extremely lucky to have a supervisor who is a great scientist and a wonderful person that cared so much about my work, and who responded to my questions and queries so promptly. Special thanks go to Prof Michelle West and Prof Simon Morley for the use of tissue culture facilities, Dr Roger Phillips for assistance with the DIC microscopy and Dr George Giamas for the use of his lab equipment when needed.

I am hugely appreciative to Dr George Giamas' lab members: Dr Thomas Simon, Dr Franz Wendler and Angeliki Ditsiou who were always willing to help and give their best suggestions. In particular, I am grateful to Dr Teresa Gagliano for her constant support, valuable advice and constructive suggestions. I also would like to thank Arnhild Grothey, a past member of Dr Giamas lab, for her help and support.

Completing this work would have been more difficult without the support and friendship provided by my colleagues particularly Aminah Barqawi, Lazarus Joseph and Moji Naciri. I thank them for their continued support and encouragement, for their companionship and for providing a so pleasurable and friendly working atmosphere.

Special thanks also go to Alicia Elhigazi a PhD student who I had the pleasure to meet. My sincere thanks also go to Dr Barbara Domanska for her support and for introducing me to Cell Biology skills.

Last but not the least, I would like to acknowledge with much appreciation the crucial role of my husband who supported me mentally and financially, my wonderful sons, my father, my mother and my sisters. I would like to thank them for their love, patience and their unconditional support, without which it would not be possible to conduct this research. I dedicate this thesis to them.

Abstract

Bacillus thuringiensis (*Bt*) is a gram positive spore forming bacterium which produces intracellular protein crystals toxic to a wide variety of insect larvae and is the most commonly used biological pesticide worldwide. More recently, *Bt* crystal proteins known as parasporins have been discovered, that have no known insecticidal activity but target some human cancer cells exhibiting strong cytotoxic activities with different toxicity spectra and varied activity levels. Amongst these parasporins, parasporin-3 most closely resembles the commercially used insecticidal toxins and presents the narrowest activity spectrum, showing moderate cytotoxicity against only two cancer cell lines, HL-60 (Human promyelocytic leukemia cells) and HepG2 (Human liver cancer cells). Parasporin-3, also called Cry41Aa, has only been shown to exhibit cytotoxic activity towards these two cell lines after being proteolytically cleaved. In order to understand this activation mechanism various mutations were made at the N- or C-terminal region of the protein and the toxicity against both HepG2 and HL-60 cell lines was evaluated. Our results indicate that only N-terminal cleavage is required for activation and that N-terminally deleted mutants show some toxicity without the need for proteolytic activation. Furthermore we have shown that the level of toxicity towards the two cell lines depends on the protease used to activate the toxin. Proteinase K-activated toxin was significantly more toxic towards HepG2 and HL-60 than trypsin-activated toxin. N-terminal sequencing of activated toxins showed that this difference in toxicity is associated with a difference of just two amino acids (serine and alanine at positions 59 and 60 respectively) which we hypothesize occlude a binding motif. Preliminary work carried out on binding showed a lack of correlation between binding and toxicity since toxin binds to both susceptible and non-susceptible cancer cell lines. In an attempt to better understand the mechanism of action of Cry41Aa against these cells, we evolved resistance in HepG2 through repeated exposure to increasing doses of the toxin. Morphological, physiological and genetic characteristics of the resistant cell line were compared with susceptible cells. Toxin was shown to bind to resistant HepG2 similarly to the susceptible line. RNA sequencing identified AQP9 as a potential mediator of resistance but extensive investigations failed to show a direct link. The involvement of

certain intracellular signalling pathways were also investigated in order to understand cell responses to the toxin and showed that in response to the toxin p38, but not ERK1/2, is activated and in a dose dependent manner.

Abbreviations

aa: amino acids

ABC: ATP-binding cassette

BBMV: brush border membrane vesicle

bp: base pairs

BSA: bovine serum albumin

Bt: *Bacillus thuringiensis*

°C: degrees Celsius

cAMP: 3', 5' - cyclic adenosine monophosphate

CAPS: 3 - (cyclohexylamino) – 1 - propanesulfonic acid

Chymo: chymotrypsin

Cry: crystal

Cyt: cytolytic

DIC: differential interference contrast

DMEM: Dulbecco's modified Eagle medium

DMSO: dimethyl sulfoxide

DNA: deoxyribonucleic acid

DPBS: Dulbecco's phosphate-buffered saline

DTT: dithiothreitol

EC₅₀: half maximal effective concentration

ECL: enhanced chemiluminescence

E. coli: *Escherichia coli*

EDTA : 2, 2', 2'', 2''' - (Ethane - 1, 2 - diylidinitrilo) tetraacetic acid

EGTA: ethylene glycol – bis (2 - aminoethylether) - N,N,N',N' - tetraacetic acid

FCS: fetal calf serum

FPLC: fast protein liquid chromatography

g: gram

HA: human influenza hemagglutinin

HRP: horseradish peroxidase

IC₅₀: the half maximal inhibitory concentration

l: litre

LB: Luria Bertani

LD₅₀: lethal dose that gives half maximal response

M: molar concentration

m: meter

min: minute(s)

MS-grade: mass spectrometry-grade

MW: molecular weight

NP-40: nonidet-P40

OD₆₀₀ :optical density measured at 600 nm

ORF: open reading frame

PAGE: polyacrylamide gel electrophoresis

PBS: phosphate - buffered saline

PBS-T: phosphate - buffered saline with Tween - 20

PCR: polymerase chain reaction

pI: isoelectric point

PK: Proteinase K

PKA: protein kinase A

PLB: planar lipid bilayer

Pres: PreScission

PSG: penicillin, streptomycin, and glutamine

RFU: relative fluorescence units

RGB: resolving gel buffer

RIPA: radio immune - precipitation assay

RLU: relative luminescence units

RPMI: Roswell Park Memorial Institute medium

RT: room temperature

SDS: sodium dodecyl sulphate

SEM: standard error of the mean

SGB: stacking gel buffer

Sol: solubilised

TBE: tris - borate EDTA

TEMED: N,N,N',N'-tetramethylethylenediamine

try: trypsin

TX-100: triton X-100

Table of Contents

1	Introduction	15
1.1	<i>Bacillus thuringiensis</i> the bacterium	15
1.2	Delta-endotoxins	17
1.2.1	Cry toxins.....	17
1.2.2	Cyt toxins.....	22
1.3	VIP.....	23
1.4	Anti-cancer toxins: Parasporins (PSs).....	24
1.4.1	Parasporin-1 (Cry31Aa1).....	25
1.4.2	Parasporin-2 (Cry46Aa1).....	27
1.4.3	Parasporin-3 (Cry41Aa and Cry41Ab)	29
1.4.4	Parasporin-4 (Cry45Aa1).....	33
1.4.5	Parasporin-5 (Cry64Aa).....	34
1.4.6	Parasporin-6 (Cry63Aa1).....	36
1.5	Different models proposed for Cry toxin mode of action.....	36
1.5.1	The pore formation models	38
	• The Bravo model.....	38
	• The Ping-Pong model.....	39
1.5.2	The signalling model	40
	• The Zhang model	40
	• The Jurat-Fuentes Model: A combination of the pore forming and the signalling models.....	42
1.6	Cry toxin receptors	44
	• The Aminopeptidases N (APNs).....	45
	• Cadherins	46

•	Alkaline phosphatases (ALPs)	46
•	ATP-binding cassette (ABC)	47
1.7	Resistance mechanisms to Cry toxins	48
1.8	Cellular response to PFT toxins	53
1.8.1	Use of cell lines to study the mode of action of <i>Bt</i> : examples of cell responses to Cry toxins.....	58
2	Aims and objectives	63
3	Materials and methods.....	64
3.1	Materials.....	64
•	Bacterial strains	64
•	Plasmids	64
•	Buffers/solutions and their compositions	65
•	Reagents, enzymes and DNA/RNA kits.....	66
•	Antibodies	67
•	Cell lines	67
•	Culture media, reagents and plasticware.....	67
•	Cell assay kits	68
3.2	Methods	68
•	Polymerase chain reaction (PCR).....	68
•	Agarose Gel Electrophoresis.....	70
•	Dpn1 digestion	71
•	Purification of PCR Products (column purification).....	71
•	Gel purification using Qiaprep kit.....	71
•	DNA ligation	72
•	Bacterial transformation by electroporation	72
•	Bacterial growth conditions.....	73

• Extraction of DNA from <i>E.coli</i> transformants using QIAprep Spin Miniprep Kit	73
• Extraction of DNA from <i>Bt</i> transformants	74
• Verification of inserts.....	74
• Protein harvesting.....	74
• Solubilisation and activation of crystal protein	75
• Protein dialysis.....	75
• Protein purification.....	75
• Protein analysis by SDS-PAGE.....	76
• Protein concentration.....	76
• Preparation of the protein for N-terminal sequencing	77
• Cell culture conditions	78
• Cell assays	78
• Statistical analysis	80
• Preparation of cell extracts.....	80
• Western blot	80
• Ligand blot	81
• Development of the resistant cell line.....	81
• Microscopy.....	82
• Determination of growth curves	83
• RNA Extraction.....	83
• RNA electrophoresis gel.....	84
• Determination of RNA concentration and RNA integrity	84
• RNA-seq and analysis.....	85
• cDNA Synthesis	86

•	qPCR.....	86
•	Transfection of resistant HepG2 using siRNA.....	87
4	Involvement of N and C-terminal cleavages in Cry41Aa toxicity	89
4.1	Introduction.....	89
4.2	Can the toxin be pre-activated by N-terminal deletion?	90
4.2.1	Deletion of 23 amino acids	92
•	Creation of FL Δ 23.....	92
•	Creation of Δ R Δ 23.....	96
4.2.2	Deletion of 40 amino acids	100
•	Creation of FL Δ 40.....	100
•	Creation of Δ R Δ 40.....	104
4.2.3	Deletion of 60 amino acids	104
•	Creation of FL Δ 60.....	104
4.3	Does C-terminal cleavage contribute to Cry41Aa toxicity?	105
4.3.1	Creation of PreScission recognition site at the 40 th aa.....	105
•	Creation of FLP40.....	105
•	Creation of Δ RP40.....	109
4.4	Discussion	120
5	Differential proteolysis of Cry41Aa can affect toxicity.....	124
5.1	Introduction.....	124
5.2	Effect on toxicity of activating with different proteases.....	125
5.2.1	Involvement of upper and/or lower band(s) in Cry41Aa toxicity.....	128
5.2.2	Cry41Aa labelling.....	141
•	Previous problems with HA tag	141
•	Creation of Δ R-HAP40.....	143
5.2.3	Binding analysis.....	146

5.3	Discussion	155
6	Probing the mechanism of action of Cry41Aa on HepG2 through the establishment of a resistant subline	163
6.1	Introduction.....	163
6.2	Generation of resistant HepG2 cell line to T/C activated Cry41Aa	164
6.3	Confirmation of the resistance to the toxin.....	165
6.4	Estimation of half maximal effective concentration (EC ₅₀)	170
6.5	Morphological changes	171
6.6	Cross resistance study	172
6.7	Assessment of membrane damage: Patch clamp analysis	174
6.8	Characterisation of HepG2R cell response to the toxin compared with the parental cell line	177
	• Activation of p38 MAP kinase pathway.....	177
	• Assessment of EGTA effect on toxin action.....	178
6.9	Stability of the resistance phenotype	180
6.10	RNA isolation and sequencing.....	182
6.10.1	Validation of <i>aqp9</i> expression level by RT-qPCR	193
6.10.2	Validation of AQP9 protein expression by western blot	196
6.10.3	Inhibition of AQP9 using MMTS inhibitor	205
6.10.4	AQP9 knock down using small interfering RNA	207
6.11	Discussion	211
7	The role of signal transduction in the mode of action of Cry41Aa	220
7.1	Introduction.....	220
7.2	Investigating the connection between Zhang model and Cry41Aa mode of action.....	221
	• EGTA effect on toxin action on HepG2 and HL-60.....	221

•	Assessment of PKA activation following toxin treatment	223
7.3	Involvement of mitogen-activated protein kinases: assessment of activation of ERK1/2 pathway	226
7.4	Discussion	228
8	General discussion	231
9	References	236

1 Introduction

1.1 *Bacillus thuringiensis* the bacterium

Bacillus thuringiensis (*Bt*) is an aerobic gram-positive spore forming bacterium, belonging to the *Bacillus cereus* group. It was first isolated in Japan in 1901 from a diseased larvae of the silkworm, *Bombyx mori*. *Bt* synthesizes crystalline parasporal inclusions during sporulation (figure 1) and this salient feature makes it distinguishable from other *Bacillus* species (Ohba et al., 2008). The inclusion proteins have been proven to be highly toxic to insects making *Bt* an entomopathogenic organism that has been widely used as a biological pesticide in the form of sprays and more recently *Bt* proteins have been expressed in transgenic plants rendering them resistant to insect attack (Sanahuja et al., 2011).

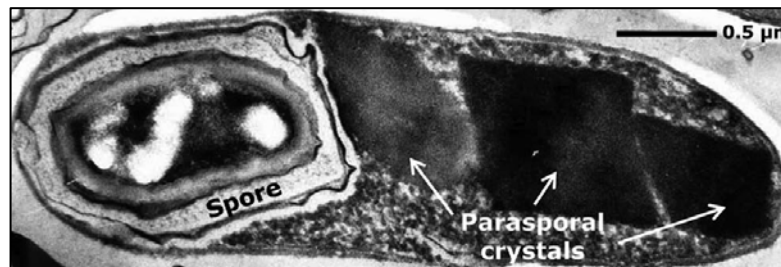


Figure 1: A sporulated cell of *Bacillus thuringiensis* subsp. *morrisoni* strain C18.

Strain C18 was isolated from a dead cotton bollworm larvae. The sporulated cell was visualised under electron microscopy (Ibrahim et al., 2010).

Bt strains show activity towards larvae of very diverse insect orders like Lepidoptera, Diptera, Coleoptera, Hymenoptera, Homoptera, Orthoptera and Mallophaga and in some cases against species from other phyla like nematodes, mites and protozoa (Schnepf et al., 1998). In addition some *Bt* strains were shown to exhibit activity against human cancer cells of various origins (Ohba et al., 2008).

The crystal inclusions produced by *Bt* during the stationary growth phase comprise one or more Cry and/or Cyt proteins (also designated as δ -endotoxins) that have potent and specific insecticidal activity (Bravo et al., 2007). Additionally, during the vegetative

growth phase *Bt* isolates are also able to produce vegetative insecticidal proteins known as Vips (Palma et al., 2014). Figure 2 represents the list of different *Bt* toxins.

Three-domain			ETX-MTX	Bin	Parasporin		
Cry1Aa	Cry2Aa	Cry8Aa	Cry15Aa	Cry31Aa	Cry40Aa	Cry58Aa	Cyt1Aa
Cry1Ab	Cry2Ab	Cry8Ab		Cry31Ab	Cry40Ba		Cyt1Ab
Cry1Ac	Cry2Ac	Cry8Ac	Cry16Aa	Cry31Ac	Cry40Ca	Cry59Aa	Cyt1Ba
Cry1Ad	Cry2Ad	Cry8Ad		Cry31Ad	Cry40Da	Cry59Ba	Cyt1Ca
Cry1Ae	Cry2Ae	Cry8Ba	Cry17Aa				Cyt1Da
Cry1Af	Cry2Af	Cry8Bb		Cry32Aa	Cry41Aa	Cry60Aa	Cyt2Aa
Cry1Ag	Cry2Ag	Cry8Bc	Cry18Aa	Cry32Ab	Cry41Ab	Cry60Ba	Cyt2Ba
Cry1Ah	Cry2Ah	Cry8Ca	Cry18Ba	Cry32Ba	Cry41Ba		Cyt2Bb
Cry1Ai	Cry2Ai	Cry8Da	Cry18Ca	Cry32Ca	Cry41Ca	Cry61Aa	Cyt2Bc
Cry1Ba	Cry2Aj	Cry8Db		Cry32Cb			Cyt2Ca
Cry1Bb	Cry2Ak	Cry8Ea	Cry19Aa	Cry32Da	Cry42Aa	Cry62Aa	Cyt3Aa
Cry1Bc	Cry2Ba	Cry8Fa	Cry19Ba	Cry32Ea			
Cry1Bd		Cry8Ga	Cry19Ca	Cry32Eb	Cry43Aa	Cry63Aa	Vip1Aa
Cry1Be	Cry3Aa	Cry8Ha		Cry32Fa	Cry43Ba		Vip1Ab
Cry1Bf	Cry3Ba	Cry8Ia	Cry20Aa	Cry32Ga	Cry43Ca	Cry64Aa	Vip1Ac
Cry1Bg	Cry3Bb	Cry8Ib	Cry20Ba	Cry32Ha	Cry43Cb		Vip1Ad
Cry1Bh	Cry3Ca	Cry8Ja		Cry32Hb	Cry43Cc	Cry65Aa	Vip1Ba
Cry1Bi		Cry8Ka	Cry21Aa	Cry32Ia			Vip1Bb
Cry1Ca	Cry4Aa	Cry8Kb	Cry21Ba	Cry32Ja	Cry44Aa	Cry66Aa	Vip1Bc
Cry1Cb	Cry4Ba	Cry8La	Cry21Ca	Cry32Ka			Vip1Ca
Cry1Da	Cry4Ca	Cry8Ma	Cry21Da	Cry32La	Cry45Aa	Cry67Aa	Vip1Da
Cry1Db	Cry4Cb	Cry8Na	Cry21Ea	Cry32Ma	Cry45Ba		
Cry1Dc	Cry4Cc	Cry8Pa	Cry21Fa	Cry32Mb		Cry68Aa	Vip2Aa
Cry1Ea		Cry8Qa	Cry21Ga	Cry32Na	Cry46Aa		Vip2Ab
Cry1Eb	Cry5Aa	Cry8Ra	Cry21Ha	Cry32Oa	Cry46Ab	Cry69Aa	Vip2Ac
Cry1Fa	Cry5Ab	Cry8Sa		Cry32Pa		Cry69Ab	Vip2Ad
Cry1Fb	Cry5Ac	Cry8Ta	Cry22Aa	Cry32Qa	Cry47Aa		Vip2Ae
Cry1Ga	Cry5Ad		Cry22Ab	Cry32Ra		Cry70Aa	Vip2Af
Cry1Gb	Cry5Ba	Cry9Aa	Cry22Ba	Cry32Sa	Cry48Aa	Cry70Ba	Vip2Ag
Cry1Gc	Cry5Ca	Cry9Ba	Cry22Bb	Cry32Ta	Cry48Ab	Cry70Bb	Vip2Ba
Cry1Ha	Cry5Da	Cry9Bb		Cry32Ua			Vip2Bb
Cry1Hb	Cry5Ea	Cry9Ca	Cry23Aa	Cry32Va	Cry49Aa	Cry71Aa	
Cry1Ia		Cry9Da		Cry32Wa	Cry49Ab		Vip3Aa
Cry1Ib	Cry6Aa	Cry9Db	Cry24Aa			Cry72Aa	Vip3Ab
Cry1Ic	Cry6Ba	Cry9Dc	Cry24Ba	Cry33Aa	Cry50Aa		Vip3Ac
Cry1Id		Cry9Ea	Cry24Ca		Cry50Ba	Cry73Aa	Vip3Ad
Cry1Ie	Cry7Aa	Cry9Eb		Cry34Aa			Vip3Ae
Cry1If	Cry7Ab	Cry9Ec	Cry25Aa	Cry34Ab	Cry51Aa	Cry74Aa	Vip3Af
Cry1Ig	Cry7Ba	Cry9Ed		Cry34Ac			Vip3Ag
Cry1Ja	Cry7Bb	Cry9Ee	Cry26Aa	Cry34Ba	Cry52Aa		Vip3Ah
Cry1Jb	Cry7Ca	Cry9Fa			Cry52Ba		Vip3Ai
Cry1Jc	Cry7Cb	Cry9Ga	Cry27Aa	Cry35Aa			Vip3Ba
Cry1Jd	Cry7Da			Cry35Ab	Cry53Aa		Vip3Bb
Cry1Ka	Cry7Ea	Cry10Aa	Cry28Aa	Cry35Ac	Cry53Ab		Vip3Ca
Cry1La	Cry7Fa			Cry35Ba			
Cry1Ma	Cry7Fb	Cry11Aa	Cry29Aa		Cry54Aa		Vip4Aa
Cry1Na	Cry7Ga	Cry11Ba	Cry29Ba	Cry36Aa	Cry54Ab		
Cry1Nb	Cry7Gb	Cry11Bb			Cry54Ba		Sip1Aa
	Cry7Gc		Cry30Aa	Cry37Aa			
	Cry7Gd	Cry12Aa	Cry30Ba		Cry55Aa		
	Cry7Ha		Cry30Ca	Cry38Aa			
	Cry7Ia	Cry13Aa	Cry30Da		Cry56Aa		
	Cry7Ja		Cry30Db	Cry39Aa			
	Cry7Ka	Cry14Aa	Cry30Ea		Cry57Aa		
	Cry7Kb	Cry14Ab	Cry30Fa		Cry57Ab		
	Cry7La		Cry30Ga				

Figure 2: List of *Bt* toxins.

Toxins listed are grouped according to their primary rank. The three domain Cry toxin family, coloured in blue, represents the majority of toxins. 13 toxins from the Binary like group are coloured in pink while 11 toxins from the ETX/MTX-like group are depicted in orange, those toxins named with red text indicate the parasporin class. Cry toxins highlighted with other colours represent toxins that are not classified into the existing Cry toxin families (Adang et al., 2014).

1.2 Delta-endotoxins

The δ -endotoxins are a superfamily of crystal proteins which can be divided into two main groups on the basis of their mechanism of action: the insect-specific Cry proteins and the generally cytolytic Cyt proteins (Butko, 2003).

Hofte and Whiteley in 1989 introduced the first systematic nomenclature for crystal proteins which was based on the spectrum of activity of proteins as well as their amino acid sequence homology (Höfte and Whiteley, 1989). The crystal toxins classification was later revised based only on amino acid sequence identity, where each protoxin acquired a name consisting of Cry (or Cyt) associated with four hierarchical ranks depending on its place in a phylogenetic tree. Proteins with a sequence identity of approximately <45%, 78%, 95% and $\leq 100\%$ differ in primary, secondary, tertiary and quaternary rank respectively (Crickmore et al., 1998).

1.2.1 Cry toxins

Their name derives from the fact that these proteins form parasporal crystals. *B. thuringiensis* Cry toxins represent the largest group of insecticidal proteins. It includes around 300 different crystal proteins and to date these toxins have been classified into 74 different types. The three-domain, binary (Bin) and ETX/MTX2 are the main families within this group (Crickmore, 2016).

Most well-studied crystal proteins are produced as inactive protoxins that are later proteolytically cleaved to form a toxic core fragment with a molecular weight in the range of 55 - 65 KDa in the larva midgut. These toxins were shown to exhibit toxicity against Lepidopterans, Coleopterans, Hemipterans, Dipterans, Nematodes, snails and human-cancer cells (figure 3) (Palma et al., 2014).

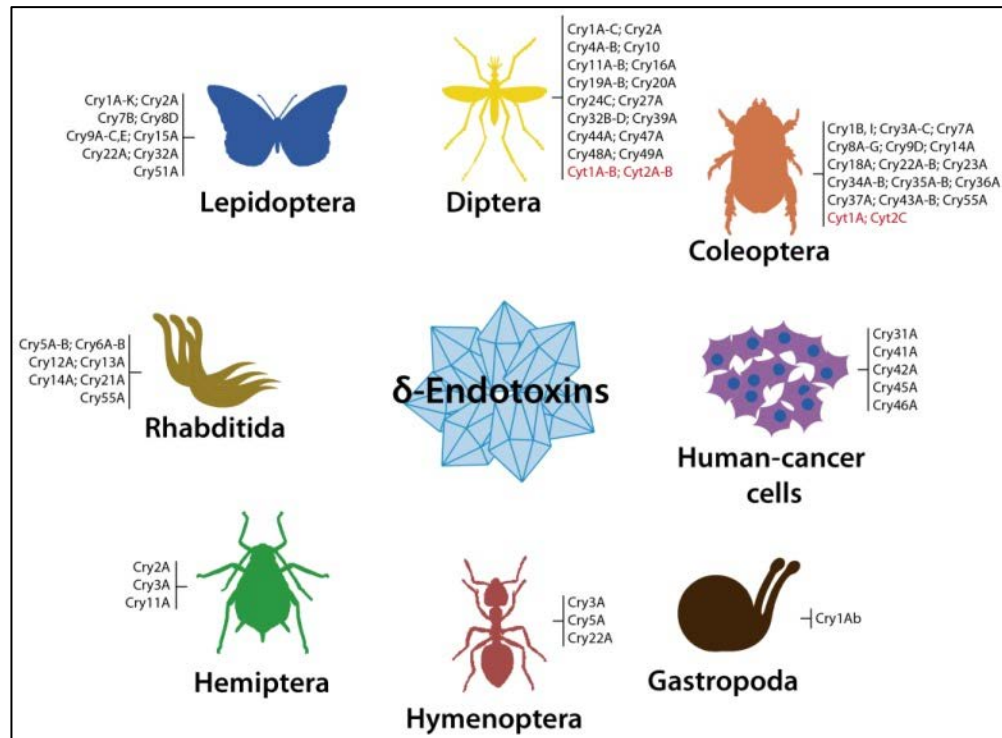


Figure 3: Host spectrum of *Bt* δ -endotoxins.

Bt δ -endotoxins (Cry and Cyt) grouped based on target specificity (Palma et al., 2014).

The three domain toxins constitute the biggest family of insecticidal *Bt* proteins. These toxins display differences in their amino acid sequences but share a similar three domain structure and five conserved blocks of amino acids believed to reside in the active toxic core. Block 1 exists in domain I, block 4 and 5 are contained in domain III while block 2 and 3 span the junction between domains I and II and domains II and III respectively (Höfte and Whiteley, 1989). These Cry proteins display toxic activity against insect species of the following orders: Lepidoptera, Diptera, Coleoptera, Hemiptera and nematodes yet, their mode of action has been studied mainly in lepidopteran insects (Palma et al., 2014).

Protoxins belonging to this family exhibit two different lengths with the larger group approximately twice as long as the majority of the toxins. The carboxy-terminal extensions of the long protoxins are not involved in toxicity and are believed to mediate the formation of bipyramidal crystals within the bacterium (de Maagd et al., 2001). Whereas, shorter protoxins (e.g., Cry3 and Cry11 toxins) of approximately 70 kDa are synthesized lacking the C-terminal region (figure 4) (Palma et al., 2014).

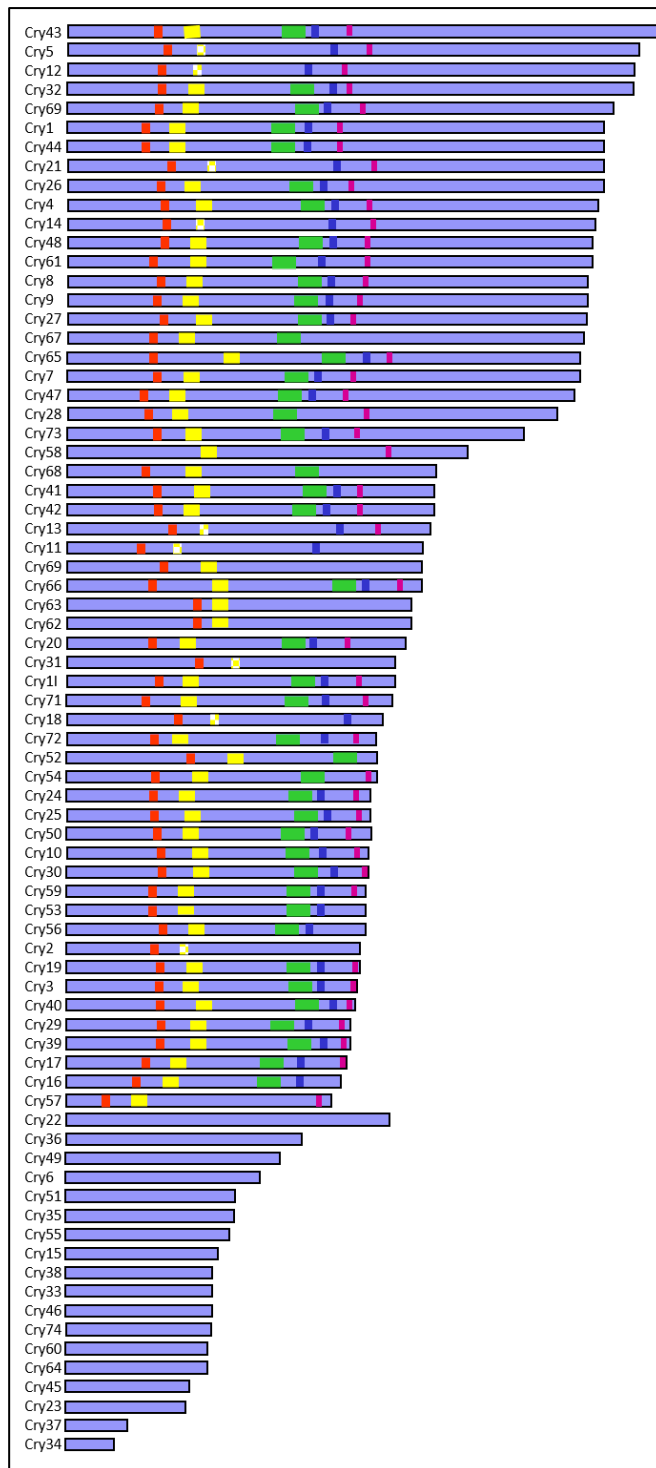


Figure 4: Cry protoxins presenting different lengths with presence/absence of the five conserved blocks and the three domains.

The three domain toxins are shown above the non-three domain ones and the coloured boxes represent the five conserved blocks (Fiuza et al., 2017).

The N-terminal Domain I or perforating domain is constituted by seven α -helices and is subjected to proteolytic cleavage during toxin activation. As suggested by the umbrella

model, the hydrophobic helical hairpin $\alpha 4$ and $\alpha 5$ are believed to insert into the membrane initiating pore formation while the other α -helices lay flat on the membrane surface in an umbrella-like shape. This helical domain is therefore responsible for toxin membrane insertion and pore formation (Deist et al., 2014).

Domain II, a β -prism, consists of three antiparallel β -sheets with exposed loop regions and is implicated in protein-receptor interactions. Due to their similarities to immunoglobulin antigen-binding sites, the loops of domain II were suggested to participate in receptor binding (Deist et al., 2014).

Domain III consists of two antiparallel β -sheet sandwich. It is proteolytically cleaved in some three-domain Cry proteins and is also involved in receptor recognition and binding and possibly in pore formation. This domain has also been shown to play a role in maintaining structural integrity of the toxin by protecting it from proteolysis (Deist et al., 2014).

The crystal structures of certain three domain toxins have been solved by X-ray crystallography. Amongst these toxins: Cry1Aa (Grochulski et al., 1995), Cry1Ac (Derbyshire et al., 2001) Cry2Aa (Morse et al., 2001), Cry3Aa (Li et al., 1991), Cry3Bb (Galitsky et al., 2001), Cry4Aa (Boonserm et al., 2006), Cry4Ba (Boonserm et al., 2005) and Cry8Ea1 (Guo et al., 2009). An example of three dimensional structure of the three domain toxin Cry8Ea1 is shown in figure 5.

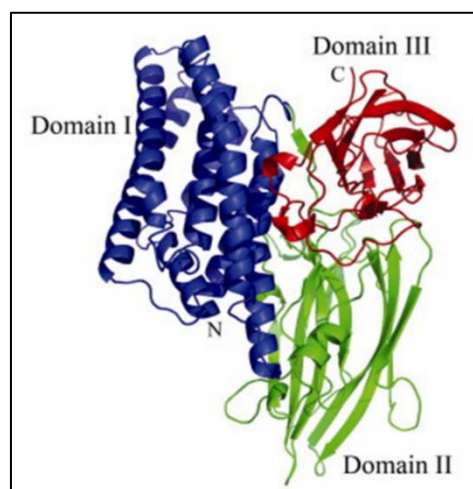


Figure 5: Three dimensional structure of Cry8Ea1 toxin.

The tertiary structure of Cry8Ea1 was determined at 3.2 Å resolution by X-ray crystallography. Domain I, II and III are represented in blue, green and red respectively (Guo et al., 2009).

The ETX/MTX2 family consists of 11 members that were classified under distinct primary rankings in the nomenclature: Cry15, Cry23, Cry33, Cry38, (Coleoptera), Cry51 (Coleoptera and Hemiptera), Cry60 (Diptera), Cry45 (Parasporin-4) and Cry64 (Parasporin-5) (human cancer cells). They all show features of the ETX/MTX2 family that includes the Mtx2 protein from *Lysinibacillus sphaericus* and the *Clostridium perfringens* epsilon toxin (Adang et al., 2014). Although their structure is significantly different from the three domain toxins, these toxins are believed to act via forming pores in the membranes of the target cells (Bokori-Brown et al., 2011). In fact, the Cry-ETX/MTX toxins showed significant similarities at the structural level with proteins from the aerolysin-like β -PFT group particularly with the tail region that has been proposed to play a role in oligomerisation and pore formation. A similar mode of action was then proposed for these Cry toxins (Liu et al., 2018). An example of the ETX/MTX structure is shown in figure 6.

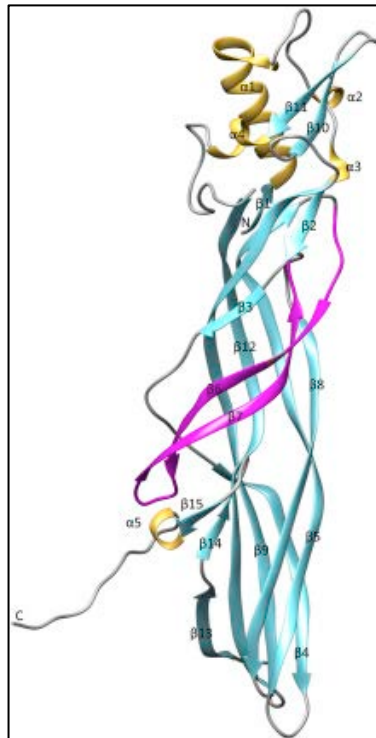


Figure 6: Three dimensional structure of Cry51Aa1.

The structure of Cry51Aa1 was solved at 1.65 Å resolution; PDB 4PKM. The secondary structure components include 5 helices and 15 β -strands presented in yellow and cyan respectively. The amphipathic β -hairpin is shown in magenta (Xu et al., 2015a).

The Bin-like toxins are a class that is composed of 13 toxins. Their name is derived from the fact that they resemble the two homologous components (Bin A and Bin B) of the mosquitocidal binary toxin from *L. sphaericus*. Although their molecular structure as well as their mechanism of action is unclear, there is some evidence that they form pores and that one of the components acts intracellularly (Berry, 2012). Figure 7 represents the 3-D structure of Bin A and Bin B of *L. sphaericus*.

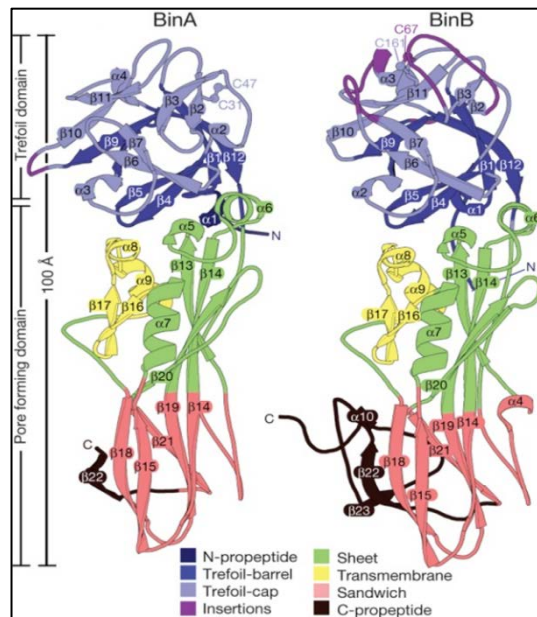


Figure 7: Three dimensional structure of Bin A and Bin B of *L. sphaericus*.

Structural similarity between Bin A and Bin B composed of trefoil and pore-forming domains. Each molecule is approximately 100 Å long and 25-30 Å in diameter. α and β represent carbohydrate-binding molecules where the structural differences are suggested to be located (Colletier et al., 2016).

1.2.2 Cyt toxins

Cytolytic toxins (Cyt) have been classified into four families (Crickmore, 2016). These toxins show mainly Dipteran specificity, some Cyt toxins, however, are able to kill coleopteran larvae such as Cyt1Aa that is toxic to *Chrysomela scripta* and Cyt2Ca which shows toxicity against *Leptinotarsa decemlineata* and *Diabrotica spp* (Soberon et al., 2013). In addition, these toxins were shown in vitro to be cytolytic to a broad range of cells including red blood cells (Promdonkoy and Ellar, 2003). They are synthesized as protoxins that are proteolytically cleaved to form the 25 kDa active toxic core (Thomas and Ellar, 1983b). The overall structure of Cyt toxins consists of a β -sheet surrounded by two α -helical layers (figure 8) (Cohen et al., 2011, Cohen et al., 2008, Li et al., 1996). The

mode of action of these toxins was suggested to involve either oligomerisation and pore formation or aggregation on the target cell surface leading to destruction of the lipid bilayer in a detergent-like manner (Butko, 2003, Rodriguez-Almazan et al., 2011).

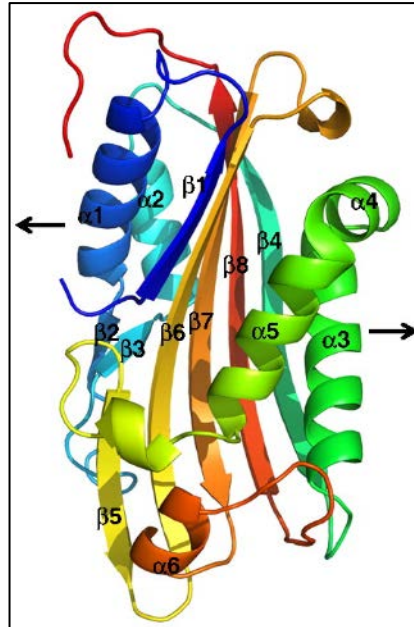


Figure 8: Three dimensional structure of Cyt1Aa toxin monomer.

The represented tertiary structure of Cyt1Aa toxin is coloured in rainbow using PyMOL; PDB 3RON. It was determined at 2.2 Å resolution. Arrows indicate the proposed movement of the helical layers to allow the pore formation by β -sheet (Cohen et al., 2011).

1.3 VIP

The vegetative insecticidal proteins (VIP) are classified into four families. They are secreted during the vegetative growth phase of *B. thuringiensis* and do not form parasporal crystal proteins. Vip1 and Vip2 constitute a binary toxin with high insecticidal activity reported against some members of Coleoptera. The Vip1 component is thought to bind to receptors in the membrane of the insect midgut while the Vip2 component enters the cell and prevents microfilament formation via ADP-ribosylation (Chakroun et al., 2016). The Vip3 toxins are active against a wide variety of lepidopteran insects, including *Agrotis ipsilon*, *Spodoptera frugiperda*, *Spodoptera exigua*, and *Helicoverpa zea*. When fed to susceptible insects, Vip3 acts in a similar way to that of Cry proteins

causing gut paralysis and lysis of midgut epithelial cells (Schnepf et al., 1998). On the other hand, the insecticidal properties of Vip4 toxins remain unknown.

1.4 Anti-cancer toxins: Parasporins (PSs)

The existence of *Bt* strains with no known insecticidal activity was first reported in 1986. From a total of 189 isolates of *Bacillus thuringiensis* producing parasporal inclusions (PIs), 36% were toxic to different orders of insects whereas the rest (64%) showed no insecticidal activity suggesting that in natural environments non-insecticidal PI-forming bacteria outnumber the insecticidal ones (Ohba and Aizawa, 1986). The fact that non-insecticidal isolates often account for >90% of the natural populations from soils and phylloplanes raised the question of whether such proteins synthesized in non-insecticidal inclusions have any undiscovered biological activity (Ohba et al., 2008). Therefore an extensive screening of *B. thuringiensis* Cry proteins with no known insecticidal activity was commenced and has led to the discovery of the proteins that target human cancer cells (Ohba et al., 2008).

A large-scale screening of 1744 *B. thuringiensis* strains was first attempted by Mizuki et al where amongst the non-hemolytic parasporal proteins produced, 42 were shown to have in vitro cytotoxic activity against MOLT-4 cells (human leukemic T-cells) retaining no significant insecticidal activities against 11 species of five orders: Lepidoptera, Diptera, Orthoptera, Dictyoptera and Isoptera. For a characterization of the anticancer activity of these proteins, three strains were chosen and were further examined. The selected proteins showed strong cytotoxic activities with different toxicity spectra and varied activity levels. The proteins of the two strains 84-HS-1-11 (A1190) and 89-T-26-17 (A1462) were of particular interest because of their ability to discriminate between leukemic and normal T-cells with a preferential activity against the cancer line (Mizuki et al., 1999). In 2000, Mizuki et al. obtained another strain A1190 producing an anticancer Cry protein which led to the creation of a new category of proteins designated as parasporins that are able to produce parasporal proteins capable of discriminately killing cancer cells (Mizuki et al., 2000).

To date 19 parasporins have been discovered. Based on the primary amino acid sequence of protoxins, they were classified into 6 first-rank groups parasporin-1, -2, -3, -4, -5 and -6 by the Committee of Parasporin Classification and Nomenclature (<http://parasporin.fitc.pref.fukuoka.jp/intro.html>). In addition, based on the sequence similarity to existing insecticidal toxins from *Bt* they were also incorporated into the Cry gene nomenclature (Crickmore et al., 1998).

Sequence analysis of parasporins revealed that they could also be categorized into two types: the three-domain type (PS-1, PS-3 and PS-6) and the ETX/MTX type of the β -pore-forming-toxin (β -PFT) family (PS-2, PS-4 and PS-5) (Akiba and Okumura, 2017).

1.4.1 Parasporin-1 (Cry31Aa1)

PS-1 derives from the *B. thuringiensis* soil isolate 84-HS-1-11 (recently designated as A1190). This three domain toxin possesses the five conserved blocks that are characteristic of three domain Cry proteins yet it only shares very low homology (<25% identity) with the existing classes of Cry and Cyt protein (Mizuki et al., 2000).

PS-1 is encoded by a gene of 2,169 bp long and is a polypeptide of 723 amino acid residues with a predicted molecular weight of 81,045 Da (Mizuki et al., 2000). Protease treatment by trypsin yields the active form of PS-1 which is a heterodimer protein consisting of 15 and 56 KDa polypeptides that are tightly associated (Katayama et al., 2007). The digestion occurs at the N-terminal region of the precursor protein (Mizuki et al., 2000). PS-1 preferentially exerts its cytotoxic effects against several cancer cell lines especially HeLa and HL-60 cell lines (their LD₅₀s are 0.12 and 0.32 μ g/mL respectively). Its cytotoxic effect was considered as moderate against Sawano and HepG2 cells but absent against the normal cells, peripheral blood T cells and MRC-5 cell line (Katayama et al., 2007).

Its crystal structure has been determined at 1.76 Å resolution (Akiba et al., 2005). It has a typical architecture characteristic of the three-domain insecticidal Cry toxins with an

additional N-terminal segment present in the active form of the protein (figure 9) (Akiba and Okumura, 2017).

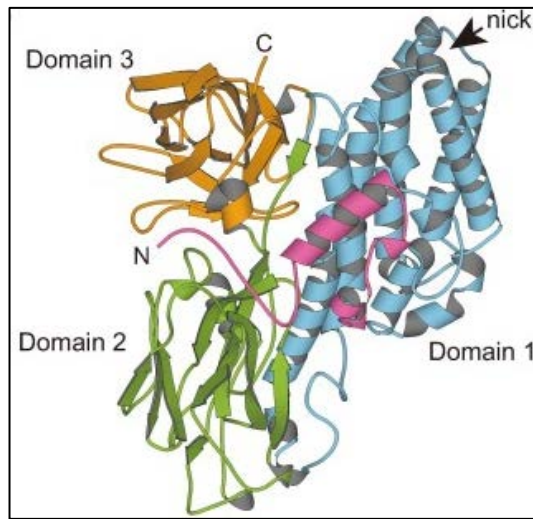


Figure 9: Orthogonal view of the ribbon representation showing the 3D-structure of the activated form of PS-1. Domains 1, 2 and 3 are indicated in light blue, green, and orange, respectively. The N-terminal extension of the protein is shown in violet. The cleavage site is represented with a black arrow (Akiba and Okumura, 2017).

Katayama et al in 2007 investigated the effect of the protein on membrane permeability, calcium homeostasis and the mode of cell death in sensitive cell lines. In their study they demonstrated that PS-1 induced an increase in Ca^{2+} influx with no observed alterations in membrane potential of intoxicated cells. This influx was considered as the first step in the pathway that underlies parasporin-1 toxicity. Heterotrimeric G-proteins or G-protein coupled receptors were shown to be involved in the induction of Ca^{2+} influx. In addition, PS-1 was proposed not to be a pore forming toxin and the mode of cell death was suggested to be most likely apoptotic (Katayama et al., 2007). It has been reported that PS-1 binds to the receptor Beclin-1 (Katayama, 2011) however the interaction between the toxin and the receptor is still to be elucidated. In figure 10, the visualised effect (cell ballooning) of PS-1 on HeLa cells is shown.

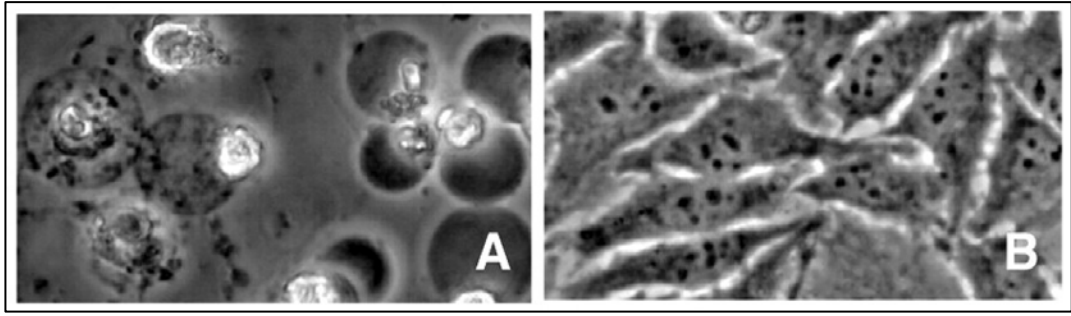


Figure 10: Morphological changes of PS-1-treated HeLa cells. A: Cells treated with toxin. B: Mock control. HeLa cells were treated with (1 μ g/ml) or without trypsin activated PS-1 then morphological changes were visualised using a phase-contrast microscope. *Bar*, 10 μ m. Figure was edited from Katayama et al. (Katayama et al., 2007).

1.4.2 Parasporin-2 (Cry46Aa1)

This toxin derives from the *Bt* strain 90-F-45-14 (recently designated as A1547). The gene encoding this protein is 1,014 bp long and the toxin is a polypeptide of 338 amino acid residues with a molecular weight of 37,446 Da. PS-2 is not a three domain Cry protein and thus lacks the block sequences conserved in these proteins. It does however, share a low sequence homology with Cry15Aa (an ETX/MTX toxin) among the established Cry and Cyt proteins (Ohba et al., 2009).

Proteolytic treatment of the 37 kDa protein with Proteinase K yields a cytotoxic 30 kDa fragment that exhibits notable cytotoxicity to certain human cancer cell lines. The digestion occurs at both N and C termini of the protein and the active core is selectively cytotoxic to HepG2, HL-60, Sawano, Jurkat and MOLT-4 cell lines (figure 11) (Ito et al., 2004, Ohba et al., 2009).

Cell	Characteristics	LD ₅₀ μg/ml
MOLT-4	Leukemic T cell	0.044
Jurkat	Leukemic T cell	0.015
HL-60	Leukemic T cell	0.066
T cell	Normal T cell	0.148
HC	Normal hepatocyte	>10
HepG2	Hepatocyte cancer	0.023
HeLa	Uterus (cervix) cancer	>10
Sawano	Uterus cancer	0.041
TCS	Uterus (cervix) cancer	>10
UtSMC	Normal uterus	9.28
MRC-5	Normal embryonic lung fibroblast	7.15
A549	Lung cancer	>10
CACO-2	Colon cancer	4.86

Figure 11: Cytocidal activity of PS-2 towards various human cells.

Cytotoxicity of proteinase K activated PS-2 (final concentrations, 0.6 ng to 10 μg) was tested on several cell lines using MTT assay and LD₅₀ was determined (Ito et al., 2004).

The crystal structure of the active form of PS-2 has been determined at 2.38 Å resolution (figure 12). It is very similar to the crystal structures of the ETX/MTX group therefore a similar mechanism of action was proposed: the toxin molecules bind to specific receptors in lipid rafts, oligomerize then insert their β-hairpins to penetrate the membrane and form pores (Akiba and Okumura, 2017).

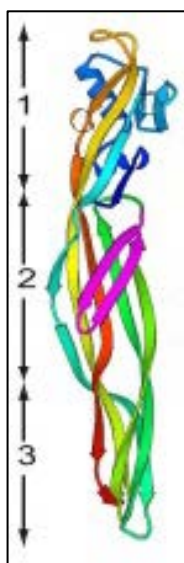


Figure 12: Crystal structure of PS-2 in ribbon representation.

Domain 1, 2 and 3 are indicated by vertical arrows on the left. The polypeptide chain of PS-2 is shown in a rainbow ramp: The N-terminus, C-terminus and amphipathic β-hairpin regions are coloured in blue and magenta respectively. Figure edited from Akiba and Okumura (Akiba and Okumura, 2017).

This proposed model was later demonstrated where the initial step in the cytotoxic action of PS-2 was shown to be the specific binding of the toxin to a putative receptor protein (GPI-anchored proteins) located in the lipid raft of plasma membrane of the susceptible cells which was followed by the formation of oligomers (>200 kDa) (Kitada et al., 2009). The 30 kDa protein was found to be a pore forming toxin which caused an increase in plasma membrane permeability. Following exposure to toxin, susceptible cells ballooned and started to detach, burst open and fragmented (figure 13). The study of DNA fragmentation and caspase activation showed that the mode of cell death was unlikely to be apoptotic in contrast to PS-1 (Ito et al., 2004, Kitada et al., 2006).

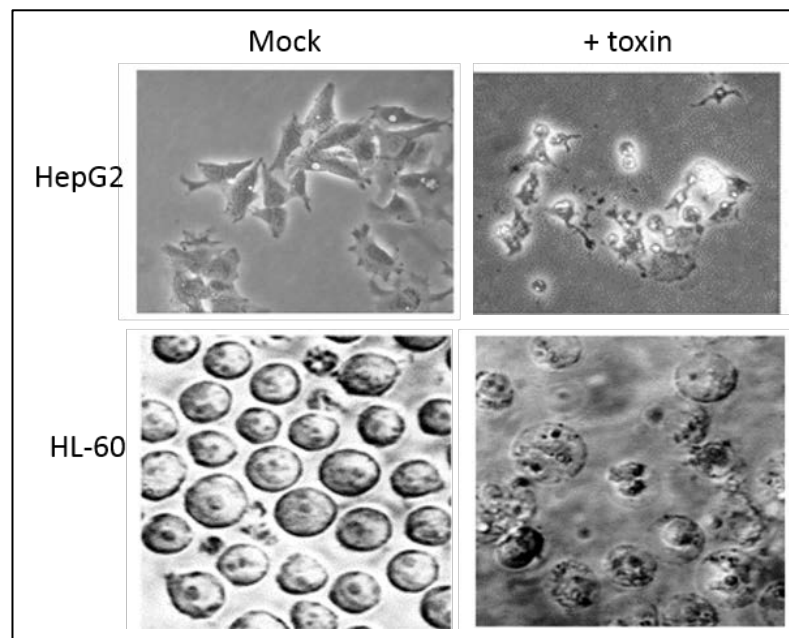


Figure 13: Visual effect of PS-2 on HepG2 cells and HL-60 cell lines.

Morphological changes of HepG2 and HL-60 cells treated with or without toxin were visualised under a phase-contrast microscopy. Figure is edited from Ito et al. (Ito et al., 2004).

1.4.3 Parasporin-3 (Cry41Aa and Cry41Ab)

Parasporin-3 was isolated from the *B. thuringiensis* strain 89-T-26-17 (recently designated as A1462) from soils of Tokyo in Japan. The protein consists of 825 amino acid residues with a deduced molecular weight of 93,689 Da sharing low homology with insecticidal Cry proteins. PS-3 has a typical three-domain structure with five block sequences commonly conserved in these Cry proteins. The C-terminal sequence of this

protein contains a β -trefoil domain similar to that of *Clostridium botulinum* hemagglutinin HA-33 (Ohba et al., 2009). PS-3 exhibits cytotoxic effect against only two tested cancer cell lines, HL-60 (myeloid leukaemia cancer) and HepG2 (liver cancer) (figure 14) and has the narrowest activity spectrum among the PS 1-4 proteins. Proteolytic digestion is required for activation of the protein which is converted to a 64-kDa toxic moiety by proteolytic processing of both N- and C-terminal regions (Ohba et al., 2009).

Cell	Origin	EC ₅₀ (ug/ml)	
		P2	P3
Human			
MOLT-4	Leukemic T cell	>10	>10
Jurkat	Leukemic T cell	>10	>10
HL60	Myeloid leukemia	1.32	1.25
HeLa	Uterus cervix cancer	>10	>10
TCS	Uterus cervix cancer	>10	>10
Sawano	Uterus cancer	>10	>10
HepG2	Hepatocyte cancer	2.80	1.86
A549	Lung cancer	>10	>10
CACO-2	Colon cancer	>10	>10
T cell	Normal T cell	>10	>10
UtSMC	Normal uterus	>10	>10
HC	Normal hepatocyte	>10	>10
MRC-5	Normal lung	>10	>10
Simian			
Vero	African green monkey kidney	>10	>10
COS-7*	African green monkey kidney	>10	>10
Murine			
NIH3T3-3	Mouse embryo	>10	>10

Figure 14: Cytotoxicity spectra and levels of PS-3.

The cytotoxic effect of proteinase K activated PS-3 was tested on several mammalian cell lines using MTT cell viability assay and EC₅₀s were determined. P2 and P3 represent Cry41Aa1 and Cry41Ab1 respectively (Yamashita et al., 2005).

Gene cloning experiments carried out by Yamashita et al in 2005 showed the existence of two genes encoding the 88-kDa Cry proteins representative of PS-3: Cry41Aa and Cry41Ab. Each gene is formed of three ORFs: ORF1, ORF2 and ORF3 that are orientated in the same direction and had putative ribosome binding sites in their upstream regions (Yamashita et al., 2005). ORF1 encodes a hypothetical protein of around 19 kDa, ORF3 encodes a protein of around 82 kDa and is believed to be involved in crystallization and expression since it shares homology with the C-terminal domain of the larger 3-domain insecticidal Cry toxins while ORF2 encodes a protein of 93 kDa which possesses the cytotoxic activity against human cancer cells and contains the aforementioned five

conserved blocks (Yamashita et al., 2005). Additionally ORF2 contains a conserved domain belonging to Ricin superfamily which is similar to HA-33 like domain present in *Clostridium botulinum* type C mammalian neurotoxin that causes botulism disease (Tsuzuki et al., 1990).

The two encoded toxins, designated as Cry41Aa1 and Cry41Ab1 by the *Bt* Toxin Nomenclature Committee (Crickmore, 2016), show a high degree of homology: 87%, 88% and 99% sequence identity between the proteins coded by ORF1, 2 and 3 respectively. Proteinase K activated toxin but not the solubilised core exhibits a cytotoxic action. Upon treatment with Proteinase K, the 88 kDa protoxin is converted to 64 kDa active core which was N-terminally sequenced and showed that N-terminal cleavage occurs at the 60th aa (Yamashita et al., 2005), while trypsin and chymotrypsin treatment result in two fragments of around 64 and 80 kDa (Yamashita et al., 2000). Cry41Aa and Cry41Ab exhibited strong cytotoxic activity only against HL-60 and HepG2 cells yet viability and membrane damage experiments showed that Cry41Aa was more toxic than Cry41Ab. Morphological observations of HepG2 cells post-toxin administration showed swelling and a serious membrane damage (figure 15) however the swelling was also detected in non-susceptible cells like HeLa (Yamashita et al., 2005).

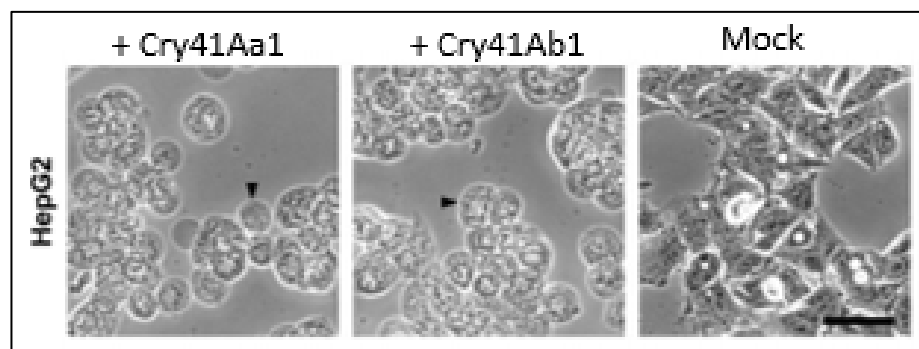


Figure 15: Morphological changes of HepG2 cells upon treatment with Cry41Aa1 and Cry41Ab1. Cells were treated with activated proteins (10 mg/ml). Phase-contrast microscopic observation was done 1 h post-administration. Arrowheads indicate swollen cells, Bar = 50 μm. Figure is edited from Yamashita et al. (Yamashita et al., 2005).

Cry41Aa was expressed by Krishnan et al in 2017. The amino acid sequence of its ORF2 is shown in figure 16. The predicted three dimensional structure of Cry41Aa protoxin was generated by Phyre2 and visualised using UCSF Chimera 1.10.1 (figure 16).

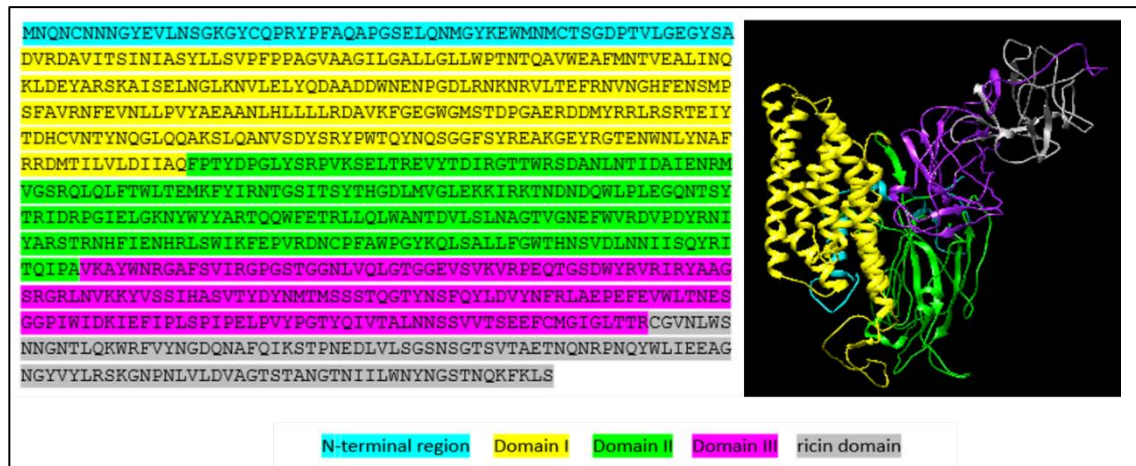


Figure 16: The amino acid sequence of Cry41Aa encoded by ORF2 and the correspondent predicted 3-D structure. The putative domains were identified based on sequence comparison with other three domain Cry toxins (Elhigazi et al. unpublished). N- and C-terminal regions as well as the ricin domain of the protoxin are also presented. 13 templates were selected to model Cry41Aa protein based on heuristics to maximise confidence, percentage identity and alignment coverage: c1ciyA, d1i5pa3, c2c9kA, c3eb7B, c4moaA, d1qxa2, c1ybiA, c1dlcA, c2ihoA, c2vsaA, c2ehiB, d1qxa1 and c1j16A presenting % identity of 29, 22, 29, 33, 30, 29, 26, 32, 22, 30, 22, 30 and 35 respectively.

Krishnan et al showed that the ricin domain was not involved in Cry41Aa toxicity. They also proposed that Cry41Aa is a pore-forming toxin and does not induce apoptosis. Upon treatment of HepG2 cells with activated Cry41Aa morphological changes (figure 17) as well as membrane damage were observed. Sequence comparison of Cry41Aa and insecticidal toxins identified loop 3 in domain II of Cry41Aa, which in insecticidal Cry toxins was previously shown to play a major role in receptor binding (Pacheco et al., 2009). This exposed loop region, was shown to be important for the activity of Cry41Aa against HepG2 cells (Krishnan et al., 2017).

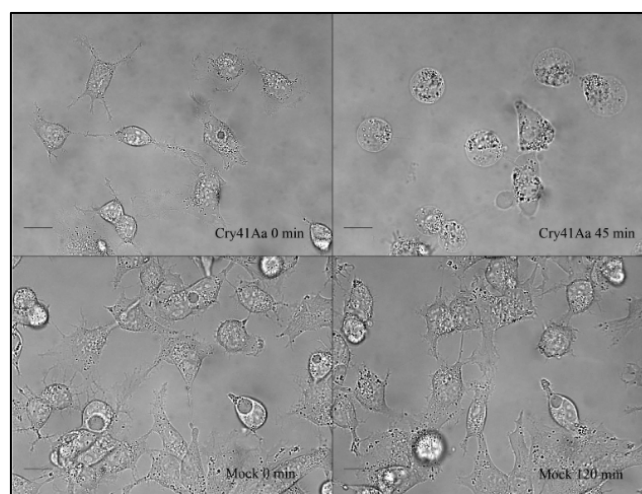


Figure 17: Morphological changes of HepG2 cells following Cry41Aa treatment. HepG2 cells were treated with Cry41Aa (5.5 µg/ml) at different time points and then viewed by DIC (differential interference contrast) microscope. The scale bar represents 20 µm (Krishnan et al., 2017).

Further work on Cry41Aa was carried out by Domanska et al. (Domanska, 2016) who investigated the mechanism of action of this toxin and established the following :

- Cell exposure to Cry41Aa resulted in membrane permeability allowing the detection of both small and large size cytotoxic markers.
- Cry41Aa induced channel formation in planar lipid bilayers (PLBs) as well as in biological membrane patches of various origins. PLB experiments confirmed the pore forming nature of Cry41Aa.
- Pre-treatment of HepG2 cells with EGTA inhibited Cry41Aa toxicity by means of metal ion chelation. EGTA acted by preventing stable interaction with the membrane and the subsequent steps of membrane damage. It was also shown to exert its protective effect by chelating cations (most likely candidates being: Ca^{2+} , Mn^{2+} and Zn^{2+}) bound to plasma membrane components.
- Cry41Aa induced p38 MAPK activation in susceptible cells however inhibition of p38 activity did not rescue cell viability.

1.4.4 Parasporin-4 (Cry45Aa1)

PS-4 was isolated from *Bt* strain A1470 (previously designated as 89-T-34-22) (Okumura et al., 2005). It consists of 275 amino acid residues with a molecular weight of 30, 078 Da and possesses only low homology (< 30%) in amino acid sequence with the existing Cry and Cyt proteins. The three-domain structure is not associated with this protein (Ohba et al., 2009). Proteolytic processing is essential for activation of the cytotoxic protein. Proteinase K treatment of PS-4 leads to the production of a 28 kDa fragment that was shown to be toxic towards various mammalian cells yet preferentially killing colonic, uterine, and blood cancer cells (Okumura et al., 2005). The protein could also be activated using pepsin leading to the production of a 27 kDa fragment that was highly cytotoxic towards CACO-2, Sawano, MOLT-4, TCS, and HL-60 cells (Okumura et al., 2011).

PS-4 treatment was shown to induce marked morphological changes in susceptible MOLT-4 and CACO-2 cells: In MOLT-4 treated cells, swelling and blebbing followed by nuclear shrinkage were observed (figure 18). PS-4 was also shown to induce the formation of large pores in the plasma membrane of target cells: It binds non-specifically (to susceptible and non-susceptible cells) to the plasma membrane and oligomerizes to form pores only in susceptible cells leading to cell death. PS-4 shares homology with ETX/MTX toxins therefore its mode of action was proved to be almost identical to that of ETX/MTX toxins however, PS-4 differs in its cholesterol independence (Okumura et al., 2011).

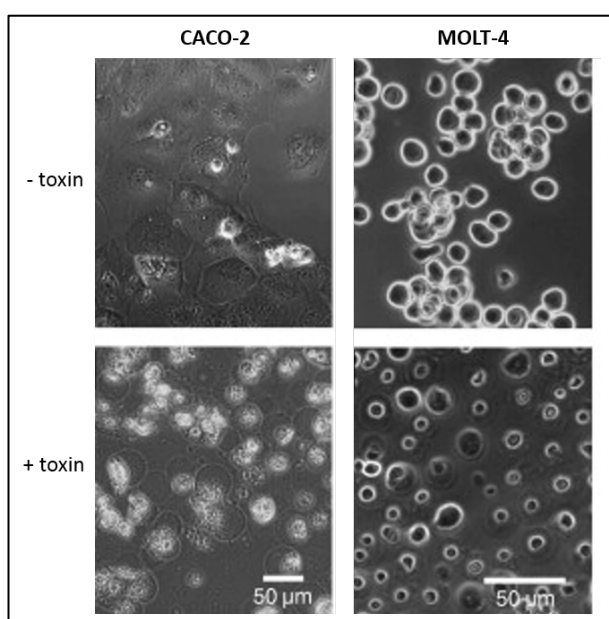


Figure 18: Morphological changes of CACO-2 and MOLT-4 cells following toxin treatment. CACO-2 and MOLT-4 cells were incubated with PS-4 at a final concentration of 4 µg/ml then were visualised under phase contrast microscopy. Figure is edited from Okumura et al. (Okumura et al., 2011).

1.4.5 Parasporin-5 (Cry64Aa)

PS-5 was isolated from *Bt* strain A1100. This protein shares some slight amino acid sequence homology with some *B. thuringiensis* Cry toxins and also with ETX/MTX toxins (Ekino et al., 2014).

PS-5 was expressed as a 33.8 kDa inactive protoxin that exhibited cytotoxic activity following proteolytic treatment with Proteinase K. The cleavage occurs at the C-terminal region of the protein to yield smaller active molecules of around 29.8 kDa.

The cytotoxic activities of the protein against various mammalian cell lines were evaluated showing that the toxin possesses strong cytotoxic effect against seven (MOLT-4, HepG2, TCS, HeLa, COS7, Vero, and Sawano cells) out of 18 mammalian cell lines, and low to no cytotoxicity to the others (figure 19) (Ekino et al., 2014).

Cell line	Origin	EC ₅₀ (µg/mL)
MOLT-4	leukemic T cell, human	0.075
CACO-2	colon cancer, human	0.30
Jurkat	leukemic T cell, human	0.124
A549	lung cancer, human	4.41
HepG2	hepatocyte cancer, human	0.049
TCS	uterus cervix cancer, human	0.046
HL60	promyelocytic leukemia cell, human	1.079
K562	myelogenous leukemia cell, human	4.249
U937	DE-4 lymphoma cell, human	>10
HeLa	uterus cervix cancer, human	0.080
COS7	kidney cell, monkey	0.045
NIH3T3	embryo cell, NIH Swiss mouse	0.321
Vero	kidney cell, monkey	0.050
CHO-K1	ovary cell, chinese hamster	0.571
Sawano	uterus cancer, human	0.065
MRC-5	normal embryonic lung fibroblast, human	0.273
UtSMC	normal uterus, human	0.223
HC	normal hepatocyte, human	>10

Figure 19: Cytotoxic activity of PS-5 protein against various mammalian cells.

The cytotoxic effect of PS-5 was evaluated on several mammalian cell lines using MTT viability assay and EC₅₀s were determined (Ekino et al., 2014).

Microscopic observation of MOLT-4 cells treated with PS-5 revealed rapid cell swelling (figure 20) however the mode of action is still unknown but is predicted to be similar to that of the β -PFTs (Ekino et al., 2014).

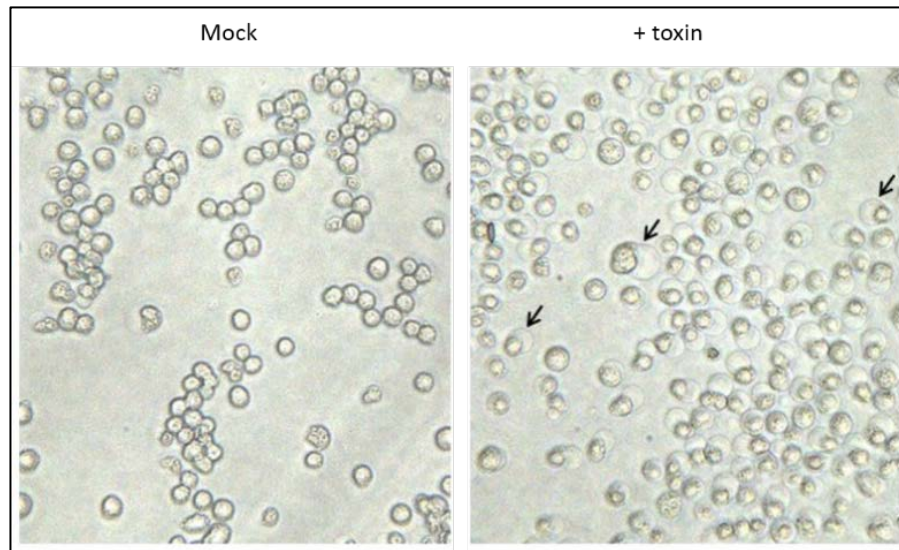


Figure 20: Visualised cytopathic effect of PS-5 on MOLT-4 cells.

The cells were treated with solubilised PS-5 for 1 hour then morphological changes were observed under a phase-contrast microscope. Arrows show the ballooning cell shape of target cells. Figure edited from Ekino et al. (Ekino et al., 2014).

1.4.6 Parasporin-6 (Cry63Aa1)

PS-6 was isolated from *Bt* strain M019. Proteolytic treatment of the 84 kDa three domain Cry protein with trypsin resulted in the cleavage at N-terminal region leading to its activation and the production of two fragments of around 14 and 59 kDa which were toxic to HepG2 and HeLa cells. Swelling and formation of vacuoles in the cytoplasm of HepG2 cells were observed with the vacuole-formation in the cytoplasm was speculated to be a secondary effect of pore-forming action (Nagamatsu et al., 2010).

1.5 Different models proposed for Cry toxin mode of action

There are two main groups of pore-forming toxins (PFT): the α -helical group, in which the α -helix regions of the toxin form the trans-membrane pore and the β -barrel toxins that form a β -barrel which inserts into the membrane (Parker and Feil, 2005). The first class of PFT includes toxins such as the colicins, exotoxin A, diphtheria toxin and Cry three-domain toxins while the second class includes aerolysin, α -hemolysin, anthrax

protective antigen, cholesterol-dependent toxins as perfringolysin O and the ETX/MTX toxins. Generally bacteria secrete their toxins which interact with specific receptors located on the host cell surface. In most cases, the activation of these PFT occurs by host proteases followed by receptor binding resulting in the formation of an oligomeric structure that inserts into the membrane (Parker and Feil, 2005).

The most accepted model of Cry toxin mode of action is based on Knowles and Ellar's work in 1987 where the colloid-osmotic lysis model was proposed (Knowles and Ellar, 1987). The model was postulated based on experiments carried out on the three domain δ -endotoxins on Lepidopteran larvae. Initially, the crystal inclusions are ingested by susceptible larvae, solubilised in the alkaline environment of the gut then activated by midgut proteases producing 60-70 kDa protease resistant proteins. The proteolytic activation of the toxin involves removal of an N-terminal peptide (25-30, 58 and 49 amino acids for Cry1, Cry3A and Cry2Aa toxins respectively) and approximately half of the remaining protein from the C-terminus in the case of the long Cry protoxins resulting in the monomeric toxin. Toxin then binds to insect midgut epithelial receptors, inserts into the membrane and forms lytic pores in microvilli of apical membranes leading to cell lysis and death (Soberon et al., 2009).

Another model was proposed: the signal transduction model. This model has the same initial steps as the pore formation model up to the binding of the toxin to a cadherin receptor. In this model, toxin interaction with the receptor stimulates the activation of a Mg^{2+} -dependent intracellular pathway resulting in cell death (Soberon et al., 2009). Figure 21 shows a diagram describing the mode of action of Cry toxins.

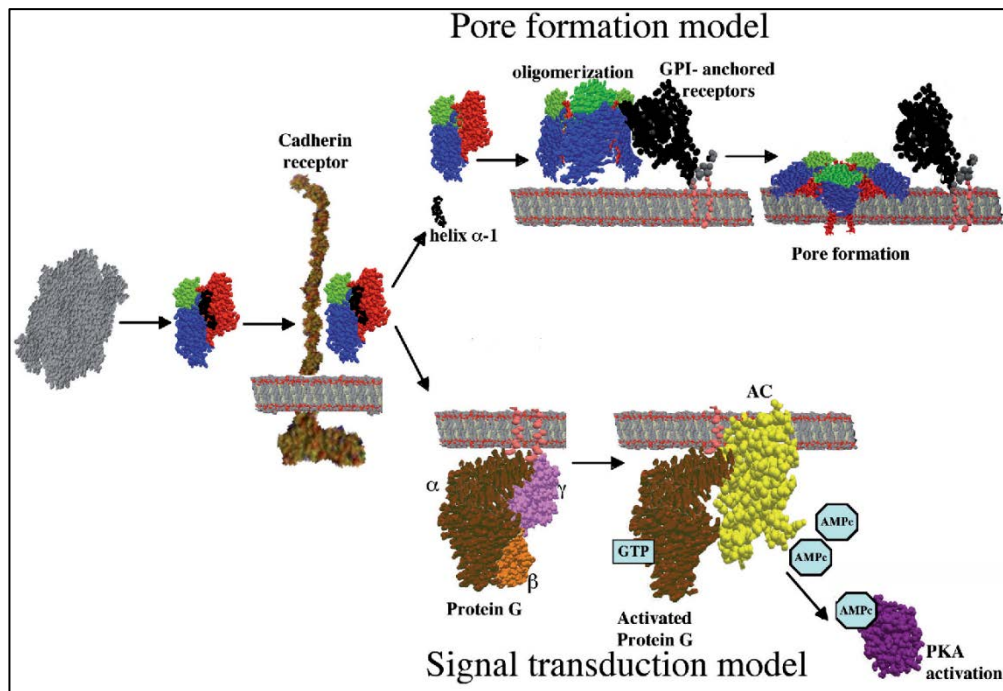


Figure 21: Diagram summarising models proposed for the mode of action of Cry toxins.

Two models were proposed for the mode of action of Cry toxins: the pore formation model and the signal transduction model (Soberon et al., 2009).

1.5.1 The pore formation models

- **The Bravo model**

The Bravo model was proposed based on experiments carried out on Cry1Ab toxin and its interactions with the brush border membrane vesicles (BBMV) of *Manduca sexta*. It suggests that Cry1Ab needs to bind to two receptor molecules (aminopeptidase N (APN) and a cadherin-like protein (Bt-R1)) to exert its effect on the target cell membrane. In fact, immunoprecipitation experiments demonstrated that initial binding of Cry1Ab toxin to cadherin is followed by binding to APN. Initially, the toxin monomer binds to cadherin which promotes cleavage of helix α -1 by a membrane-bound protease resulting in formation of oligomeric toxin which then binds to APN. This latter interaction facilitates the migration of the pre-pore complex towards the detergent-resistant membrane (DRM) where toxin insertion occurs leading to formation of pores and subsequent cell lysis and death (figure 22). The fact that APN was more efficiently detected in samples immunoprecipitated with the oligomeric structure of Cry1Ab while

cadherin was preferentially detected in samples immunoprecipitated with the monomeric Cry1Ab suggested that the two receptors interact sequentially with different structural state of the toxin to facilitate its efficient membrane insertion (Bravo et al., 2004).

This finding was supported by previous work where the Cry1Ab oligomer was shown to be toxic towards *M. sexta* (Gomez et al., 2002) and that it inserts more efficiently into membrane vesicles compared with the monomeric Cry1Ab suggesting that the oligomerization process is required for toxin insertion into target cell membranes (Rausell et al., 2004b). The important role of APN in toxin activity was also demonstrated in a previous study where silencing APN in *S. litura* resulted in insect resistance to Cry1C toxin (Rajagopal et al., 2002a).

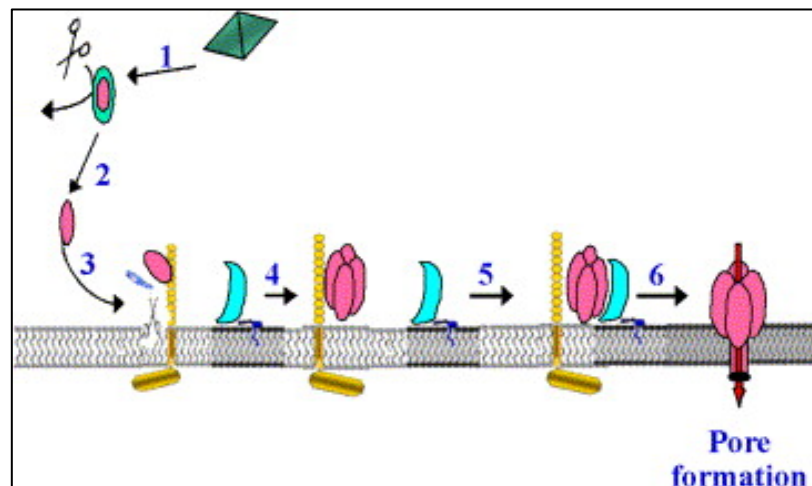


Figure 22: Sequential steps proposed in the mode action of Cry toxins.

The different steps in the mode of action of Cry toxins are: **1:** Solubilisation of crystal protein, **2:** Proteolytic processing of the protoxin, **3:** Binding of toxin monomer to Bt-R1 and cleavage of helix α -1, **4:** Pre-pore oligomeric structure formation, **5:** Binding of toxin oligomer to APN and mobilization to DRM, **6:** Pore formation (Bravo et al., 2004).

- **The Ping-Pong model**

This model was proposed by Pacheco et al where the Cry1Ab monomer was shown to bind initially with low affinity to the highly abundant APN through loop 3 of domain II before the high affinity interaction with the low-abundant cadherin occurs through other regions of domain II in addition to loop 3. The latter interaction with cadherin promotes cleavage of helix α -1 and formation of the pre-pore oligomer that binds to APN which facilitates its insertion into the membrane (figure 23) (Pacheco et al., 2009).

Pacheco et al showed that mutations located in loop3 of domain II affected binding of Cry1Ab to both receptors and insecticidal activity against *Manduca sexta* larvae and that the interaction with these receptors depends on the oligomeric state of the toxin. In fact, in the case of APN, binding of monomers of loop 3 mutants to this receptor was reduced, in contrast the oligomeric form of these mutants was not affected in binding to APN suggesting that loop 3 is involved in the binding with receptor molecules depending on the oligomeric state of the toxin (Pacheco et al., 2009).

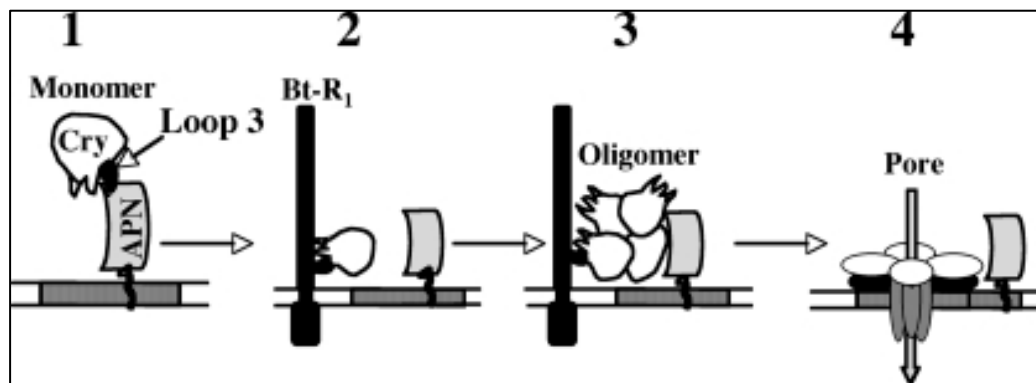


Figure 23: Schematic representation of the Ping pong binding model of Cry1Ab toxin.

1: Binding of Cry1Ab monomer to APN through loop 3 of domain II, **2:** The monomer binds to Bt-R1 through regions of domain II (loops α -8, 2, and 3), **3:** Formation of an oligomeric form of the toxin that binds to Bt-R1 through loop 3 and to APN through domain III, **4:** Membrane insertion and pore formation (Pacheco et al., 2009).

1.5.2 The signalling model

- **The Zhang model**

This model was proposed based on experiments performed using Cry1Ab and cells originating from ovarian cells of the cabbage looper, *Trichoplusia ni*. These cells (H5) which don't express the cadherin receptor, were shown to become sensitive to Cry1Ab following transfection with the receptor molecule (transfected cells were named S5) (Zhang et al., 2005). It was suggested that monomeric but not the oligomeric form of Cry1Ab can specifically bind to cadherin receptor and induce toxicity. Toxin oligomer

was also shown to be unable to form lytic pores into target cell membrane. The cell death was rather correlated with an activation of Mg^{2+} -dependent cellular signalling pathway following binding of the Cry1Ab toxin monomer to cadherin (Zhang et al., 2005).

These findings came from the fact that Cry1Ab toxin oligomer was shown to insert into membranes in cells stably expressing cadherin (susceptible) as well as in receptor-free (non-susceptible) cells while monomeric form of the toxin was incorporated only into the membranes of cells expressing cadherin. In addition, blocking the receptor active site of the toxin resulted in lack of interaction of toxin monomer with cadherin and prevented toxicity and cell death however incorporation of oligomeric toxin into the cell membrane was observed and was inconsequential. The toxin oligomers were also shown to be incorporated into the cell membrane of H5 cells and were maintained there through several generations without any toxic effect (Zhang et al., 2005).

Zhang et al in 2005 also showed that in the presence of EDTA and EGTA chelators, the binding of the toxin (Cry1Ab) to the receptor (cadherin) still occurred however only EDTA prevented subsequent cell death. Addition of Mg^{2+} to susceptible cells pre-exposed to EDTA restored cytotoxicity of Cry1Ab and microscopic observations showed that removal of this cation prevented the susceptible cells from swelling. These findings proposed that Cry1Ab binding to Bt-R1 and subsequent cell death were linked to a Mg^{2+} -dependent signaling pathway (Zhang et al., 2005).

The model proposed an intracellular cascade response involving protein G, adenylyl cyclase (AC) and protein kinase A (PKA) following interaction with membrane receptor (figure 24). Specific binding of the Cry1Ab toxin to cadherin receptor (Bt-R1) was shown to stimulate G protein ($G_{\alpha s}$) and adenylyl cyclase (AC) causing the accumulation of cAMP and activation of protein kinase A (PKA). These events were shown to disturb both structural and functional integrity of the host cell leading to its death (figure 24) (Zhang et al., 2006).

Induction of the adenylyl cyclase/protein kinase K pathway was manifested by membrane blebbing, appearance of ghost nuclei, cell swelling and lysis (Zhang et al., 2006). Pre-treatment of S5 cells with PKA inhibitors prevented these phenotypic changes of cells and protected them from Cry toxin action. In addition, inhibition of $G_{\alpha s}$

(NF449) and AC (ddADP) resulted in lack of cAMP production and reduced the Cry1Ab cytotoxicity while the activator (FSK) and potentiator (pCPT-cAMP) of cAMP sensitized the cells and enhanced cytotoxicity (Zhang et al., 2006).

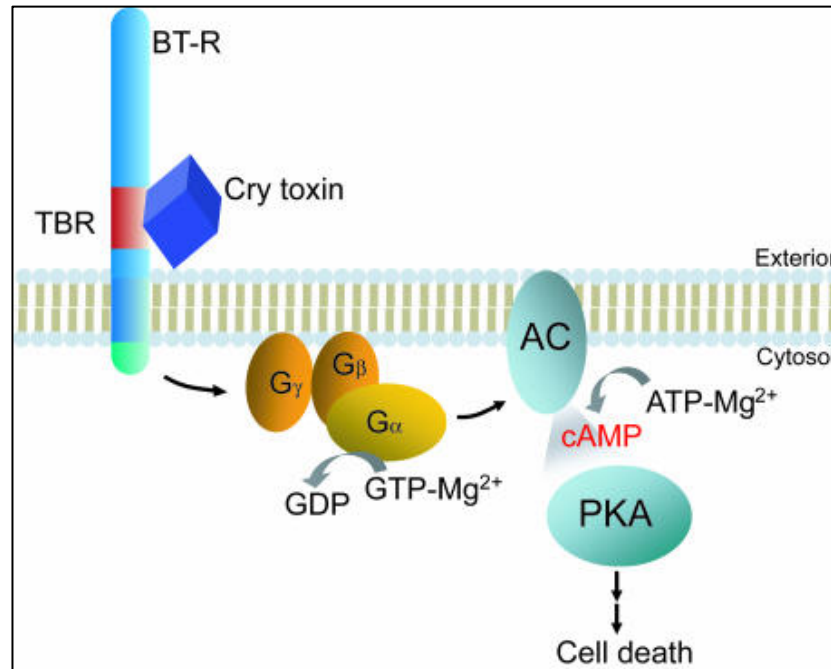


Figure 24: The signalling pathway model proposed for the action of Cry toxin.

Cry toxin binds to Bt-R1 and stimulates G protein and AC causing accumulation of intracellular cAMP and activation of PKA. PKA activation causes destabilisation of the structural and functional integrity of the cell leading to cell death (Zhang et al., 2006).

- **The Jurat-Fuentes Model: A combination of the pore forming and the signalling models**

This model was proposed to explain the mode of action of Cry1Ac against *H. virescens* (Jurat-Fuentes and Adang, 2006). The model suggests that both osmotic lysis and cell signalling contribute to the cytotoxicity and thus elements of both the Bravo model and the Zhang model are combined in the toxin mode of action (Figure 25). Initially the monomeric form of Cry1Ac binds to the cadherin-like protein (HevCaLP) resulting in the activation of an intracellular signaling cascades regulated by phosphatases. Proteomic analysis of BBMVs of susceptible and resistant larvae indicated the involvement of

phosphatases. In fact, resistant strains were shown to have lower alkaline phosphatase activity when compared to susceptible larvae of *H. virescens* (Jurat-Fuentes and Adang, 2006).

A direct interaction between Cry1Ac and actin was suggested to have a possible effect on the signalling (Jurat-Fuentes and Adang, 2006, McNall and Adang, 2003). The interaction of this cytoskeletal protein (actin) with the cytosolic domain of cadherins through tyrosine phosphatases, catenin and actinin was previously observed (Lilien and Balsamo, 2005). After binding to HevCaLP, Cry1Ac toxin monomers oligomerize then bind to GPI anchored proteins HvALP and APN. The Cry1Ac oligomers are driven to DRMs where toxin insertion occurs inducing osmotic shock as well as activation of signaling pathways, which may activate apoptotic responses, leading to cell death (Jurat-Fuentes and Adang, 2004).

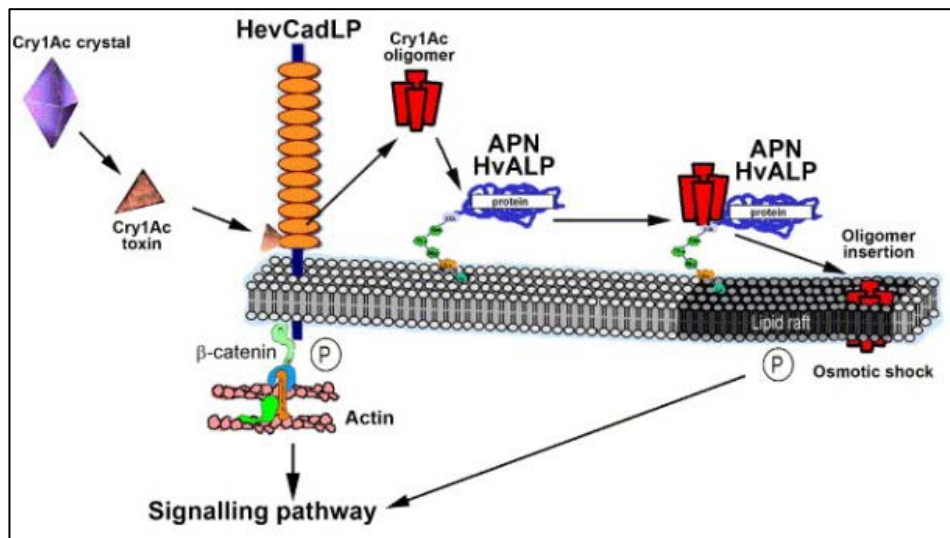


Figure 25: Proposed model describing the mode of action of Cry1Ac toxin in *H. virescens*.

Following proteolytic processing of the toxin in the insect midgut, activated Cry1Ac binds to HevCaLP. Oligomerization then occurs followed by binding to GPI-anchored HvALP receptor which leads to membrane insertion and pore formation. Binding to cadherin may also induce activation of signalling pathway after the interaction between cadherin intracellular domain and actin, which is regulated by phosphatases (P) (Jurat-Fuentes and Adang, 2006).

1.6 Cry toxin receptors

Cry toxin binding to insect midgut epithelial receptors has been demonstrated to be a key determinant of specificity. Positive correlation between binding to the brush border membrane and toxicity has been confirmed in many cases. In fact, early studies showed that Cry1Ba toxin, lethal to *Pieris brassicae*, bound specifically to the insect's brush border membrane vesicles (BBMV) but not to BBMV prepared from rat intestine (Hofmann et al., 1988a). Moreover, it was shown that Cry1Ab and Cry1Ba which are toxic to *P. brassicae* bound specifically to the insect's BBMV, yet only Cry1Ab bound to BBMV prepared from *Manduca sexta* since this toxin but not Cry1Ba is toxic to the insect (Hofmann et al., 1988b). However later studies presented data where no correlation between binding and toxicity was observed. Cry1Ac was shown to have a relatively stronger binding affinity to *Lymantria dispar's* BBMV compared with Cry1Ab which is more toxic to the insect (Wolfersberger, 1990). Moreover, specific binding of Cry1Ac was found to be similar between BBMVs prepared from resistant and susceptible larvae of *Pectinophora gossypiella* (Ocelotl et al., 2015). It was then concluded that the binding is necessary but not sufficient for Cry toxicity (Fiuza et al., 2013). On the other hand previous work carried out on binding kinetics demonstrated that irreversible binding, identified as the toxin-membrane association step, correlates better with toxicity than the reversible binding which is defined as toxin-receptor interaction step (Liang et al., 1995).

Interactions between *Bt* Cry toxins and putative/functional receptors have been extensively investigated. The best characterized receptors are aminopeptidase N (APN) and cadherin-like receptors identified in lepidopteran insects. Glycolipids were identified as Cry toxin receptors in nematodes in addition to other putative receptors including alkaline phosphatases (ALPs) reviewed by Pigott and Ellar (Pigott and Ellar, 2007). In case of Cry1A toxins, at least four different binding-proteins: a cadherin-like protein (CADR) (Gahan et al., 2001), a GPI-anchored aminopeptidase-N (APN) (Wei et al., 2016), a GPI-anchored alkaline phosphatase (ALP) (McNall and Adang, 2003) and a 270 kDa glycoconjugate (Valaitis et al., 2001) have been described in different

lepidopteran insects (figure 26). Recent reports on resistance to *Bt* Cry toxins support the role of ABC transporters as putative Cry toxins receptors (Heckel, 2012).

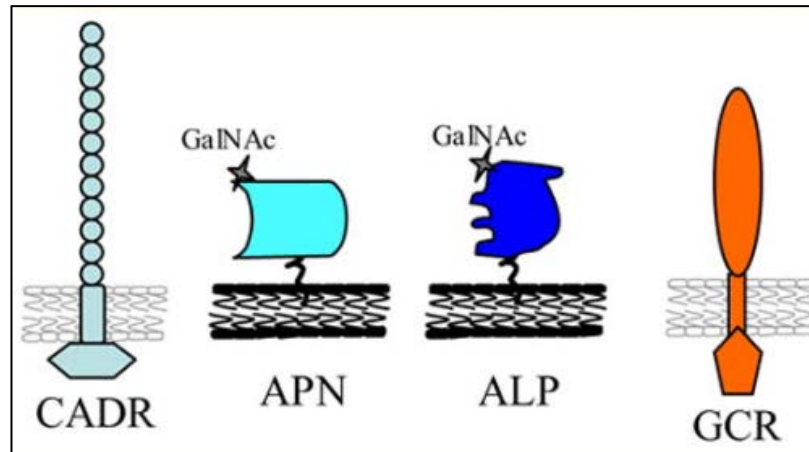


Figure 26: Representation of different receptor molecules of Cry1A toxins.

Cadherin, aminopeptidase-N, alkaline phosphatase, and 270 kDa glyco-conjugate receptors are designated as CADR, APN, ALP and GCR respectively (Bravo et al., 2007).

- **The Aminopeptidases N (APNs)**

The Aminopeptidases N (APNs) are a class of metalloproteases that cleave amino acids at the N terminus of polypeptides in microorganisms, plants and animals (Sanz, 2007). In the Lepidopteran larval midgut it plays a role in the digest of proteins derived from the insect's diet (Wang et al., 2005). The proteins are mainly bound to microvillar membranes of midgut cells via a C-terminal glycosylphosphatidylinositol (GPI) anchor. Glycosylation was shown to be important for some Cry toxin-APN interactions. Carbohydrate structures including GalNAc are believed to be particularly important for some interactions between Cry1Ac and APN (Knight et al., 1994) and RNAi knock down of APN1 was shown to protect midgut cells from the toxic effect of Cry1Ac (Wei et al., 2016). Previous studies have reported binding of different Cry toxins to APNs of various insects. For example Cry1Aa, Cry1Ab, Cry1Ac were shown to bind to *M. sexta* and *H. virescens* APNs (Masson et al., 1995a, Luo et al., 1997), binding of Cry11Ba to *A. gambiae* APN was also observed (Zhang et al., 2008), Cry1Ba was shown to bind to *E. postvittana*

APN (Simpson and Newcomb, 2000) while binding of Cry1Ca to *S. litura* (Rajagopal et al., 2002b) and Cry1Fa binding to *H. virescens* APNs were reported (Banks et al., 2001).

- **Cadherins**

Cadherins belong to a family of calcium-dependent transmembrane glycoproteins playing a variety of functions including cell adhesion, migration, and morphogenesis (Angst et al., 2001). Midgut cadherins have been identified as receptors or putative receptors of *Bacillus thuringiensis* (*Bt*) Cry toxins in several orders of insects, including at least 7 Lepidoptera, 3 Coleoptera and 2 Diptera (Wu, 2014). The expression of cadherin has been shown to vary with larval developmental stage and its role was proposed to be to maintain midgut epithelial organization. Cadherins have been shown to be important receptors for Cry1A toxins, especially in some lepidopteran species where mutations in the cadherin gene have been linked to resistance to Cry1A toxins (Gahan et al., 2001). Different Cry toxins have been reported to bind to cadherins in various insects. For example Cry1Aa, Cry1Ab and Cry1Ac were shown to bind to *M. sexta* Bt-R1 cadherin (Hua et al., 2004), Cry11Aa bound to *A. aegypti* cadherin (Chen et al., 2009), binding of Cry3Ba to *T. castaneum* cadherin was reported (Contreras et al., 2013) and Cry4Ba was shown to bind to *A. gambiae* cadherin (Hua et al., 2008).

- **Alkaline phosphatases (ALPs)**

Alkaline phosphatases (ALPs) are GPI-anchored membrane glycoproteins and undergo glycosylation similarly to APNs. Different Cry toxins have been reported to bind to ALPs of various insects. For example Cry1Ac was shown to bind to *M. sexta* ALP (McNall and Adang, 2003), binding of Cry11Aa and Cry4Ba to *A. aegypti* ALPs was observed (Fernandez et al., 2006, Buzdin et al., 2002) and Cry11Ba was shown to bind to *A. gambiae* ALP (Hua et al., 2009).

- **ATP-binding cassette (ABC)**

The ABC transporters belong to one of the largest superfamilies of membrane proteins. Their common architecture comprises two nucleotide-binding domains (NBDs) and two transmembrane domains (TMDs), often with additional domains. The intracellular domain binds and hydrolyses ATP to transport (import/export) molecules across lipid bilayer membrane. There are eight major families, denoted by the letters A–H, which are classified based on sequence similarity in the conserved ATP binding domains. Members of ABCB and ABCC families have been implicated in cancer chemotherapy resistance (Theodoulou and Kerr, 2015). The interaction of Cry toxins with particularly the subfamilies C2 and A of the members of the ATP binding cassette (ABC) protein family has been previously described (Jurat-Fuentes and Crickmore, 2017). In fact, specific interaction between Cry1A toxin and ABCC2 was observed (Bretschneider et al., 2016). Alterations in these ABC proteins are linked with resistance against Cry1 (Heckel, 2012) and Cry2Ab toxins (Tay et al., 2015). For example ABCC2 transporter was linked to *B. mori* resistance to Cry1A toxins (Atsumi et al., 2012) . The exact role of these proteins is still unclear however it has been proposed that they may act as receptors.

Besides these membrane proteins, other components that were shown to be able to interact with Cry toxins such as glycolipids (Griffitts et al., 2005) or intracellular proteins, such as V-ATPase subunit A and actin have been identified (McNall and Adang, 2003, Krishnamoorthy et al., 2007).

The identification of Glycolipids as a class of putative Cry toxin receptor was demonstrated using the *Caenorhabditis elegans* strains resistant to Cry5Ba (Griffitts et al., 2005). Four genes named as *bre 2*, *bre 3*, *bre 4* and *bre 5* that could restore toxin susceptibility were identified. These resistance genes appeared to encode glycosyltransferases which synthesize a component that is important for the interaction between toxin and intestinal cells (Griffitts et al., 2003, Griffitts et al., 2001).

Two additional types of receptors were also identified: a 270-kDa anionic brush border membrane glycoconjugate isolated from *L. dispar* called BTR-270 and a 252-kDa protein

named as P252 which was isolated from *B. mori* brush border membranes. The first was shown to bind strongly to Cry1Aa, Cry1Ab, and Cry1Ba but displays a weaker affinity to Cry1Ac (Valaitis et al., 2001) while the second bound to Cry1Aa, Cry1Ab, and Cry1Ac under non denaturing conditions (Hossain et al., 2004).

In the case of parasporins, Beclin-1 a tumor suppressor protein was identified as a PS-1 receptor in HeLa cells (Katayama, 2011). In addition, glyceraldehyde-3-phosphate dehydrogenase (GAPDH) was identified as a binding protein on the plasma membrane of CEM-SS cells for parasporin-like protein *Bt18* (Krishnan et al., 2010).

The following table presents different Cry toxins and their correspondent putative/functional receptors.

Table 1: Different Cry toxins and their correspondent putative/functional receptors (see text for references)

Toxin	Putative/functional receptor(s)									
	APN	Cadherin	ALP	Glycolipid	ABCC2	Beclin-1	Actin	GAPDH	BTR-270	P252
Cry1Aa	✓	✓			✓				✓	✓
Cry1Ab	✓	✓			✓				✓	✓
Cry1Ac	✓	✓	✓		✓		✓		✓	✓
Cry1Ca	✓									
Cry1Ba	✓								✓	
Cry1Fa	✓									
Cry3Ba		✓								
Cry4Ba		✓	✓							
Cry5Ba				✓						
Cry11Aa		✓	✓							
Cry11Ba	✓		✓							
PS-1						✓				
Cry toxin from <i>Bt 18</i> strain								✓		

✓ Reported functional receptor where its presence was correlated with toxicity.

✓ Reported putative receptor where binding was observed.

1.7 Resistance mechanisms to Cry toxins

Insect pests are one of the major problems in agriculture. This problem has become significantly worrying since a dramatic increase in the number of resistant insects to insecticides has been observed. In fact, over 500 species evolved resistance to different

kinds of insecticides (Denholm et al., 2002). Since 1996 transgenic crops producing *Bt* toxins, known as *Bt* crops, have been grown worldwide. The use of this transgenic technology has been proven to reduce crop damage efficiently and helped to decrease the use of chemical insecticides (Kleter et al., 2007). However, the long term future of *Bt* crops applications is threatened by the development of resistance in insects. In order to counter this phenomenon, understanding how *Bt* toxins work, and how insects become resistant, are key factors for resistance management, therefore the resistance mechanisms have been studied. In theory, alteration in any step in the mechanism of action of Cry toxins could result in resistance. In fact potential resistance mechanisms were proposed for Cry1A toxins based on their mode of action (figure 27).

Cry1A toxin mode of action	Potential mechanisms of resistance
Solubilization of Cry protein to release protoxin	Incomplete solubilization
Proteolytic activation of protoxin	Deficient activation, differential processing, or toxin degradation by proteases
Primary toxin-receptor binding	Lack of/decreased toxin-receptor binding due to toxin immobilization, altered posttranslational processing of toxins and decreased affinity, modified receptors, or modulated gene expression
Cleavage of α -helix by host proteases	Lack of cleavage of α -helix (no reports to date for this mechanism)
Pre-pore oligomerization	Lack of pre-pore oligomerization due to toxin immobilization and/or sequestration
Secondary toxin-receptor binding	Lack of/decreased toxin-receptor binding due to toxin sequestration, altered posttranslational processing of toxins and decreased affinity), modified receptors (mutations/modulated gene expression/MAPK <i>trans</i> -regulation) or receptor shedding
Binding of oligomer to ABC transporter protein	Lack of binding due to modified protein
Membrane insertion	Lack of membrane insertion due to altered membrane components/properties
Pore formation	Lack of pore formation due to epithelial healing

Figure 27: Potential mechanisms of resistance of Cry1A toxins.

Alterations in any step of the mechanism of action of Cry1A toxins was considered as a potential factor that could induce resistance (Peterson et al., 2017).

However, the most frequently proposed mechanisms of Cry toxin-resistance involve defects in receptor binding (Ferré and Van Rie, 2002), altered activation of Cry toxins by midgut proteases (Sayyed et al., 2001) or elevated immune response (figure 28) (Ma et al., 2005a).

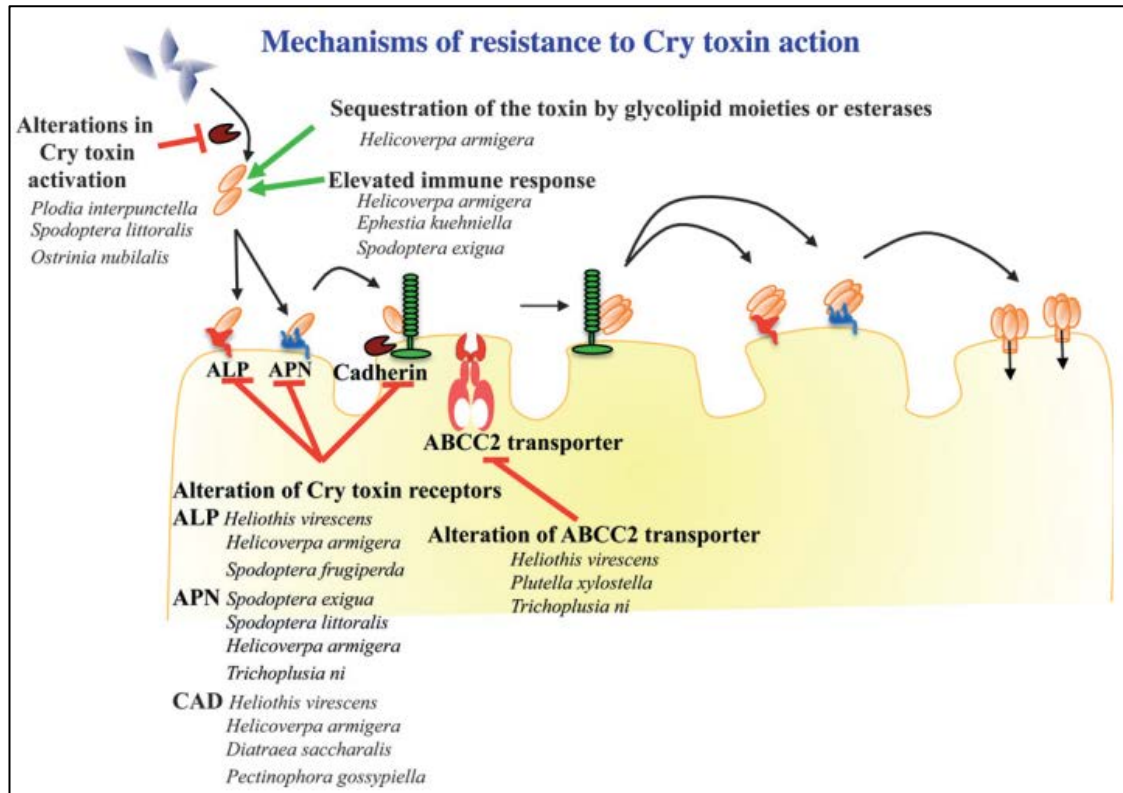


Figure 28: Schematic representation of the different mechanisms of resistance to Cry toxins described in lepidopteran insects (Pardo-Lopez et al., 2013).

The most common type of resistance was reported to involve changes in the binding of toxin to a putative midgut receptor (Heckel et al., 2007). In some lepidopteran pests such as *Plutella xylostella* and *Heliothis virescens* these characteristics were regularly observed. Resistance of *Plodia interpunctella* to Cry1Ab was also correlated with reduced binding of the toxin to larval brush border membrane vesicles (Van Rie et al., 1990). Moreover, reduced expression or mutation of Cry toxin receptors has been considered as a potential biomarker for resistance to diverse Cry proteins. *Trichoplusia ni* evolved resistance to Cry1Ac by differential alteration of two midgut aminopeptidases N (APN1 and APN6) (Tiewisiri and Wang, 2011). Additionally, alteration of the cadherin gene was correlated with resistance to *Bt* crops. For example, resistance of *Manduca*

sexta to Cry1Ab, *Heliothis virescens* to Cry1Ac and *Spodoptera exigua* to Cry1Ac and Cry2Aa were all associated with alterations in a cadherin gene (Soberon et al., 2007, Tabashnik, 2001, Qiu et al., 2015). In addition, mutations in the gene encoding ATP-binding cassette transporter gene (*ABCC2*) was associated with resistance. For example, a single amino acid mutation in *ABCC2* gene rendered *Bombyx mori* resistant to Cry1Ab (Atsumi et al., 2012). In *H. armigera* and *H. punctigera*, resistance to Cry2Ab was also conferred by mutations in ABC transporter gene (Coates and Siegfried, 2015, Tay et al., 2015).

Proteolytic activation of Cry toxins has been shown to be a crucial step in their mechanism of action. Impairment of this process was correlated with resistance. Resistance of *H. armigera* to Cry1Ac was associated with a mutation in the promoter region of one trypsin gene *HaTryR*. The insect adapted to Cry1Ac by decreasing the expression of this gene which, when knocked down in susceptible larvae fed on diets containing Cry1Ac, resulted in an increase in their survival (Liu et al., 2014). In *Plodia interpunctella*, resistance to Cry1Ac was shown to be linked to defects in midgut protease activities manifested by lack of a major BApNA-hydrolyzing enzyme (T1) that affected the activation of Cry1A protoxins (Oppert et al., 1997).

Since previous findings have shown the importance of carbohydrates in *Bt* toxicity, another resistance mechanism was proposed. This mechanism, manifested by the loss of a carbohydrate modifying enzyme (e.g. Bre 5), was considered dangerous and more serious than a mutation in a single receptor. In fact the loss of Bre 5 in *Caenorhabditis elegans* intestine resulted in resistance to Cry5B. Bre-5 mutants exhibited resistance to Cry14A which is lethal to nematodes and insects. Therefore the loss of such a particular modifier could affect the binding of various *Bt* toxins to several receptors which would result in a high level of resistance to a single toxin as well as cross-resistance to other *Bt* toxins (Griffitts et al., 2001).

Esterase sequestration and elevated immune response are other causes for developing resistance to *Bt* toxins. An *H. armigera* Cry1Ac-resistant strain showed increased production of gut esterase which bound and sequestered Cry1Ac toxin preventing the progress of the intoxication process (Gunning et al., 2005, Ma et al., 2005a). In addition, feeding a sub-lethal dose of Cry1Ac toxin to *Ephestia kuehniella* led to tolerance to

Cry1Ac toxin that correlated with an elevated immune response associated with the production of pro-coagulants such as hexamerin for *H. armigera* or lipophorin for *E. kuehniella*. (Rahman et al., 2004, Rahman et al., 2007, Ma et al., 2005b).

Transcriptomic analysis of resistant and susceptible larvae has served well in the characterisation of the resistance mechanism and this is why selection of resistant insects was considered as a tool to overcome this problem. For example, a resistant population of Asian corn borer to Cry1F was established through selection experiments under laboratory conditions. It was shown that the resistance trait to this toxin has autosomal inheritance which was due to more than one locus (Wang et al., 2016). In addition, a commercial formulation of Cry1Ac protoxin was incorporated in *Helicoverpa armigera*'s diet in order to establish a resistant strain that served well in finding that resistance to Cry1Ac was linked with a mutation in a gene encoding a transporter protein ABCC2 (Xiao et al., 2016).

It is worthwhile mentioning that the cross resistance to other *Bt* Cry toxin(s) has been observed in several insects resistant to a single Cry toxin. For example, a cross resistance study performed on diamondback moth (*Plutella xylostella*) showed that a Cry1C-resistant strain, obtained after selection with the toxin in the laboratory, had strong cross-resistance to Cry1Ab, Cry1Ac, and Cry1F but low to moderate cross-resistance to Cry1Aa and Cry9Ca (Liu et al., 2001). When selected with Cry1Ab, the insects showed marked (40-fold) cross-resistance to Cry1Ac, while selection with Cry1Ac resulted in little cross-resistance to Cry1Ab, Cry1Ca and Cry1Da (3-, 2- and 3-fold respectively compared with unselected population) (Sayyed Ali and Wright Denis, 2001).

Assessment of cross-resistance risks associated with combination of *Bt* proteins would contribute in improving control strategies, based on *Bt* crop carrying pyramided Cry proteins, for pests in the field.

1.8 Cellular response to PFT toxins

In general, the mode of action of PFTs consists of receptor recognition, activation by proteases, and formation of oligomeric-structures that, following insertion into the

membrane, form ionic pores. Additionally, as in the case of anthrax or diphtheria toxins produced by *Bacillus anthracis* and *Corynebacterium diphtheria* respectively, PFTs may have other effects during their interaction with their target cells such as intra-cellular signaling or transport of other enzymatic components (Parker and Feil, 2005).

Understanding the mechanism of action of PFTs as well as the host responses to toxin action is useful to counter existing/emerging pathogens and also to improve the action of toxins that may have biotechnological applications (Cancino-Rodezno et al., 2010b).

Following exposure to various biotic and abiotic stresses, eukaryotic cells have developed defense responses. Two general defense responses: the innate and the adaptive immune responses have been previously outlined. The innate immune system allows cells to have a quick and broad spectrum of responses. Macrophages and dendritic cells are innate immune cells that are able to eliminate pathogenic microorganisms via phagocytosis or expression of specific proteins such as cytokines and chemokines that contribute to pathogen elimination (Akira et al., 2006). When the innate host defense is overwhelmed, the induction of an adaptive immune response is required. The adaptive system which consists of B- and T-cells is mediated by antigen receptors located on lymphocytes and is able to develop a more comprehensive response that is memorized (Cancino-Rodezno et al., 2010b).

In response to PFTs, the host may trigger sophisticated mechanisms including adaptive or innate immunity responses as well as cellular non-immune defenses (Aroian and van der Goot, 2007). PFTs perturb the plasma membrane integrity affecting cytoplasmic ion composition, such as Ca^{2+} or K^{+} ions and also induce changes in osmotic pressure. Toxin-induced membrane permeabilization may activate pathways involved in either cell survival or cell death (Los et al., 2013).

Apoptosis is a programmed cell death process that is regulated and controlled. The apoptosis pathway involves a metabolic cascade started by initiator caspases (caspase-2, -8, -9 and -10) followed by activation of the effector caspases (caspase-3, -6 and -7) that will cleave a set of target proteins in order to produce the morphological (nuclear and cytoplasmic condensation and cellular fragmentation) and biochemical features associated with apoptosis (Fink and Cookson, 2005). On the other hand, cell death by

oncosis is characterized by cellular and organelle swelling, blebbing and increase in membrane permeability. Oncotic cell death may result from toxic agents that cause alterations in ATP generation, in cellular energy consumption or in intracellular Ca^{2+} levels (Trump and Berezsky, 1994).

Depending on the cell type and the dose of PFT used, cell death may be induced by either oncosis or apoptosis. In fact, when used at low concentrations some PFTs induce apoptosis, yet when high doses are used, cells die quickly by oncosis or necrosis. This is the case of *Clostridium prefringens* enterotoxin (CPE) which, when used at low concentrations, induces apoptotic cell death in mammalian Caco2 cells manifested by DNA fragmentation, chromatin condensation, mitochondrial membrane depolarization and activation of caspases-3 and -7. Yet, a high dose of CPE induces cell death by oncosis manifested by random DNA shearing (McClane and Chakrabarti, 2004). In addition, T-lymphoma cells undergo apoptosis when treated with a sub-nM concentrations of aerolysin however when high concentrations of the toxin are used, the cells die quickly and the apoptotic pathway was not triggered (Nelson et al., 1999).

Pyroptosis is another form of cell death which is dependent on caspase-1 and involves the secretion of the pro-inflammatory-cytokines such as IL-1 β and IL-18 (Fernandes-Alnemri et al., 2007). It was shown that treatment of macrophages with pneumolysin (PLY) induces the production of IL-1 α , IL-1 β and IL-18 following the formation of inflammasome complexes. This response was not produced following treatment with *S. pneumoniae* mutant that lacks the *ply* gene suggesting that PLY plays an important role in promoting cell death through pyroptosis (Shoma et al., 2008).

In regards to defense mechanisms evolved by eukaryotic cells to PFTs, the following are some examples. Previous studies have shown that the two mitogen-activated protein kinase (MAPK) pathways: p38 and c-Jun N-terminal kinase (JNK)-like were up-regulated in *Caenorhabditis elegans* in response to Cry5B toxin. Both of these MAPK pathways provided a significant cellular defense against the toxin and this defense was shown to be conserved in mammalian cells attacked by PFTs (Huffman et al., 2004). It was demonstrated that epithelial cells start an early immune response, involving activation of MAPK p38 pathway following exposure to low concentrations of several PFTs that are

able to initiate a proinflammatory response involved in defense to PFT and cell survival (Ratner et al., 2006a).

Phosphorylation of MAPK p38 protein was also shown to be correlated with the pore formation activity of these toxins. In fact, previous studies have shown that toxins where mutations are made in the regions essential for pore formation activity, were unable to induce the p38-response. In addition, the protective role of MAPK p38 pathway was previously observed in human epithelial cells (HaCaT). Following treatment of HaCaT cells with a low concentration (<10 ng/ml) of α -toxin, phosphorylation of MAPK p38 was activated. The pore formation activity of the toxin was correlated with activation of p38 since a pore formation mutant was unable to induce this activation. Additionally, inhibition of MAPK p38 with the specific SB203580- inhibitor was shown to inhibit the recovery process of cells (Husmann et al., 2006).

Moreover, the endoplasmic reticulum stress response to unfolded proteins (UPR) was shown to be induced in response to cellular stress stimulated by PFTs. This pathway increases phospholipid biogenesis to defend against the toxin and was previously shown to be implicated in the reestablishment of cellular homeostasis (Bravo et al., 2013). Activation of MAPK p38 in *C. elegans* treated with Cry5 or in HeLa cells treated with aerolysin was shown to induce the endoplasmic reticulum stress response to unfolded proteins. Loss of this pathway was demonstrated to cause hypersensitivity in *C. elegans* and HeLa cells to Cry5B and aerolysin respectively. It was then proposed that cells have adapted the UPR pathway to promote cellular defense to PFTs (Bischof et al., 2008).

Ion movements have also been shown to contribute to cell survival. Potassium efflux, a consequence of the pore formation activity of PFT, was shown to induce caspase-1 which activates sterol regulatory element-binding proteins (SREBPs) that are involved in membrane lipid biogenesis promoting cellular survival (Gurcel et al., 2006). Pore formation induced by PFTs also results in Ca^{2+} influx. GAS SLO-induced calcium influx was shown to trigger the exocytosis of lysosomes and extracellular release of the lysosomal enzyme acid sphingomyelinase. The latter was found to subsequently induce endocytosis, which contributed to membrane repair (Idone et al., 2008).

Other cell-survival responses to PFTs have been outlined. In fact, epithelial cells were shown to respond to PFT treatment by the activation of central regulators involved in membrane biogenesis (Gurcel et al., 2006). Endocytic mechanisms were also implicated in cell repair. In the case of PFTs that induce Ca^{2+} influx such as SLO, the lesion could be repaired in kidney and HeLa cells by a process that involves endocytosis to remove the SLO containing pores from the plasma membrane (Idone et al., 2008). Another survival mechanism, autophagy, was mentioned since it may restrict the infection by sequestering the pathogens and further degradation in lysosomes (Deretic, 2006). In fact, a PFT called *Vibrio cholerae cytotoxin* (VCC) was shown to modulate autophagy in Caco2 cells and inhibition of this cellular defense pathway resulted in decreased survival of Caco2 cells upon treatment with the toxin (Gabriel Gutierrez et al., 2007). Figure 29 summarizes the mentioned cell responses to PFTs which lead to either cell death or recovery.

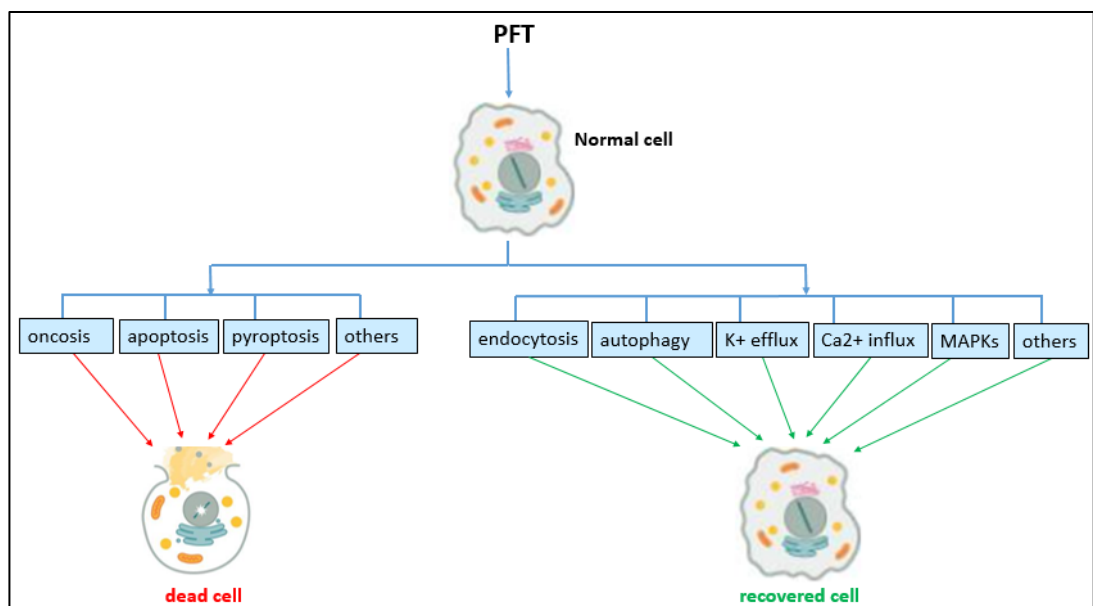


Figure 29: Examples of different cell responses/pathways leading to cell death or survival following PFT attack. Schematic representation of healthy and dead cells were taken from Fink and Cookson (Fink and Cookson, 2005).

Additionally, a new family of proteins named REPAT (response to pathogen) was identified following intoxication of *Spodoptera exigua* with either *Bt* Cry1Ca toxin or baculovirus. The 18 kDa glycosylated proteins were shown to be specifically expressed

in the insect gut and were suggested to play a role in a defensive response to the infection of *S. exigua*. This was revealed by a delay in the progression of the infection in larvae intoxicated with a recombinant baculovirus expressing the REPAT1 protein (Herrero et al., 2007). Moreover, these proteins have been shown to be constitutively up-regulated in a *Bt*-resistant *S. exigua* (Hernández-Martínez et al., 2010).

Arylphorin from the hexamerins gene family have also been associated with midgut response to *Bt* intoxication. Due to its mitogen activity as well as its role in cell proliferation and regeneration, these genes were suggested to be involved in the immune response (Hakim et al., 2009). Arylphorin was shown to be upregulated in *S. exigua* treated with *Bt* toxins as well as in the *Bt*-resistant strain (Hernández-Martínez et al., 2010). It has been proposed that REPAT genes, as transcriptional regulators, (Hernández-Rodríguez et al., 2008) may participate in arylphorin expression (Castagnola and Jurat-Fuentes, 2016).

Another aspect in the defensive response produced by insects intoxicated with *Bt* Cry toxins was reported: the regeneration of the epithelium by replacing diseased with newly differentiated midgut cells. An enhanced gut regenerative response that is proposed to be controlled by increased production of mitogenic factors, was suggested to play an important role in the resistance of *H. virescens* to several Cry toxins (Castagnola and Jurat-Fuentes, 2016).

1.8.1 Use of cell lines to study the mode of action of *Bt*: examples of cell responses to Cry toxins

Cell lines have been extensively used for the study of the mode of action of different pore forming toxins produced by different bacterial species. In case of *Bt* toxins, in order to understand the mechanism of action of 3-domain Cry toxins, experiments carried out with brush border membranes (BBM) isolated from midgut of various insects have been very useful (Pardo-Lopez et al., 2013). Several other studies performed in established insect cells as well as mammalian cell lines have helped to understand the mechanism

of action of different *Bt* toxins. The fact that these cells are simple, have a low cost/benefit ratio, reproducible and could be used for high throughput screening, they have proven to be reliable models (Smagghe, 2007).

Functional studies have been performed on some insect cell lines that are naturally susceptible to certain 3d-Cry toxins (table 2).

Table2: Different cell lines used to study the mode of action of *Bt* Cry toxins.

Cell line	Origin	Susceptibility	References
Sf21	primary explants of <i>Spodoptera frugiperda</i> pupal tissue	Cry1Ab, Cry1C	(Vaughn et al., 1977, Johnson, 1994, Teixeira Correa et al., 2012)
Sf9	derived from sf21 cells	Cry1C	(Summers and Smith, 1987, Kwa et al., 1998)
TnH5	Ovarian cells of <i>Trichoplusia ni</i>	Cry1Ac	(Wickham et al., 1992, Liu et al., 2004)
CF1	<i>Choristoneura fumiferana</i> neonate larvae	Cry1Ab, Cry1Ac and Cry1C	(Gringorten et al., 1999, Thomas and Ellar, 1983a)
C6/36	<i>Aedes albopictus</i> larvae	Cry11 and Cry4Aa	(Igarashi, 1978, Teixeira Correa et al., 2012)

Amongst the cell lines mentioned above Sf9, Sf21, TnH5 and C6/36 as well as certain mammalian cell lines have been used as recipients for transformation with different Cry toxin-binding proteins to study their role as receptors in the mode of action of Cry toxins. Mammalian cell lines were also used to study the anticancer activity of parasporins (Soberón et al., 2018).

Correlations between findings on the interaction of insect cell lines and Cry toxins and that of insects and Cry toxins have been observed. For example, Cry1C which was toxic towards sf9 cells (EC_{50} of 0.2 $\mu\text{g/ml}$) was shown to bind to a protein of 40kDa (Kwa et al., 1998, Sakai et al., 2007). The interaction between these cells and the toxin proved the importance of lipid rafts for Cry1C toxicity (Avisar et al., 2005), this is consistent with previous findings demonstrating binding of several 3-domain Cry toxins to receptors such as ALP and APN which are localized in lipid rafts of insects (Zhuang et al., 2002). In addition, previous study showed that the cytotoxic effects of different Cry1Ab mutants was similar in *Manduca sexta* and CF1 cells (Portugal et al., 2014).

Morphological changes were observed upon treatment of susceptible cell lines to Cry toxins. For instance, upon treatment with Cry1Ab (0.6 $\mu\text{g/ml}$), transformed COS-7 and HEK-293 cells with the cadherin protein from *M. sexta* (MsCAD) presented dramatic morphological changes followed by death (Dorsch et al., 2002). In addition, at a concentration of 187 nM, Cry4Ba induced membrane blebbing, cell swelling and lysis in the TnH5 cells transfected with cadherin gene from *Anopheles gambiae* (AgCAD) (Ibrahim et al., 2013). Sf21 transformed with APN1 from *H. armigera* (HaAPN) became susceptible to Cry1Ac showing aberrant morphology, swelling and lysis (Sivakumar et al., 2007). In the case of cancer cell lines, HepG2 cells showed morphological alterations including cell blebbing, alterations in the cytoskeleton and mitochondrial and endoplasmic reticulum fragmentation in response to PS-2 (0.1 $\mu\text{g/ml}$) (Kitada et al., 2006). Intoxication of MOLT-4 cells with PS-4 (2 $\mu\text{g/ml}$) toxin resulted in blebbing, nuclear shrinkage and formation of ballooned shaped cells (Okumura et al., 2011).

The pore forming activity of certain Cry toxins in several cell lines was observed through the study of ion movements. Cry1C was shown to induce efflux/influx of Na^+ , H^+ and K^+ and membrane depolarization in Sf9 cells (Guihard et al., 2000, Vachon et al., 1995) suggesting that Cry toxins open non-specific pores in the target membranes,

alternatively this could also be explained by the fact that Cry toxins affect existing channels in the cells (Soberón et al., 2018). Moreover, Cry1Ac and Cry1Ab toxins increased CF1 membrane permeability to Ca^{2+} and K^+ (Potvin et al., 1998, Portugal et al., 2017). These findings suggest that different toxins could form similar pores in CF1 cells (Soberón et al., 2018). The swelling induced in transfected sf9 cells with cadherin from *B. mori* following Cry1Aa intoxication was correlated with disturbances in the osmoregulation of the cells manifested by opening of ion currents. On the other hand cells transfected with a BmCAD that has a mutation in the CR9-region did not bind Cry1Aa and did not show ion channel responses supporting the role of BmCAD and its CR9 region in the pore formation activity of Cry1Aa toxin (Yasunori et al., 1999). In addition, studying the interaction between PS-3 and HepG2 cells proposed that this toxin acts as pore forming toxin resulting in ATP depletion, cell swelling and membrane damage (Krishnan et al., 2017). The initial response of MOLT-4 to PS-2 is a fast depolarization of the membrane. Additionally, the efflux of cytoplasmic lactate dehydrogenase (LDH) and the influx of propidium iodide (PI) have supported the pore formation activity of the toxin (Kitada et al., 2006). PS-4 was proposed to form pores in the plasma membrane of susceptible cells since it induces the leakage of lactate dehydrogenase and influx of extracellular FITC-dextran (Okumura et al., 2011).

In relation to the intracellular responses, It was also reported that depending on the time of the exposure to the toxin from *Bt* AA1-9 strain, apoptosis or necrosis are induced in midgut cells isolated from *H. virescens* (Loeb et al., 2000). Previous studies have shown that following treatment with Cry1Ab and Cry1Ac, CF1 cells developed a defense response involving phosphorylation of MAPK p38 (Portugal et al., 2017). On the other hand studies performed on mosquitoes have shown that a programmed cell death associated with apoptosis was induced in the gastric caeca cells as well as in the midgut cells from *Culex pipiens* larvae upon intoxication with Cry toxins produced by *Bt* subsp. *israelensis* (Smouse and Nishiura, 1997). Moreover, it was shown that upon treatment of CF1 with Cry1Ab and Cry1Ac, the intracellular signal transduction cascade of Protein kinase A/Adenylate cyclase (PKA/AC) was not activated. Yet, this pathway was proposed to trigger cell death in a TnH5 cell line transfected with CAD receptor from *M. sexta* (MsCAD) (Zhang et al., 2006). Zhang et al showed that binding of Cry1Ab to MsCAD

stimulates a G-protein that activates adenylate cyclase activity resulting in increased levels of intracellular cAMP that in turn activates a PKA. Activation of PKA induces membrane blebbing, ghost nuclei, cell swelling and lysis (Zhang et al., 2006). In contrast to the Zhang et al findings in 2006, Cry1Ab and Cry1Ac toxins were shown to be unable to activate the intracellular signal transduction cascade of Protein kinase A/Adenylate cyclase (PKA/AC) in CF1 cells and that cell death was triggered through an apoptotic pathway. Inhibition of apoptosis resulted in lower mortality of these cells when intoxicated with the EC₅₀ concentration of Cry1A toxins (Portugal et al., 2017). In the case of anticancer Cry toxins, the proposed mechanism of action of PS-1 includes apoptosis. Inhibitors of apoptosis was shown to block the cytotoxic activity of PS-1 against HeLa cells (Katayama et al., 2007). In addition, it was also reported that the death response induced by PS-2 toxin involves activation of apoptosis in prostate cancer cells PC-3 (Brasseur et al., 2015a). Therefore apoptosis can be activated in both conditions (death and defense responses).

2 Aims and objectives

This research study aims to better understand the mechanism of action of Cry41Aa. Different aspects in the mode of action of the protein are going to be investigated:

- The activation mechanism of the toxin is going to be studied through creation of various mutations at the N-terminal or C-terminal region of the protein as well as the use of N-terminal sequencing.
- The effect of differential proteolysis of Cry41Aa on toxicity is going to be assessed in both HepG2 and HL-60 cell lines.
- A resistance to the toxin is going to be evolved in susceptible HepG2; morphological, physiological and genetic characteristics of the established resistant cell line are going to be compared with the susceptible line. An understanding of which genes are involved in resistance may help us understand how this toxin targets human cancer cells.
- Involvement of certain intracellular signalling pathways are going to be investigated in order to understand cell responses to the toxin.

3 Materials and methods

3.1 Materials

- **Bacterial strains**

E. coli DH5 α : was used for routine cloning applications.

E. coli GM2163: this strain is deficient in both *dam* and *dcm* genes. It was used to obtain unmethylated DNA and therefore to facilitate the transformation of *B. thuringiensis*.

Bt 4D7: a crystal minus derivative of *Bacillus thuringiensis* subspecies *kurstaki*. It was obtained from *Bacillus* Genetic Stock Center, Department of Biochemistry, Ohio State University.

- **Plasmids**

pSVP2741Aa (10392 bp): this is an *E. coli* - *B. thuringiensis* shuttle vector with the promoter from the *cyt1A* toxin gene of *B. thuringiensis* subsp. *israelensis* upstream of the cloned ORF2 and ORF3 of *cry41Aa* operon (Krishnan et al., 2017). This plasmid contains both *E. coli* and *Bt* origin of replication and ampicillin and chloramphenicol antibiotic resistance genes.

pSVP2741Aa Δ R (9984 bp): same characteristics as for SVP2741Aa except that *cry41Aa* gene is missing the region coding for the ricin domain.

pSVP2741Aa Δ R-HA (10011 bp): same characteristics as for pSVP2741Aa Δ R but with a C-terminal HA tag sequence introduced (Etherington et al., unpublished).

- **Buffers/solutions and their compositions**

Table 3: Different buffers/solutions used

Name	Composition
TBE (5x)	108 g of tris, 55 g of boric acid, 40 ml of 0.5 M EDTA, 2 l of dH ₂ O, pH 8.0.
RGB	18.18 g tris, 0.4 g SDS, 100 ml of dH ₂ O, pH 8.8.
SGB	6.06 g tris, 0.4 g SDS, 100 ml of dH ₂ O, pH 6.8
Protein gel sample loading buffer (2x)	2 g SDS, 6 mg EDTA, 20 mg Bromophenol Blue, 5 ml of RGB, 50 ml glycerol, 100 ml of dH ₂ O.
SDS running buffer (10x)	7.6g tris-HCl, 36g glycine, 2.5g SDS, 250 ml of dH ₂ O
Coomassie Blue	methanol, dH ₂ O, acetic acid (10:9:1 v/v/v), Brilliant Blue R-250 (0.25%, w/v)
Destain	methanol, dH ₂ O, acetic acid (10:9:1, v/v/v).
PBS (10x)	80 g of 1.37 M NaCl, 2 g of 27 mM KCl, 14.4 g of 100 mM Na ₂ HPO ₄ , 2.4 g of 18 mM KH ₂ PO ₄ , 1 l of dH ₂ O, pH 7.4
CAPS (10mM)	2.21g CAPS, 1l dH ₂ O pH10.5
CAPS (10mM)+ NaCl (1M)	2.21g CAPS, 1M NaCl, 1l dH ₂ O pH10.5
NP-40	150 mM NaCl, 1.0% NP-40 or Triton X-100, 50 mM tris, pH 8.0.
RIPA	150 mM NaCl, 1.0% NP-40 or Triton X-100, 0.5% sodium deoxycholate, 0.1% SDS, 50 mM tris, pH 8.0.
Dry blot	39 M glycine, 48 mM tris, 0.0375% SDS, 20% methanol.
Tris-HCL	20 mM Tris HCl, dH ₂ O pH 7.5
ECL solution	10 ml of 100 mM tris pH 8.5, 3 µl of H ₂ O ₂ , 25 µl of 14.7 mg/ml p-coumaric acid, 50 µl of 88.6 mg/ml luminol.

- **Reagents, enzymes and DNA/RNA kits**

Reagents obtained from Sigma-Aldrich: β -mercaptoethanol, Bromophenol Blue, Brilliant Blue R-250, ammonium persulfate, TEMED, acrylamide/bis-acrylamide 30%, SDS, tris base, tris-HCl, CAPS, sodium carbonate, hydrogen peroxide, DMSO, chloramphenicol, etoposide, 5-Fluorouracil, S-methylmethanethiosulfonate (MMTS), EGTA, p-coumaric acid, luminol, sodium orthovanadate, sodium arsenite, proteinase K, lysozyme, formaldehyde solution, RNase ZAP, ethanol absolute for molecular biology.

Reagents obtained from Biotum: GelRed nucleic acid gel stain.

Reagents obtained from Fluka Analytical: EGTA.

Reagents/kits obtained from QIAGEN: Gene solution siRNA, hyperfect, RNeasy Plus Mini kit, QIAshredder, QIA prep Spin Mini prep kit.

Reagents obtained from Melford: trypsin, agarose low EEO, MOPS, ampicillin

Reagents obtained from AnalaR BDH: glucose, NaCl, NaOH, Ponceau S, NP-40, TX-100, EDTA, ethanol, sodium hydrogen carbonate.

Reagents obtained from Fisher Scientific: Acetic Acid Glacial

Chemicals/kits obtained from Thermo Fisher Scientific: glycine, methanol, 1-butanol, phosphate, acetic acid, trypsin (MS-grade), HRV 3C Protease, RNase inhibitor, High Capacity cDNA Reverse Transcription kit, Power Syber Green PCR master Mix, glycerol, glycine.

Chemicals obtained from New England Biolabs: Pre-stained Protein Ladder (7-175, 11-245 and 10-230 kDa), 1 Kb DNA ladder, *DpnI*, T4 DNA ligase

Chemicals obtained from Tocris: BSA, PKi (14-22 amide, myristoylated), 8-bromo-cAMP

Chemicals obtained from Calbiochem: Microcystin

Chemicals obtained from Promega: *HaeIII*, buffer C

- **Antibodies**

- Rabbit polyclonal antibodies against phosphorylated and total ERK (Cell Signaling Technology (9215S, 9102 respectively)).
- Rabbit polyclonal antibodies against total p38 (Cell Signaling Technology (9101S)).
- Rabbit monoclonal antibody against phosphorylated p38 (Thr180+Tyr182) (Thermo Fisher Scientific (MA5 15182)).
- Rabbit monoclonal against CD59 (abcam (ab126777)).
- Chicken polyclonal anti-HA tag HRP (abcam (ab1190)).
- Rabbit monoclonal anti-CREB phospho S133 (abcam (ab32096)).
- Human polyclonal anti-AQP9 (Thermo Fisher scientific) (PA5-51285).
- Secondary HRP conjugated goat anti-rabbit antibody (abcam (ab97051)).

- **Cell lines**

- HepG2: human hepatocyte carcinoma cell line was purchased from ECACC, Salisbury, UK.
- HepG2R: a Cry41Aa resistant subline of HepG2 developed in the lab.
- HepG2 Rev: a reverted line from HepG2R.
- HeLa: cervical carcinoma cells that were a gift from Dr George Giamas (University of Sussex, UK).
- HL-60: human promyelocytic leukemia cell line that was purchased from ECACC, Salisbury, UK.

- **Culture media, reagents and plasticware**

DMEM, RPMI 1640, OPT-MEM, PSG, DPBS, trypsin/EDTA (0.05% trypsin and 0.53 mM EDTA) and Trypan Blue (0.4%) were obtained from Gibco (Life Technologies).

FCS, 40 µm Nylon Mesh Cell Strainer and Nalgene 2.0 mL cryogenic vials were obtained from Fisher Scientific.

25, 75 and 175 cm² flasks; 60 mm dishes; 6, 12, 24 and 96-well clear and black-walled clear flat bottom plates were obtained from Nunc.

- **Cell assay kits**

- CellTiter-Blue Cell Viability Assay (Promega).
- CellTiter-Glo Luminescent Cell Viability Assay (Promega).

3.2 Methods

- **Polymerase chain reaction (PCR)**

PCR reactions were performed in order to create the desired mutations. The program of PCR was called PFU ULTRA 10 kb and was set as follows:

Table 4: Different settings of PCR program.

Type of reaction	Number of cycles	Temperature(°C)	Duration
Initial denaturation	1	98	2 minutes
Denaturation	30	92	40 seconds
Primer annealing	30	55	8 minutes
Extension	30	68	5.3 minutes
Final extension	1	68	5 minutes

For the reaction the volumes used were: 1 μ l of 100 pmol/ μ l of each primer (obtained from Eurofins Genomics), 25 μ l of high fidelity PFU Ultra II Hotstart 2 x master mix (Agilent technologies), 1 μ l of template DNA and 22 μ l of sterile distilled water.

The list of templates and primers used in the mutagenesis experiments is as follows:

Table 5: List of mutants created and their correspondent primers and template used.

Mutant created	Template	Forward and reverse primers (5' \longrightarrow 3')
FL Δ 23	SVP2741Aa	FP: TATCCTTTTGCGCAGGCAC RP: CATTGACAATCCTCCATTCCA
Δ R Δ 23	SVP2741Aa Δ R	Same as for FL Δ 23
FL Δ 40	SVP2741Aa	FP: GAGTGGATGAATATGTGTACTAGTGG RP: CATTGACAATCCTCCATTCC
Δ R Δ 40	SVP2741Aa Δ R	Same as for FL Δ 40
FL Δ 60	SVP2741Aa	FP: GATGTAAGGGATGCCGTTATTAC RP: CATTGACAATCCTCCATTCCA
FLP60	SVP2741Aa	FP: TTTCAGGGTCCAGTTATTACAAGTATAAAT ATC RP: AAGTACTTCTAATCCCTCCCCCAGGAC
FLP40	SVP2741Aa	FP: TTTCAAGGTCCTATGAATATGTGTACTAGT GG RP: AAGTACTTCAAGTAGTTCAGAACCTGGTG C
Δ RP40	SVP2741Aa Δ R	Same as for FLP40

Δ R-HAP40	SVP2741Aa Δ R-HA	Same as for FLP40
FL-HA	SVP2741Aa	FP: TTCCAGATTATGCTTAAAGGTGTGCAACTA TCCCTG RP: CATCATATGGATAAGTGGTTAAGCCAATACC CATAC
AK	SVP2741Aa	FP: AAAGATGTAAGGGATGCCGTTATTAC RP: GCTGTATCCCTCCCCCAG
RA, TD and TA	Δ R-HAP40	FP: ASGGMTGCCGTTATTACAAGTATAAATATC G RP: TACATCTGCGCTGTATCCCTCC

- **Agarose Gel Electrophoresis**

In this study 1% agarose concentration was used: 0.3 g of Agarose Low EEO was added to 30 ml of 1x TBE (Tris-Borate-EDTA) and heated until completely dissolved. The mixture was allowed to cool then 1.5 μ l of a 1 in 3 dilution of Gel Red was added before pouring the solution onto a gel casting tray. The gel was allowed to cast, then 5 μ l of purified product was added to 1 μ l of loading buffer and a total of 6 μ l of each sample was loaded onto gel.

1 Kb ladder (New England Biolabs) was used as a marker depending on the desired fragment size. The gels were run at 120 Volt in 1x TBE buffer in electrophoresis chamber then the bands of amplified products were visualised under ultraviolet light and in some instances excised from the gel for further use and analysis.

- ***DpnI* digestion**

DpnI enzyme was used in this study to digest methylated template DNA: 1 μ l of *DpnI* was added to 45 μ l of PCR product and the mixture was incubated for 1 hour at 37°C prior to purification.

- **Purification of PCR Products (column purification)**

QIAquick PCR Purification Kit (QIAGEN) was used in order to separate the PCR products from the other components present in the mixture.

To 1x volume of PCR product, 5x volumes of chaotropic buffer PB were added and mixed. The sample was then added to a spin column, placed in 2 ml collection tube, and centrifuged for 1 minute at 13000 rpm. The flow through was discarded and 750 μ l of PE buffer was then added to the column and spun for 1 minute at 13000 rpm. The flow through was again discarded and the spin column was further centrifuged for 1 minute in order to remove any traces of buffer.

The column was placed in a new 1.5 ml eppendorf tube and 30 μ l of EB buffer (10 mM Tris-Cl, pH 8.5) was added, allowed to stand for 1 minute, then the column was centrifuged for 1 minute for elution of the DNA.

- **Gel purification using Qiaprep kit**

The bands representing the amplicon(s) were excised from the gel and placed into separate tubes. To each tube, 600 μ l of QG buffer was added and placed in 55°C water bath for approximately 10 minutes until the gel slices were completely dissolved. The contents were then transferred into spin columns placed in 2 ml collection tubes. The samples were centrifuged for 1 minute at 13000 rpm (all centrifugation of samples were

carried out at 13000 rpm) and the flow through was discarded. 600 µl of QG buffer was then added and spun for 1 minute. The flow through was discarded, 750 µl of PE buffer was added to each sample and columns were centrifuged for 1 minute. The flow through was again discarded and columns were spun for an additional 1 minute.

The spin columns were then placed in clean 1.5 ml microcentrifuge tubes. To elute the DNA, 30 µl of EB buffer was added, allowed to stand for 1 minute then spun for 1 minute for the recovery of the product.

- **DNA ligation**

In order to self-ligate the purified PCR products, 0.5 µl of T4 DNA ligase and 1 µl of its corresponding buffer were added to 8.5 µl of the DNA of interest. The mixture was incubated over night at room temperature then stored at -20°C for future use.

- **Bacterial transformation by electroporation**

100 ml of broth solution containing a bacterial strain (GM2163, DH5α or 4D7), scraped from agar plate, was incubated in the shaker for approximately 2 hours until the optical density (OD₆₀₀) of the cells reached 0.4-0.8.

The mixture was then transferred into a sterile centrifuge bottle which was spun at 10000 rpm for 10 min at 4°C. The broth was discarded, 100 ml of cold water was added to the resultant pellet and the tube was again centrifuged for additional 10 minutes at 10000 rpm. The supernatant was discarded and the pellet was re-suspended in 1ml of cold distilled water. The cells were transferred into eppendorf tube and spun for 1 minute at 13000 rpm. The water was again discarded and 200 µl of cold water was added and mixed with the pellet. 50 µl of competent cells were mixed with 1-2 µl of DNA, then transferred into cooled electroporation cuvette which were then placed in Gene Pulser II machine (Bio-Rad) set to 1.8 KV, 200 Ohms, 25 µF. Following transformation, a sterile

Pasteur pipette was used to wash out cuvette with 500 µl of LB broth then to transfer the mixture into a sterile bottle that was incubated for 1 hour at 37°C before being plated onto LB agar plates containing the appropriate antibiotic. The plates were finally incubated overnight at 37°C to obtain the colonies with the desired DNA.

- **Bacterial growth conditions**

E.coli DH5α and GM2163 transformants were grown at 37°C over night on LB (Luria-Bertani) agar plates containing ampicillin (100 µg/ml) whereas *Bt* transformants were grown on nutrient LB agar plates supplemented with chloramphenicol (5 µg/ml). For harvesting of the toxin proteins, *Bt* transformants were grown for 3-4 days at 30°C.

- **Extraction of DNA from *E.coli* transformants using QIAprep Spin Miniprep Kit**

Scraped from agar plates, the bacterial cells were re-suspended in 250 µl of P1 buffer and thoroughly mixed in a microcentrifuge tube. 250 µl of P2 buffer was then added to lyse the cells and the mixture was inverted 6 times for proper mixing. Next, 350 µl of neutralising buffer N3 was added and the mixture was again inverted 6 times before centrifugation for 10 minutes at 13000 rpm. The resultant supernatant was then transferred to a QIAprep spin column which was centrifuged for 30 seconds at 13000 rpm. The flow through was discarded and 500 µl of PB buffer was added to the sample which was then spun for additional 60 seconds. The flow through was discarded and 750 µl of PE buffer was added. The column was spun first for 30 seconds, the flow through was again discarded and the column was further re-spun for 1 minute in order to remove any traces of buffer. The column was later placed in a clean 1.5 ml microcentrifuge tube and 30-50 µl of Elution Buffer was added. The sample was allowed to rest for 1 minute then centrifuged for 1 minute at 13000 rpm and the eluted DNA was finally collected.

- **Extraction of DNA from *Bt* transformants**

Transformed *Bt* cells were scraped off a chloramphenicol supplemented plate and resuspended in 250 µl of buffer P1 containing 10 mg/ml lysozyme. The mixture was then incubated at 37°C for 1 hour in order to enhance the lysis of the cell wall. The rest of the protocol was carried out using the same methodology as for the extraction of DNA from *E.coli* cells (described above).

- **Verification of inserts**

Initially, restriction digestion using *HaeIII* enzyme was performed on the plasmids thus extracted to verify the integration of the correct insert. 2 µl of plasmid DNA were digested by adding 0.5 µl of *HaeIII*, 1 µl of corresponding buffer and 6.5 µl of sterile distilled water to make up a total volume of 10 µl. The reaction mix was incubated at 37°C for 30 min then run on a 1% agarose gel for comparison with the predicted banding profile produced by NEBcutter software.

Final confirmation was carried out using DNA sequencing carried out by Eurofins Genomics.

- **Protein harvesting**

Bt transformants were grown in LB agar plates containing chloramphenicol (5 µg/ml) for 3 days at 30°C. Sporulation and production of crystals were monitored using a phase contrast microscope. The sporulated cells were scraped off the plate and added to 30 ml of sterile cold water. The cells were then sonicated for 4 minutes (1 minute on 1 minute off) then centrifuged at 10000 rpm for 10 minutes at 4°C. The supernatant was discarded, 30 ml of fresh cold water was again added and the mixture was further sonicated then centrifuged for 10 minutes at 10000 rpm. The pellet obtained was re-suspended in 1 ml of distilled water. The spore/crystal mixture was later stored at -20°C until use.

- **Solubilisation and activation of crystal protein**

Crystal proteins were solubilised in 50mM sodium carbonate at pH 10.5 in the presence of 5 mM Dithiothreitol (DTT) at 37°C for 1 hour. The mixture was then spun for 1-5 minutes at 13000 rpm. The supernatant was collected and treated with the appropriate protease. Following addition of trypsin (1 mg/ml final concentration) or proteinase K (0.01 mg/ml final concentration) the mixture was incubated at 37°C for 1 hour while for activation with PreScission protease (130 µg/ml), the sample was incubated at 4°C for 16 hours. Complete mini EDTA-free protease inhibitor was finally added to the activated samples to stop further proteolysis.

- **Protein dialysis**

Prior to the purification process, the samples were dialysed against 1 litre of 10 mM CAPS (pH 10.5) using 12 kDa MWCO Dialysis Tubing Cellulose Membrane (D9777-100FT Sigma). After purification of the proteins of interest, the pooled fractions were dialysed against 1 litre of PBS (pH 7.4). In both cases, the dialysis process occurred over night at 4°C using a magnetic stirrer.

- **Protein purification**

In all the cytotoxicity assays carried out in this study, toxins used were ÄKTA purified except for ΔR-HAP40.

Successful purification was achieved with a 1 ml Resource Q column (strong anion exchange, GE Healthcare Life Sciences) connected to an ÄKTA Purifier-FPLC System. All the buffers and toxin samples utilized in this procedure were filtered using 0.22 µm Millex-GP filters (Millipore) prior to use. Sample was injected in 10 mM CAPS (pH 10.5)

and linear increase in the gradient of NaCl (0 to 1 M) was applied at a flow rate of 1 ml/min for 25 min. 0.8 fractions were collected then analysed by SDS-PAGE.

A gel filtration method was also used in this study using Sephacryl S-200 High Resolution (Amersham) resin. Around 0.5 ml of the protease treated toxin was applied to a column filled with 15 ml of resin which was initially washed with ethanol and equilibrated with PBS buffer (pH 7.4). Collected fractions (50 μ l) that were eluted with around 10 ml of buffer, were analysed using SDS-PAGE.

- **Protein analysis by SDS-PAGE**

Based on the size(s) of the protein(s) in question, 7.5% and 12% gels were used in this study. Initially samples were mixed 1:1 with sample loading buffer in the presence of β -mercaptoethanol (5%), boiled for 3-10 min then spun for 30 s. The supernatant of each sample was loaded on to a gel which is composed of two parts (stacking and resolving). Electrophoresis was carried out at 200 V for 35 min in MiniPROTEAN® II Electrophoresis Cell (Bio-Rad) using tris-glycine running buffer. Gels were later stained with Coomassie Blue for 20 min then de-stained until clear visualisation of the bands of interest. The fragment sizes were estimated using a protein ladder (New England BioLabs).

- **Protein concentration**

Following protein purification and SDS-PAGE analysis, the fractions containing the purified fragment(s) were pooled together and concentrated using Vivaspin500 or Vivaspin6 columns (GE Healthcare).

The concentrations of *Bt* crystal proteins were determined by densitometry using different dilutions of bovine serum albumin (BSA) as protein standard which are run alongside the protein of interest on SDS-PAGE gel then examined using the Image J program.

However for determination of the concentration of the proteins present in cell extracts used in western blot and ligand blot experiments, Bradford method was applied using a Bio-Rad Protein Assay Kit (Bio-Rad) with BSA used as the standard. The concentration of each sample was determined by comparing its absorbance against a BSA standard curve.

- **Preparation of the protein for N-terminal sequencing**

- **Using gel slices**

All buffers, detergents and proteases were freshly made. Cry41Aa was initially solubilised then activated with trypsin (Promega) as described previously. The resultant protein was then concentrated by the use of Vivaspin 500, 10 KDa MWCO tube. The tube was first pre-rinsed by adding 500 µl of 50mM of Na₂CO₃ and spun for 10 minutes at 15000 rpm in order to get rid of traces of glycerine and sodium azide present in the membrane. The concentrator was then filled with the sample and placed in the centrifuge to be spun for around 2 hours at 15000 rpm to obtain 100 µl of concentrated sample.

The sample was next mixed with loading buffer and either incubated for 30 minutes at 65°C or boiled for 3-5 minutes before loading on 7.5% protein gel which was later stained then destained until clear visualisation of the band of interest.

The bands were then excised aseptically from the gel, placed in eppendorf tube and sent to Alta Bioscience company for sequencing.

- **Using PVDF membrane**

The purified activated Cry41Aa with either proteinase K, trypsin (Promega) or trypsin (MS grade) was resolved in a 4-20% precast gel. The gel was then soaked in dry blot buffer for 10 min with gentle rotation. Using a Trans-Blot Semi-Dry transfer Cell (Bio-Rad), the protein(s) was transferred onto a PVDF membrane (for 1 hour at 100 mA)

which was later stained with Ponceau S stain, destained with distilled water, left to dry for few minutes then sent to Alta Biosciences company for sequencing.

- **Cell culture conditions**

Adherent cell lines (HepG2, HeLa) were cultured in Dulbecco's modified Eagle's medium (DMEM) provided with 1% penicillin-streptomycin-neomycin (PSN) antibiotic mixture and 10% fetal bovine serum (FBS) in a humidified atmosphere containing 5% CO₂ at 37°C whereas suspension cells (HL-60) were cultured in Roswell Park Memorial Institute medium (RPMI) 1640 supplemented with 10% FCS and 1% PSG.

When a confluency of around 70% was reached, the adherent cells were split. The splitting process begins with washing the cells twice with DPBS after removal of the medium. The cells were then detached by trypsinization (trypsin/EDTA containing 0.05% trypsin and 0.53 mM EDTA) at 37°C for 5 - 10 minutes. To neutralize the trypsin action, medium was added followed by spinning (150 x g for 5 min) and the resultant pellet corresponding to the cells was resuspended in fresh medium. After counting, the cells were seeded at a desired density in sterile polystyrene 75 cm² flasks (Nunc).

In the case of HL-60, the cells were passaged when they reach a density of 10⁶ cells/ml.

- **Cell assays**

Assays were performed in 96-well plates (Nunc). Each well received 90 µl of cell suspension at a density of 22,500 cells per well and cultured overnight (at 37°C/5% CO₂ humidified air) before 10 µl of the test sample was added. The experiments were set up in triplicates.

The mock control wells received 90 µl of cell suspension and 10 µl of the appropriate buffer (Na₂CO₃, PBS and DMSO). The wells that contained 100 µl of appropriate cell culture medium served as background fluorescent/luminescent controls.

The readings were carried out using GloMax-Multi Detection System (Promega) according to the assay(s) instructions. The fluorescent or luminescent signal in the background control wells was subtracted from each experimental value.

CellTiter-Blue cell viability assay

The number of viable cells in culture was monitored using CellTiter Blue (Promega). This assay relies on the conversion of resazurin (a redox dye) into resorufin (fluorescent product) which could only be enabled by viable cells knowing that the non-viable ones are not able to generate the fluorescent signal due to the loss of their metabolic capacity. 20 µl of the reagent (resazurin) was added at the end of toxin exposure period and the reading was taken after an additional 2 hours of incubation. Using fluorescent plate reader, fluorescence was measured with a green filter with excitation wavelength at 560 nm and emission wavelength at 590 nm.

CellTiter-Glo luminescence cell viability assay

The number of viable cells in culture was determined based on quantitation of the ATP present knowing that post lysis the cells lose the ability to synthesize ATP which makes ATP a reliable viability marker. A direct correlation exists between luminescent output (corresponding to the ATP levels) and viable cells in this assay. 100 µl of the lyophilized CellTiter-Glo® substrate were added to each well in an opaque-walled 96 well plate at the end of toxin exposure period. The plate was placed in an orbital shaker for 5 min to induce cell lysis then equilibrated with its content at room temperature for 20 min to stabilize luminescent signal before the reading was taken.

- **Statistical analysis**

EC₅₀s of the proteins of interest were determined using SPSS software version 22.0 (IBM, 2013), Probit Regression.

- **Preparation of cell extracts**

Initially the cells were seeded on plates (6-24 wells) or dishes (60 mm) then after reaching the desired confluency and performing the appropriate treatment (depending on the aim of the experiment), the medium was removed and the cells were washed twice with cold DPBS. Next they were gently scraped, spun at low speed (2.5 rpm) and supernatant was discarded. Pellet containing intact cells was suspended in adequate volume of either lysis buffers RIPA or NP-40 or 20 mM of Tris-HCL sample buffer (the latter was used when dealing with whole cells). These buffers contained: protease inhibitors, phosphatase inhibitors (2 mM sodium orthovanadate + 1 μM microcystin), 1 mM EGTA and 1 mM EDTA. In case of whole cells suspended in Tris-HCL, the samples were stored immediately at -20°C while to ensure cell lysis with RIPA or NP-40, the mixture was later incubated on ice for 30 min, spun for another 30 min at 13000 rpm and the supernatant containing the cell extracts was collected then stored at -20°C.

For the preparation of HL-60 extracts, the same procedure was followed except that no scraping was used since these cells grow in suspension culture.

- **Western blot**

10-25 μg of proteins were loaded per well. The proteins were initially run on SDS-PAGE gels (7.5-12%). The gels as well as the nitrocellulose membranes were soaked in dryblot buffer for 10 min with rotation at room temperature. Using a Bio-Rad Trans-Blot Semi-Dry Transfer Cell system (100 mA for 30-75 min), the proteins were transferred to a

nitrocellulose membrane (Bio-Rad, 0.45 μm). The membrane was washed with PBS then incubated with the blocking solution (PBS containing 0.02% Tween-20 (PBST) and 3% BSA or 5% non-fat dry milk). The membrane was washed with PBST 3 times for 15 min then incubated with the appropriate ligand at 4°C overnight in the shaker.

- 3% BSA and primary antibody diluted in PBST (1:1000 v/v dilution for antibodies against total and phosphorylated ERK and p38; 1:50000 v/v dilution for anti-CD59 antibody, 1:500 v/v dilution for anti-AQP9 antibody).
- 5% non-fat dry milk and primary antibody diluted in PBST (1 $\mu\text{g}/\text{ml}$ final for antibody against phosphorylated CREB)

The next day, the membrane was washed 3 times with PBST for 15 min then incubated for 1 hour at room temperature with the secondary antibody diluted 1:2000 in PBST containing 5% non-fat dry skimmed milk.

Another wash with PBST was carried out 3 times for 15 min then the membrane was incubated in the chemiluminescent detection solution and finally either exposed to X-ray film (FUJI medical X-ray film) or placed in UVP ChemStudio imaging system (analytikjena).

- **Ligand blot**

Same procedure was followed as for the western blot experiment except that instead of the primary antibody, $\Delta\text{R-HAP40}$ diluted in PBST was used.

- **Development of the resistant cell line**

HepG2 cells were cultured in step-wise increases of purified T/C activated Cry41Aa. Initially, the cells were seeded at around 20% confluency and the toxin treatment was carried out after 24 hours with a commencing dose of 0.1 $\mu\text{g}/\text{ml}$.

As the cells become confluent, they were sub-cultured in the usual manner and the increase of the toxin dose generally followed the pattern of doubling the concentration unless the cells appeared not to have tolerated the drug treatment, in which case, they were allowed to recover in drug-free medium and be exposed to a less concentrated dose. A range of different concentrations was used (0.1; 0.2; 0.3; 0.4; 0.8; 1.6; 2.6; 4; 8; 10; 15; 20; 30; 50 $\mu\text{g/ml}$) during a period of 8 months.

Two flasks are set up for this experiment: one flask is used to grow treated cells and the other flask is used to grow each passage in drug-free medium which was used as a supply of "resistant cells". Regular freezing of cells was carried out at each passage.

- **Microscopy**

- For monitoring the morphological features of cells during the culturing process and prior/post treatment with toxin or other compounds, Nikon Eclipse TS100 inverted microscope was used.
- For observation of morphological changes between susceptible and resistant HepG2: HepG2 and HepG2R cells were seeded at the density of 4×10^4 cells/ml in a microscope chamber slide. The next day, pictures were taken using Zeiss Axiovert 200M, 63x DIC objective.
- For monitoring swelling/recovery of HepG2 and HepG2R over time following toxin exposure: HepG2 and HepG2R cells were seeded at the density of 25×10^4 cells/ml, in 6 well plates. The next day cells were dosed with purified T/C activated Cry41Aa (1.5 $\mu\text{g/ml}$ and 110 $\mu\text{g/ml}$ respectively) or buffer. Morphological changes were visualised using EVOS FL imaging system 10x objective.

- **Determination of growth curves**

HepG2, HepG2R and HepG2 Rev cell lines were seeded at the same cell density (25×10^4 cells/ml) in 6 well plates. The growth of cells was monitored by counting cells using Trypan blue reagent and haemocytometer chamber. Three replicates were used for each determination and four cell counts for each replicate from each cell line were made every 24 hours for 5 days.

- **RNA Extraction**

RNA extraction was performed using QIAGEN RNeasy Plus Mini Kit according to the manufacturer's instruction. Initially the cells were grown in a monolayer then trypsinized and spun for 5 min at 300 x g. The supernatant was discarded and the pellet was suspended in RLT buffer containing β -ME to ensure lysis. The lysate was next placed into a QIAshredder spin column and spun for 2 min at maximum speed. For genomic DNA elimination, the homogenized lysate was then transferred to a gDNA Eliminator spin column and spun for 30 seconds at 9000 g. The column was discarded and to the flow through 1 volume of 70% ethanol was added. Next, the mixture was transferred to RNeasy spin column and centrifuged for 15 seconds at 9000 g. The flow through was discarded and 700 μ l of buffer RW1 was added to the RNeasy spin column which was spun for 15 seconds at 9000 g. The flow through was discarded and 500 μ l of RPE was added to the column and spun for 15 seconds at 9000 g. The flow through was again discarded and another 500 μ l of RPE was added then the mixture was centrifuged for 2 min at 9000 g. The RNeasy column was placed in a new 2 ml collection tube, centrifuged for additional 1 min and was finally placed in a new 1.5 ml collection tube. For RNA elution, 30-50 μ l of RNase-free water was added directly to the spin column membrane which was spun for 1 min at 9000 g. The eluted RNA samples were stored at -80°C until use.

- **RNA electrophoresis gel**

Electrophoretic separation of RNA samples was carried out on agarose-formaldehyde gel. 0.5 g of agarose was added to 36 ml of H₂O and warmed up until it was dissolved. 2.75 ml formaldehyde and 5 ml formamide were pre-warmed separately and added to the warm agarose solution in a fume hood where 2 µl of Gel Red (1 in 3 dilution) was added to the solution and the mixture was poured into a cast tray. After it was set, the tray was placed in an electrophoresis system where 1 x 3-(N-morpholino) propanesulfonic acid (MOPS) buffer was used as the running buffer.

The RNA samples were then denatured: 2 µl of each RNA sample was added to 2 µl of formaldehyde, 4 µl of H₂O, 2 µl of 10 x MOPS buffer and 9 µl of formamide. The mixture was then heated at 70°C for 10 minutes. Next the sample was cooled in ice for 1-3 min and 4 µl of RNA loading buffer was then added. Each RNA sample was then loaded into each well of the RNA gel which was finally run for up to 2 hours at 120 V.

- **Determination of RNA concentration and RNA integrity**

NanoDrop spectrophotometer

Using a NanoDrop ND-2000 spectrophotometer, the amount of RNA in ng/µl and the A₂₆₀/A₂₈₀ ratio were determined. Following the software's instruction, 1 µl of elution water was loaded into the instrument and the machine was blanked. After wiping the Nanodrop sensor, 1 µl of the sample was next loaded and the measure button was then clicked. Concentration of the sample as well as A₂₆₀/A₂₈₀ ratio were finally displayed.

Agilent Bioanalyser 2100

The Agilent Bioanalyser 2100 was used as per manufacturer's instructions using a RNA 6000 Nano Kit. Briefly, before beginning the chip preparation protocol, the chip priming station and the bioanalyser were ensured to be set up and ready to use. The program on the computer was then started and the electrodes were decontaminated. Initially the gel was prepared, then to 65 μ l of filtered gel, 1 μ l of RNA 6000 Nano dye concentrate was added. 9 μ l of this Gel-Dye Mix was loaded into each of the marked wells on an RNA Nanochip placed on the chip priming station. After loading 5 μ l of the RNA 6000 Nano Marker in each of the appropriate wells, 1 μ l of each of the ladder and the sample were then loaded into the Chip which was later inserted in the Agilent 2100 Bioanalyser. The Chip Run was finally started.

- **RNA-seq and analysis**

RNA-seq was performed by a third party. GATC Biotech who undertook the RNA-seq (INVIEW™ Transcriptome) of the purified RNA using Illumina sequencing. The first step in the technique involves isolation of subsets of RNA molecules using different protocols such as the poly-A selection or a ribo-depletion to enrich for polyadenylated transcripts or to remove ribosomal RNAs respectively. Next, the population of RNA to be sequenced is converted into cDNA fragments (a cDNA library) by reverse transcription and sequencing adaptors are ligated to the ends of the cDNA fragments. The cDNA library is then analyzed by NGS, producing short sequences which correspond to either one or both ends of the fragment. These reads, of which there will be many millions by the end of the workflow, can then be aligned to a genome of reference and assembled to produce an RNA sequence map that spans the transcriptome (Kukurba and Montgomery, 2015).

The generated FASTQ files were next analysed using Galaxy software (usegalaxy.org).

- **cDNA Synthesis**

Aliquots of 2 µg of total RNA were reverse transcribed to cDNA using High-Capacity cDNA Reverse Transcription Kit (Applied Biosciences) according to the manufacturer's instruction. 20 µl reaction was placed in a thermo-cycler that was set up as follows: 25°C for 10 minutes followed by 37°C for 120 minutes, then 85°C for 5 minutes before finally held at 4°C indefinitely.

- **qPCR**

Syber Green-based qPCR was performed. A 96 well plate was set up with a final reaction volume of 20 µl containing the following: 10 µl of Syber Green master mix (Applied Biosystems), 1 µl of cDNA, 1 µl of forward primer (200 mM), 1 µl of reverse primer (200 mM) and 7 µl of H₂O. AQP9 was used as the target gene while GAPDH was used as the endogenous control, and all reactions were performed in triplicate.

RNAs that were subjected to cDNA synthesis without the reverse transcriptase were used as non-genomic DNA controls, while wells lacking the cDNA served as negative controls.

The qPCR was run on an Applied Biosystems StepOne™ Real-Time PCR System. Relative gene expression was calculated using the comparative cycle threshold ($2^{-\Delta\Delta CT}$) method. PCR cycling conditions are described in the following diagram:

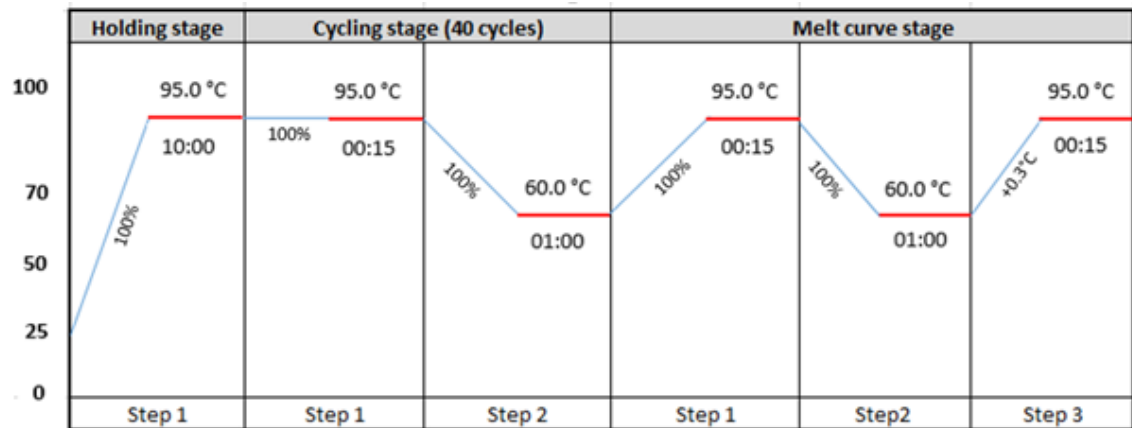


Figure 30: Different settings used in the qPCR reaction.

The primers used in this experiment for AQP9 and GAPDH were:

AQP9

- FP: CTGGTGGAAAACCTGCTGATCG
- RP: CTGCAAATGCGTTCGCCAGAG

GAPDH

- FP: ATCCCTGAGCTGAACGGGAA
- RP: GGCAGGTTTTTCTAGACGGC

• **Transfection of resistant HepG2 using siRNA**

AQP9 knock down was achieved through the use of RNA interference (FlexiTube GeneSolution-QIAGEN). This kit consists of 4 alternative siRNA molecules targeted to AQP9.

The experiment was optimised using different conditions: transfection reagents (Hyperfect, Lipofectamine, and Hyperfect), type of transfection (Fast-forward, reverse), concentration of siRNA, volume of the transfection reagent and incubation time (12, 24, 48 hours).

The protocol that led to successful AQP9 knock down was:

Initially, the transfection solution was prepared: 4 μl of Hyperfect, 1 μl of each siRNA (giving a total concentration of 20 nM) and 95 μl OPT-MEM. The mixture was then vortexed and incubated for 5-10 min at room temperature to allow the formation of the transfection complexes. Next, 1×10^5 cells per well were seeded in a 24 well plate to which the transfection solution was added. The plate was incubated in a humidified atmosphere containing 5% CO_2 at 37°C and gene silencing was monitored after 12 hours using RT-qPCR and western blot.

4 Involvement of N and C-terminal cleavages in Cry41Aa toxicity

4.1 Introduction

Processing of the Cry protoxin into its active form is essential for toxin activity and this processing is mediated by proteases that cleave the protoxin polypeptide at specific points to produce the mature active toxin. Proteolytic processing was initially considered as a toxin activation step following a study where similar levels of mortality were observed after protoxin and activated toxin were fed to susceptible insects and the level of toxicity of the former was diminished in the presence of protease inhibitors reviewed by Deist et al in 2014 (Deist et al., 2014). In fact, a possible correlation between low susceptibility and lack of proper proteolytic activation or degradation of toxin to inactive peptides, by cleavage at inappropriate sites, was suggested.

Proper proteolytic activation was shown to facilitate the recognition and binding of *Bt* toxins to insect gut receptors. These two steps are crucial in toxicity and modification of either or both of them can result in altered host range and/or altered toxicity reviewed by Jurat-Fuentes and Crickmore in 2017 (Jurat-Fuentes and Crickmore, 2017).

In the case of anticancer Cry toxins, proteolytic cleavage was also shown to be indispensable for toxin activity. N/C-terminal cleavage (s) of the proteins was shown to be important to convert them into potent toxins exhibiting high cytopathic effect against cancer cell lines (Ohba et al., 2008). Yamashita et al, in 2005, showed that alkali-solubilised parasporin-3 had no cytotoxic activity against HepG2 cells whereas strong cytopathic effect was observed after activation of the toxin with proteases. A more recent study is in good agreement with this finding showing that it is only upon proteolytic treatment with trypsin that parasporin-3 (Cry41Aa) induces a rapid and significant decrease in HepG2 metabolic activity (Krishnan et al., 2017).

In order to understand the activation mechanism of Cry41Aa, various mutations were created in this protein as shown in figure 31 in order to answer two key questions:

- Can the toxin be pre-activated by N-terminal deletion?
- Which of N or C-terminal cleavage is important in Cry41Aa toxicity?

In order to understand the activation mechanism of *Bt* crystal proteins, various approaches have previously been implemented. Amongst these approaches the use of toxin truncation and modification of protease cleavage sites (Walters et al., 2008b, Zhou et al., 2014).

Deletions ($\Delta 23$, $\Delta 40$, $\Delta 60$) were then made at the N-terminal region of the protein based on possible trypsin cleavage sites. However another approach was followed in order to investigate the role of N and C-terminal cleavage(s) in toxicity and involved the insertion of PreScission protease cleavage sites to ensure cleavage of Cry41Aa solely at the N-terminus (figure 31).

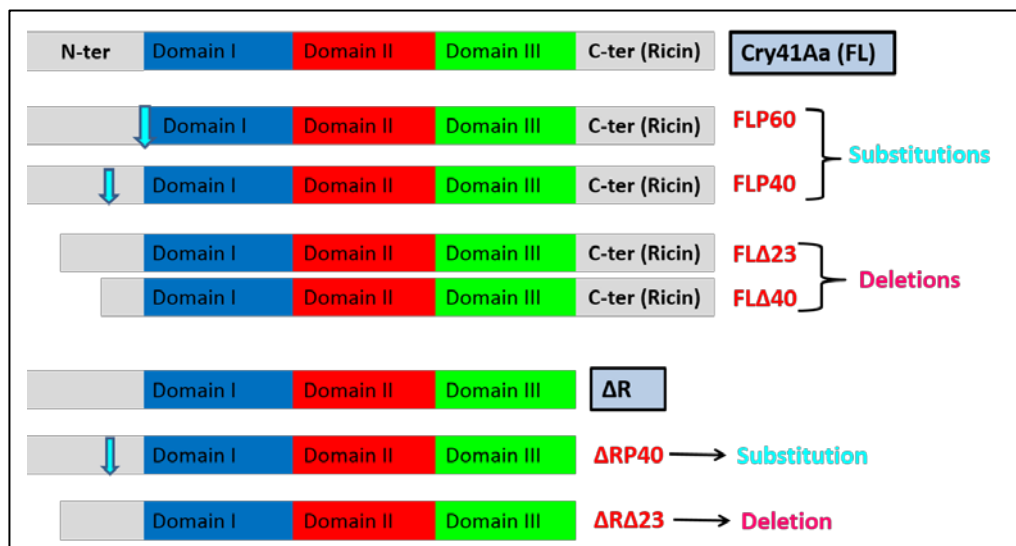


Figure 31: Schematic presentation of various created mutants.

The blue arrows indicate the regions where PreScission protease cleavage sites were inserted (40th and 60th aa). Only successfully expressed proteins are presented in this diagram. Mutations were created in Cry41Aa full length (FL) and Cry41Aa missing the ricin domain (ΔR) in parallel.

4.2 Can the toxin be pre-activated by N-terminal deletion?

Sequencing of trypsin activated Cry41Aa was needed in order to create an N-terminally deleted variant that would resemble a product produced by cleavage by trypsin.

The protein of interest was concentrated to obtain the required intensity in order to facilitate the sequencing protocol. After being concentrated, the toxin sample was run in 3 lanes on 7.5% SDS-PAGE gel and the resultant bands of interest were then excised from the gel and sent for sequencing. However the outcome was failure of N-terminal sequencing of the protein (data not shown). Therefore based on the potential N-terminal cleavage sites of trypsin (figure 32) (after arginine (R) or lysine (K)), deletions were created. These cleavage sites were predicted based on Yamashita et al findings in 2005 where the N-terminal cleavage site of the major band produced (64 kDa) after proteolytic activation of Cry41Aa resides after the 60th aa.

```

MNQNCNNGYEVLNSGKGYCQPRYPFAQAPGSELQNMGYKEWMMNCTSGDPTVLGEGYSA
DVRDAVITSINIASYLLSVFPFPAGVAAGILGALLGLLWPTNTQAVWEAFMNTVEALINQ
KLDEYARSKAISELNGLKNVLELYQDAADDWNEPGLDLRNKNRVLTFEFRNVNGHFENSMP
SFAVRNFEVNLLPVYAEAANLHLLLRDAVKFGEWGMSDTPGAERDDMYRRLRSRTEIY
TDHCVNTYNQGLQQAQSLQANVSDYSRYPWTQYNQSGGFSYREAKGEYRGTENWNLYNAF
RRDMTILVLDIIAQFPTYDPGLYSRPVKSELTREVTDIRGTTWRSDANLNTIDAIENRM
VGSRQLQLFTWLTEMKFYIRNTGSITSYTHGDLMVGLEKKIRKTNNDNQWLPLEGQNTSY
TRIDRPGIELGKNYWAYRTQQWFETRLLQLWANTDVLSLNAGTVGNEFWVRDVPDYRNI
YARSTRNHFIENHRLSWIKFEPVRDNCPPAWPGYKQLSALLFGWTHNSVDLNNIISQYRI
TQIPAVKAYWNRGAFSVIRGPGSTGGNLVQLGTGGEVSVKVRPEQTGSDWYRVRIRYAAG
SRGLNVKKYVSSIHASVTYDYNMTMSSSTQGTYNQYLDVYNFRLAEPEFEVWLTNES
GGPIWIDKIEFIPLSPIPELPVYPGTQIVTALNNSVVTSEEFCMGI GLTTRCGVNLWS
NNGNTLQKWRFFVYNGDONAFQIKSTPNEDLVLSGSNSGTSVTAETNQNRPNQYWLIEEAG
NGYVYLRKGNPNLVLDVAGTSTANGTNI LLWNYNGSTNQKFKLS

```

Figure 32: Illustration of Cry41Aa amino acid sequence.

The sequence highlighted in red corresponds to the ricin domain and the letters written in bold present the potential N-terminal cleavage sites by trypsin.

Inverse PCR was used to create the deletions. The templates used were pSVP2741Aa, a plasmid used to express Cry41Aa full length (FL) and pSVP2741Aa Δ R, a plasmid used to express Cry41Aa missing the ricin domain (Δ R) (figure 33). The mutations were created in both plasmids in parallel.

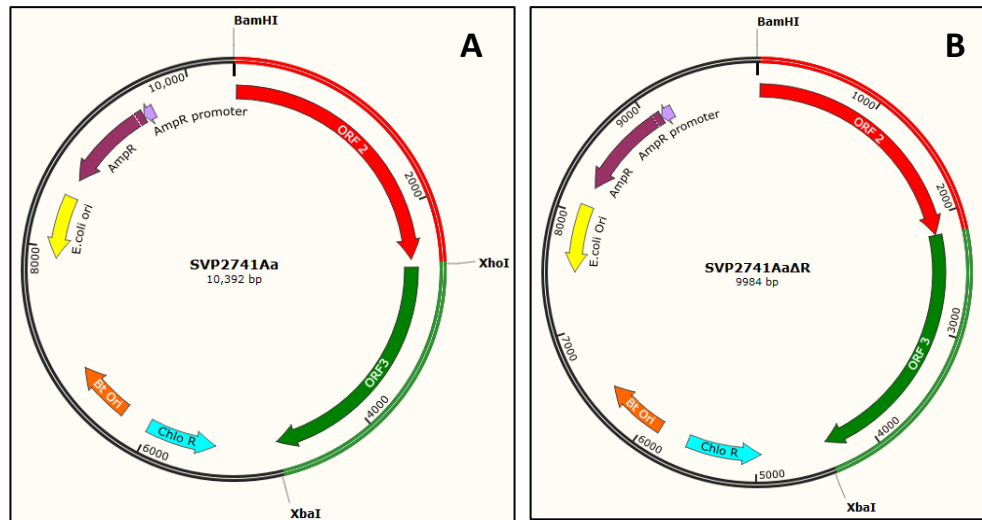


Figure 33: Plasmids used to create the desired mutations (constructed using Snapgene program).

A: a plasmid used for the expression of *Cry41Aa* gene using *E. coli* - *Bt* expression vector pSVP27A under the control of *Cyt1A* promoter (Krishnan et al., 2017). This plasmid has both chloramphenicol and ampicillin resistance genes. **B:** same plasmid as **A** except that *cry41Aa* gene is missing the region coding for the ricin domain.

4.2.1 Deletion of 23 amino acids

- **Creation of FLΔ23**

Based on the corresponding amino acid sequence (figure 32), primers were designed (figure 34) using PCR primer stats and PRIMER SELECT programs in order to generate an N-terminally deleted variant of *Cry41Aa* that would mimic a product produced by cleavage by trypsin at the 23rd aa (arginine).

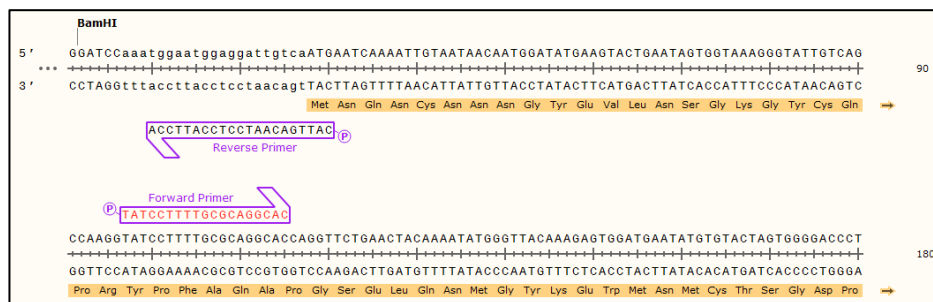


Figure 34: Schematic representation of forward and reverse primers used in the PCR reaction.

Both primers were phosphorylated in order to ensure the ligation of the amplicon using T4 DNA ligase. The part highlighted in orange represents the translated amino acid sequence.

PCR (PFU ULTRA 10 kb) reaction was performed overnight on SVP2741Aa plasmid. The resultant PCR product was digested with *DpnI* (to remove methylated template DNA), purified using QIAquick kit then run on 1% agarose gel (figure 35).

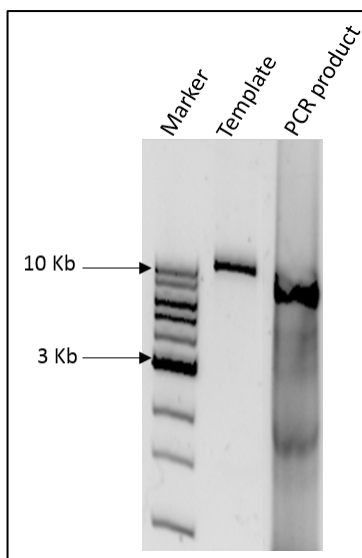


Figure 35: Confirmation of the presence of amplified PCR product.

PCR product was digested with *DpnI*, purified using QIAquick kit then run on 1% agarose gel along with the template and 1 Kb ladder (Marker) for size comparison.

According to figure 35, the size of the amplified product present in lane 3 was around 10 kb which corresponded to the expected size of the product.

The amplified construct was self-ligated prior to introduction into DH5 α , *E. coli* competent cells used to maximize transformation efficiency. After being sequenced, the extracted DNA from these cells, was introduced into another *E. coli* strain called GM2163 which does not methylate DNA and facilitates the transformation of *B. thuringiensis*. Following *Bt* transformation, the extracted DNA was again introduced into DH5 α for final confirmation. The verification of the introduction of the right plasmid was initially carried out using restriction digestion with *HaeIII* enzyme. This is by comparing the size of fragments (expected bands) given by NEBcutter program (figure 36) with the size of the resultant bands after digestion with the enzyme which were run on 1% agarose gel (figure 37B).

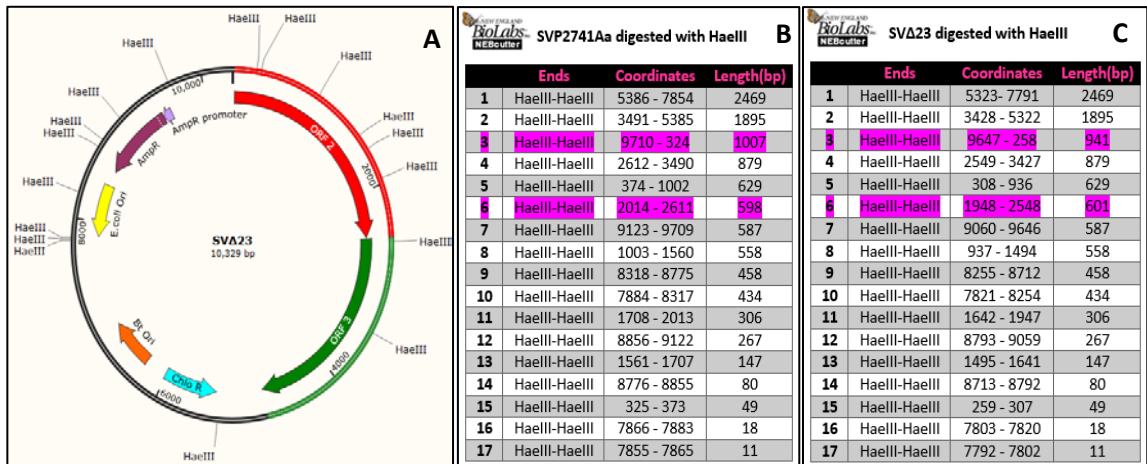


Figure 36: A: Schematic representation of SVΔ23 plasmid and localisation of different restriction sites of *HaeIII*, **B** and **C:** Sizes of different fragments yielded by digestion of SVP2741Aa and SVΔ23 with *HaeIII* enzyme respectively (NEB-Cutter program). The parts highlighted in pink are the predicted differences.

According to figure 36, a difference in size between the fragments around 1007 bp and 941 bp of digested SVP2741Aa and SVΔ23 respectively is expected to be visible on the gel whereas the difference between the two other bands is too small to be visualised. This is also shown in figure 37A which represents the predicted banding pattern of digested DNAs (SVP2741Aa (lane 2) and SVΔ23 (lane 3)) and confirmed by 1% agarose gel where digested DNAs were run (figure 37B) showing that the bands around 1007 bp and 879 bp look distant whereas those around 941 bp and 879 bp look much closer.

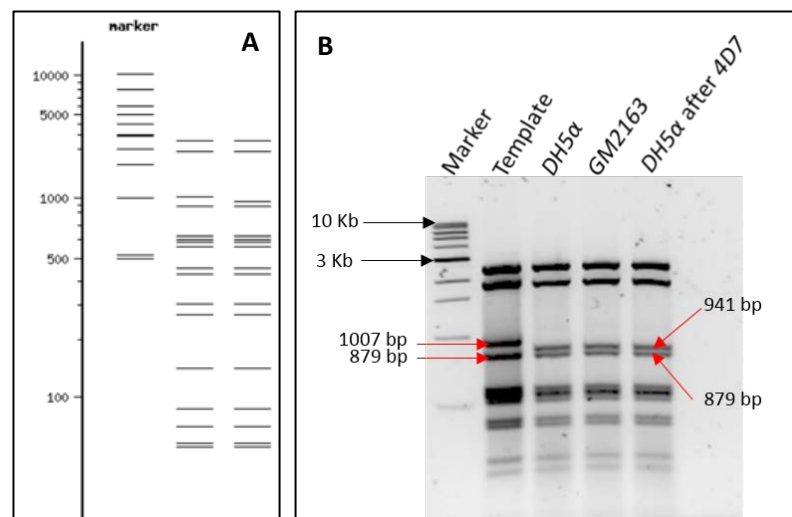


Figure 37: DNA banding pattern after *HaeIII* digestion.

A: Predicted *HaeIII* digestion profile of SV2741Aa (lane 2) and SVΔ23 (lane 3) (NEBcutter), **B:** DNAs were miniprepred after each transformation step using QIAprep kit, digested with *HaeIII* then run on 1% agarose gel along with the digested template (SVP2741Aa).

The mutation created was finally confirmed by sequencing where the alignment of the sequenced DNA (Seq) with the expected sequence of the mutated DNA (SVΔ23), using Clustal Omega software, showed perfect identity (figure 38).

```

SVΔ23      -----GGATCCaatggaatggaggattgtcaATGTATCCTTTGCGC
Seq        TTTAATGTTGAAAGGGGGATCCAAATGGAATGGAGGATTGTCAATGTATCCTTTGCGC
          *****

SVΔ23      AGGCACCAGGTTCTGAACTACAAAATATGGGTTACAAAGAGTGGATGAATATGTGTACTA
Seq        AGGCACCAGGTTCTGAACTACAAAATATGGGTTACAAAGAGTGGATGAATATGTGTACTA
          *****

SVΔ23      GTGGGGACCCTACCGTCCTGGGGGAGGATACAGCGCAGATGTAAGGGATGCCGTATTA
Seq        GTGGGGACCCTACCGTCCTGGGGGAGGATACAGCGCAGATGTAAGGGATGCCGTATTA
          *****

SVΔ23      CAAGTATAAATATCGCTTCCTATCTTCTTTCAGTCCCATTCCCTCCAGCTGGAGTAGCCG
Seq        CAAGTATAAATATCGCTTCCTATCTTCTTTCAGTCCCATTCCCTCCAGCTGGAGTAGCCG
          *****

```

Figure 38: Alignment of the predicted sequence of SVΔ23 (SVΔ23) and the sequence produced by sequencing of the DNA extracted from GM2163 cells (Seq).

The sequence of the DNA obtained from GM2163 transformation and the expected sequence of SVΔ23 were aligned using Clustal Omega software. The deletion site is shown with a yellow arrow.

4D7 (SVΔ23) was then grown and the protein was harvested then run on 7.5% SDS-PAGE along with Cry41Aa (full length) for size comparison (figure 39).

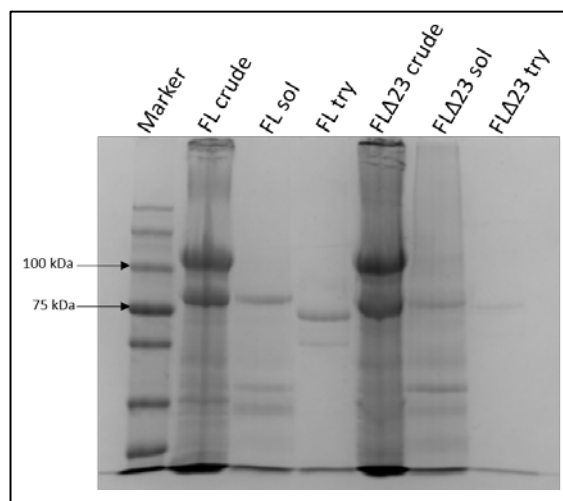


Figure 39: SDS-PAGE analysis of FLΔ23 protein levels and sizes compared with Cry41Aa full length (FL).

Crude FLΔ23 and Cry41Aa (FL) were solubilised for 1 hour at 37°C in 50 mM sodium carbonate (pH 10.5) in the presence of 5 mM DTT and activated with trypsin (1 mg/ml) for 1 hour at 37°C. The samples (crude, solubilised and activated) were then run on 7.5% SDS-PAGE gel.

SDS-PAGE showed that the mutant FL Δ 23 was successfully expressed. However, by comparing the trypsin activated protein to the solubilised core we can see that there is only a small shift in size in case of FL Δ 23 suggesting that either the cleavage site is beyond 23 aa or there might be cleavage at the C-terminus of the protein.

The level of toxicity of FL Δ 23 was then evaluated on HepG2 cell line. According to figure 40, at a concentration of 100 μ g/ml, the solubilised FL Δ 23 had no significant effect on the cell line similar to the protoxin (solubilised Cry41Aa), unlike the trypsin activated Cry41Aa which caused a considerable decrease in cell viability at a concentration of 12 μ g/ml. Therefore deletion of 23 aa at the N-terminus of Cry41Aa does not lead to the pre-activation of the toxin.

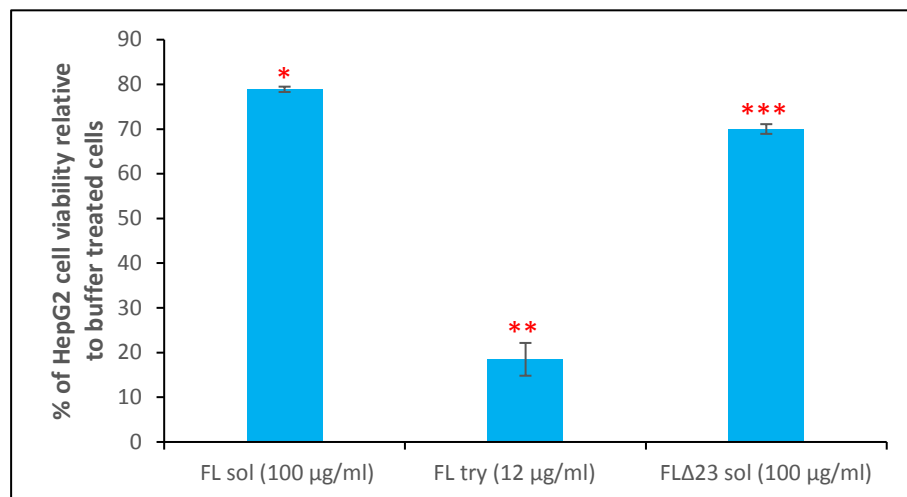


Figure 40: Evaluation of the level of toxicity of solubilised FL Δ 23.

HepG2 cells were seeded at a density of 25×10^4 cells/ml. The next day the cells were treated with solubilised FL (100 μ g/ml), solubilised FL Δ 23 (100 μ g/ml) and trypsin activated FL (12 μ g/ml). 24 hours later, cell viability was measured using CellTiter-Blue. Ttest was used to calculate the p values: * $p=0.08$, ** $p=1.35E-06$ and *** $p=0.06$

- **Creation of Δ R Δ 23**

In order to generate an N-terminally deleted variant of Δ R that would mimic a product produced by cleavage by trypsin at the 23rd aa (arginine), the primers used were the same as the ones utilized for the creation of SV Δ 23 (figure 34).

The PCR (PFU Ultra 10 Kb) was set up overnight on SVP2741AaΔR plasmid, then the resulting PCR product was first digested with *DpnI*, purified and finally run on 1% agarose gel (figure 41).

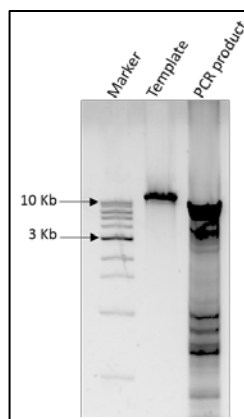


Figure 41: Confirmation of the presence of amplified PCR product.

PCR product was digested with *DpnI*, purified using QIAquick kit then run on 1% agarose gel along with the template and 1 Kb ladder (Marker) for size confirmation.

The amplified band of around 10 kb, present in lane 3, was identified as the desired band of interest.

The product was later self-ligated, introduced into DH5 α , then into GM2163 and finally into *Bt* and the introduction of the correct DNA, after each transformation step, was initially confirmed using *HaeIII* restriction enzyme then finally confirmed by sequencing (figures 42, 43 and 44).

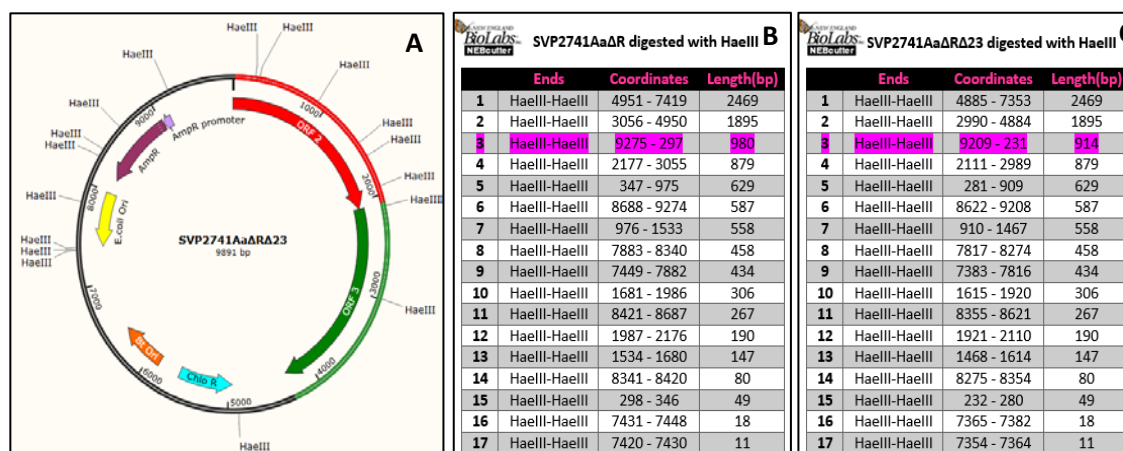


Figure 42: A: Schematic representation of SVP2741AaΔRΔ23 plasmid and localisation of different restriction sites of *HaeIII*, B and C: Sizes of different fragments yielded by digestion of SVP2741AaΔR and SVP2741AaΔRΔ23 with *HaeIII* enzyme respectively (NEBcutter program). The parts highlighted in pink are the predicted differences.

According to *HaeIII* restriction profile, the fragment around 980 bp of digested SVP2741Aa Δ R becomes smaller to around 914 bp in case of SVP2741Aa Δ R Δ 23. This difference in fragment sizes is shown in figure 43A which represents the predicted banding pattern of digested DNAs (SVP2741Aa Δ R (lane 2) and SVP2741Aa Δ R Δ 23 (lane 3)) and confirmed by 1% agarose gel where digested DNAs were run (figure 43B) showing a bigger distance between 980 bp and 879 bp fragments compared with 914 bp and 879 bp bands which look closer.

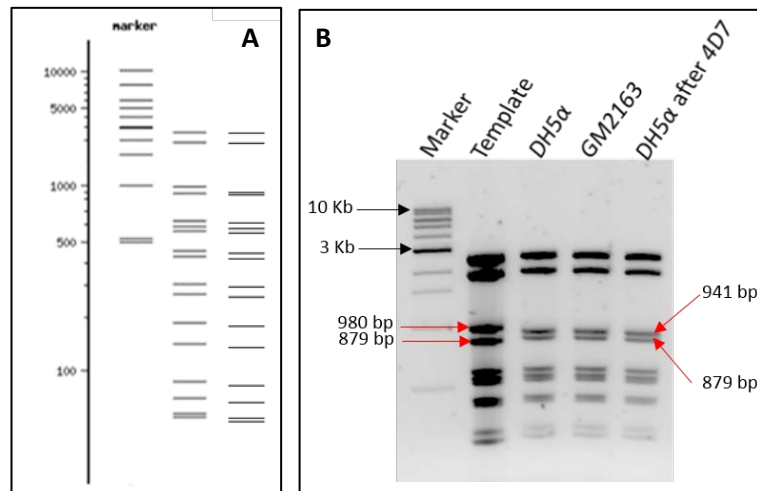


Figure 43: DNA banding pattern after *HaeIII* digestion.

A: Predicted DNA banding pattern of SV2741Aa Δ R (lane 3) and SVP2741Aa Δ R Δ 23 (lane 2) after *HaeIII* digestion (NEBcutter), **B:** DNAs were miniprepped after each transformation step using QIAprep kit, digested with *HaeIII* then run on 1% agarose gel along with the digested template (SVP2741Aa Δ R).

Then the extracted DNA was sequenced and the sequencing result shown in figure 44 confirmed the creation of the desired mutation.

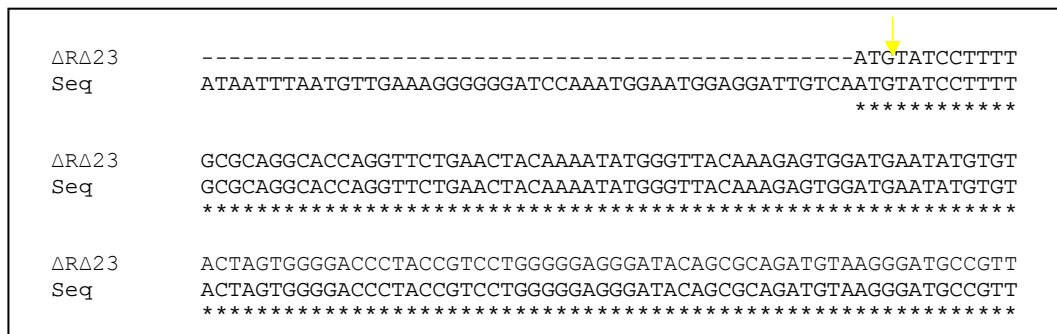


Figure 44: Alignment of predicted sequence of SVP2741Aa Δ R Δ 23 (Δ R Δ 23) and the sequence of the DNA extracted after GM2163 transformation (Seq).

The sequence of the DNA obtained from GM2163 transformation and the expected sequence of SVP2741Aa Δ R Δ 23 were aligned using Clustal Omega software. The deletion site is shown with a yellow arrow.

4D7($\Delta R\Delta 23$) was then grown and the protein was harvested and run on 7.5% SDS-PAGE gel along with Cry41Aa full length (FL) and Cry41Aa missing the ricin domain (ΔR) for comparison between protein levels and sizes (figure 45).

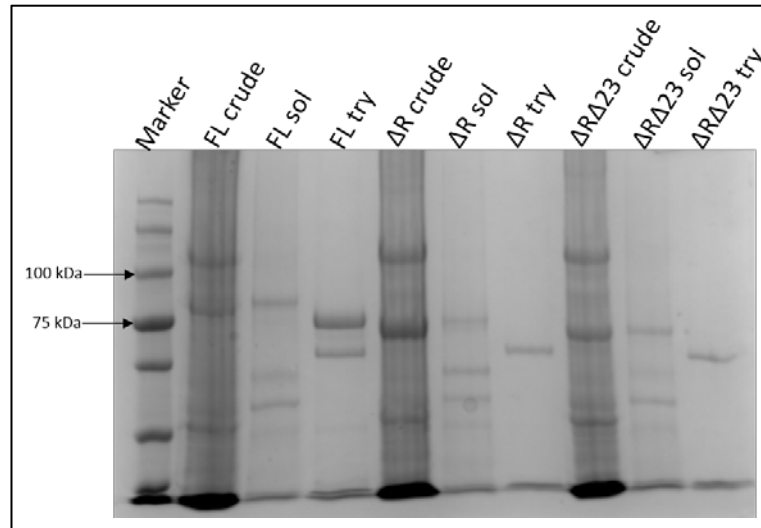


Figure 45: SDS-PAGE analysis of $\Delta R\Delta 23$ protein levels and sizes compared with Cry41Aa full length (FL) and Cry41Aa missing the ricin domain (ΔR).

Crude $\Delta R\Delta 23$, ΔR and Cry41Aa (FL) were solubilised for 1 hour at 37°C in 50 mM sodium carbonate (pH 10.5) in the presence of 5 mM DTT and activated with trypsin (1 mg/ml) for 1 hour at 37°C. The samples were then run on 7.5% SDS-PAGE gel.

According to figure 45, the mutated protein was successfully expressed. Trypsin activated $\Delta R\Delta 23$ looked much smaller than solubilised $\Delta R\Delta 23$ suggesting that trypsin cleavage is downstream of the 23rd aa or there might be cleavage occurring at the C-terminal region of the protein.

Trypsin activation of ΔR and $\Delta R\Delta 23$ yielded a single band of around 65 kDa whereas it produced two bands of around 76 and 65 kDa in case of full length protein. This result suggested that the upper band corresponds to a partial digestion while the lower band corresponds to a complete digestion and loss of the ricin domain.

The toxicity of $\Delta R\Delta 23$ was then evaluated on HepG2 cell line and according to the result, it appeared that there is only a negligible difference in the level of toxicity between solubilised FL $\Delta 23$ and solubilised $\Delta R\Delta 23$ suggesting no crucial role of C-terminal cleavage

at the ricin domain position in Cry41Aa toxicity (figure 46). This result confirmed Krishnan et al finding in 2017.

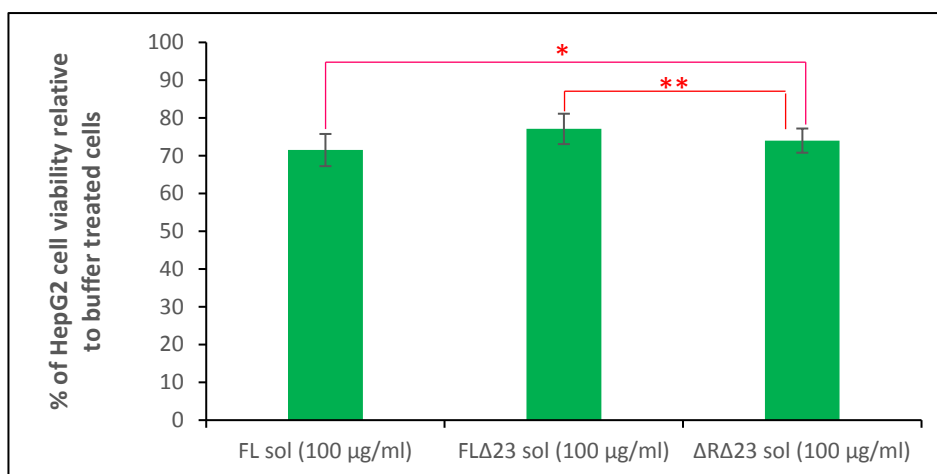


Figure 46: Evaluation of the level of toxicity of ΔRΔ23.

HepG2 cells were seeded at a density of 25×10^4 cells/ml. The next day the cells were treated with solubilised FL (100 µg/ml), solubilised FLΔ23 (100 µg/ml) and solubilised ΔRΔ23 (100 µg/ml). 24 hours later, readings were taken using CellTiter-Blue assay. Ttest was used to calculate the p values: *p=0.32 and **p=0.28

Since deletion of the N-terminal 23 aa was not sufficient to produce an active form of the toxin, we moved on to the deletion of 40 aa at the N-terminus in order to see if this deletion would do so.

4.2.2 Deletion of 40 amino acids

- **Creation of FLΔ40**

The same procedure was followed as used to create the previous mutants in order to delete 40 aa at the N-terminus of Cry41Aa. The primers were designed as shown in figure 47.

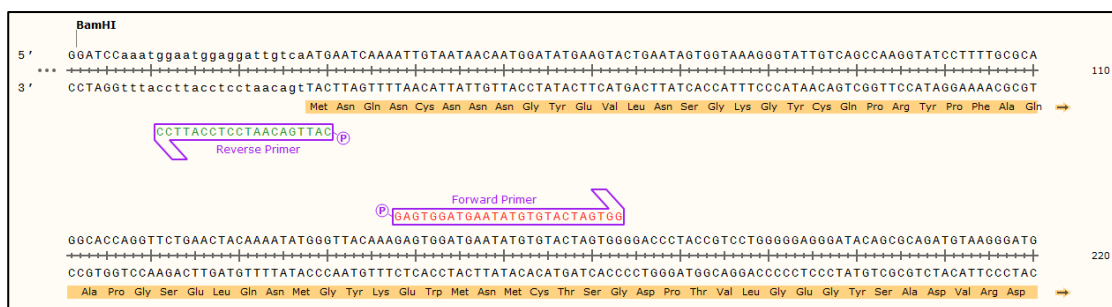


Figure 47: Schematic representation of forward and reverse primers used in the PCR reaction.

Both primers were phosphorylated in order to ensure the ligation with T4 DNA ligase. The part highlighted in orange represents the translated amino acid sequence.

The PCR (PFU ULTRA 10 kb) reaction was setup overnight on SVP2741Aa and the resultant amplicon was digested with *DpnI*, purified then run on 1% agarose gel (figure 48).

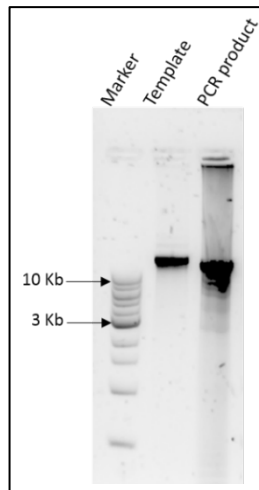


Figure 48: confirmation of the presence of amplified PCR product.

PCR product was digested with *DpnI*, purified using QIAquick kit then run on 1% agarose gel along with the template and 1 Kb ladder (Marker) for size confirmation.

According to figure 48, the amplified band shown in lane 3 appeared to have the right expected size of around 10 kb.

The amplified product was self-ligated using T4 DNA ligase then introduced into DH5 α . After confirmation of the mutation by the mean of restriction digestion and sequencing, the DNA was introduced into GM2163 and finally *Bt* for protein expression. The introduction of the right plasmid was initially confirmed by restriction analysis with *HaeIII* enzyme (figures 49 and 50).

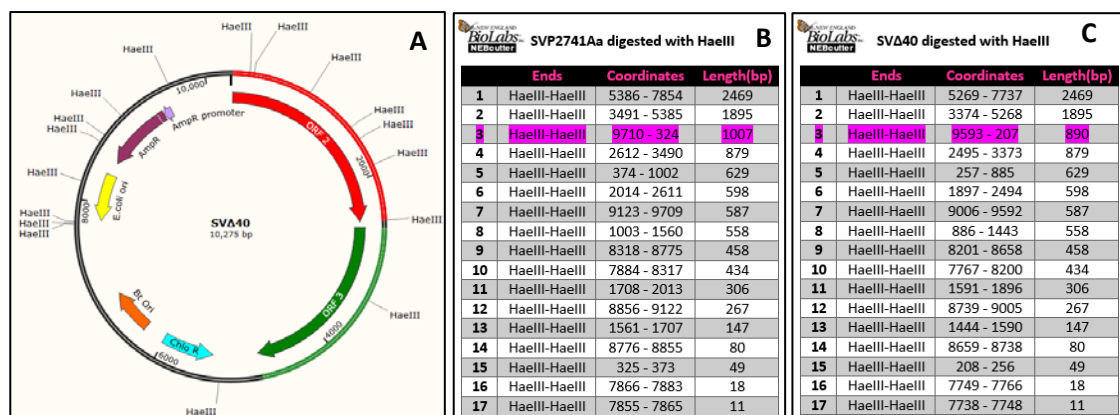


Figure 49: A: schematic representation of SVΔ40 plasmid and localisation of different restriction sites of HaeIII, B and C: sizes of different fragments yielded by digestion of SV2741Aa and SVΔ40 with HaeIII enzyme respectively (NEBcutter program). The parts highlighted in pink are the predicted differences.

According to figure 49, we should expect to see a difference between the size of fragments at around 1007 bp and 890 bp of digested SVP2741Aa and SVΔ40 respectively. This is shown in figure 50A (NEBcutter) and confirmed by 1% agarose gel where digested DNAs were run showing two distinguishable bands around 1007 bp and 879 bp for SVP2741Aa whereas only a single band representing the 890 bp and 879 bp fragments for SVΔ40 (figure 50B).

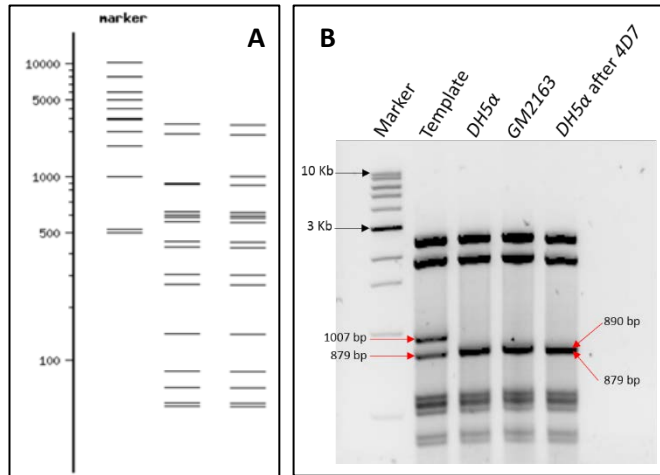


Figure 50: DNA banding pattern after *HaellI* digestion.
A: Predicted DNA banding pattern of SV2741Aa (lane 3) and SVΔ40 (lane 2) after *HaellI* digestion (NEB Cutter), **B:** DNAs were minipreped after each transformation step using QIAprep kit, digested with *HaellI* then run on 1% agarose gel along with the template (SVP2741Aa).

Then for final confirmation, the DNA was sequenced and as per figure 51 the result suggested that the desired mutation was made and this is by comparing the sequencing result (Seq) to the expected sequence of the mutant (SVΔ40).

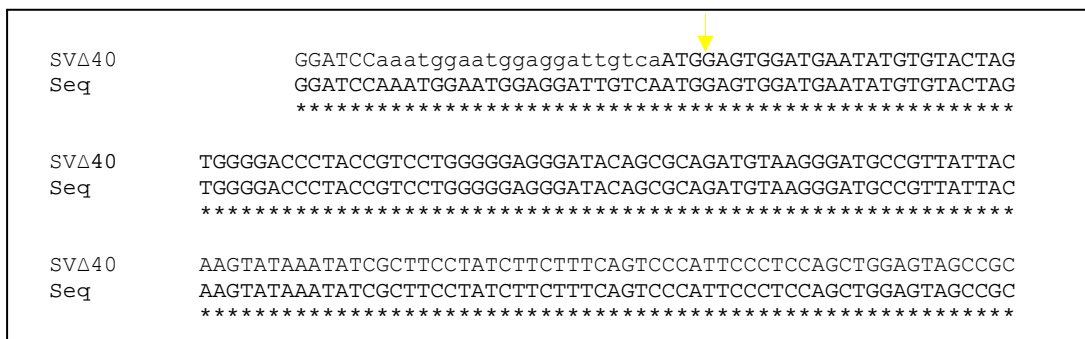


Figure 51: Alignment of the predicted sequence of SVΔ40 (SVΔ40) and the sequence of the DNA extracted from transformed GM2163 (Seq).

The sequence of the DNA obtained from GM2163 transformation and the expected sequence of SVΔ40 were aligned using Clustal Omega software. The deletion site is shown with a yellow arrow.

4D7(SVΔ40) was grown and the protein was harvested and run on 7.5% SDS-PAGE along with Cry41Aa full length (FL) for size comparison and for checking the level of expression of the protein of interest (figure 52).

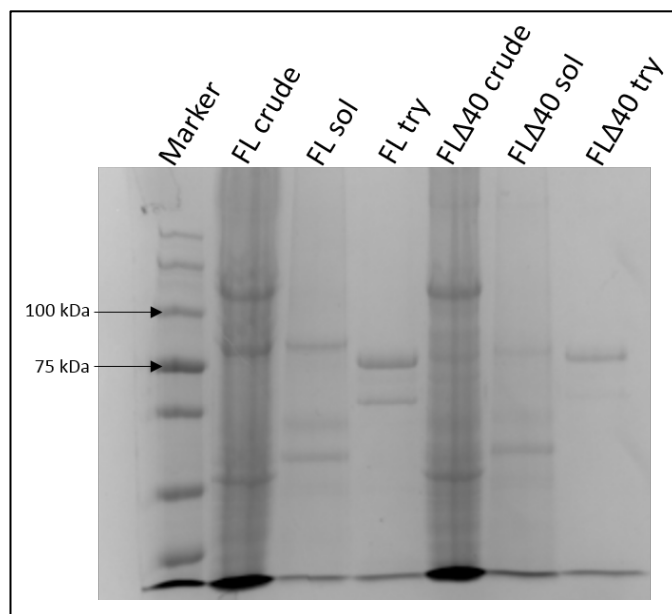


Figure 52: SDS-PAGE analysis of FLΔ40 protein levels and sizes compared with Cry41Aa full length (FL).

Crude FLΔ40 and Cry41Aa (FL) were solubilised for 1 hour at 37°C in 50 mM sodium carbonate (pH 10.5) in the presence of 5 mM DTT and activated with trypsin (1 mg/ml) for 1 hour at 37°C. The samples were then run on 7.5% SDS-PAGE gel.

SDS-PAGE gel showed a weak expression of the mutated protein. In fact, the band representing the solubilised protein which should be around 88 kDa, presented in lane 6, was faint and so the trypsin activated toxin shown in lane 7 was concentrated due to a very low intensity of the band produced post activation. This result is consistent with previous finding about the role of N-terminus of Cry toxins in expression/crystallisation (Oppert, 1999). Also, according to the gel, the size of trypsin activated FLΔ40 was smaller compared with the solubilised protein suggesting a possibility of the cleavage site being downstream of the 40th aa, or at the C-terminus.

The cytotoxicity of the created mutant was then tested on HepG2 and according to figure 53, at a concentration of 10 μg/ml, solubilised FLΔ40 showed higher toxicity level towards this cell line compared with the solubilised FL or solubilised FLΔ23 at a concentration of 100 μg/ml. Therefore N-terminal cleavage at amino acid 40 appears to be sufficient for Cry41Aa toxicity.

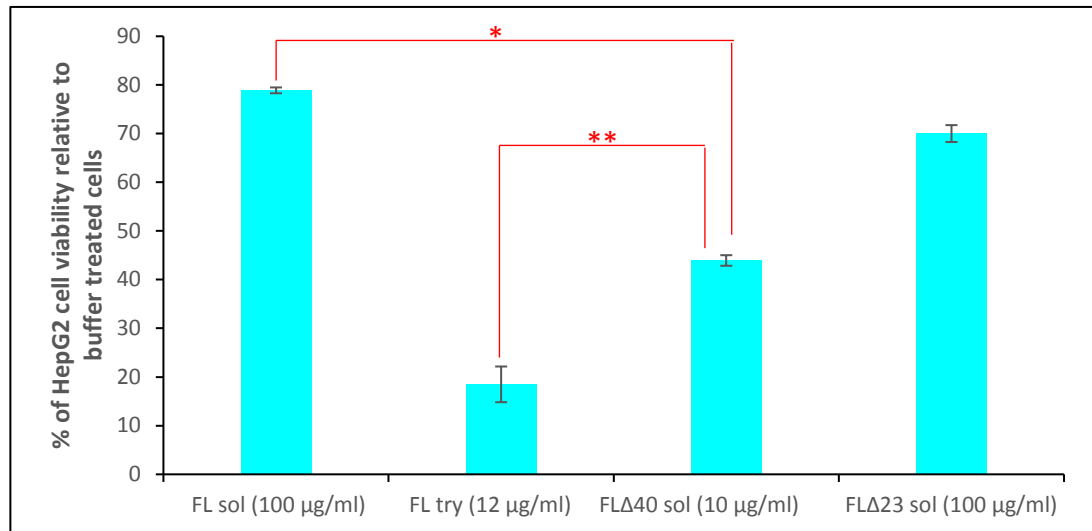


Figure 53: Evaluation of the level of toxicity of solubilised FLΔ40.

HepG2 cells were seeded at a density of 25×10^4 cells/ml. The next day the cells were treated with solubilised FL (100 µg/ml), solubilised FLΔ23 (100 µg/ml), solubilised FLΔ40 (10 µg/ml) and trypsin activated FL (12 µg/ml). 24 hours later, cell viability was measured using CellTiter-Blue. Ttest was used to calculate the p values: * $p=0.0002$ and ** $p=0.006$

- **Creation of ΔRΔ40**

The procedure followed to create this mutant protein was the same as previously used for the creation of the other mutants however the expression of this protein was not successful. Therefore a deletion of 40 aa in ΔR causes alteration in the protein expression/stability.

Since solubilised FLΔ40 gave partial activity, we decided to make a further deletion to the 60th aa which corresponds to the site identified by Yamashita et al in 2005.

4.2.3 Deletion of 60 amino acids

- **Creation of FLΔ60**

The same technique as used for the creation of the previous mutants was performed for the creation of FLΔ60. However, the created protein was not stable which could be explained by a possible important role of the deleted peptides in protein folding.

Because solubilised FLΔ40 only showed partial toxicity compared with the trypsin activated Cry41Aa towards HepG2 cell line therefore the question was whether C-

terminal cleavage, or N-terminal cleavage beyond amino acid 40, may play a role in toxicity.

4.3 Does C-terminal cleavage contribute to Cry41Aa toxicity?

4.3.1 Creation of PreScission recognition site at the 40th aa

The reason behind using PreScission was based on the knowledge that this protease has a rare and specific recognition site where it solely cleaves between glutamine and glycine. After a thorough examination of Cry41Aa sequence, it appeared that there is no similarity with the PreScission recognition site suggesting that if this site is introduced into Cry41Aa sequence, the cleavage by PreScission would only occur at one position.

- **Creation of FLP40**

This was achieved by the substitution of 8 amino acids at the N-terminal region of the protein with the PreScission protease recognition site (LEVLFQGP). PreScission activation of the resulting protein will be similar to that of trypsin activation being at the 40th amino acid (K) and this is based on the knowledge that PreScission protease cuts between glutamine (Q) and glycine (G) residues as explained in figure 54.

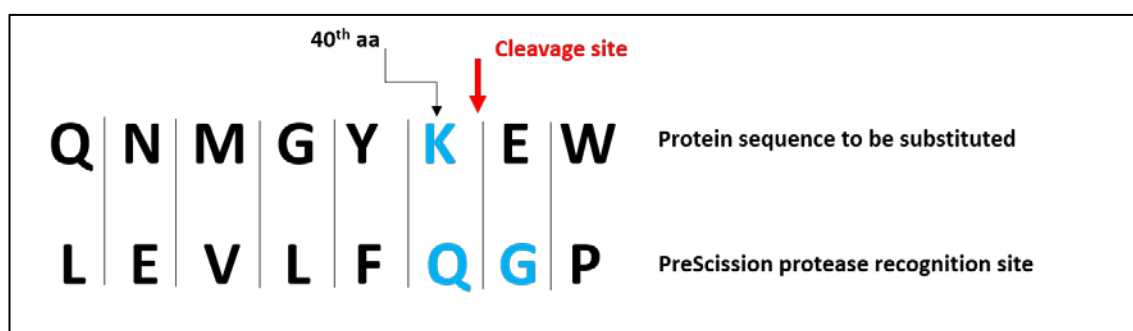


Figure 54: Schematic explanation of insertion of PreScission cleavage site in order to ensure cleavage at the 40thaa in the N-terminal region of Cry41Aa.

The oligonucleotides carrying the desired mutation were designed in order to insert the PreScission protease recognition site at the right position (figure 55).

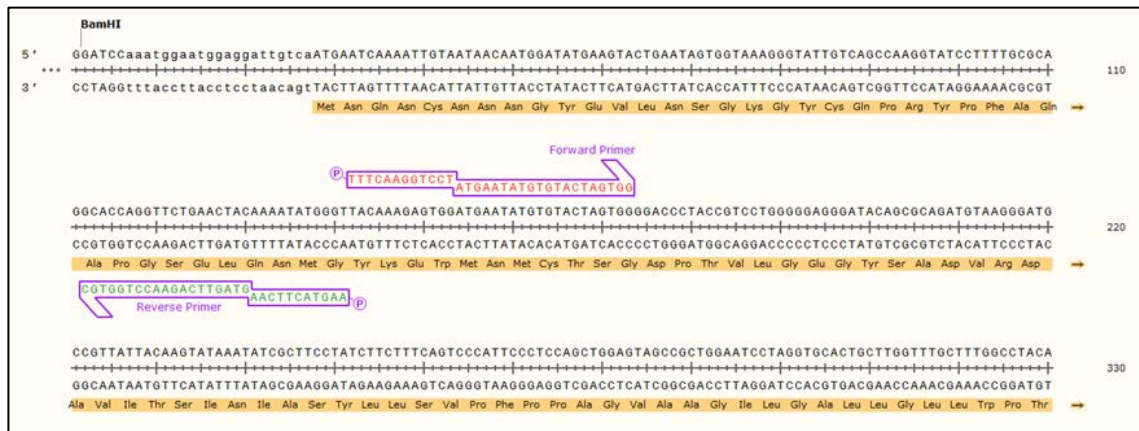


Figure 55: Schematic representation of forward and reverse primers used in the PCR reaction.

Both primers were phosphorylated in order to ensure the ligation with T4 DNA ligase and each of the staggered sequences presented in the schema corresponds to half of the PreScission recognition sequence. The corresponding amino acid sequence is highlighted in orange.

Then, the PCR (PFU Ultra 10 Kb) was setup on SVP2741Aa overnight and the amplified DNA was purified and run on 1% agarose gel (figure 56).

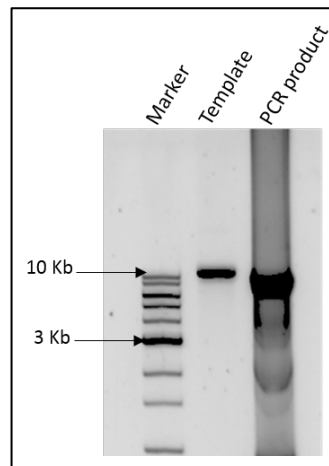


Figure 56: Confirmation of the presence of amplified PCR product.

PCR product was digested with *DpnI*, purified using QIAquick kit then run on 1% agarose gel along with the template and 1 Kb ladder (Marker) for size confirmation.

According to the gel, an amplified band of around 10 kb was observed suggesting that it corresponds to the desired amplicon.

The amplified DNA was self-ligated, introduced into DH5 α , GM2163 then into *Bt* for protein expression. *Hae*III digestion was regularly performed in order to check the introduction of the right plasmid after each transformation step (Figures 57 and 58).

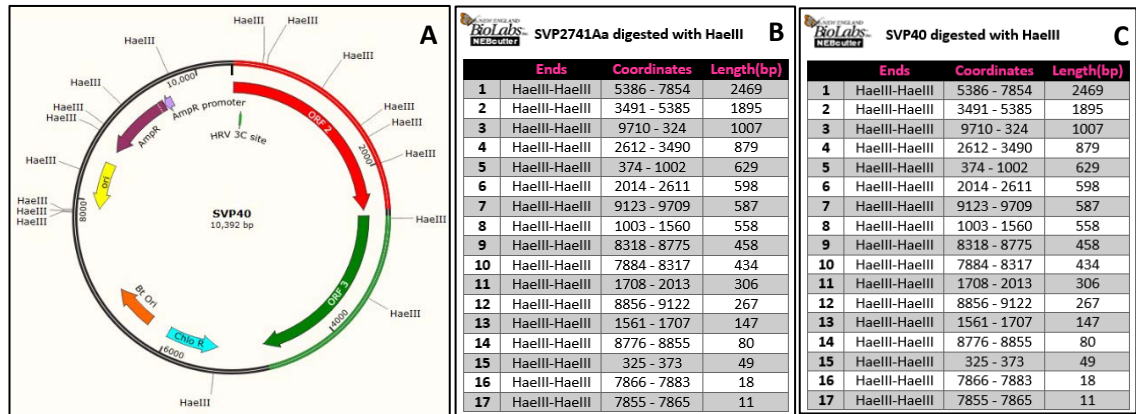


Figure 57: A: Schematic representation of SVP40 plasmid and localisation of different restriction sites of *Hae*III, **B** and **C:** Sizes of different fragments yielded by digestion of SV2741Aa and SVP40 with *Hae*III enzyme respectively (NEBcutter program).

According to figure 57, we should expect to see no difference between the fragments produced after digestion of SVP2741Aa and SVP40 with *Hae*III enzyme. This was confirmed by 1% agarose gel where digested DNAs were run showing similar banding patterns (figure 58B).

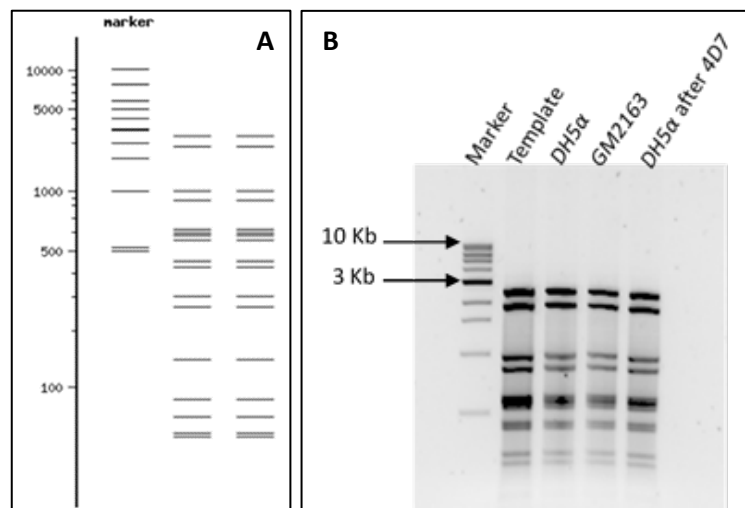


Figure 58: DNA banding pattern after *Hae*III digestion.

A: Predicted DNA banding pattern of SV2741Aa (lane 3) and SVP40 (lane 2) after *Hae*III digestion (NEBcutter), **B:** DNAs were miniprepred after each transformation step using QIAprep kit, digested with *Hae*III then run on 1% agarose gel along with the template (SVP2741Aa).

For a definitive confirmation, the DNA was sequenced and the sequencing result showed that the desired mutation was successfully introduced. This is by comparing the predicted mutated sequence (SVP40) to the sequencing result (Seq), highlighted in yellow, which look identical (figure 59).



Figure 59: Alignment of the predicted sequence of SVP40 (SVP40) and the sequence of the DNA extracted after GM2163 transformation (Seq).

The sequence of the DNA obtained from GM2163 transformation and the expected sequence of SVP40 were aligned using Clustal Omega software. The mutated region is highlighted in yellow.

Then the created mutant was grown and the protein was harvested and run on 7.5% SDS-PAGE along with Cry41Aa (FL) for protein levels and sizes comparison (figure 60).

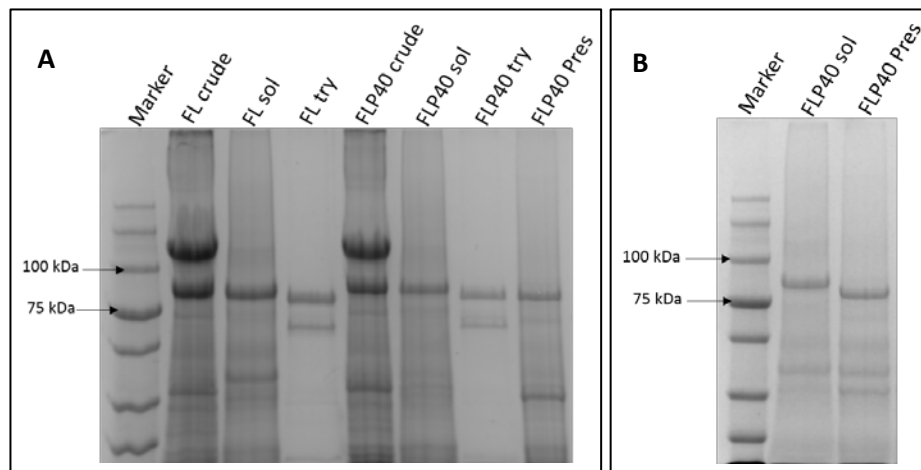


Figure 60: SDS-PAGE analysis of FLP40 protein levels and sizes compared with Cry41Aa full length (FL).

Crude FLP40 and Cry41Aa (FL) were solubilised for 1 hour at 37°C in 50 mM sodium carbonate (pH 10.5) in the presence of 5 mM DTT and activated with trypsin (1 mg/ml) for 1 hour at 37°C or with PreScission (130 µg/ml) for 16 hours at 4°C. The samples were then run on 7.5% SDS-PAGE gel.

SDS-PAGE gel showed a successful expression of the mutated protein. The molecular weight of PreScission activated toxin looked smaller to that of the solubilised core (figure 60B) suggesting that the cleavage with PreScission protease was successful but similar to trypsin digestion.

The level of toxicity of this mutant was then evaluated on HepG2 and the results showed that the PreScission activated toxin significantly decreased cell viability (figure 61). Therefore Cry41Aa toxin could be activated with PreScission protease and N-terminal activation alone is sufficient for toxicity.

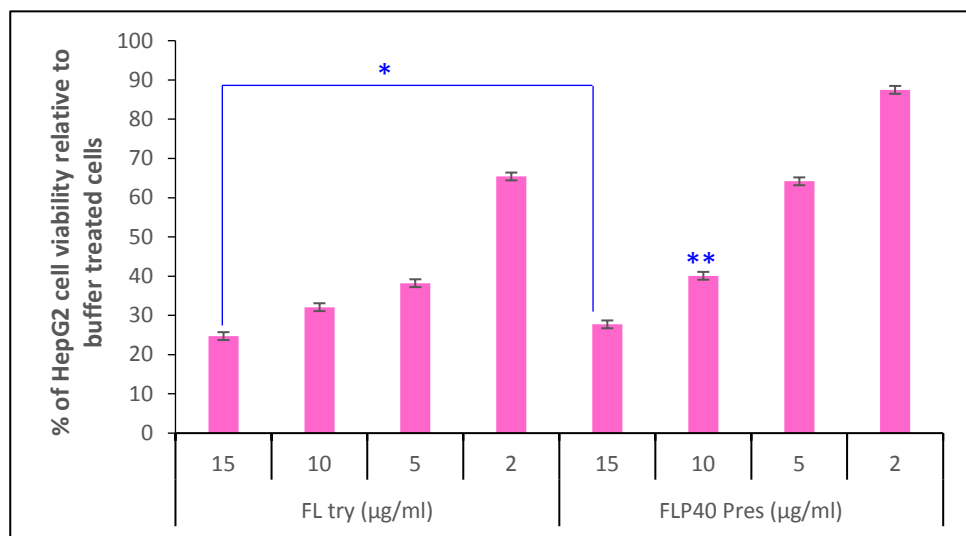


Figure 61: Evaluation of the level of toxicity of FLP40

HepG2 cells were seeded at a density of 25×10^4 cells/ml. The next day the cells were treated with different concentrations of trypsin activated Cry41Aa (FL try) (15, 10, 5, 2 µg/ml) and PreScission activated FLP40 (FLP40 Pres) (15, 10, 5, 3, 2 µg/ml). 24 hours later, cell viability was measured using CellTiter-Blue. Ttest was used to calculate the p values: *p= 0.19 and **p=8.4E-05

- **Creation of Δ RP40**

The same primers as the ones utilized for the creation of FLP40 were used in order to ensure the substitution of the 8 aa (PreScission protease recognition site) at the N-terminus of the protein and therefore to create a protein that could be cleaved with PreScission protease only at the 40th aa in the N-terminal region.

The PCR (PFU Ultra 10 Kb) was set up overnight on SVP2741AaΔR plasmid and the resultant amplicon was then digested with *DpnI*, purified and run on 1% agarose gel (figure 62).

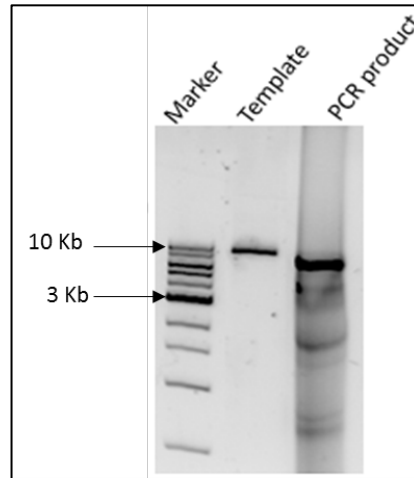


Figure 62: Confirmation of the presence of amplified PCR product.

PCR product was digested with *DpnI*, purified using QIAquick kit then run on 1% agarose gel along with the template and 1Kb ladder (Marker) for size confirmation.

The amplified band shown in figure 62 lane 3 was considered as the DNA of interest since the size was around 10 kb similar to the size of the template used in the PCR reaction.

The amplicon was later self-ligated, inserted into DH5 α , GM2163 and finally into *Bt. Haelll* digestion as well as sequencing were carried out after each transformation step to verify the presence of the correct construct (figures 63, 64 and 65).

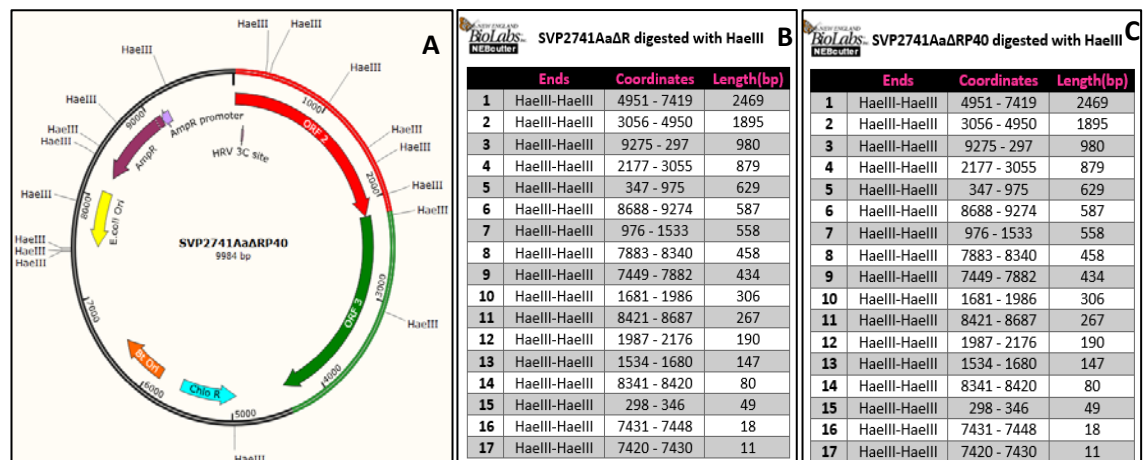


Figure 63: A: Schematic representation of SVP2741AaΔRP40 plasmid and localisation of different restriction sites of *Haelll*, B and C: Sizes of different fragments yielded by digestion of SV2741AaΔR and SVP2741AaΔRP40 with *Haelll* enzyme respectively (NEBcutter program).

The comparison between the fragment sizes produced by digestion of SVP2741AaΔRP40 and SVP2741AaΔR shows no differences (figures 63). This was confirmed by *HaeIII* digests run on 1% agarose gel (figure 64B). In fact, there is no differences between the bands generated after digestion of the DNAs thus extracted and the plasmid used as a PCR template. This result is consistent with them being the correct plasmids.

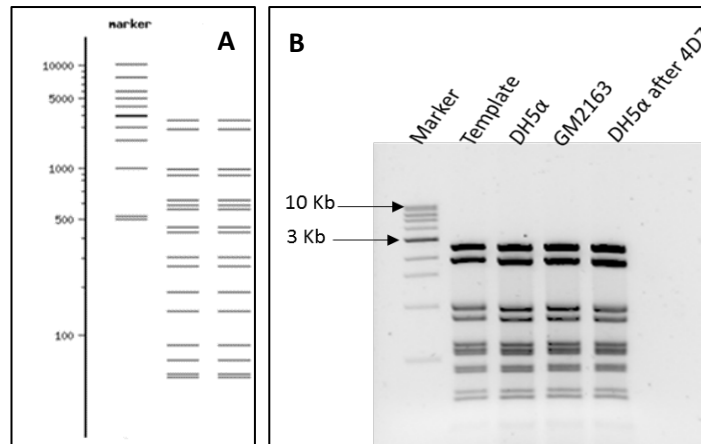


Figure 64: DNA banding pattern after *HaeIII* digestion.

A: predicted DNA banding pattern of SV2741AaΔR (lane 3) and SVP2741AaΔRP40 (lane 2) after *HaeIII* digestion (NEBcutter), **B:** DNAs were minipreped after each transformation step using QIAprep kit, digested with *HaeIII* then run on 1% agarose gel along with the template (SVP2741AaΔR).

The DNA was then sequenced for final confirmation and according to figure 65 the right mutation was created. In fact based on the alignment of the sequencing result (Seq) and the expected DNA sequence of the mutated protein (ΔRP40), we can see that the mutated region (highlighted in yellow) is identical.



Figure 65: Alignment of predicted sequence of SVP2741AaΔRP40 (ΔRP40) and the sequence of the DNA extracted after GM2163 transformation (Seq).

The sequence of the DNA obtained from GM2163 transformation and the expected sequence of SVP2741AaΔRP40 were aligned using Clustal Omega software. The mutated region is highlighted in yellow.

4D7 (Δ RP40) was grown and the protein of interest was harvested then run on 7.5% SDS-PAGE along with Cry41Aa full length for size comparison (figure 66).

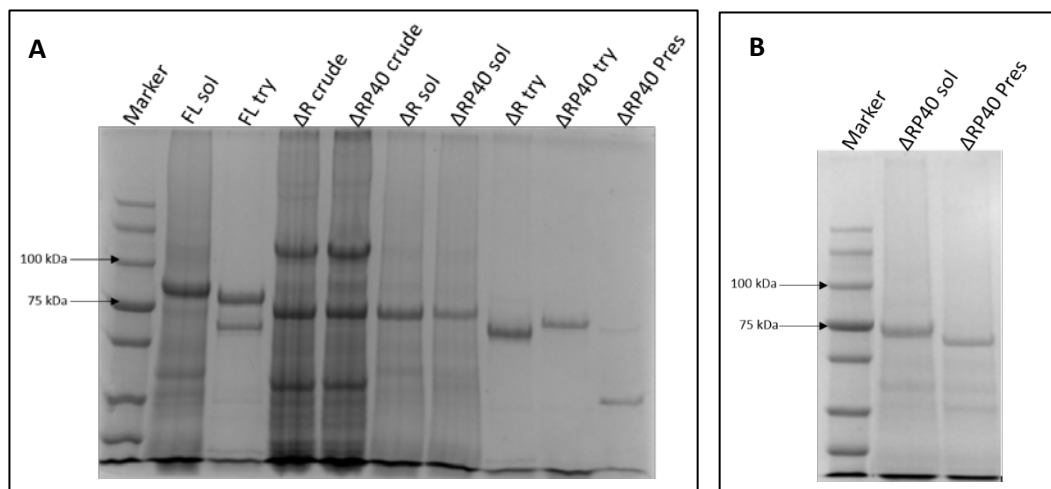


Figure 66: SDS-PAGE analysis of Δ RP40 protein levels and sizes compared with Cry41Aa full length (FL) and Cry41Aa missing the ricin domain (Δ R).

Crude Δ RP40, Δ R and Cry41Aa (FL) were solubilised for 1 hour at 37°C in 50 mM sodium carbonate (pH 10.5) in the presence of 5 mM DTT and activated with trypsin (1 mg/ml) for 1 hour at 37°C or with PreScission (130 μ g/ μ l) for 16 hours at 4°C. The samples were then run on 7.5% SDS-PAGE gel.

According to figure 66, the protein was well expressed and could be cleaved with PreScission protease producing smaller protein compared with the solubilised core (figure 66B). SDS-PAGE gel also showed that Δ RP40 Pres looks slightly bigger than the trypsin activated Δ R suggesting that possibly, the cleavage site of trypsin is downstream of the 40th aa which is consistent with the previous finding and/or the existence of C-terminal cleavage.

Δ RP40 toxicity level towards HepG2 was later evaluated and showed that it exhibits only slightly higher effect than FLP40 suggesting that C-terminal cleavage plays little or no role in toxicity unless cleavage occurs before the ricin domain junction (figure 67).

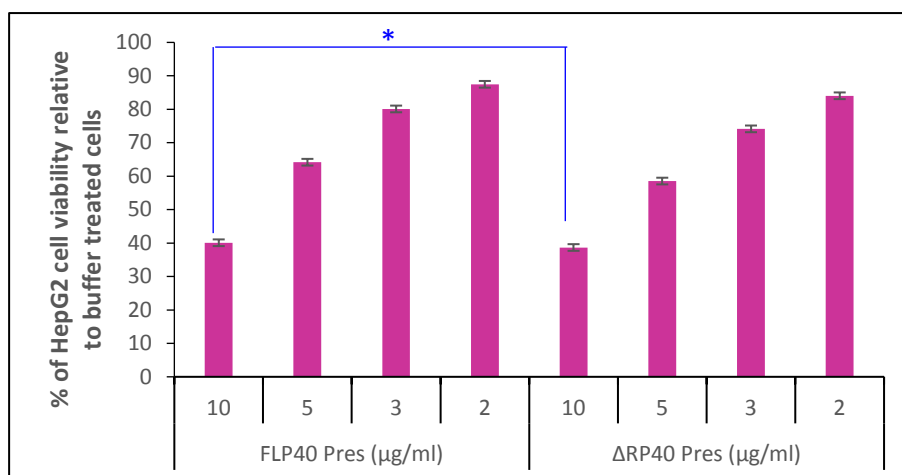


Figure 67: Evaluation of the level of toxicity of FLP40.

HepG2 cells were seeded at a density of 25×10^4 cells/ml. The next day the cells were treated with different concentrations of PreScission activated FLP40 (FLP40 Pres) (10, 5, 3, 2 μg/ml) and PreScission activated ΔRP40 (ΔRP40 Pres) (10, 5, 3, 2 μg/ml). 24 hours later, cell viability was measured using CellTiter-Blue. Ttest was used to calculate the p value: * $p=0.4$ (p values for all other concentrations used were calculated and are >0.05)

Because the level of toxicity of the P40 mutants was slightly lower than that of the trypsin activated Cry41Aa full length, the question was whether C-terminal cleavage could have affected the activity of the protein.

To confirm the previous findings, the created mutants (activated/solubilised) as well as full length protein were purified using anion exchange FPLC. Their concentrations were determined by densitometry using different dilutions of bovine serum albumin (BSA) as protein standard and the Image J program. The level of toxicity of these mutants was evaluated on HepG2 cell line using CellTiter-Blue cell viability assay and their EC_{50} s (Effective concentration of the drug that gives half-maximal response) were determined using SPSS software (Statistical Package for the Social Sciences), Probit Regression analysis (figures 68 and 69). This would enable us to investigate if the mutations created on Cry41Aa would have affected the structure of the protein leading to a possible change of cleavage site(s) and therefore possibility of affecting the protein functionality.

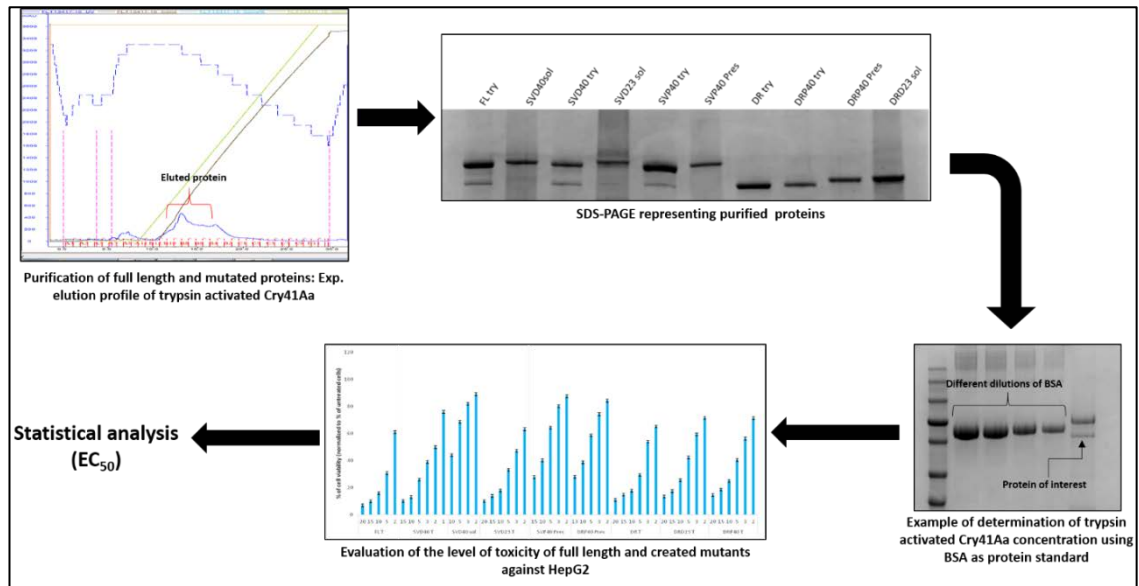


Figure 68: Diagram summarising different steps followed for EC₅₀ determination of the proteins of interest.

After harvest, solubilisation and activation with the appropriate protease, the proteins of interest were ÄKTA purified and run on SDS-PAGE gel for size comparison. After determination of their concentrations, their cytotoxic effect was assessed on HepG2 cells using CellTiter-Blue assay, then EC₅₀s were determined using SPSS software, Probit Regression analysis.

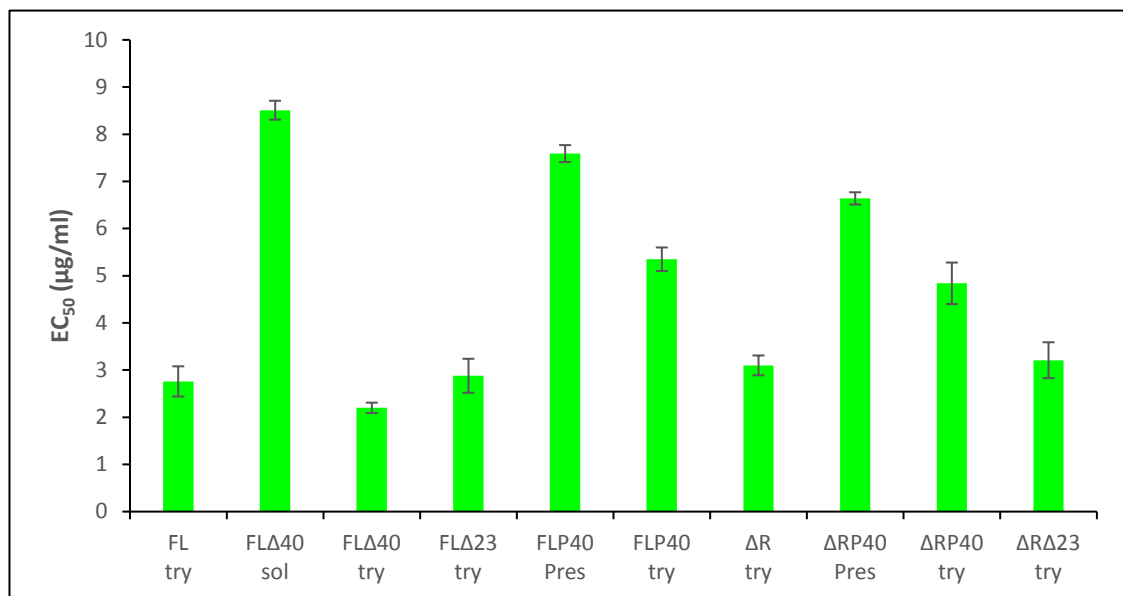


Figure 69: Evaluation of the level of toxicity of purified (solubilised/activated) mutants on HepG2 cell line.

HepG2 cells were seeded at a density of 25×10^4 cells/ml. The next day the cells were treated with different concentrations of purified trypsin activated Cry1Aa and solubilised/activated mutants. 24 hours later, cell viability was measured using CellTiter-Blue. The EC₅₀s were determined using SPSS software.

According to figure 69, substitutions but not deletions created at the N-terminus of Cry41Aa seem to have an effect on the activity of the protein. In fact, trypsin activated mutants which comprise the deletions presented similar EC_{50} as the trypsin activated full length unlike trypsin activated P40 mutants.

PreScission activated P40 mutants were still less toxic than trypsin activated Cry41Aa suggesting that either the lysine (40th aa) is not the trypsin N-terminal cleavage site, C-terminal cleavage is involved in toxicity or the insertion of the recognition site of PreScission protease may have affected the protein functionality.

The hypothesis where the cleavage site might be different from the lysine (40th aa) was adopted. This is based on Yamashita et al finding in 2005 where they sequenced the N-terminus of PK activated Cry41Aa showing that the cleavage occurs at the 60th aa. Moreover, the presence of an arginine (trypsin cleavage site) at the 63rd amino acid position and because PK and trypsin activated Cry41Aa showed almost the same sizes of bands: upper band around 76 kDa and lower band around 65 kDa (figure 70), this led to the hypothesis that cleavage with trypsin might occur at this region. Based on this hypothesis, a mutation was created at this position where PreScission recognition site was introduced.

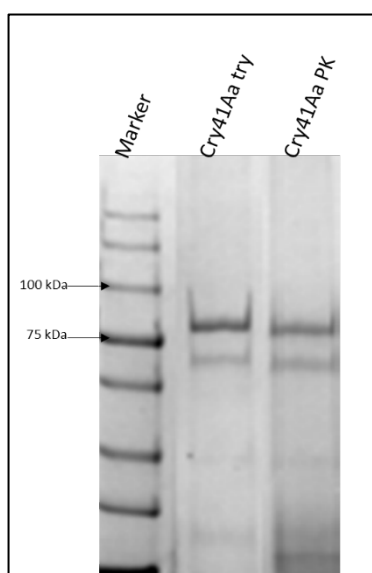


Figure 70: SDS-PAGE gel showing similar protein banding profile between trypsin and PK activated Cry41Aa.

Crude Cry41Aa full length was solubilised for 1 hour at 37°C in 50 mM sodium carbonate (pH 10.5) in the presence of 5 mM DTT and activated with trypsin (1 mg/ml) or proteinase K (0.01 mg/ml) for 1 hour at 37°C. The samples were then run on 7.5% SDS-PAGE gel.

The engineered protein (FLP60) was successfully expressed however cleavage by PreScission was unsuccessful (data not shown).

In order to reveal the N-terminal cleavage site of trypsin activated Cry41Aa, another attempt at N-terminal sequencing was carried out using another technique for sample preparation. As per manufacturer's instructions, sample was activated with trypsin (MS-grade), purified using anion exchange chromatography, desalted then blotted on Polyvinylidene difluoride (PVDF) membrane. The membrane was stained with Ponceau S, destained with distilled water then sent for sequencing (figure 71).

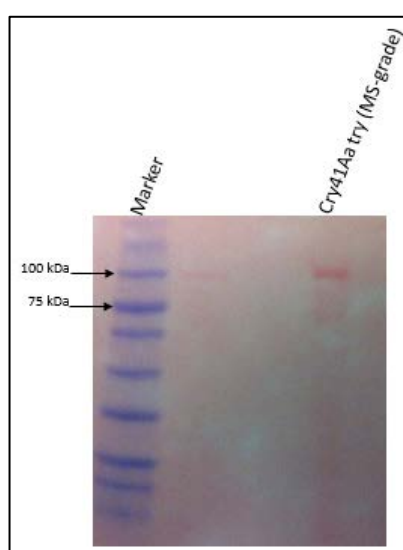


Figure 71: PVDF membrane showing blotted Cry41Aa activated with MS-grade trypsin along with protein marker. Crude Cry41Aa full length was solubilised for 1 hour at 37°C in 50 mM sodium carbonate (pH 10.5) in the presence of 5 mM DTT and activated with MS grade trypsin (1 mg/ml) for 1 hour at 37°C. The toxin was then purified using anion exchange chromatography, desalted, concentrated then run on precast 4-20% gel. The protein was blotted onto a PVDF membrane which was stained with Ponceau S, destained with distilled water then sent for sequencing.

The sequencing was successful and showed that the N-terminal cleavage site occurs at the 23rd aa (figure 72). A surprising result especially because it is not consistent with the previous finding where deletion of the N-terminal 23 aa did not lead to the activation of the toxin in addition to no major role of C-terminal cleavage in toxicity.

N terminus		A	
Residue			
1	Y		
2	P		
3	F		
4	A		
5	Q ?		
6			
7			

B	
MNQNCNNGYEV LNSGKGYCQP	R YFFAQAP
GSELQNMGYKEWMNMCTSGDPTVLGEGYSA	

Figure 72: A: Protein sequence report (Alta Bioscience). B: N-terminal region of Cry41Aa: with the letter written in bold corresponds to the 23rd aa (arginine) and the sequence highlighted in red is the sequence downstream the arginine residue.

Therefore, the level of toxicity of the same sample, which was used for sequencing, towards HepG2 was evaluated. According to our results, it appeared that this toxin had no effect on HepG2 cell line (figure 73).

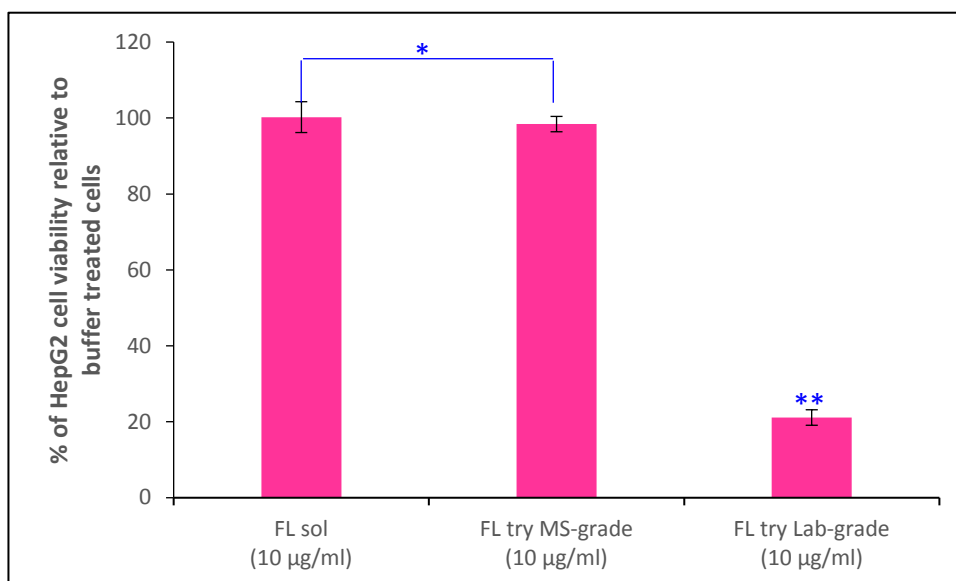


Figure 73: Assessment of the level of toxicity of Cry41Aa activated with MS-grade trypsin.

HepG2 cells were seeded at a density of 25×10^4 cells/ml. The next day the cells were treated with a concentration of 10 µg/ml of solubilised Cry41Aa, activated Cry41Aa with pure MS-grade trypsin and activated Cry41Aa with lab-grade trypsin (Promega). 24 hours later, cell viability was measured using CellTiter-Blue. Ttest was used to calculate the p values: *p=0.34 and **p=1.51E-06

According to figure 73, at a concentration of 10 µg/ml, Cry41Aa activated with MS-grade trypsin had no effect on HepG2 cell line similarly to the protoxin (FL sol). On the other

hand this protein, when activated with lab-grade trypsin, significantly decreased HepG2 cell viability.

Therefore we decided to sequence Cry41Aa activated with lab-grade trypsin (same sample that was used in the above cell assay). Same protocol was used for sample preparation (figure 74).

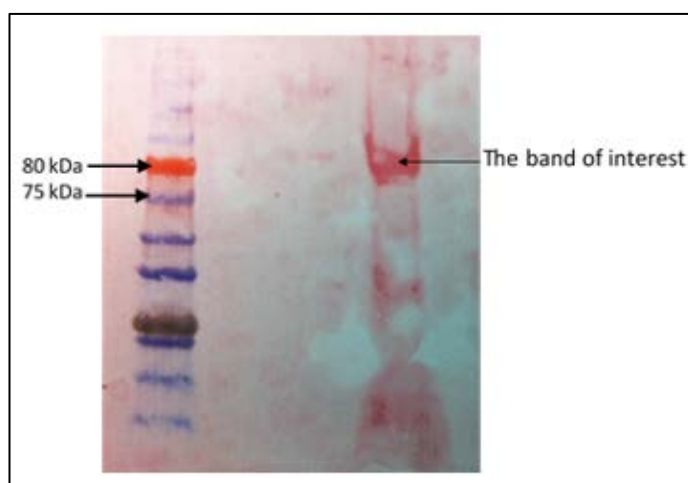


Figure 74: PVDF membrane showing blotted Cry41Aa activated with non-pure trypsin along with protein marker. Crude Cry41Aa full length was solubilised for 1 hour at 37°C in 50 mM sodium carbonate (pH 10.5) in the presence of 5 mM DTT and activated with lab-grade trypsin (1 mg/ml) for 1 hour at 37°C. The toxin was then purified using anion exchange chromatography, desalted, concentrated then run on precast 4-20% gel. Then the protein was blotted on PVDF membrane, stained with Ponceau S, destained then was sent for sequencing.

The N-terminal sequencing of this protein was successful. Surprisingly the result showed that the cleavage site resides after the 58th aa which corresponds to a tyrosine (figure 75).

N terminus			A
Residue		Minor	
1	S	d ?	
2	A		
3	D		
4	V		
5	-		
6			
7			

B

MNQN CNNGYEVLNSGKGYCQPRYPFAQ
 APGSELQNMGYKEWMNMCTSGDPTVLGE
 G**Y**SADVRDAVITSINIASY

Figure 75: A: Protein sequence report (Alta Bioscience). B: N-terminal region of Cry41Aa: with the letter written in bold corresponds to the 58th aa (tyrosine) and the sequence highlighted in red is the sequence downstream the tyrosine residue.

According to figure 75, it appeared that cleavage occurs at the tyrosine residue which is not a trypsin cleavage site. Therefore the 99% pure trypsin from Melford is contaminated with an enzyme that can cleave here –most likely chymotrypsin and this cleaves the N-terminus of Cry41Aa at that position leading to protein activity.

The importance of the residues downstream of this chymotrypsin cleavage site in toxicity was also observed with FLP60 mutant which lost its toxicity when activated with lab-grade trypsin (figure 76). This could be explained by the fact that the tyrosine residue was substituted with the PreScission protease recognition site.

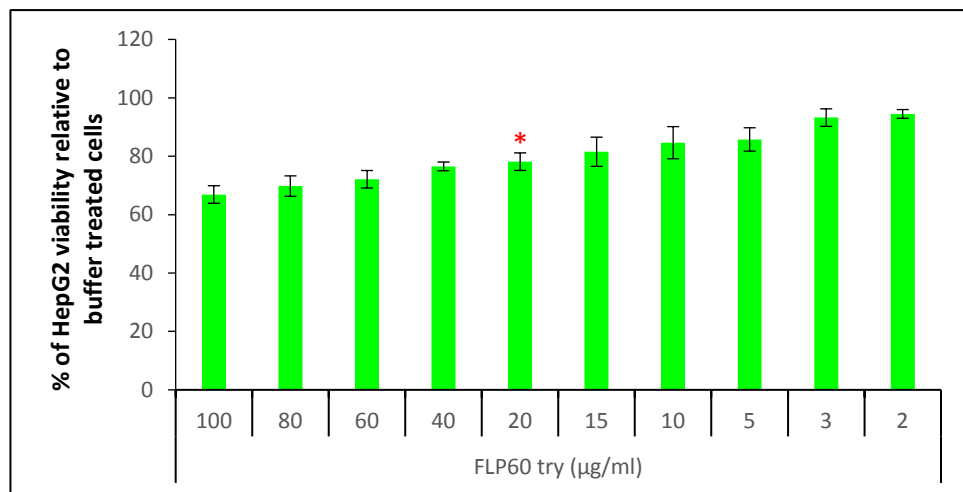


Figure 76: Evaluation of the level of toxicity of activated FLP60 with lab-grade trypsin.

HepG2 cells were seeded at a density of 25×10^4 cells/ml. The next day the cells were treated with different concentrations of trypsin activated FLP60 (FLP60 try) (100, 80, 60, 40, 20, 15, 10, 5, 3, 2 µg/ml). 24 hours later, cell viability was measured using CellTiter-Blue. Ttest was used to calculate the p value: *p=0.02

In fact, a significant effect of the toxin on HepG2 cell line could be seen starting from a concentration of 20 µg/ml. The EC_{50} of this mutant is greater than 100 µg/ml which is more than 50 fold compared with the EC_{50} of trypsin activated Cry41Aa (2.76 µg/ml) (figure 69).

4.4 Discussion

The processing of Cry protoxins which belong to the 3-domain group has been well described. Cleavage of these toxins usually results in the removal of N-terminal peptides, and occasionally C-terminal peptides in larger protoxins. It has previously been shown that the N-terminal cleavage is essential for toxin action. This is the case for insecticidal and anti-cancer Cry toxins. In fact, according to our results N-terminal cleavage alone was sufficient to activate Cry41Aa. This was shown by the deletion of 40 aa at the N-terminus (FL Δ 40) which caused a significant decrease in HepG2 cell viability, also P40 showed a high cytotoxic effect on this cell line when cleaved at the 40th aa at the N-terminus with PreScission protease. Previous studies have shown that cleavage of the N-terminus of parasporin-2 toxin was essential for its cytotoxic activity against MOLT-4 cell line, whereas C-terminal digestion was required for rapid cell injury (Kitada et al., 2006). In addition, protease processing of Parasporin-1 (81 kDa) occurs on the N-terminal region and produces an active form consisting of 15 and 56 kDa polypeptides toxic to cancer cells (Ohba et al., 2009). In case of insecticidal toxins, lack of cleavage at the N-terminus of a variant of *Bt* Cry1Ac by trypsin was unable to form pores in vitro in *Manduca sexta* brush border membrane vesicles and had reduced insecticidal activity in vivo (Bravo et al., 2002). Besides, the full-length (72 kDa) form of Cry11A was highly toxic to mosquito larvae whereas the truncated form of the protein with a 9.6 kDa deletion at the N-terminus was non-toxic. Based on this result, Pang et al suggested that most of the N-terminal region either directly or indirectly is required for toxicity (Pang et al., 1992).

Although PreScission activated FLP40 caused a significant decrease in HepG2 cell viability, its toxic effect was still lower than that of trypsin activated full length. This could be due to a possible role of C-terminal cleavage in toxicity, N-terminal cleavage not occurring at the 40th aa or the mutations made causing miss-folding of the protein. This difference in toxicity between full length and truncated toxins was previously observed in the Cry1Ac crystal protein from *B. thuringiensis subsp kurstaki* strain HD-73 where the 68 kDa N-terminal peptide was shown to be sufficient to kill *Manduca sexta* insects but at a lower level than the full length gene product. Based on this result Adang

et al suggested that this may be due to the loss of an active region located in the C-terminus of the protein (Adang et al., 1985). Various other studies showed that C-terminal cleavage plays an important role in Cry toxicity. In fact, Parasporin-5, expressed as a 33.8 kDa inactive protein, exhibited cytotoxic activity towards human leukemic T cells (MOLT-4) only when degraded by protease at the C-terminus to produce an active protein consisting of 29.8 kDa (Ekino et al., 2014). On the other hand, it has been demonstrated that the carboxy-terminal extensions of many Cry toxins mediate the formation of bipyramidal crystals and have no major role in some Cry toxins activity. In fact, deletion of the C-terminal sequence of Cry15Aa showed that this sequence is not required for activity against the codling moth (*Cydia pomonella*) (Naimov et al., 2011). In addition, approximately 400 aa can be removed from the C-terminus of crystal proteins from the Cry1Ab gene from *Bt Berliner* 1715 and *Bt kurstaki* HD-1-Dipel and Cry1Ac of *Bt kurstaki* HD-73 without significant loss of larvicidal activity (Deist et al., 2014).

The insertion of PreScission protease recognition site at the N-terminal region of Cry41Aa may have caused conformational changes that affected the protein functionality. In fact this could be justified by trypsin activated P40 mutants that were still less toxic than the trypsin activated full length. This is also the case of FLP60 that exhibited a significant effect on HepG2 cells only at high concentrations starting from 20 µg/ml. Previous work suggested that some alterations made at the 5' and 3' end to Cry toxin (the Cry1Ab gene from crystals of *B. thuringiensis subsp. kurstaki HD-1-Dipel*) could lead to conformational changes and cause modifications in the proteolytic cleavage patterns of the protein (Schnepf and Whiteley, 1985).

According to our results, the position of N-terminal cleavage was important in Cry41Aa toxicity. In fact, deletion of 40 but not 23 aa at the N-terminus produced an active toxin that was capable of killing HepG2 cells. This could be explained by the fact that it has been previously suggested that the presence of the N-terminal peptide might prevent binding to insect gut membranes which does only occur after proteolytic removal of this peptide.

For instance, proteolytic activation of the Cry2A protoxin with the trypsin results in the removal of 42 aa. It has been proposed that the deletion of this fragment serves to

expose the binding region of the Cry2 toxin suggesting that “this amino terminal cleavage is a rate-limiting step in the toxin binding of Cry2A” which resulted in a 3 fold increase in Cry2A toxicity against *Spodoptera littoralis* and *Agrotis ipsilon* (Mandal et al., 2007). In addition, the structures for the Cry3Aa and Cry1Aa toxins revealed that the N-terminal region masks a region of the toxin believed to be involved in the interaction between the toxin and the brush border membrane of the target insect (Bravo et al., 2002). Therefore the hypothesis is that as for the other 3 domain toxins mentioned above, the N-terminal region of Cry41Aa may be interfering with binding and deletion of the first 23 aa was not sufficient to expose the binding site of Cry41Aa whereas deletion of 40 aa led to the exposure of this region. In order to confirm this finding structural and binding analysis of both mutants needed to be carried out.

We have also shown that the N-terminus of the protein plays an important role in protein expression/crystallization. In fact deletion of 40aa at the N-terminus led to a weak expression of the protein. Deletion of 60 aa led to major conformational changes resulting in failure of the protein expression. Research with mutant toxins indicated that toxin stability and or/expression levels are affected by N-terminal amino-acid sequence. In fact, expression of Cry1C toxins with truncated N-termini was not successful suggesting that the requirement of the N-terminus is important to cell viability and toxin stability and/or expression (Oppert, 1999). It has previously been observed that the lack of N-terminal peptide of engineered Cry1Ab toxin expressed in *Escherichia coli* severely affected the growth of these cells. The expression level of N-terminally truncated Cry1Ca toxin expressed in *Bt* was much lower than the full-length toxin and the formation of crystals was repressed (Martens et al., 1995).

Prediction of the N-terminal cleavage site was not possible from the created mutations and their effect on the level of toxicity of Cry41Aa neither from the approximate size(s) of fragment(s) yielded after proteolytic activation due to a possible combination of C- and N-terminal cleavages. Mass spectrometry technique was attempted to identify the N-terminal peptide of trypsin activated Cry41Aa. However the results were inconclusive due to the presence of numerous false positives (data not shown). N-terminal sequencing was then the alternative. The method used for the preparation of the sample played an important role in producing comprehensive results. In fact, sequencing failed

when samples (bands) that were sent for sequencing were excised from SDS-PAGE gel however sequencing of the samples that were electroblotted onto a PVDF membrane was successful. This could be explained by the fact that the preferred final purification method mostly used to analyse N-terminal sequence of intact proteins is the use of one-dimensional or two-dimensional gels followed by electroblotting to a high-retention PVDF membrane. Things that could have altered the sequencer performance with the first method maybe presence of high levels of salt, purity or concentration of the sample which according to Speicher et al in 2009, are critical parameters that have to be taken into consideration (Speicher et al., 2009).

N-terminal sequencing of the activated protein revealed that the N-terminal cleavage site occurs at a tyrosine (58th aa) which is a chymotrypsin cleavage site. Chymotrypsin was not able to activate parasporin-1 (Mizuki et al., 2000), however this serine protease was shown to be one of the proteases that has been used to activate Cry toxins that exhibit insecticidal activity. In fact chymotrypsin processing of Cry3A was essential to obtain a toxic product that binds to *L- decemlineata* gut membranes causing the death of these insects (Oppert, 1999). In addition, Cry1A protoxins corresponding to around 130-135 kDa have shown to be able to produce an active 65 kDa toxin core after proteolytic cleavage with chymotrypsin and trypsin-like proteases (Bah et al., 2004).

It is worthwhile mentioning that we concluded that our lab stock of trypsin must have been contaminated with Chymotrypsin.

Conclusions

- 1- N-terminal cleavage alone can partially activate Cry41Aa toxin
- 2- Either C-terminal cleavage or the precise position of N-terminal cleavage may affect toxin activity.
- 3- Cry41Aa cannot be activated by trypsin but presumably by contaminating chymotrypsin in some stocks.

5 Differential proteolysis of Cry41Aa can affect toxicity

5.1 Introduction

Noticeable differences in anticancer cytotoxicity spectra and activity levels were observed between PS-1, PS-2, PS-3 and PS-4 with PS-2 and PS-4 presenting the widest cytotoxicity spectra where both induced cell death in six out of nine human cancer cell lines while PS-3, a typical three domain-type Cry protein, presented the narrowest activity spectrum, showing moderate cytotoxic effect against only two cancer cell lines, HL-60 (Human promyelocytic leukemia cells) and HepG2 (Human liver cancer cells) reviewed by Okassov et al in 2015 (Okassov et al., 2015).

Since activation is a crucial step to achieve toxicity, it has been suggested that the type and/or abundance of proteases is important in contributing to toxin specificity. According to Yamashita et al in 2005, upon treatment with Proteinase K, PS-3 (Cry41Aa) exhibits cytotoxic activity against HepG2 and HL-60 cell lines. It has also been shown that proteolytic activation with proteinase K leads to the production of a major band of 64 kDa that was identified as the toxic moiety. In the previous chapter we have shown that trypsin/chymotrypsin (T/C) activated Cry41Aa is highly toxic to HepG2 and that T/C and PK (Proteinase K) activation produce similar protein banding profiles. In addition Domanska et al in 2016 observed differences in the cytotoxic effect between the two activated forms of the protein on HepG2 cells (Domanska, 2016), therefore it was worthwhile to compare the cytotoxic effect of both activated forms of toxin towards the two cell lines.

In addition, the protein profile of activated Cry41Aa with either T/C or PK led to the production of differential intensity of the upper and lower bands with the upper band in most cases being the major one in contrast to Yamashita et al finding in 2005 (figure 77).

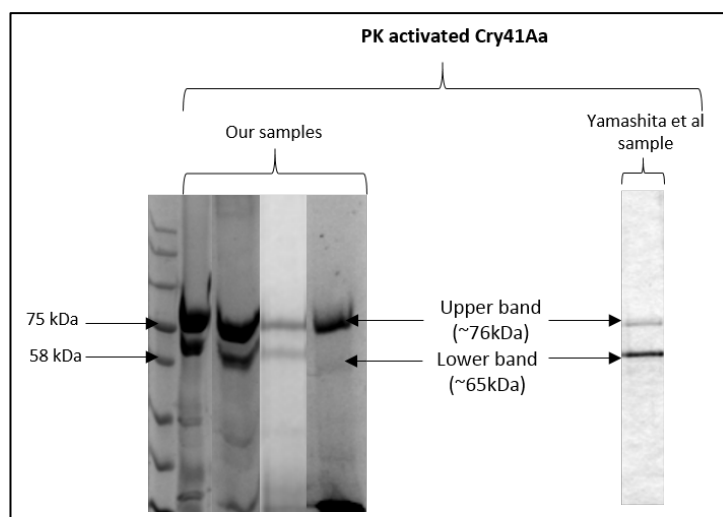


Figure 77: Different intensities of upper and lower bands produced after proteolytic activation of Cry41Aa with PK. Different crude samples of Cry41Aa full length were solubilised for 1 hour at 37°C in 50 mM sodium carbonate (pH 10.5) in the presence of 5 mM DTT and activated with Proteinase K (0.01 mg/ml) for 1 hour at 37°C. The samples were then run on 7.5% SDS-PAGE gel and compared to the PK activated Cry41Aa shown by Yamashita et al in 2005.

Therefore, it was also interesting to figure out which of the two band represents the toxic moiety and whether this is similar for both cell lines.

Based on the multi-step mode of action of Cry toxins where receptor binding is considered one of the critical steps that may have a significant effect on toxin activity/specificity (Jurat-Fuentes and Crickmore, 2017), a preliminary binding study was also carried out in this work in order to investigate the interactions between Cry41Aa and human cancer cells.

5.2 Effect on toxicity of activating with different proteases

PK and T/C activated toxins were purified using anion exchange chromatography. The fractions were desalted, concentrated and the buffer was exchanged. Their concentrations were determined by densitometry using different dilutions of bovine serum albumin (BSA) as protein standard and the Image J program. To assess their toxic effect, CellTiter-Blue cell viability assay was used and their EC_{50} s were determined using SPSS software (figure 78).

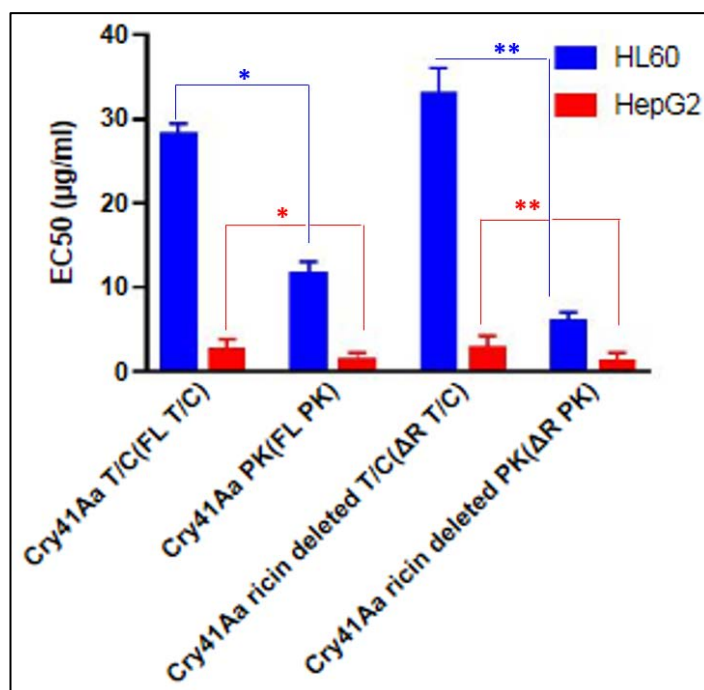


Figure 78: Comparison between the level of toxicity of T/C and PK activated Cry41Aa full length and ΔR on HepG2 and HL-60 cell lines.

HepG2 and HL-60 cells were seeded at a density of 25×10^4 cells/ml. The next day the cells were treated with different concentrations of purified trypsin/chymotrypsin and PK activated Cry41Aa full length and ΔR. 24 hours later, cell viability was measured using CellTiter-Blue assay. The EC₅₀s were determined using SPSS software. * $p=0.001$, ** $p=0.0009$, * $p=0.04$ and ** $p=0.02$

According to figure 78, proteinase K (PK) activated full length (FL) and ricin deleted Cry41Aa (ΔR) are significantly more toxic to HL-60 and HepG2 than when they are activated with trypsin/chymotrypsin (T/C) although the effect is most dramatic with HL-60.

Therefore the toxicity towards the two cell lines (HepG2 and HL-60) depends on the protease used to activate the toxin.

In recent study (Domanska, 2016), it has been shown that Cry41Aa activates P38 MAPK in HepG2 cells. In order to figure out if this response to the toxin is similar in HL-60 cells and whether the difference in toxicity between the two activated forms of Cry41Aa is reflected in p38 phosphorylation, western blot technique was performed using extracts from both cell lines that were exposed to PK or T/C activated Cry41Aa full length or ΔR, T/C activated Cry1Ca, sodium arsenite (AS) or buffer (figures 79 and 80).

Sodium arsenite (a potent p38 inducer) was used as a positive control while T/C activated Cry1Ca was tested as a negative control in this experiment. The reason behind

choosing this insecticidal toxin is that it is expressed in the same acrySTALLiferous *Bt* strain as recombinant Cry41Aa, and that it shares a similar three domain Cry toxin fold with Cry41Aa in addition to exhibiting activity against lepidopteran insects and having no known cytotoxic effect on human cells.

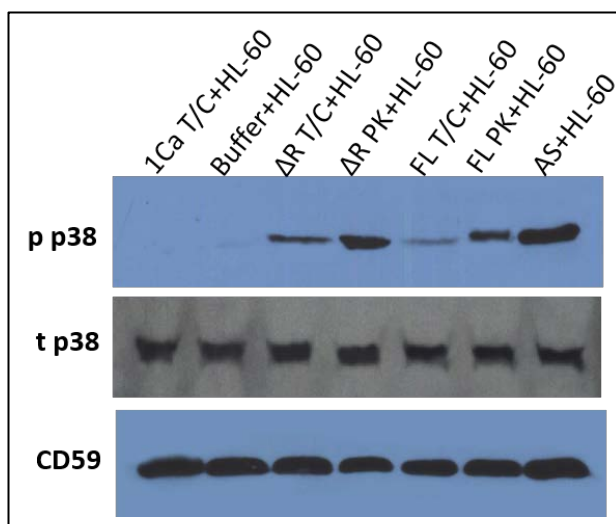


Figure 79: Assessment of p38 activation in toxin treated HL-60 cells.

HL-60 cells were treated with purified T/C, PK activated Cry41Aa or ΔR (12 $\mu\text{g}/\text{ml}$), buffer, sodium arsenite (0.5 mM), or T/C activated Cry1Ca (12 $\mu\text{g}/\text{ml}$) for 30 minutes. Next, cells were lysed in RIPA buffer. 15 μg of protein from each sample were loaded in each lane and analysed by western blot for the presence of total (t p38) or phosphorylated (p p38) p38. CD59 was used as the loading control.

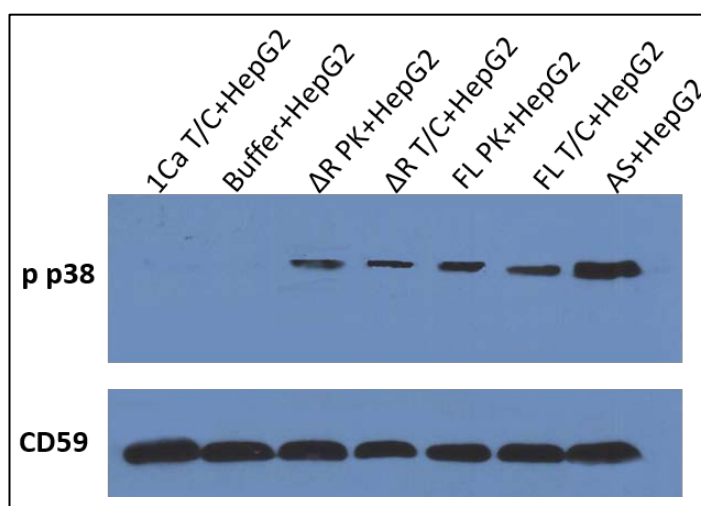


Figure 80: Assessment of p38 activation in toxin treated HepG2 cells.

HepG2 cells were treated with purified T/C activated Cry41Aa (12 $\mu\text{g}/\text{ml}$), buffer, sodium arsenite (0.5 mM), or Cry1Ca (12 $\mu\text{g}/\text{ml}$) for 10 minutes. Next, cells were lysed in RIPA buffer. 15 μg of protein from each sample were loaded in each lane and analysed by western blot for the presence of phosphorylated p38. CD59 was used as the loading control.

Our results showed that p38 phosphorylation was elevated in sodium arsenite treated HepG2 and HL-60 cells yet no signal was produced from the extracts of cells that were exposed to Cry1Ca or buffer.

Regardless of the protease used to activate the toxin, a high signal was produced from the extracts of cells that were exposed to Cry41Aa FL and ΔR in both cell lines. A higher signal was detected in extracts from cells that were treated with PK activated toxin compared with the T/C treated ones particularly in the case of HL-60.

These results indicated that the higher toxic effect of PK activated toxin compared with the T/C treated one towards HepG2 and HL-60 cell lines is reflected in p38 activation.

5.2.1 Involvement of upper and/or lower band(s) in Cry41Aa toxicity

As previously mentioned, the activation of Cry41Aa with either T/C or PK leads to the production of two bands which are around 76 and 65 kDa (figure 70).

In order to investigate the importance of each of the two proteins for toxicity, many attempts were carried out to separate them and assess their individual cytotoxic effect. Initially, purification with gel filtration resin Sephacryl S-200 was used, however the separation was unsuccessful since the two fragments of interest co-eluted (data not shown). Anion exchange chromatography was then used where we were successfully able to separate the upper band from the mixture (figures 81 and 82).

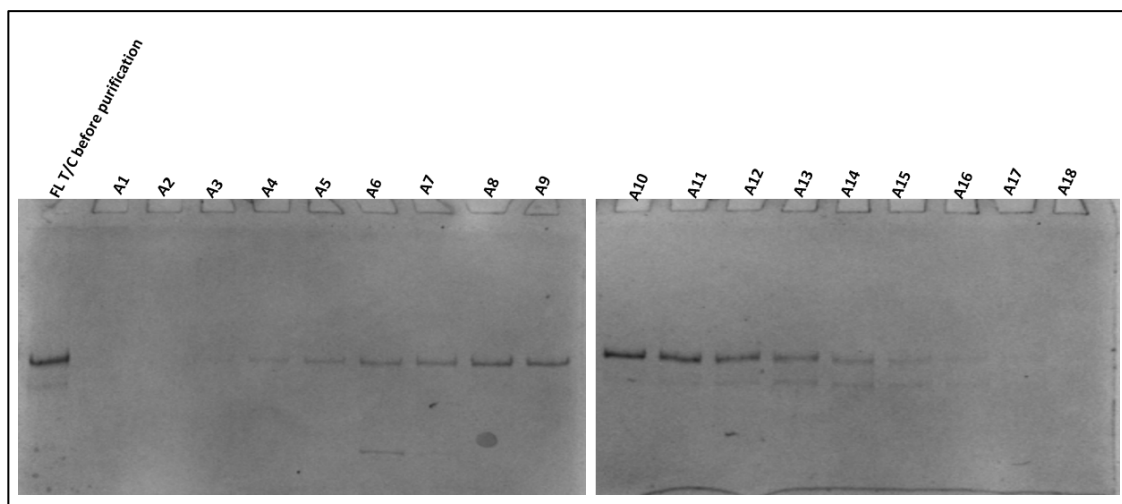


Figure 81: SDS-PAGE representing different fractions (A1 to A18) eluted from FL T/C purification using anion exchange chromatography FPLC.

Fragments produced by T/C activation of Cry41Aa were ÄKTA purified using 10 mM CAPS at a pH of 10.5 and a linear increase of gradient of salt from 0 to 1 M. 0.8 ml fractions were collected and run on 7.5% gel.

According to the gels, the fractions from A3 to A9 except for A6 and A7 (which include a lower molecular weight protein) represent the purified 76 kDa protein. While from fraction A10, the 64 kDa protein started to appear and was co-eluted with the upper one in the rest of the fractions collected.

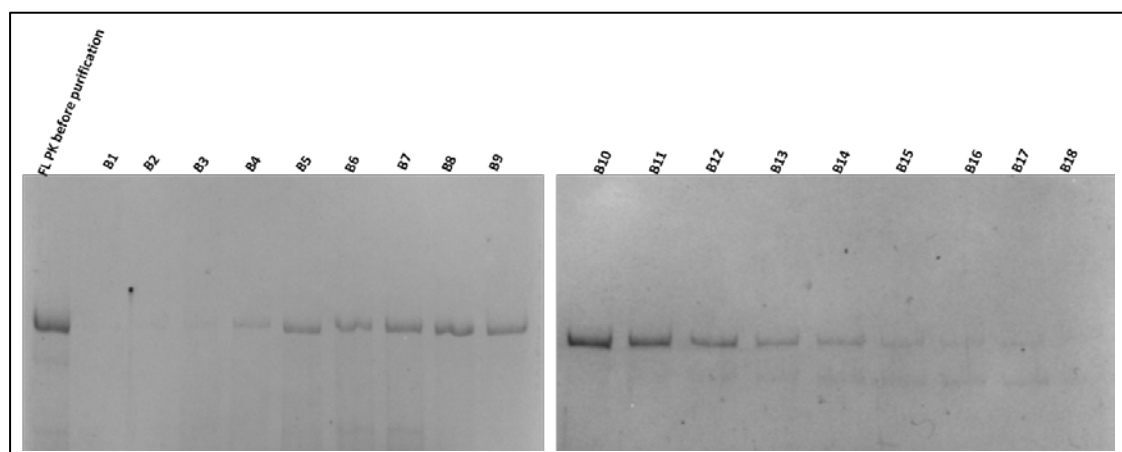


Figure 82: SDS-PAGE representing different fractions (B1 to B18) eluted from FL PK purification using anion exchange chromatography FPLC.

Fragments produced by PK activation of Cry41Aa were ÄKTA purified using 10 mM CAPS at a pH of 10.5 and an increasing gradient of salt from 0 to 1 M. 0.8 ml fractions were collected and run on 7.5% gel

According to figure 82, it appears that B8 and B9 fractions represent the purified upper band whereas from fraction B10 onwards the two bands were co-eluted.

The selected fractions, comprising the upper band, of both activated forms of toxin were desalted, concentrated then run on a 7.5% gel along with purified toxins that include the two fragments in order to check for the presence/absence of the lower band (figure 83).

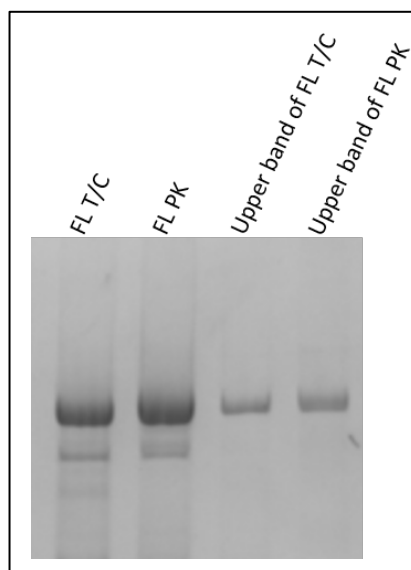


Figure 83: SDS-PAGE showing successful separation of the upper band from the mixture yielded after Cry41Aa activation.

Selected fractions comprising only the upper band of T/C and PK activated Cry41Aa were desalted, concentrated then run on 7.5% gel along with ÄKTA purified toxins which contain the two fragments.

Despite the difference in concentration, our results indicate a successful separation of the 76 kDa protein for both activated forms of Cry41Aa.

The comparison between the cytotoxicity of the upper band and the two bands together would then answer the question of whether the upper band is sufficient for toxicity. Cytopathic effects of the fragments of interest were assessed on both HepG2 and HL-60 cell lines (figures 84 and 85).

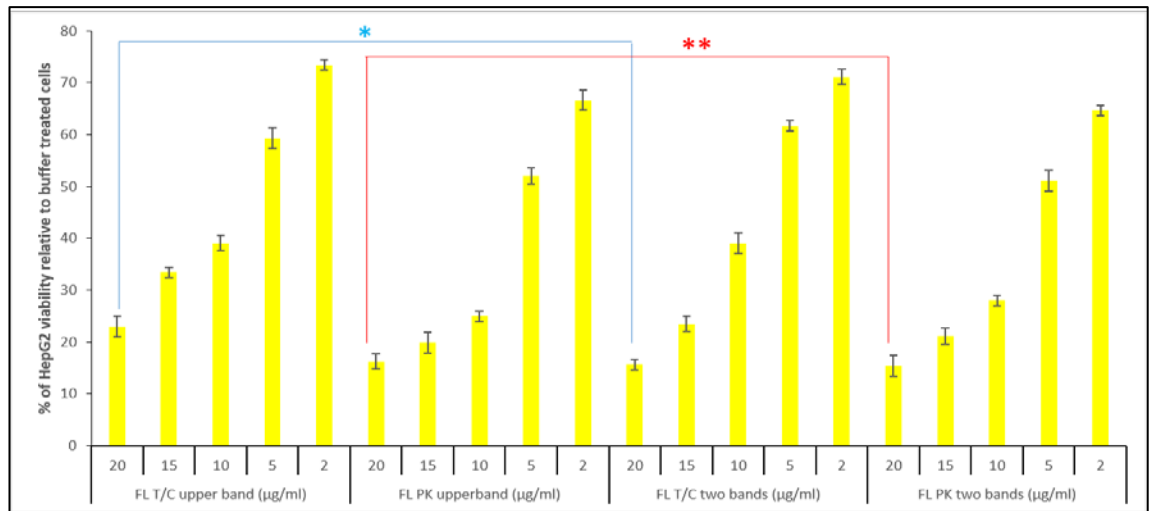


Figure 84: Evaluation of the level of toxicity of T/C and PK activated Cry41Aa and the upper bands yielded post activation on HepG2 cell line.

HepG2 cells were seeded at a density of 25×10^4 cells/ml. The next day the cells were treated with different concentrations of purified T/C and PK activated Cry41Aa and the upper bands produced after activation. 24 hours later, cell viability was measured using CellTiter-Blue. Ttest was used to calculate the p values: * $p=0.15$ and ** $p=0.35$ (p values for all other concentrations used were calculated and are >0.05)

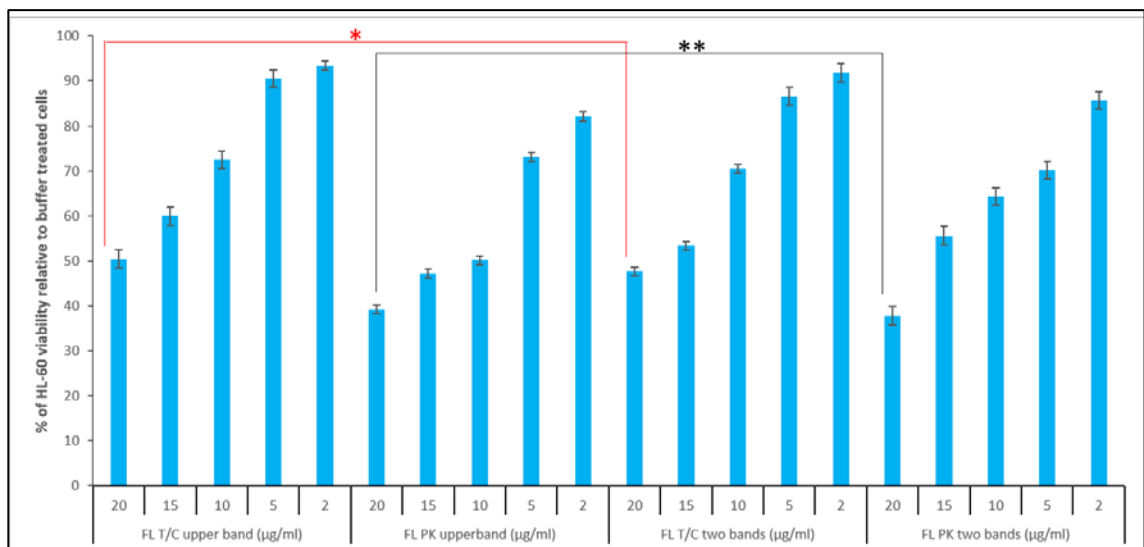


Figure 85: Evaluation of the level of toxicity of T/C and PK activated Cry41Aa and the upper bands yielded post activation on HL-60 cell line.

HL-60 cells were seeded at a density of 25×10^4 cells/ml. The next day the cells were treated with different concentrations of purified T/C and PK activated Cry41Aa and the upper bands produced after activation. 24 hours later, cell viability was measured using CellTiter-Blue. Ttest was used to calculate the p values: * $p=0.11$ and ** $p=0.26$ (p values for all other concentrations used were calculated and are >0.05)

According to our results, it appears that there was no major difference in the level of toxicity between the upper protein and the two proteins together towards HepG2 and

HL-60 cell lines. Therefore the upper band is sufficient for toxicity and no further activation (leading to the production of the lower band) is then needed.

Based on these results and knowing that there is a similar protein banding pattern produced by activation with both trypsin/chymotrypsin and PK, two possibilities were considered: either difference in N-terminal cleavages or C-terminal ones are behind this difference in toxicity.

Knowing the N-terminal cleavage of T/C activated Cry41Aa, sequencing the N-terminus of FL PK was worthwhile to see whether there was a difference in the cleavage site(s).

The same technique, as explained previously (chapter 4 page 113), was used for sample preparation. The protein of interest was blotted onto a PVDF membrane which was then sent for sequencing.

Sequencing the N-terminus of the protein of interest was successful and showed that the N-terminal cleavage of proteinase K occurred after the 60th aa (alanine) (figure 86) which is in agreement with N-terminal sequencing of the lower band protein by Yamashita et al in 2005. Therefore the difference between the upper and lower bands must be the C-terminal cleavage.

A			
N terminus			
Residue			
1	D		
2	V		
3	R		
4	D		
5	A		
6			

B
MNQNCNNGYEVLNSGKGYCQPRYP
FAQAPGSELQNMGYKEWMNMCTSGD
PTVLGEGYS A DVRDAVITSINIAS
YLLSVFPFPPA

Figure 86: A: Protein sequence report (Alta Bioscience). B: N-terminal region of Cry41Aa: with the letter written in bold corresponds to the 60th aa (alanine) and the sequence highlighted in red is the sequence downstream the alanine residue.

The possibility that there might be some cleavage occurring at the C-terminus of the upper band protein which might influence in Cry41Aa higher toxicity, was investigated.

A construct was created where human influenza hemagglutinin (HA) tag was attached to the end of the ricin domain sequence. Following proteolytic activation of the resultant protein, loss or presence of the tag would indicate if cleavage at the C-terminal region of the protein had occurred. The protein designated as FL-HA was created using the same technique that was utilised to create previous variants (see chapter 4 section 4-2-1). The primers used were: forward Primer: TTCCAGATTATGCTTAAAGGTGTGCAACTATCCCTG and reverse primer: CATCATATGGATAAGTGGTTAAGCCAATACCCATAC. FL-HA was successfully created and expressed (figure 87).

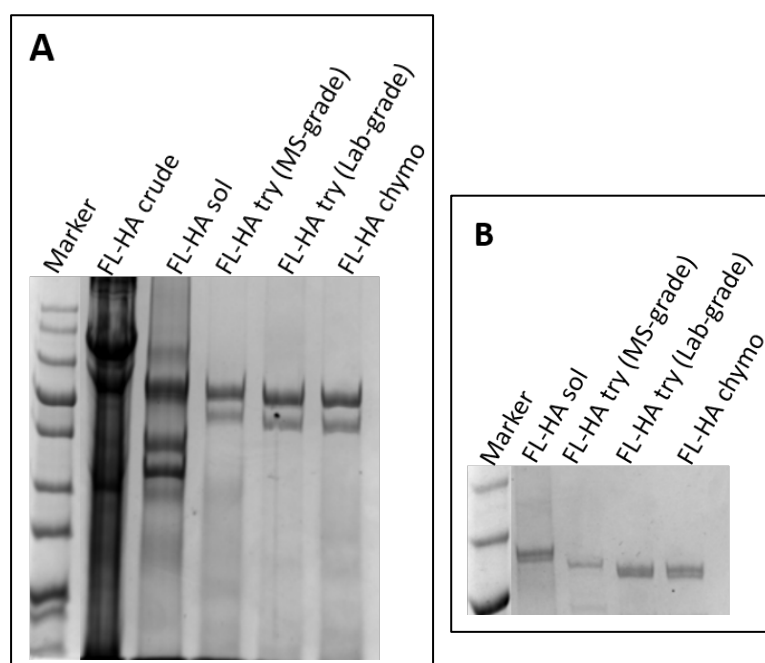


Figure 87: SDS-PAGE showing the expression levels of FL-HA before and after proteolytic activation.

Crude FL-HA protein was solubilised for 1 hour at 37°C in 50 mM sodium carbonate (pH 10.5) in the presence of 5 mM DTT and activated with trypsin (MS-grade), chymotrypsin or trypsin (Lab-grade) (1 mg/ml) for 1 hour at 37°C. The samples were then run on 7.5% SDS-PAGE gel along with protein ladder. **B:** Same samples except for the crude one were diluted and the gel was run for longer time.

According to figure 87A, FL-HA was successfully expressed. The two bands produced by trypsin (MS-grade) activation look slightly bigger than those produced after proteolytic activation with either trypsin (Lab-grade) or chymotrypsin which appeared to have similar banding profile. The difference between the size of the upper bands produced and that of the solubilised core was not clearly visualised. Therefore in order to confirm that these proteins were cleaved, the gel was run for longer time to ensure efficient

separation (figure 87B). The upper bands produced appeared to have smaller size compared with solubilised FL-HA suggesting that cleavage occurred. The protein when cleaved with trypsin (MS-grade) was shown to have a bigger size compared to when it was cleaved with trypsin (Lab-grade) or chymotrypsin. This was consistent with the N-terminal sequencing of the upper bands which showed that trypsin (MS-grade) cleaves at the 23rd aa (figure 72) while trypsin (Lab-grade) which appeared to be contaminated with chymotrypsin, cleaves at the 58th aa (figure 75).

A western blot was later carried out to detect the presence of HA tag in FL-HA before and after proteolytic activation, Δ R-HA (previously created by Etherington et al., unpublished) was used as a positive control and untagged solubilised FL which was used as a negative control (figure 88).

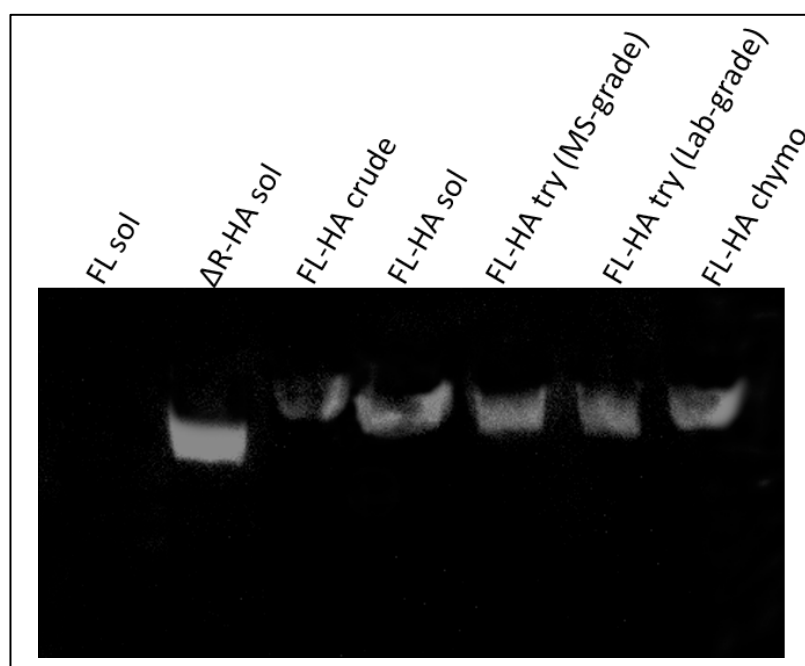


Figure 88: Western blot analysis of HA-tag attachments to FL-HA before and after proteolytic digestion.

Solubilised full length (untagged), tagged Δ R and crude, solubilised and activated (trypsin (MS-grade), trypsin (Lab-grade) and chymotrypsin) FL-HA were run on 7.5% SDS-PAGE gel. 5 μ g of proteins were loaded in each lane. After transfer, the membrane was blocked with 5% milk then incubated with the HRP conjugated anti-HA antibody followed by ECL detection.

According to our results, HA tag was detected in solubilised Δ R-HA but not in solubilised FL which were used as positive and negative controls respectively. The tag was detected in crude, solubilised and activated FL-HA proteins. Regarding the activated samples, HA

was only detected in the upper bands suggesting that no cleavage occurs at the C-terminal region of the protein while it does occur in the lower band which was indicated by the loss of the tag.

These results in addition to previous finding about the upper band being sufficient for Cry41Aa toxicity suggest that C-terminal cleavage does not influence toxicity.

Therefore, we tried to test if only the precise position of N-terminal cleavage might influence Cry41Aa toxicity towards HL-60 cells. For confirmation, the levels of cytopathic effect of the mutants previously created (see chapter 4) were evaluated on HL-60 (figure 89).

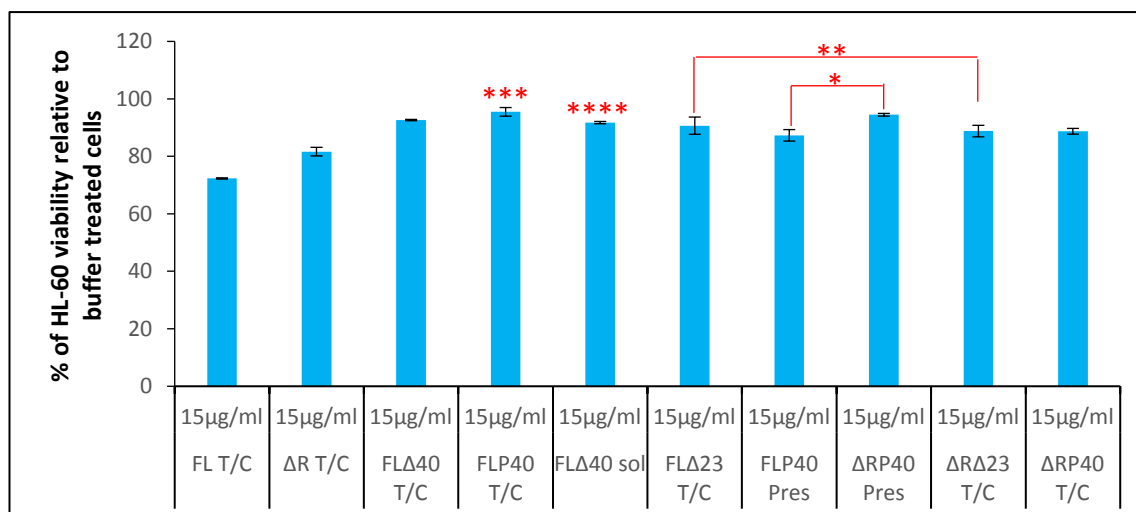


Figure 89: Evaluation of the level of toxicity of purified (solubilised/activated) mutants, Cry41Aa full length and ΔR on HL-60 cell line.

HL-60 was seeded at a density of 25×10^4 cells/ml. The next day the cells were treated with a concentration of 15 µg/ml of purified solubilised/activated mutants, T/C activated Cry41Aa and T/C activated ΔR. 24 hours later, cell viability was measured using CellTiter-Blue. Ttest was used to calculate the p values: * $p=0.19$, ** $p=0.23$, *** $p=0.08$ and **** $p=0.06$

According to our results the created mutants had a negligible cytotoxic effect towards HL-60. In fact, PreScission activated P40 mutants and solubilised FLΔ40 which were toxic to HepG2 cells had no major effect on this cell line. Therefore N-terminal cleavage at the 40th aa does not activate the toxin against HL-60.

Additionally the same cytotoxic effect was observed for PreScission activated FLP40 and Δ RP40, also for FL Δ 23 T/C and Δ R Δ 23 T/C confirming that there is no major role of C-terminal cleavage in toxicity.

Based on these findings:

1. No role of C-terminus in Cry41Aa toxicity.
2. FLP60 (where YSADVRDA residues were substituted with the PreScission protease recognition site) had lost its activity against both HepG2 and HL-60 cell lines when cleaved with either PK or trypsin/chymotrypsin (data not shown).
3. PK activated Cry41Aa is more toxic towards the two cell lines than when activated with trypsin/chymotrypsin.
4. PK cuts two aa beyond T/C.

We formed a hypothesis that DVRDA might be a possible binding site and that the Ser and Ala amino acids are interfering with this binding/toxicity particularly against HL-60.

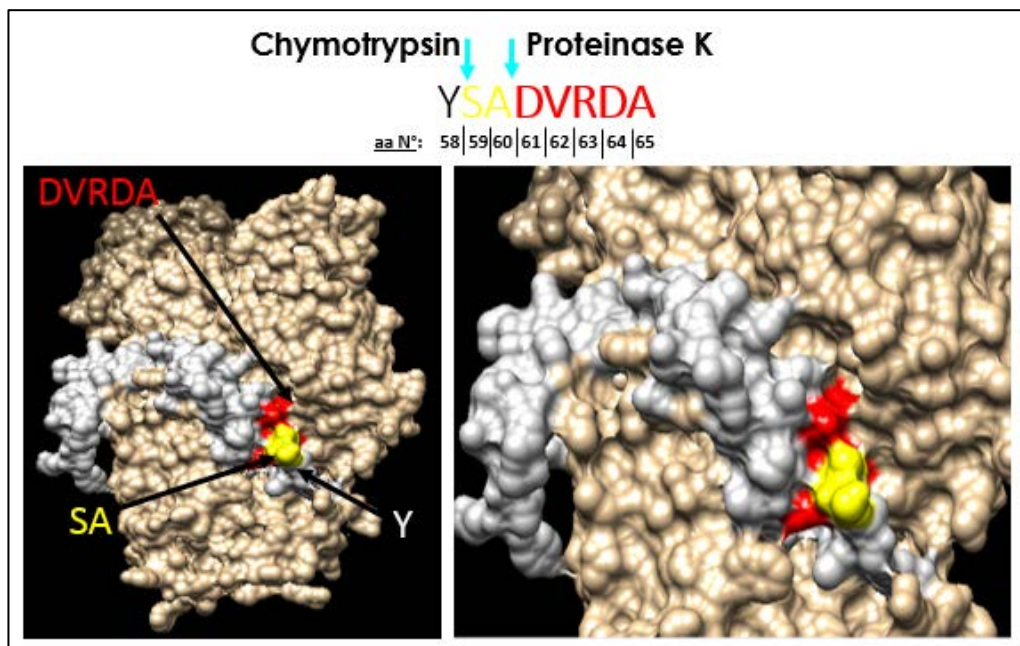


Figure 90: Diagrams showing the surface view of the structure of Cry41Aa modelled by Phyre2 and visualised by Chimera software

The red part represents DVRDA hypothesized to correspond to the binding epitopes, the yellow part represent Ser and Ala aa thought to be interfering with binding and the grey part represents the N-terminal region containing the tyrosine (Y), T/C cleavage site. The figure on the right is the zoomed in form.

According to the predicted 3-D structure of Cry41Aa (figure 90), it is possible that the N-terminal region of the protein is partially obscuring the DVRDA motif. If the 58 amino acids are removed, DVRDA would be partially revealed, however, removal of the Ser and Ala aa as well would result in great exposure of the motif.

To confirm that cleavage after amino acid 60 was responsible for the increased toxicity, we substituted the alanine (60th aa) to a lysine (trypsin cleavage site) in order to ensure cleavage of this protein with trypsin (MS grade) at the same site where PK cleaves. This activated protein should then have the same cytotoxic effect as Cry41Aa when activated with PK.

The engineered protein (AK) was successfully created (forward primer: AAAGATGTAAGGGATGCCGTTATTAC and reverse primer: GCTGTATCCCTCCCCCAG) and expressed. SDS-PAGE analysis suggested that cleavage with MS-grade trypsin was more likely to have occurred at the 23rd aa as previously observed with Cry41Aa full length due to the lack of size difference following cleavage (figure 91).

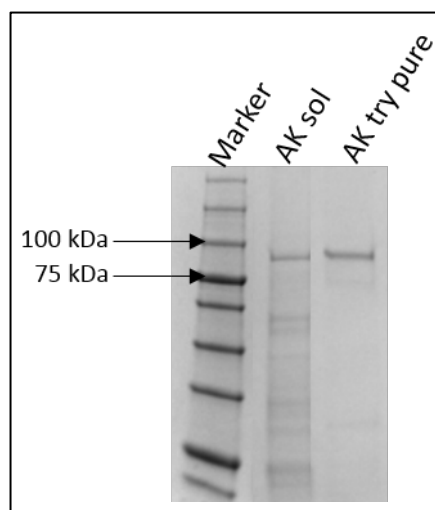


Figure 91: SDS-PAGE showing unsuccessful N-terminal cleavage of AK at the 60th aa.

Crude AK was solubilised for 1 hour at 37°C in 50 mM sodium carbonate (pH 10.5) in the presence of 5 mM DTT and activated with MS-grade trypsin (1 mg/ml) for 1 hour at 37°C. The samples were then run on 7.5% SDS-PAGE gel along with protein ladder.

According to the gel, the MW of both solubilised and trypsin activated AK look similar suggesting that the cleavage at the 60th aa was unsuccessful and it is more likely that, as

in the case of FL, the trypsin did cut at the 23rd aa, a difference in size that has proved difficult to visualise on this gel system.

Bioassays were then performed on HepG2 using this AK mutant treated with different proteases (figure 92).

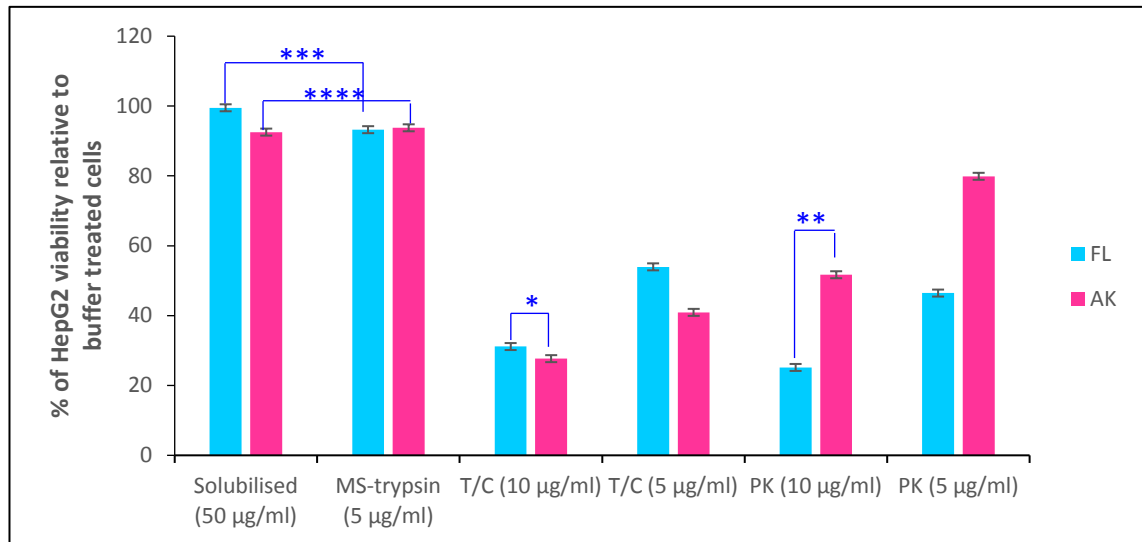


Figure 92: Assessment of the level of toxicity of AK mutant.

HepG2 was seeded at a density of 25×10^4 cells/ml. The next day the cells were treated with different concentrations of trypsin/chymotrypsin, PK and trypsin (MS-grade) activated AK and Cry41Aa full length. 24 hours later, cell viability was measured using CellTiter-Blue. Ttest was used to calculate the p values: * $p=0.2$, ** $p=0.0005$, *** $p=0.11$ and **** $p=0.41$

When activated with MS-grade trypsin, negligible toxic effect was observed for the mutant AK and FL similar to the solubilised proteins. Similar cytopathic effects were observed for trypsin/chymotrypsin activated FL and AK which could be explained by the fact that T/C cleavage site was not changed. However, when activated with PK, AK showed a reduced cytotoxic effect compared with FL which could be due to the substitution of the PK cleavage site that might have led to PK cleaving elsewhere.

An examination of the predicted structure of Cry41Aa in particular the section representing DVRDA, shows that the side chain of the second aspartic acid is protruding from the structure which would provide an easily accessible binding site (figure 93). The positively charged arginine in that sequence might also be important especially that previous study showed that a positively charged aa (lysine) also exists at that position in Cry41Ab (Yamashita et al., 2005), in addition, the importance of positively charged

amino acids in Cry toxin activity was previously observed (explained in the discussion part). Therefore, in order to investigate the possible important role of these amino acids in toxicity, mutations were created at those sites where single substitutions were made to change Arg to Thr (R to T) and Asp to Ala (D to A) in addition to double substitution where RD was changed to TA. This was to figure out whether both Arg and Asp are important or just one of them is crucial for activity.

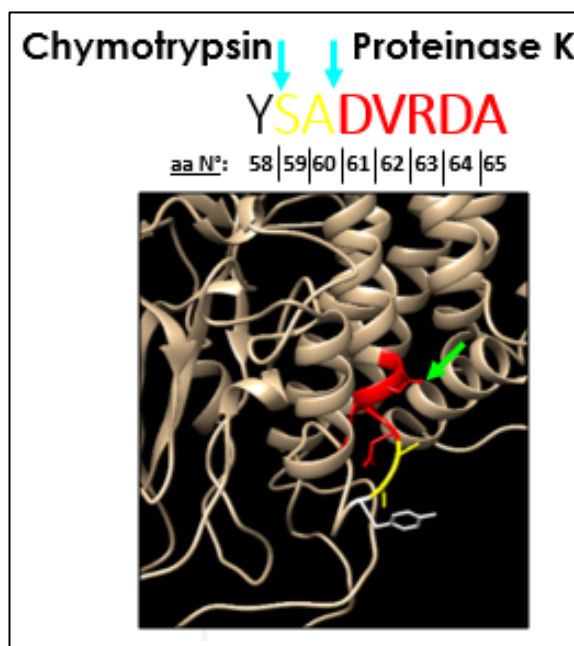


Figure 93: Diagram showing the schematic view of the structure of Cry41Aa modelled by Phyre2 and visualised by Chimera

The green arrow shows the side chain of the aspartic acid that is sticking out of the structure. The red part represents DVRDA, the yellow section corresponds to Ser and Ala residues and the grey part represents the tyrosine (T/C cleavage site).

The mutations were created on a tagged construct (Δ R-HAP40) which will be explained in detail in the next section. The mutants were successfully created and expressed and their cytotoxicity levels were assessed on HepG2 (figure 94) and HL-60 (figure 95) cell lines in order to investigate the effect of the mutations created on the protein activity. Recent study has shown that Cry41Aa is a pore forming toxin (Krishnan et al., 2017) and previous work has shown that the effect of pore forming Cry toxins is initiated with binding and that lack of binding correlates with loss of toxicity. Therefore, if those two amino acids that were substituted are important in binding, the mutants created should be non-toxic.

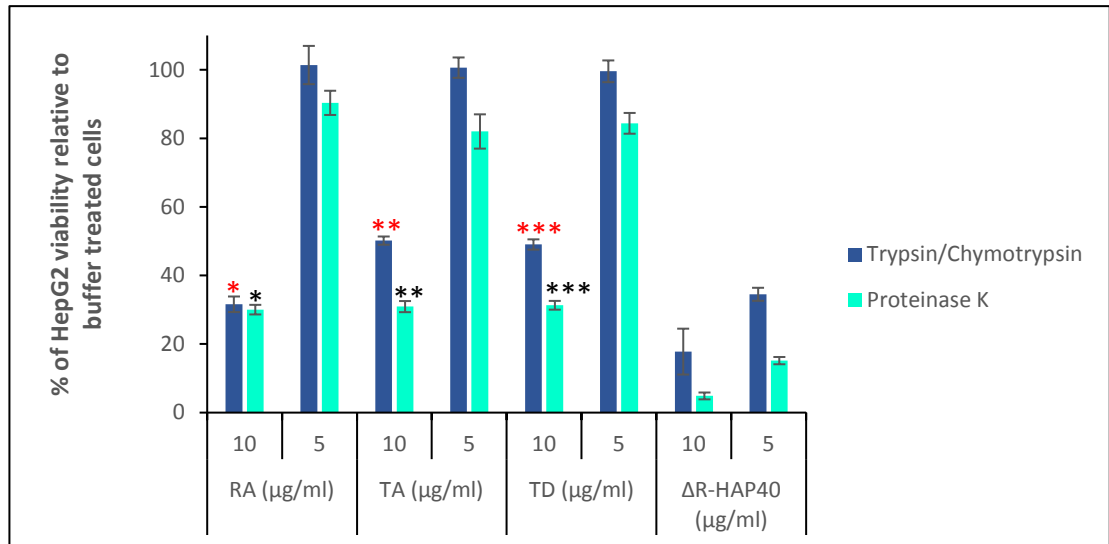


Figure 94: Effect of the mutations created on Cry41Aa protein activity against HepG2.

HepG2 was seeded at a density of 25×10^4 cells/ml. The next day the cells were treated with different concentrations of trypsin/chymotrypsin and PK activated Δ R-HAP40, TD, RA and TA. 24 hours later, cell viability was measured using CellTiter-Blue. Ttest was used to calculate the p values: * $p=0.02$, * $p=4.3E-05$, ** $p=1.53E-04$, ** $p=0.0001$, *** $p=1.4E-04$ and *** $p=4.4E-05$

According to our results, the two activated forms (T/C and PK) of all of the created mutants (RA, TA and TD) presented a reduced toxicity towards HepG2 compared with Δ R-HAP40 protein. Both single and double mutations have affected the protein function. The same result was observed towards HL-60 cell line (figure 95).

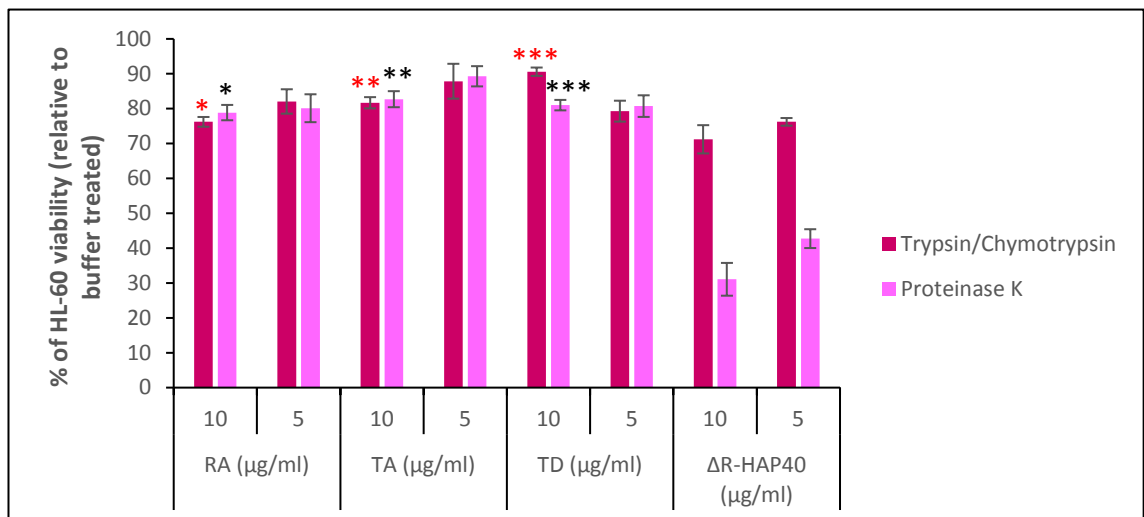


Figure 95: Effect of the mutations created on Cry41Aa protein activity against HL-60.

HL-60 cells were seeded at a density of 25×10^4 cells/ml. The next day the cells were treated with different concentrations of trypsin/chymotrypsin and PK activated Δ R-HAP40, TD, RA and TA. 24 hours later, cell viability was measured using CellTiter-Blue. Ttest was used to calculate the p values with * $p=0.2$, * $p=3.01E-05$, ** $p=0.14$, ** $p=3.5E-05$, *** $p=0.04$ and *** $p=8.24E-05$

This reduced toxicity might be due to the binding possibly being affected. Therefore we set about devising a binding assay.

5.2.2 Cry41Aa labelling

- **Previous problems with HA tag**

Epitope tagging is a technique where a short immunoreactive epitope is fused to a recombinant protein to facilitate its detection. Amongst the epitope tags that are commonly used, HA which is derived from the human influenza hemagglutinin. It has been widely used as a general epitope tag in expression vectors (Zhao and Meresse, 2015).

Knowing that its amino acid sequence (YPYDVPDYA) does not contain an arginine or lysine which would prevent enzymatic processing during activation and because it is easily accessible for detection with antibodies, HA tag was chosen for Cry41Aa labelling.

Based on the knowledge that the ricin domain had no role in Cry41Aa toxicity (Krishnan et al., 2017), which was also confirmed with our results explained in chapter 4, HA tag was attached to ΔR (Etherington et al., unpublished). However, a problem was encountered in tag detection suggesting that the loss of the tag was due to its instability during proteolytic processing or a possible cleavage at the C-terminus of the protein.

To overcome this problem, the lysine which is at the 668th position at the C-terminus, where the T/C cleavage site was suspected to be, was substituted to an alanine. The mutant protein ΔRK -HA was successfully created and expressed.

The proteins of interest were then run on 7.5% gel for checking their sizes and their expression levels (Figure 96).

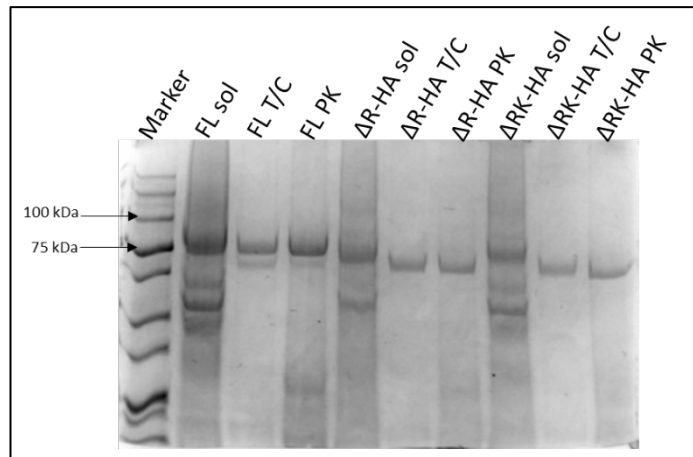


Figure 96: SDS-PAGE showing the expression levels of HA tagged proteins and untagged full length protein.

Crude HA tagged proteins and untagged full length protein were solubilised for 1 hour at 37°C in 50 mM sodium carbonate (pH 10.5) in the presence of 5 mM DTT and activated with trypsin/chymotrypsin (1 mg/ml) or Proteinase K (0.01 mg/ml) for 1 hour at 37°C. The samples were then run on 7.5% SDS-PAGE gel along with protein ladder.

According to the gel, HA tagged proteins were successfully expressed. Solubilised, trypsinised and PK activated ΔR -HA and ΔRK -HA showed the same MWs. PK and T/C digestion led to the production of a single band unlike the full length where proteolytic digestion with PK and T/C yielded two bands which could be explained by the fact that the mutations were created on ΔR . The lack of difference in size between the T/C digested ΔR -HA and ΔRK -HA suggests that C-terminal cleavage might not occur at the lysine substituted. This is based on the knowledge that if it is the case then 46 aa would be lost, a difference in size that should be visualised on a gel.

A western blot was then carried out to detect the presence of HA tag attached to ΔR and ΔRK before and after proteolytic processing using anti-HA antibody (figure 97).

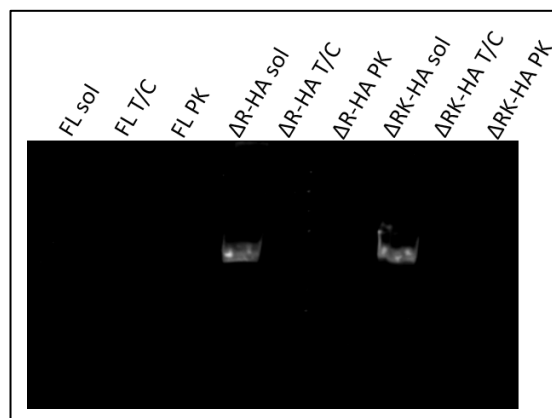


Figure 97: Western blot analysis of HA-tag attachments to proteins before and after proteolytic digestion.

Solubilised, T/C and PK activated full length (untagged) and tagged ΔR were run on 7.5% SDS-PAGE gel. 3 μ g of proteins were loaded in each lane. After transfer, the membrane was blocked with 5% milk then incubated with the HRP conjugated anti-HA antibody followed by ECL detection.

Our results suggested that both proteases (proteinase K and trypsin/chymotrypsin) cleave at the C-terminus of the ΔR proteins as the HA tag was only detected in solubilised ΔR -HA and ΔRK -HA. It also suggests that T/C does not cleave at the lysine which was suspected to be the C-terminal cleavage site because if this was the case we should expect to detect HA in T/C activated ΔRK -HA, however another possibility is that cleavage could occur at this position and somewhere else as well. HA-tag was not detected in solubilised and activated untagged full length which was used as negative control.

The fact that the tag was detected after proteolytic activation of FL-HA but not in the case of ΔR -HA suggest that the C-terminal cleavage site is difficult to be accessed by proteases in the full length form of the protein but becomes more exposed after deletion of the ricin domain.

Knowing that PreScission activation leads to just N-terminal cleavage and because the ricin domain has no role in toxicity, we decided to create ΔR -HAP40 mutant where we could study the binding of this protein without loss of the tag.

- **Creation of ΔR -HAP40**

The primers utilized were the same as used for the creation of P40 mutants (figure 55) in order to ensure the substitution of 8 aa of the protein with the PreScission protease recognition site and therefore to create a protein that could be cleaved with PreScission protease only at the 40th aa in the N-terminal region. The template used in this case was SVP2741Aa ΔR HA plasmid. Same procedure was followed as to create the previous mutants which was explained in detail in chapter 4 (Figure 98).

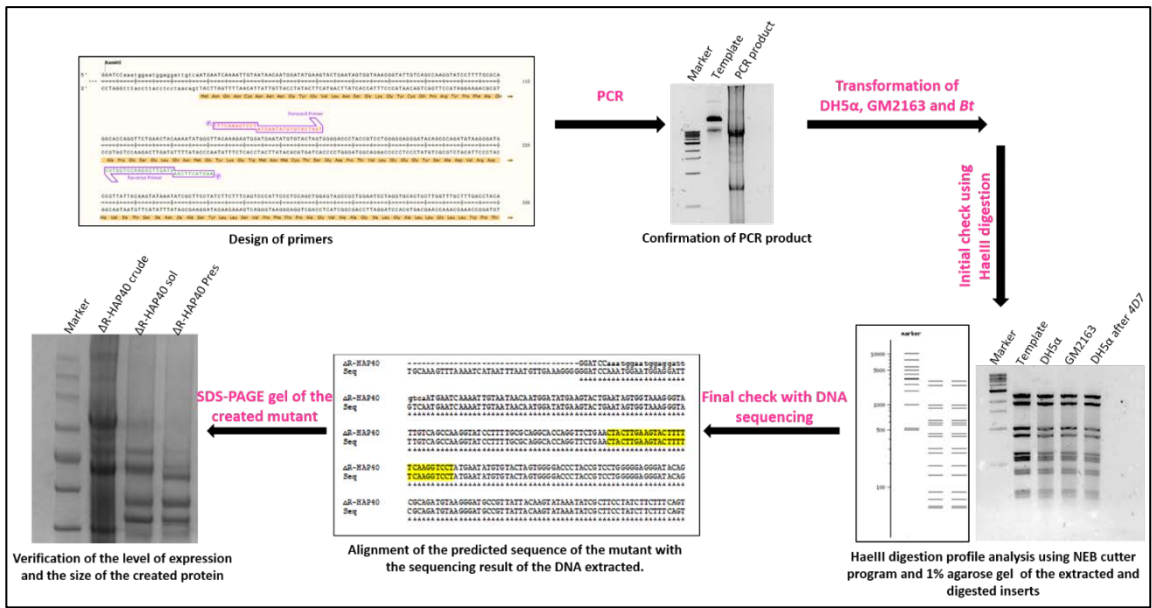


Figure 98: Diagram summarising different steps followed for the creation of ΔR-HAP40.

According to our results, ΔR-HAP40 was successfully expressed. The molecular weight of the PreScission activated toxin was smaller than that of the solubilised core suggesting that the protein was cleaved with the protease. In order to check whether the HA-tag interferes with toxin activity, the level of toxicity of the created mutant on both HepG2 and HL-60 cell lines was assessed (figure 99 and 100).

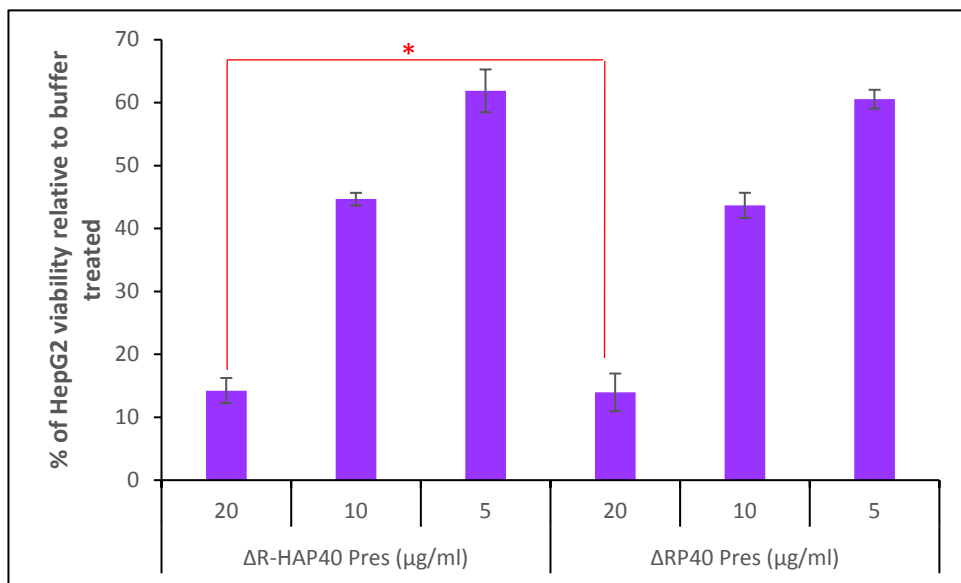


Figure 99: The effect of HA tag on protein activity towards HepG2 cell line.

HepG2 was seeded at a density of 25×10^4 cells/ml. The next day the cells were treated with different concentrations of PreScission activated ΔR-HAP40 and ΔRP40. 24 hours later, cell viability was measured using CellTiter-Blue. Ttest was used to calculate the p value: * $p=0.3$ (p values for all other concentrations used were calculated and are >0.05).

According to our results, HA tag seemed to have no effect on protein activity. In fact same level of toxicity was observed in case of Δ RP40 and Δ R-HAP40 towards HepG2 cell line.

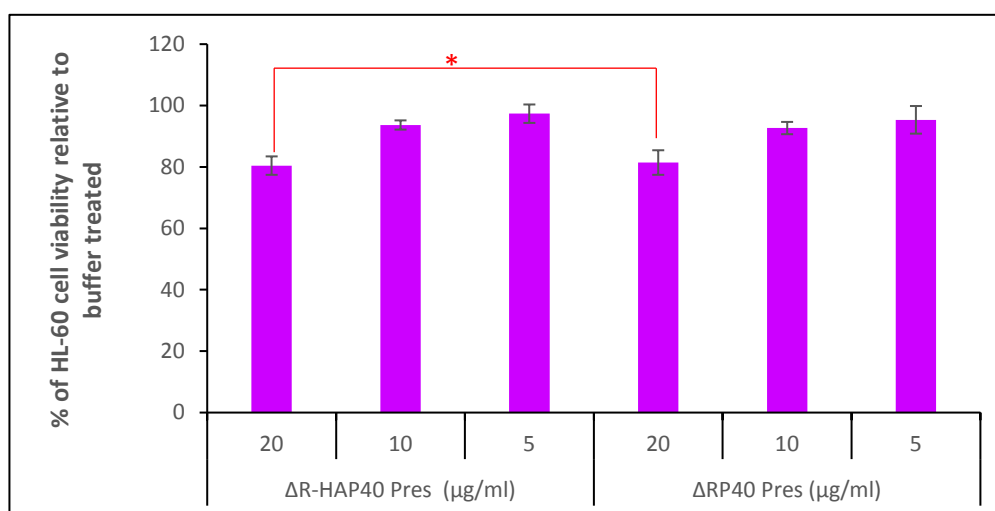


Figure 100: The effect of HA tag on protein activity towards HL-60 cell line.

HL-60 was seeded at a density of 25×10^4 cells/ml. The next day the cells were treated with different concentrations of PreScission activated Δ R-HAP40 and Δ RP40. 24 hours later, cell viability was measured using CellTiter-Blue. Ttest was used to calculate the p value: * $p=0.23$ (p values for all other concentrations used were calculated and are >0.05)

As for HepG2, the HA tag seemed to have no effect on the protein activity against HL-60 cell line.

Western blot was later carried out to detect the presence of HA tag in Δ R-HAP40 after proteolytic activation with PreScission protease (figure 101).

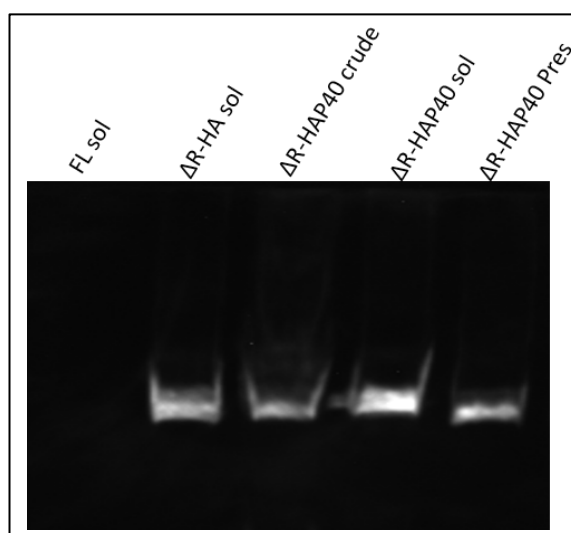


Figure 101: Western blot analysis of HA tag attachments to proteins before and after proteolytic digestion.

Solubilised full length (untagged), solubilised Δ R-HA and crude, solubilised and PreScission activated Δ R-HAP40 were run on 7.5% SDS-PAGE gel. 3 μ g of proteins were loaded in each lane. After transfer, the membrane was blocked with 5% milk then incubated with the HRP conjugated anti-HA antibody followed by ECL detection.

Our results showed that there was no tag detection in solubilised FL (negative control), tag was detected in solubilised ΔR -HA (positive control) and in crude, solubilised and PreScission activated ΔR -HAP40. Therefore, the problem of HA-tag retention after proteolytic processing was resolved.

5.2.3 Binding analysis

Binding assays were carried out initially on susceptible HepG2 cell line where western blot and ligand blot techniques were used in order to investigate whether we could detect the binding of the toxin onto these cells (figures 102 and 103).

Cell extracts were initially prepared using two lysis buffers: non-ionic mild NP-40 and harsh denaturing ionic RIPA.

Whole cell samples were also used in this study in order to minimize proteolysis, dephosphorylation and denaturation since all begin to occur once the cells are disrupted. Tris-HCl, a detergent-free sample buffer was utilized in this case.

HepG2 cells were treated with ΔR -HAP40 at a concentration of 15 $\mu\text{g}/\text{ml}$ (a dose that induced a significant decrease in cell viability). The incubation time (30 min) was determined based on microscopic observations where as soon as toxin effect on cells started to be visualized (beginning of swelling in around 10% of cells), the extracts were prepared. Protein concentrations were measured using Bradford protein assay where BSA was utilized as a protein standard.

Because of the denaturing conditions of SDS-PAGE, which would cause the dissociation of the toxin from the receptor, a band of similar molecular weight to the toxin is expected to be detected in a western blot of the extracts where cells were pre-incubated with toxin before lysis.

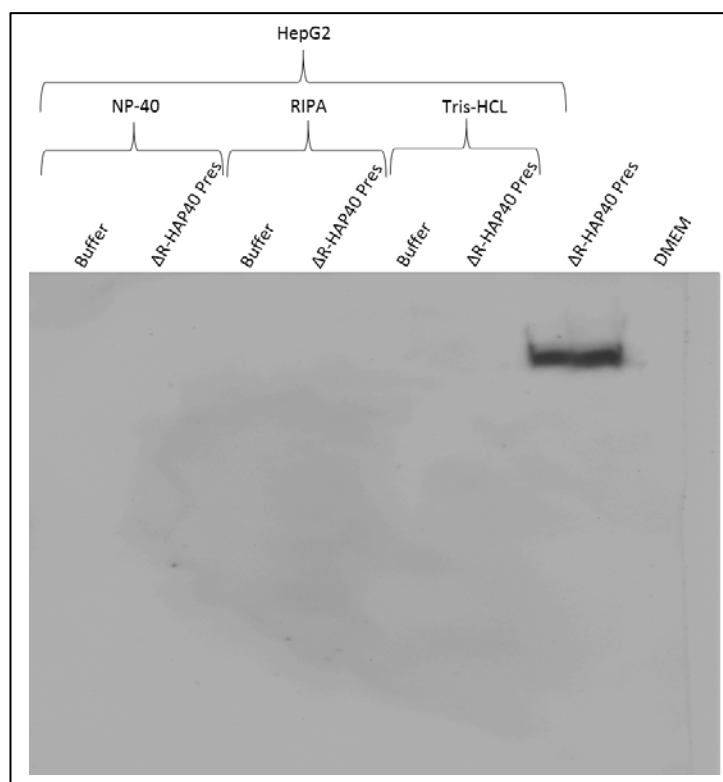


Figure 102: Western blot analysis of extracts from HepG2 cells that were treated with Δ R-HAP40 or buffer.

HepG2 cells were treated with Δ R-HAP40 (15 μ g/ml) or PBS for 30 min before either being lysed with NP-40 and RIPA or extracted and suspended in 20 mM Tris-HCL. Samples were run on 12% SDS-PAGE. 20 μ g of proteins were loaded per well and 3 μ g of Δ R-HAP40 was loaded as positive control. After transfer the membrane was incubated with anti-HA antibody followed by ECL detection.

However, no signal was produced in all the lanes containing the extracts of cells incubated with or without toxin and prepared with different lysis buffers. In order to check whether the incubation time was too short for the toxin to start binding to cell membrane and it remained in the medium (DMEM), the medium removed during the preparation of cell extracts was kept, vivaspun for toxin concentration (in case the concentration of the toxin in the sample loaded was too low for detection) then loaded on SDS-PAGE along with the cell extracts. Yet, no bands were detected suggesting that toxin at this stage was bound to the cell membrane. Thus, it is more likely that the tag might get cleaved after binding occurs. High signal was produced from PreScission activated Δ R-HAP40 with cross-reactive binding was not observed on other polypeptides of parasporal proteins, indicating the specificity of the antibody towards the protein of interest.

As an alternative approach, ligand blot technique was used where extracts that contain cells incubated for 30 min with buffer only, which were used in the western blot experiment, were loaded onto 12% SDS-PAGE gels. After transfer, the nitrocellulose membranes were incubated with or without toxin (figure 103).

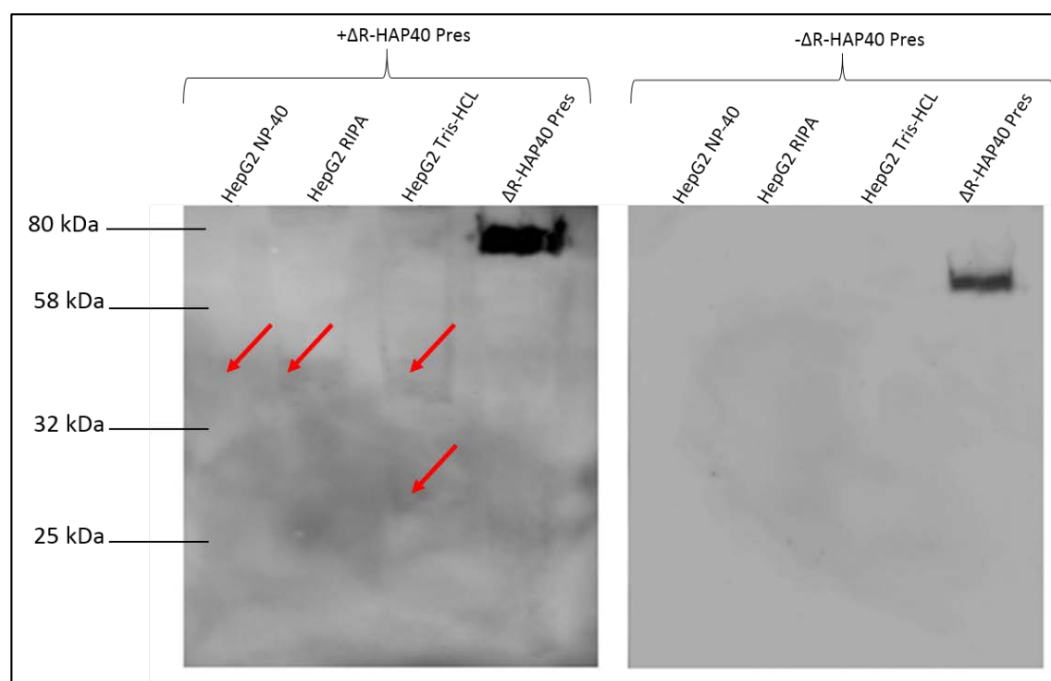


Figure 103: Ligand blot analysis of extracts from HepG2 cells.

20 μ g of extracts from HepG2 cells were loaded into 12% SDS-PAGE. 3 μ g of Δ R-HAP40 was loaded as a control. After transfer, the membrane was blocked and was either incubated with Δ R-HAP40 in PBS (10 μ g/ml) or PBS only over night at 4°C. The next day membranes were washed, incubated with anti-HA antibody and signal was detected with ECL. Red arrows indicate the bands detected.

Our results showed a signal produced at around 46 kDa which was present in all extracts however a lower molecular weight band of around 30 kDa was only detected in the whole cells sample. A high signal was produced from Δ R-HAP40 sample which was used as positive control while no bands were detected in the extracts blotted onto the second membrane that served as a negative control as there was no toxin incubated with the membrane.

Therefore, it seems that there might be binding of the toxin to proteins of 46 and 30 kDa present in the extracts. In order to confirm binding of the toxin to these proteins, the membrane was washed thoroughly and the bands detected were excised, boiled with SDS loading buffer then run on SDS-PAGE gel which was stained with Coomassie blue

then destained and analysed. Some other parts of the membranes, where no proteins were blotted, were also excised in order to check that the membrane was properly washed and no unbound toxin remained (figures 104 and 105).

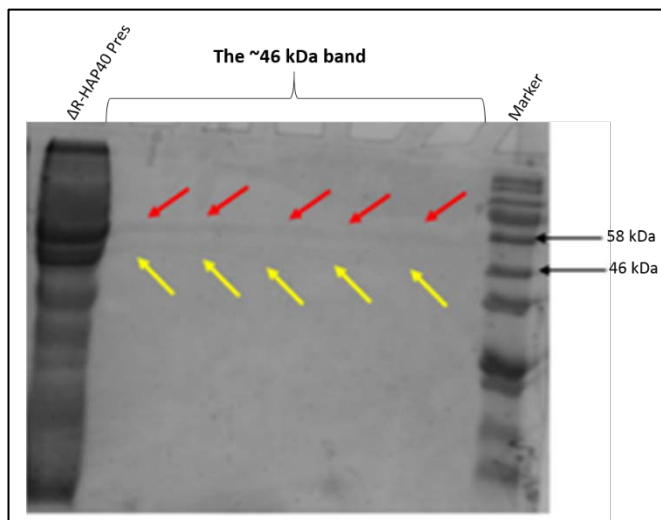


Figure 104: SDS-PAGE showing composition of excised 46 kDa band.

The upper band detected was excised from the membrane, boiled with SDS-loading buffer and loaded on SDS-PAGE gel. The red arrows corresponds to an upper band and the yellow arrows show a lower molecular weight protein

The upper band was suspected to be the PreScission activated protein as of similar molecular weight while the lower one is expected to be the protein(s) that the toxin was bound to.

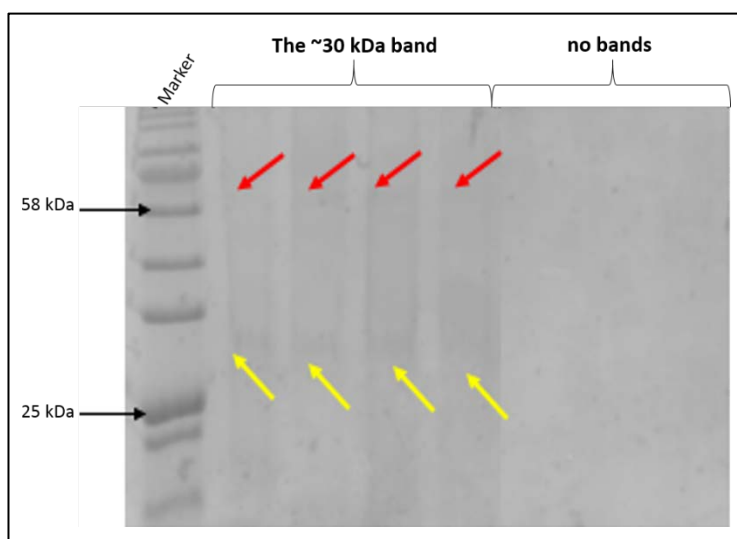


Figure 105: SDS-PAGE showing composition of the excised 30 kDa band.

The lower band detected and other parts of the membrane, where no proteins were blotted, were excised from the membrane, boiled with SDS-loading buffer and loaded on SDS-PAGE gel. The red arrows corresponds to an upper band and the yellow arrows represents a lower molecular weight protein.

The upper band in this case is suspected to be the toxin showing similar MW to that of the PreScission activated ΔR -HAP40 whereas the lower molecular weight band represents the proteins where the toxin was bound.

The parts of the membrane where no proteins were blotted showed no band indicating that no unbound toxin remained.

These results indicate that the signal detected from the ligand blot experiment was produced from the toxin.

We then wanted to analyse the binding of the created mutants (TD, RA, and TA) which presented a reduced toxicity compared with the non-mutated toxin. This was in order to investigate the correlation between reduced toxicity and binding (figure 106).

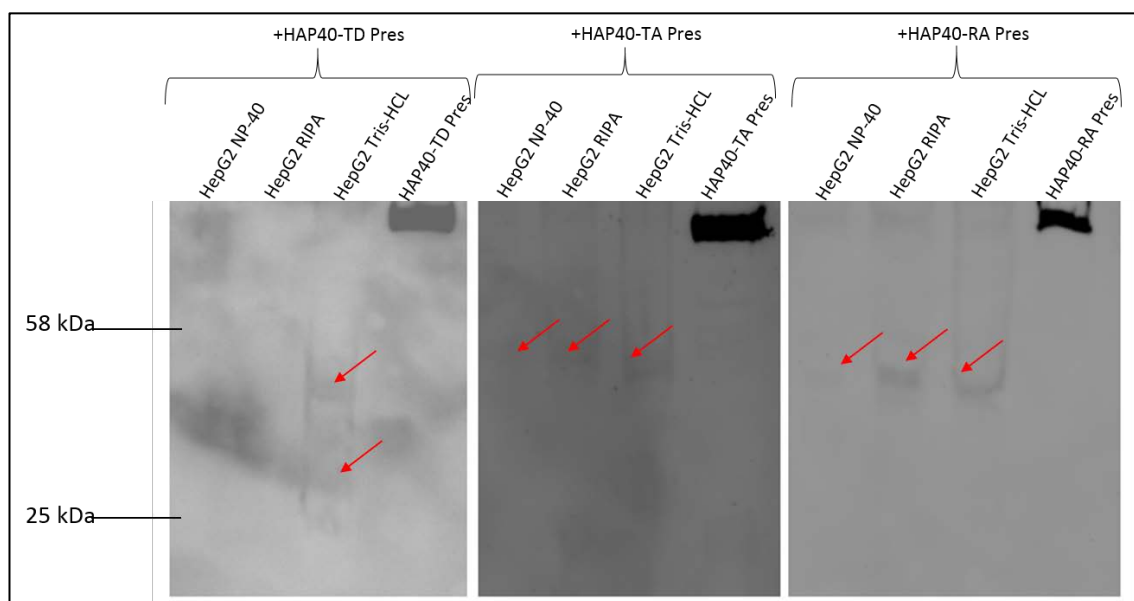


Figure 106: Ligand blot analysis of extracts from HepG2 cells.

20 μ g of extracts from HepG2 cells were loaded into 12% SDS-PAGE. 3 μ g of PreScission activated HAP40-TD, HAP40-TA and HAP40-RA were loaded as controls. After transfer the membranes were blocked and were incubated with either HAP40-TD, HAP40-TA or HAP40-RA (10 μ g/ml each) over night at 4°C. The next day membranes were washed, incubated with anti-HA antibody and signal was detected with ECL.

According to our results, despite the reduced toxicity of the created mutants, the band around 46 kDa was still detected, yet, it is only with TD incubation that the signal around 30 kDa was produced.

To investigate the possibility of this process measuring non-specific or non-productive binding, a binding study of the toxin ΔR -HAP40 to less susceptible (HL-60) and non-susceptible (HeLa) cell lines was performed.

Western blot technique was initially carried out on HL-60 cell line where the cells were pre-incubated with the toxin at a concentration of 15 $\mu\text{g}/\text{ml}$ for 1 hour. The incubation time was determined the same way as for HepG2, where, as soon as the swelling started to be microscopically visualised in around 10% of the total cells, the extracts were prepared. Then the extracts were run on 12% gel along with controls and medium in order to eliminate the possibility of the toxin still remaining in the medium in case of lack of signal (figure 107).

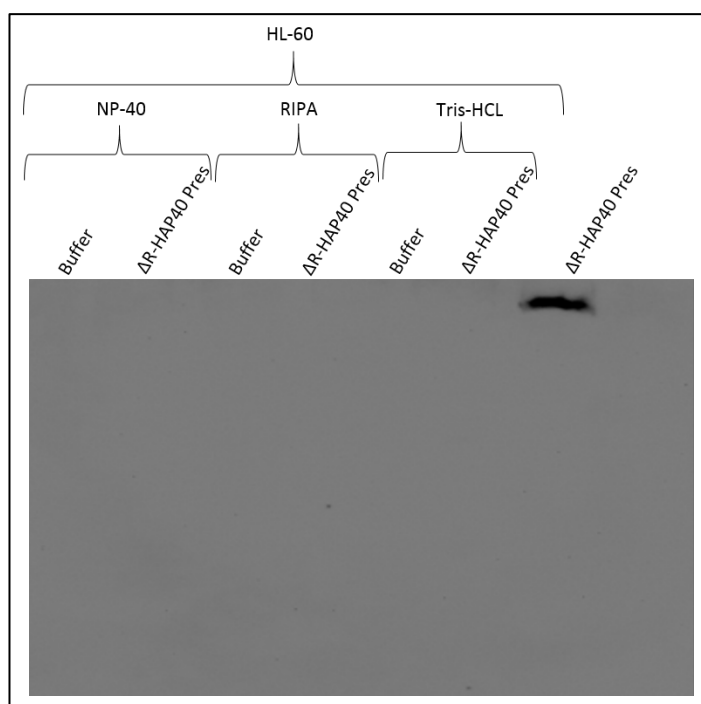


Figure 107: Western blot analysis of extracts from HL-60 cells that were treated with ΔR -HAP40 or buffer.

HL-60 cells were treated with ΔR -HAP40 (15 $\mu\text{g}/\text{ml}$) or PBS for 60 min before either being lysed with NP-40 and RIPA or extracted and suspended in 20 mM Tris-HCL. Samples were run on 12% SDS-PAGE. 20 μg of proteins were loaded per well and 3 μg of ΔR -HAP40 was loaded as a positive control. After transfer the membrane was incubated with anti-HA antibody followed by ECL detection.

No bands were detected in the lanes where the extracts of cells, incubated with or without toxin and prepared with different lysis buffers, were loaded. No signal was also produced in the RPMI medium sample showing that no unbound toxin still remained in

the medium at that stage. This is because we eliminated the possibility that the toxin continued to exist in the medium at extraction time but the tag was cleaved due its instability in those conditions. This was by running the same sample on SDS-PAGE gel which was later stained with Coomassie blue to check the presence of the toxin however no bands were visualised confirming that the binding occurred during 1 hour of incubation with the cells (data not shown).

The same extracts containing cells with buffer that were used in the western blot experiment were run again on 12% SDS-PAGE gel which was used in the ligand blot experiment where, after transfer, the nitrocellulose membrane was blocked with 5% milk then incubated with PreScission activated Δ R-HAP40 at a concentration of 10 μ g/ml over night at 4°C. The membrane was later washed, incubated with anti-HA antibody and signal was detected with ECL (figure 108).

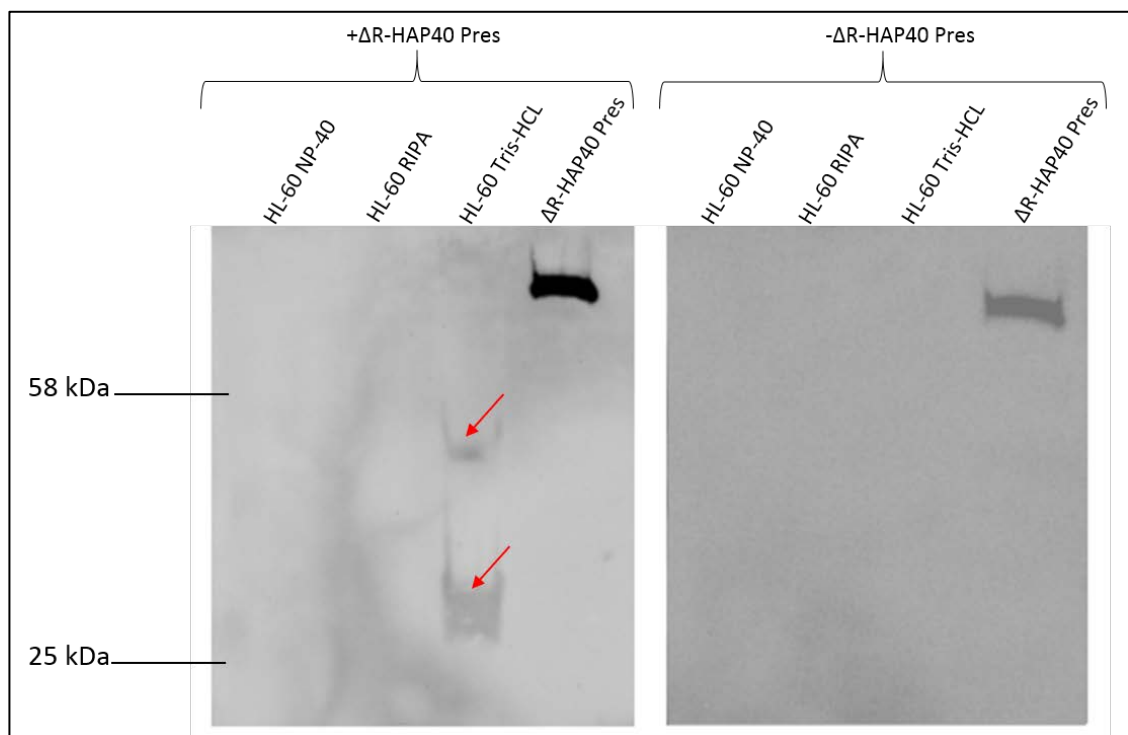


Figure 108: ligand blot analysis of extracts from HL-60 cells.

20 μ g of extracts from HL-60 cells were loaded into 12% SDS-PAGE. 3 μ g of Δ R-HAP40 was loaded as a control. After transfer the membrane was blocked with 5% milk and was either incubated with Δ R-HAP40 in PBS (10 μ g/ml) or PBS only over night at 4°C. The next day membranes were washed, incubated with anti-HA antibody and signal was detected with ECL.

Two bands of around 46 kDa and 30 kDa were only detected in the whole cell lysate sample (Tris-HCl buffer). A high signal was produced from Δ R-HAP40 samples which served as positive control while no signal was detected in the extracts blotted onto the second membrane which, incubated without toxin, was used as a negative control.

The lack of signal produced in extracts prepared with NP-40 and RIPA could be due to sample preparation.

Although less susceptible cells were used, binding is still detected which could suggest that there is no correlation between binding and susceptibility.

In order to confirm this hypothesis, a non-susceptible cell line (HeLa) was later used where western blot (figure 109) and ligand blot (figure 110) techniques were applied following the same principle as utilized for HepG2 and HL-60 cell lines.

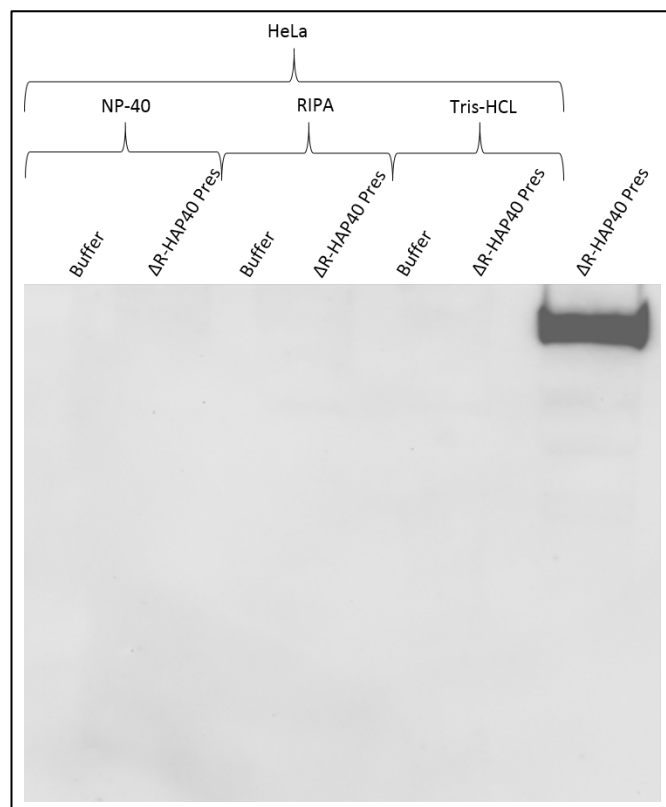


Figure 109: Western blot analysis of extracts from HeLa cells that were treated with Δ R-HAP40 or buffer.

HeLa cells were treated with Δ R-HAP40 (15 μ g/ml) or PBS for 1 hour before either being lysed with NP-40 and RIPA or extracted and suspended in 20 mM Tris-HCL. Samples were run on 12% SDS-PAGE. 20 μ g of proteins were loaded per well and 3 μ g of Δ R-HAP40 was loaded as positive control. After transfer the membrane was blocked, incubated with anti-HA antibody followed by ECL detection.

Same as for HepG2 and HL-60 cell lines, western blot analysis showed no bands detected in the cell extracts prepared with different lysis buffers. Knowing that HeLa cells are non-susceptible to the toxin, therefore this result could suggest that probably the toxin is not binding however, because using the same technique, there was no bands detected in case of susceptible HepG2 cells, this result can't be reliable.

Therefore ligand blot technique was used next (figure 110).

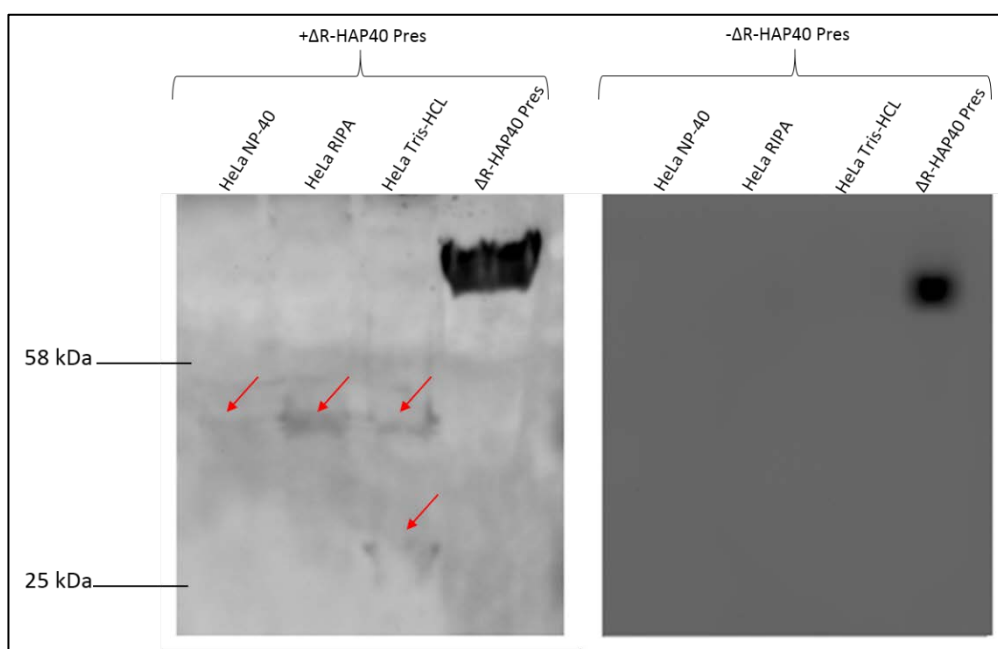


Figure 110: Ligand blot analysis of extracts from HeLa cells.

20 μ g of extracts from HeLa cells were loaded into 12% SDS-PAGE. 4 μ g of Δ R-HAP40 was loaded as a control. After transfer the membrane was blocked and was either incubated with Δ R-HAP40 in PBS (30 μ g/ml) or PBS only over night at 4°C. The next day membranes were washed, incubated with anti-HA antibody and signal was detected with ECL.

Same as for HepG2, a band of around 46 kDa was detected in all extracts while it is only in the whole cell lysate sample that the 30 kDa band was detected. An expected high signal was produced from Δ R-HAP40 sample while no signal was produced from the extracts blotted onto the second membrane that was used as a negative control.

Although HeLa cells are non-susceptible to the toxin, binding still occurs. These results are consistent with the fact that there is lack of correlation between binding and susceptibility.

5.3 Discussion

Our results showed that the toxic effect of Cry41Aa towards HepG2 and HL-60 cell lines depends on the protease used to activate the toxin. This result agrees with previous studies where the type of protease used was important in Cry toxicity/specificity. In fact, it has been shown that it is only upon treatment with Proteinase K or trypsin is parasporin-1 toxic to MOLT-4 cells while no cytotoxic activity was produced with chymotrypsin treatment. This result was explained by the fact that same proteolysis profile was produced by treatment with trypsin and PK while chymotrypsin activation gave a different protein banding pattern where a band of 56 kDa was not produced (Mizuki et al., 2000).

In the case of parasporin-2, no cytotoxic activity was observed after trypsin treatment of solubilised crystal proteins whereas proteinase K activated proteins were highly cytotoxic to HepG2, MCF-7, KLE, Hec-1A, MDA-MB231 and PC-3 cells (Brasseur et al., 2015b).

In insect models, specific proteolytic activation was proved to be essential and could determine the toxin specificity. In fact, the main digestive proteases of Coleoptera are cysteine and aspartic proteases, whereas those of Lepidoptera and Diptera are serine proteases. The insecticidal specificity of Cry toxin from *B. thuringiensis* var. *colmeri* was influenced by the source of enzymes which come from different insect guts. The activation of the toxin with these enzymes produce different sizes of toxins that depending on their aa compositions show different specificity (Haider et al., 1986).

In addition, activation of Cry3 protoxin with different proteases was shown to affect toxin activity since chymotrypsin but not trypsin activated Cry3Ba was able to bind to BBMV of Colorado potato beetle *Leptinotarsa decemlineata*. The loss of binding of trypsin activated Cry3Ba toxin was suggested to be due to structural changes related to proteolysis or to processing of important binding epitopes in the toxin (Rausell et al., 2004a).

It has been previously shown that following exposure of different organisms to PFT, the mitogen-activated protein kinase p38 pathway (MAPK p38) is activated in order to stimulate a defense response. This aspect has been observed in *M. sexta* and *A. aegypti* where Cry1Ab and Cry11Aa respectively caused phosphorylation of p38 in a dose dependent manner. The important role of MAPK p38 in defense mechanism was confirmed by gene silencing resulting in hypersensitivity of these insect species to Cry toxin intoxication (Cancino-Rodezno et al., 2010a). In addition, Domanska et al. in 2016 showed that Cry41Aa activates p38 and this phosphorylation appeared to be dose dependent (Domanska, 2016). Therefore knowing that PK activated Cry41Aa is more toxic than the T/C activated toxin, we wanted to see if this difference in toxicity is reflected in p38 phosphorylation. Our results indicated that higher activation of p38 MAPK was observed in cells treated with PK activated toxin.

The separation of the two fragments produced by activation of Cry41Aa with either trypsin/chymotrypsin or PK was unsuccessful using gel filtration resin Sephacryl S-200 method (where the two fragments were co-eluted) but was partially successful when anion exchange chromatography FPLC was used leading to the purification of the upper band of around 76 kDa. The co-elution of Cry fragments produced after activation was previously seen in the case of Cry1A: when digested with *M. sexta* midgut juice, the protoxin produces two fragments of around 30 and 58 kDa. Using different purification methods, the two monomers were co-eluted and were both detected using anti-Cry1A anti body suggesting that the treatment with midgut proteases does not unfold the structure of the protein but only makes some peptide bond cleavages (Miranda et al., 2001).

The co-elution of the two bands of activated Cry41Aa could be explained by the fact that looking at the elution profile (chapter 4 figure 39), the peaks of the two fragments seemed to be merged together. The first peak corresponds to the upper band that gets eluted first. While it is still eluting the second peak appears corresponding to the elution of the lower band. Because of their different amino acid composition, the two bands acquires different ionic properties explaining why they get detached from the column at different time. In the future, because linear gradient of salt was used, the next step is

to try to use step-wise increase of salt gradient where we will increase the time (to 3 to 5 column volume for example) when the upper band started to get eluted. This prolonged step will ensure enough time for the elution of the upper protein on its own then the lower one will be eluted individually.

According to our N-terminal sequencing of the upper band and the N-terminal sequencing of the lower band of Cry41Aa carried out by Yamashita et al in 2005, it appears that both proteins have the same N-terminal cleavage site and the difference actually resides in the C-terminal cleavage. Similar result was previously observed where the *B. thuringiensis* strain M15 crystal produces two major bands of approximately 86 and 79 kDa. N-terminal sequencing was carried out for both proteins showing that they shared identical 20-amino acid residues. One of the possibilities that was suggested to explain this result is that the 86-kDa protein might have been processed at the C-terminus to yield the 79 kDa protein (Jung et al., 2007).

Because the level of cytotoxic activity of the upper band of activated Cry41Aa was similar to that of both bands together and knowing that cleavage solely occurs at the N-terminus of the protein therefore C-terminal cleavage does not seem to play a role in HepG2 and HL-60 toxicity. This agrees with previous studies, as discussed in chapter 1, which showed that C-terminal cleavage in most Cry toxins is not involved in toxicity.

N-terminal sequencing was one of the molecular approaches that was extensively used in order to understand the difference in toxicity of Cry toxins activated with different proteases. In fact, in the case of anti-cancer Cry toxins, in order to understand the difference in toxicity between chymotrypsin, PK and trypsin activated Cry31Aa2 which could correlate with difference in activation, N-terminal sequences were determined for all fragments to identify the proteases cleavage sites (Jung et al., 2007).

The 76 kDa proteins produced by PK and T/C activation of Cry41Aa toxins showed different N-terminal cleavage site where T/C cuts after tyrosine (58th aa) and PK cleaves after alanine (60th aa). Only two aa difference (Ser and Ala) that seem to be important in Cry41Aa toxicity. Based on the predicted 3-D structure of Cry41Aa these two aa seem to be partially covering the N-terminal sequence of PK activated toxin. Therefore based on previous work which showed that cleavage affects binding and assuming that the

DVRDA motif is important in binding, the hypothesis adopted was that the Ser and Ala residues are interfering with binding.

A similar concept was observed In case of parasporin-2 where it has been suggested that the difference in toxicity between the trypsin and PK activated toxins could be due to the trypsin and proteinase K cleavage sites being different. Brasseur et al in 2015 hypothesized that without proper protease activation, the PS2Aa1 protoxin could not be recognized by cell receptors. It was assumed that when cleaved with proteinase K, specific regions of the activated PS2Aa1 can bind to receptor while, when cleaved with trypsin the binding is prevented because these binding epitopes can only be partially exposed or not at all.

Various other studies showed that position of N-terminal cleavage of insecticidal Cry toxins is important in binding. Amongst them Cry2Aa where based on structural predictions, the first 49 aa fragment, which gets cleaved during protease activation, was shown to occlude a domain II hydrophobic patch proposed to be involved in receptor interaction and deletion of 42 amino acid residues from the N-terminus resulted in a 4 to 6 fold increase in toxicity against *Spodoptera littoralis*, *Helicoverpa armigera* and *Agrotis ipsilon* (Morse et al., 2001).

The introduction of trypsin cleavage site in AK mutant was designed to improve the toxin activity since PK activated toxin is more toxic than T/C activated one therefore moving the trypsin cleavage site to that of PK would result in enhancement of toxin activity. However, unfortunately cleavage of the created protein at that position was unsuccessful. This method was previously used where introduction of protease cleavage site enhanced a toxins' activity (Walters et al., 2008a). In case of our Cry toxin, this was confirmed when a PreScission protease cleavage site was introduced at the N-terminal 40th aa which led to a great increase in Cry41Aa activity compared to the protoxin. In insect models, the introduction of a chymotrypsin/cathepsin G site in the loop between helix α -3 and helix α -4 of Cry3A toxin has increased its toxicity to 3 fold against neonate *D. virgifera* larvae. It has been proposed that cleavage of this toxin at this proteolytic site permitted the subsequent binding of the activated toxin to the receptors present in the midgut cells (Walters et al., 2008b).

The receptor-binding step has been studied extensively, as it was shown to be a key factor for insect specificity, toxicity and resistance where the loss of toxicity was correlated with reduced binding affinity to brush border membrane vesicles (BBMV). Because the DVRDA motif was speculated to be involved in binding, two residues R and D, hypothesized to be important in binding, were substituted. Therefore the mutants created should show reduced or loss of binding. The choice of the residues to be substituted were based on the 3-D predicted structure of Cry41Aa where the side chain of the Aspartic acid (64th aa) was sticking out making it possible to be involved in binding. Being positively charged, the Arginine at that position seemed to be important especially that according to previous work positively charged aa were shown to play an important role in binding. In fact, the functional role of the positive charges in specific region of the domain II loop 2 in Cry1Ab and Cry1Ac was examined by introducing mutations at the arginine residues that were replaced with alanine, glutamic acid and lysine. Toxicity and binding assays of the created mutants showed that removal of the charge or introduction of negative charges affected toxicity as well as binding supporting the view that arginine residues in the loop 2 region are important for initial binding to receptor sites (Lee et al., 2000).

However, despite these mutants showing reduced activity, binding of Cry41Aa mutants to HepG2 cell extracts was detected suggesting that either this binding is non-specific, the mutations created might have affected post-binding processes or the binding affinity of these mutants was reduced but was not lost completely therefore a quantitative binding study has to be performed.

The latter approach was previously used to examine the effect of the mutations on receptor binding. In fact, in case of Cry1Ab toxin, in order to provide quantitative data on the effects of Trp mutations on receptor binding, heterologous binding competition of Cry1Ab wild type and mutated toxins to brush border membrane vesicles (BBMV) was performed. The results suggested that the mutants bind BBMV with lower affinity than wild type Cry1Ab toxin (Padilla et al., 2006).

The effect of mutations on post-binding processes was also observed in previous studies. In fact, mutations in some residues of domain I in 3-domain Cry toxins resulted in complete loss of toxicity to *M. sexta* larvae. The nontoxic mutants showed altered oligomerization or membrane insertion which was shown to be seriously affecting pore

formation. However, these mutants presented similar binding affinity with the cadherin receptor to the wild-type toxin. This binding was therefore proved to be not sufficient for toxicity and that oligomerization and pore formation are the crucial steps for killing insect larvae (Jimenez-Juarez et al., 2007).

Previous studies showed a strong correlation between toxicity and binding which was also validated by the fact that resistance correlated with loss of binding. In fact, this was confirmed by absence of binding of Cry1Ab and Cry1Ac toxins to the midgut brush border membranes in the resistant *Trichoplusia ni* larvae (Wang et al., 2007). In addition to the loss of binding of Cry2Ab to BBMV prepared from *H. armigera* and *H. punctigera* resistant insect larvae (Caccia et al., 2010).

According to our results, Cry41Aa binding was detected in susceptible HepG2, in less susceptible HL-60 and in non-susceptible HeLa indicating that regardless of susceptibility, binding of Cry41Aa to these cancer cell lines occurs. Therefore, there might be no correlation between binding and susceptibility where the difference might reside in post binding procedures or the binding detected being non-productive. The lack of correlation between binding and toxicity was previously observed in insecticidal Cry toxins where although Cry1Ca and Cry1Bb showed different toxicity against *S. exigua* and *S. frugiperda* insects, they bound similarly to the BBMVs of the two species. On the other hand, Cry1Ac, which is not toxic to *S. exigua* and *S. frugiperda*, bound strongly to their BBMVs. It was then concluded that Cry1 toxin binding is necessary but not sufficient for toxicity (Luo et al., 1999).

Specific binding of Cry1Ac was also found to be similar between BBMVs prepared from resistant and susceptible larvae of *Pectinophora gossypiella*. It was then speculated that this binding is not sufficient to confer susceptibility to Cry1Ac (Ocelotl et al., 2015). The binding kinetics for Cry1Ac did not differ significantly between susceptible and resistant *P. xylostella* larvae. Regardless of susceptibility, Cry1Ac was able to specifically bind to their BBMVs. These results suggest that factors other than binding may be altered in the resistant insects and that binding is not sufficient for toxicity (Masson et al., 1995b).

Knowing that the binding assays presented in this chapter were only preliminary data, in the future binding should be confirmed using competition studies in order to

investigate the binding of mutated toxins compared with the full length protein. Besides, the candidate binding proteins where the toxin bound to should be identified using mass spectrometry. Identification of the cell receptor(s) is expected to provide some insight into the mechanism of target specificity and cytotoxicity. Once identified, receptor knock down in susceptible or overexpression in non-susceptible cell lines should be considered. In addition, the hypothesis suggesting that there is no correlation between binding and toxicity should be confirmed where post binding processes should be studied like toxin oligomerization, pore forming activity as well as the stability of pores and cellular recovery pathways. Previous work has shown, in insect models, the importance of post-binding processes in Cry toxicity. For instance, in case of Cry1Ab, helix $\alpha 3$ in domain I was shown to contain sequences important for oligomerization. Mutations created in this helix did not affect interactions with membrane proteins where the mutants bound receptors with similar affinity as the wild-type toxin, yet, oligomerization, pore formation and toxicity against *Manduca sexta* larvae were severely damaged. These results indicated that the pre-pore oligomer and toxin pore formation play a major role in the toxic effect of Cry1Ab on insect larvae (Jimenez-Juarez et al., 2013). The control of intracellular death pathways as well as differential defensive responses to Cry intoxication were also shown to be important events that may contribute to determine Cry specificity. In fact, a previous study has confirmed that resistance of *Heliothis virescens* to Cry1Ac was correlated with repair of damaged gut epithelium (Forcada et al., 1999).

It is therefore interesting to develop resistance in susceptible HepG2 as comparison between responses of the two cell lines to Cry41Aa intoxication would help more in the understanding of the mechanism of action of the toxin.

Conclusions

- 1- The toxicity towards HepG2 and HL-60 cell lines depends on the protease used to activate the toxin.

- 2- The higher toxic effect of PK activated toxin compared with the T/C treated one towards HepG2 and HL-60 cell lines is reflected in p38 activation.
- 3- The N-terminal cleavage is sufficient for Cry41Aa toxicity and serine (59th) and alanine (60th) residues are behind the difference in toxicity between PK and T/C activated forms of the protein.
- 4- Cry41Aa binds to proteins of around 46 and 30 kDa in susceptible and non-susceptible cell lines suggesting no correlation between binding and susceptibility.

6 Probing the mechanism of action of Cry41Aa on HepG2 through the establishment of a resistant subline

6.1 Introduction

The development of resistance to treatments used to counter diseases is a major obstacle. This phenomenon was observed in insect models that developed resistance to *Bt*-based biopesticides as well as in cancer patients who developed resistance to chemotherapeutic agents. Understanding the basis of the resistance mechanisms was then important for developing management strategies.

In insect models, the proposed mechanisms of resistance were associated with alteration in any step in the mechanism of action of *Bt* Cry toxins. The most frequently observed mechanisms of Cry toxin-resistance involve defects in receptor binding (Ferré and Van Rie, 2002), altered activation of Cry toxins by midgut proteases (Sayed et al., 2001), elevated immune response (Ma et al., 2005a) or enhanced esterase production (Gunning et al., 2005).

On the other hand the principal mechanisms that were associated with resistance of cancer cells to chemotherapy treatment include altered membrane transport involving the P-glycoprotein product of the multidrug resistance (MDR) gene as well as other associated proteins, altered target enzyme (e.g. mutated topoisomerase II), decreased drug activation, increased drug degradation due to altered expression of drug-metabolizing enzymes, drug inactivation due to conjugation with increased glutathione, subcellular redistribution, drug interaction, enhanced DNA repair and failure to apoptose as a result of mutated cell cycle proteins such as p53 (Luqmani, 2005).

One of the main approaches that has been utilized to study the resistance mechanisms in insects and cancer cell lines was to evolve a resistant population/subline to the toxic agent. The molecular alterations associated with resistance can then help in the clarification of the mechanisms of this change in phenotype.

In this study, HepG2 resistant to Cry41Aa was generated. Cellular and molecular changes were investigated in order to help unravel the mechanism of action of this toxin.

6.2 Generation of resistant HepG2 cell line to T/C activated Cry41Aa

Several methods were previously proposed that could be used to establish a cancer resistant cell line to an anti-cancer drug. These included pulse treatment method where cells are repeatedly exposed to a high concentration (generally the IC50 dose) of the drug in question followed by a recovery period. Another strategy which corresponds to growing in step-wise increases in the toxic agent was the most commonly used method. Due to its sensitivity, several parameters are crucial to consider to ensure its success such as good record keeping, regular freezing down of the evolving resistant variant, monitoring the progress of the development of the resistance phenotype, allowing the cells to recover in drug-free medium when needed etc.

In this study, HepG2 cells were cultured in step-wise increases of purified T/C activated Cry41Aa. The cells were seeded at around 20% confluency and the drug treatment was carried out after 24 hours with a commencing dose of 0.1 µg/ml.

As the cells become confluent, they were sub-cultured in the usual manner and the increase of the toxin dose generally followed the pattern of doubling the concentration unless the cells appeared not to have tolerated the drug treatment, in which case, they were allowed to recover in drug-free medium and be exposed to a less concentrated dose. As shown in figure 111, a range of different concentrations was used (0.1; 0.2; 0.3; 0.4; 0.8; 1.6; 2.6; 4; 8; 10; 15; 20; 30; 50 µg/ml) during a period of 8 months.

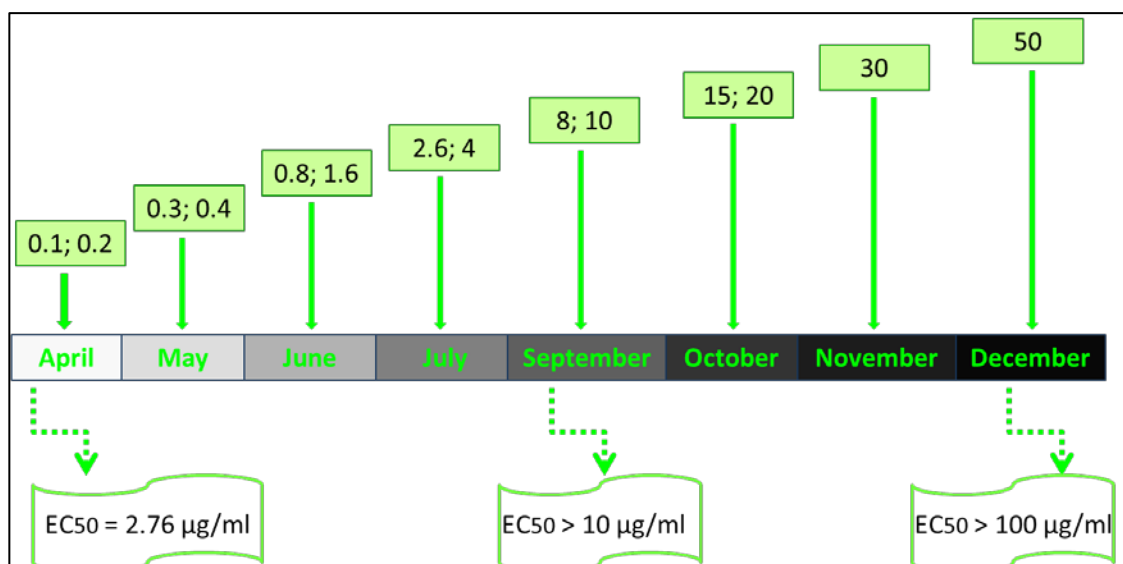


Figure 111: Diagram showing the establishment of resistant HepG2 cell line to T/C activated Cry41Aa over time. HepG2 cells were treated with step wise increasing doses of ÄKTA purified T/C activated Cry41Aa ranging from 0.1 to 50 µg/ml over a period of 8 months. Sensitivity of cells to the toxin was monitored during the selection using cell viability assays.

According to figure 111, the establishment of resistance profile in HepG2 cell line was successful showing that after 8 months of selection, HepG2 cells became resistant to T/C activated toxin tolerating a dose of 50 µg/ml and presenting an EC₅₀ that was greater than 100 µg/ml.

6.3 Confirmation of the resistance to the toxin

During the selection, monitoring the progress of the development of the toxin-resistant line was carried out. This was achieved by using two types of cell viability assays: CellTiter-Blue and CellTiter-Glo which measure metabolic capacity and ATP levels respectively.

➤ Confirmation using CellTiter-Blue cell viability assay

At the stage when the cells were tolerating a dose of 8 µg/ml which corresponds to around 3 fold the EC₅₀ of the susceptible cell line, comparison between the sensitivity of the selected and parental HepG2 cell lines to T/C activated Cry41Aa was performed (figure 112).

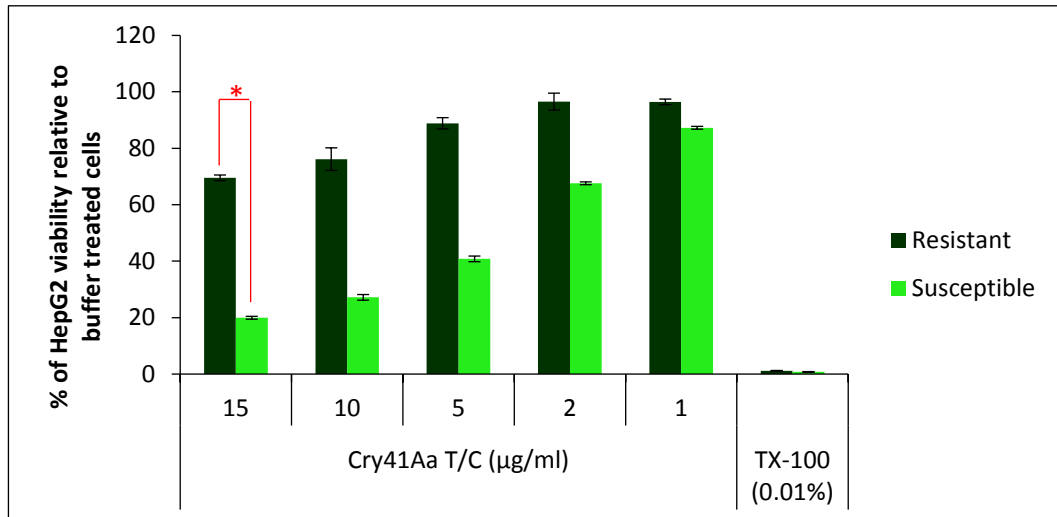


Figure 112: Assessment of the level of toxicity of T/C activated Cry41Aa on susceptible and HepG2 tolerating 8 µg/ml.

Susceptible and HepG2 tolerating 8 µg/ml were seeded at the density of 25×10^4 cells/ml. The next day the cells were treated with different concentrations (15, 10, 5, 2, 1 µg/ml) of ÄKTA purified T/C activated Cry41Aa. 24 hours later, cell viability was measured using CellTiter-Blue assay. Ttest was used to calculate the p value: * $p=1.46E-06$

According to our results, a difference in sensitivity to the toxin was observed which became significant at high doses of T/C activated Cry41Aa. In fact a concentration of 15 µg/ml resulted in a sharp and moderate decrease in viability of susceptible and resistant HepG2 respectively. TX-100 (0.01%) treatment, which was used as a positive control, caused a sharp decrease in viability for both cell lines.

When the cells were tolerating the toxin at a concentration of 30 µg/ml, the level of resistance was again assessed (Figure 113).

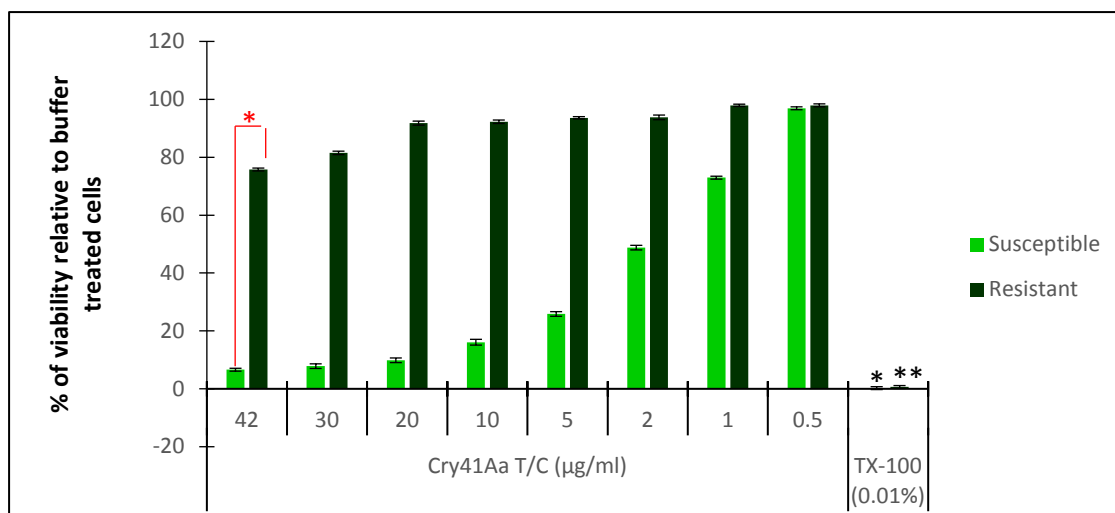


Figure 113: Assessment of the level of toxicity of T/C activated Cry41Aa on susceptible and HepG2 tolerating 30 µg/ml.

Susceptible and HepG2 tolerating 30 µg/ml were seeded at the density of 25×10^4 cells/ml. The next day the cells were treated with different doses (42, 30, 20, 10, 5, 2, 1, 0.5 µg/ml) of AKTA purified T/C activated Cry41Aa. 24 hours later, cell viability was measured using CellTiter-Blue assay. Ttest was used to calculate the p value: * $p=2.06E-06$, * $p=7.47E-08$ and ** $p=6.41 E-08$

Our results showed that there was a considerable difference in the level of toxicity of T/C activated Cry41Aa between susceptible HepG2 (EC_{50} around 3 µg/ml) and resistant HepG2 ($EC_{50} > 42$ µg/ml). A significant viability decrease was again shown for both cell lines upon treatment with TX-100 (0.01%).

At the stage when the cells were tolerating a dose of 50 µg/ml, the resistance phenotype was again checked (figure 114).

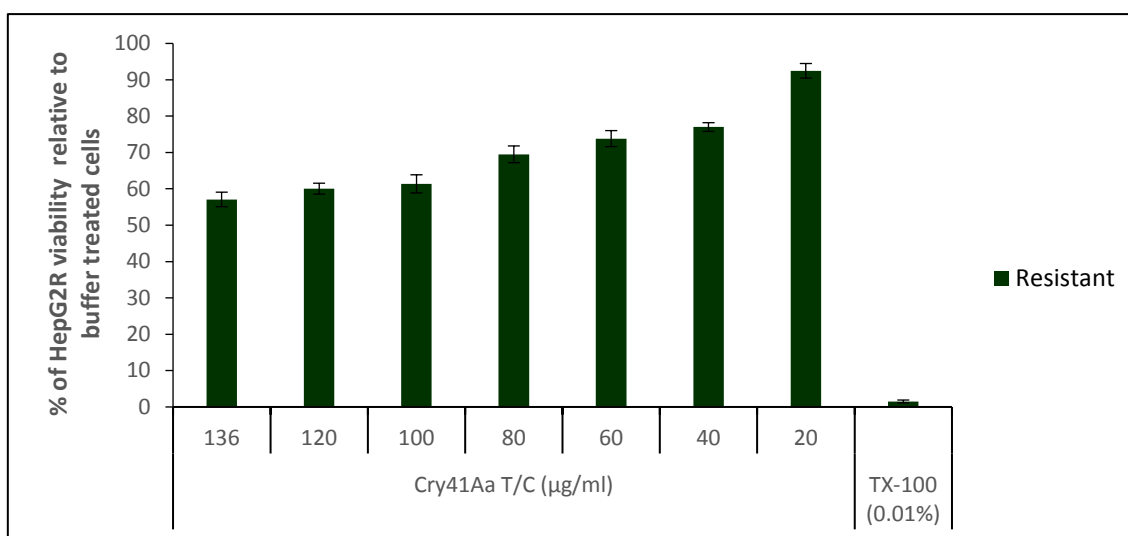


Figure 114: Assessment of the level of toxicity of T/C activated Cry41Aa on HepG2 tolerating 50 µg/ml.

HepG2 cells that were tolerating 50 µg/ml were seeded at the density of 25×10^4 cells/ml. The next day the cells were treated with different concentrations (136, 120, 100, 80, 60, 40, 20 µg/ml) of T/C activated Cry41Aa. 24 hours later, cell viability was measured using CellTiter-Blue.

According to our results, the resistance to the toxin reached a very high level. In fact, around 50% of cells were still viable upon treatment with the toxin at a concentration of 136 µg/ml which corresponds to around 50 fold more the EC_{50} of the parental cell line.

➤ **Confirmation using CellTiter-Glo Luminescence cell viability assay**

Total ATP levels, another indicator for cell viability, were measured in both susceptible and resistant HepG2 (tolerating 50 µg/ml) cell lines (Figures 115 and 116).

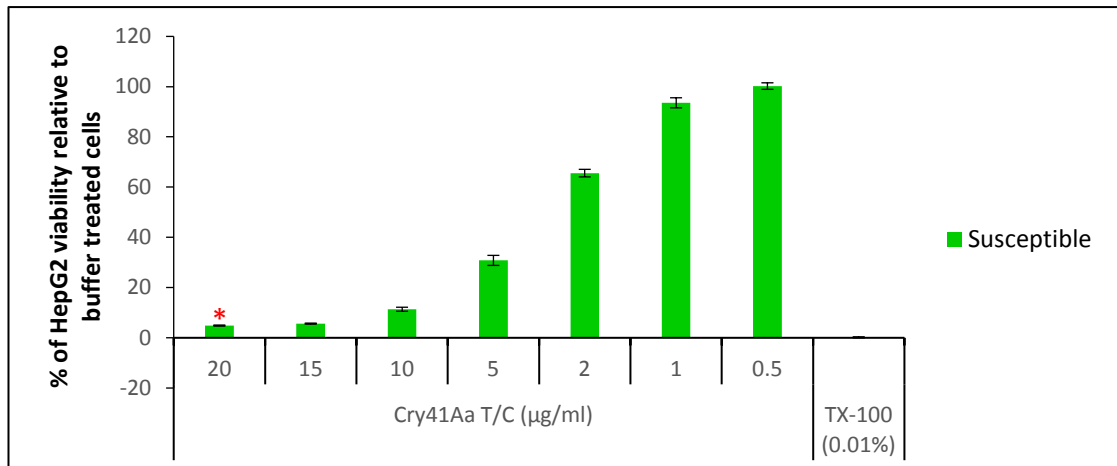


Figure 115: Assessment of ATP levels in susceptible HepG2 cells after exposure to T/C activated Cry41Aa.

HepG2 cells were seeded at the density of 25×10^4 cells/ml, in a white wall 96-well plate. The next day cells were dosed with different concentrations of purified T/C activated Cry41Aa (20, 15, 10, 5, 2, 1, 0.5 µg/ml), Triton X-100 (0.01%) or buffer. 24 hours later, cell viability was measured using CellTiter-Glo assay. Ttest was used to calculate the p value: * $p=2.15 \text{ E-}05$

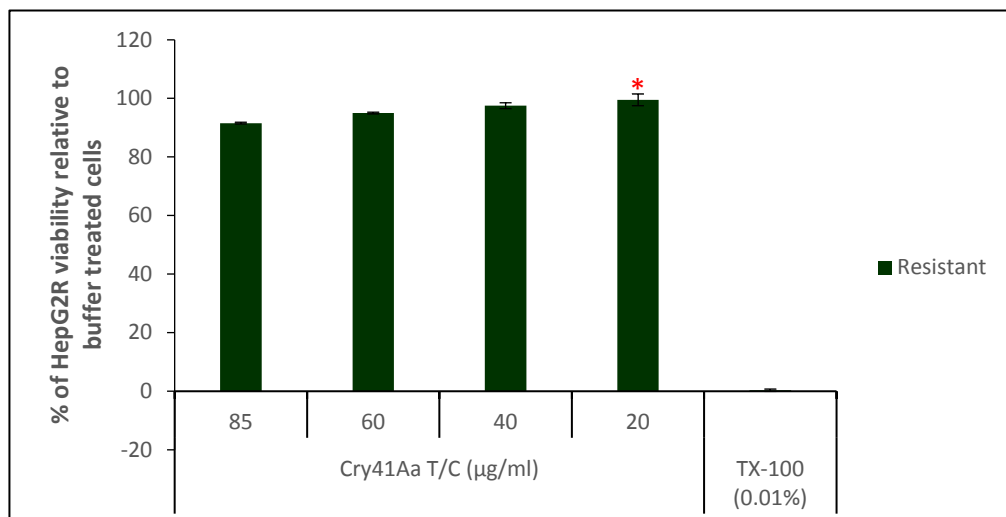


Figure 116: Assessment of ATP levels in resistant HepG2 cells after exposure to T/C activated Cry41Aa.

HepG2R cells were seeded at the density of 25×10^4 cells/ml, in a white wall 96-well plate. The next day cells were dosed with different concentrations of T/C activated Cry41Aa (85, 60, 40, 20 µg/ml) or buffer. 24 hours later, cell viability was measured using CellTiter-Glo assay. Ttest was used to calculate the p value: * $p=0.34$

Our results indicated that ATP levels were significantly reduced in susceptible HepG2 but not in resistant HepG2 exposed to higher concentrations of toxin.

Both types of cell viability assays showed that the selected cells presented a high level of resistance to the toxin. At this stage, the selection process was stopped and the resistant HepG2 cell line, grown in the EC_{50} dose of toxin (see next section), was used for further analyses.

6.4 Estimation of half maximal effective concentration (EC₅₀)

The level of toxicity of T/C activated Cry41Aa was evaluated on the susceptible and the established resistant HepG2 (HepG2R) cell lines using CellTiter-blue cell viability assay and the EC₅₀ values (effective concentration of the drug that gives half-maximal response) were determined using SPSS software (Statistical Package for the Social Sciences), Probit Regression analysis (Figures 117 and 118).

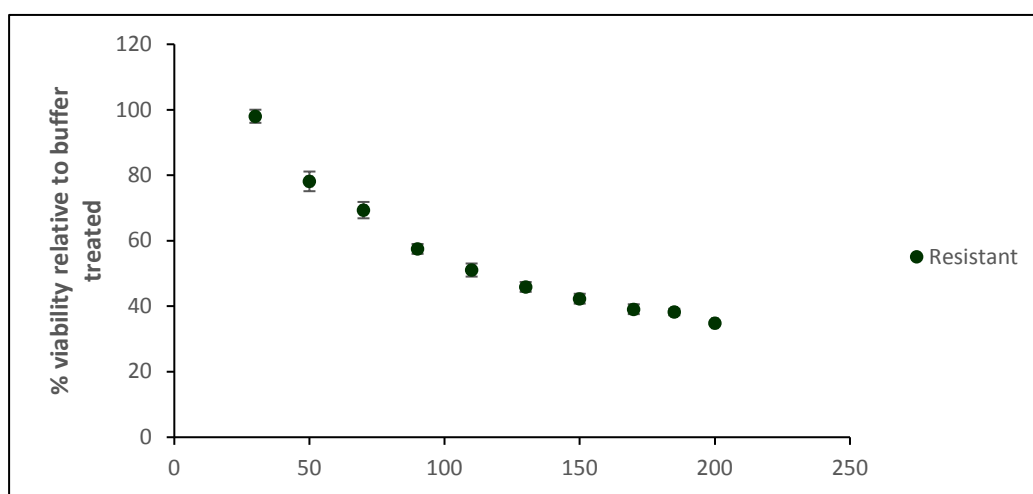


Figure 117: Evaluation of the level of resistance to the toxin in resistant HepG2 (HepG2R).

HepG2R cells were seeded at the density of 25×10^4 cells/ml. The next day cells were incubated with different doses of ÄKTA purified T/C activated Cry41Aa (30 - 200 µg/ml). Cell viability was measured after 24 hours using CellTiter-Blue.

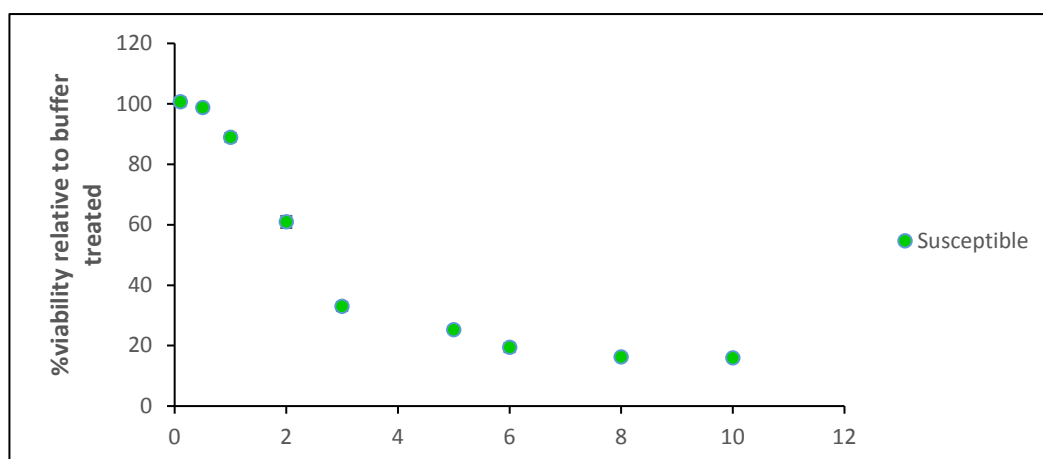


Figure 118: Assessment of the sensitivity of susceptible HepG2 to the toxin.

HepG2 cells were seeded at the density of 25×10^4 cells/ml. The next day cells were incubated with different doses of ÄKTA purified T/C activated Cry41Aa (0.1 - 10 µg/ml). Cell viability was measured after 24 hours using CellTiter-Blue.

According to our results the EC₅₀s of the resistant and susceptible HepG2 were 113.3 µg/ml and 2.76 µg/ml respectively therefore the resistance index was equal to 41, a value that is considered high compared with previous work where resistant cells to chemotherapeutic agents were studied.

6.5 Morphological changes

During the development of the resistance process, cell morphology was visualized at different stages. The most obvious aspect was the morphological difference between the cells cultured in toxin-free medium and when they were cultured in the presence of the toxic agent. In fact, when the cells were cultured in the presence of toxin, they showed an extended pseudopodia-like phenotype, however, this morphological aspect disappeared when the toxic agent was removed from the medium (figure 119).

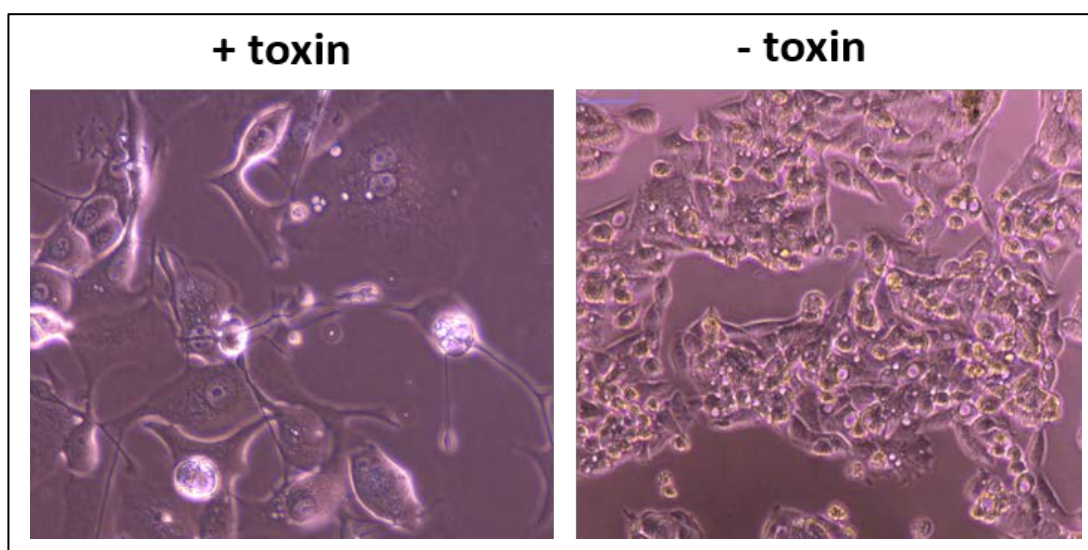


Figure 119: Microscopic observation of resistant HepG2 cultured in medium +/-toxin.

HepG2R were seeded at the density of 4×10^4 cells/ml in 2 wells of 6 well plate. The next day, the toxin (80 µg/ml) was added to one of the wells. After 4 days, the pictures were taken using Nikon Eclipse TS100 inverted microscope 10X objective. The picture of cells with toxin was zoomed in for clarification of the phenotype.

Morphological changes between the susceptible and resistant (cultured in toxin-free medium) cell lines were also examined using Differential Interference Contrast microscopy (DIC) which ensures good visualization of morphological features for unstained specimens (Figure 120).

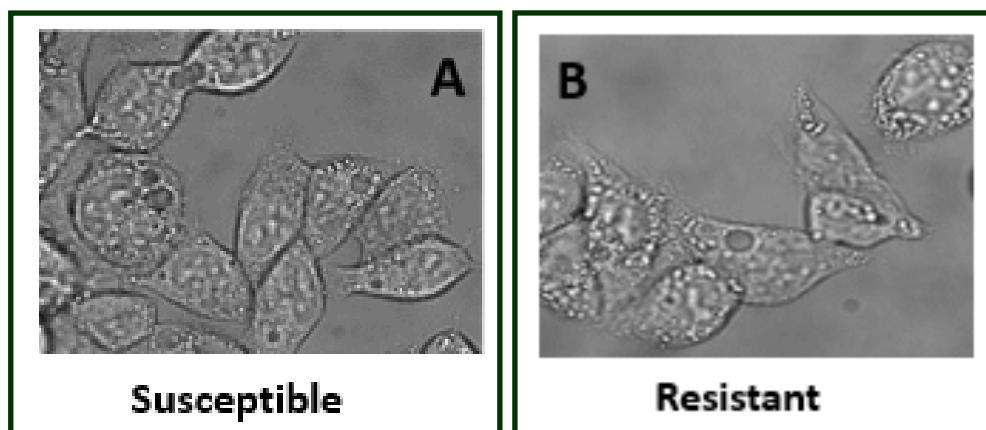


Figure 120: Morphological changes analysis between susceptible and resistant HepG2 cell lines. HepG2 and HepG2R cells were seeded at the density of 4×10^4 cells/ml in a microscope chamber slide. The next day, pictures were taken using Zeiss Axiovert 200M, 63x DIC objective.

According to our results, no obvious morphological alterations between susceptible HepG2 (A) and resistant HepG2 (B) were observed in the absence of toxin.

6.6 Cross resistance study

The acquisition of resistance to multiple anticancer drugs by human cells results in a serious problem in chemotherapy and it is also one of the reasons for tumour relapse and metastasis.

Previous attempts to generate resistant cancer cell line(s) to a particular chemotherapeutic drug(s), showed that most cells appeared to acquire a cross-resistance profile. In order to investigate if it is the case for resistant HepG2, two chemotherapeutic drugs were used (figure 121):

- Etoposide: works by blocking an enzyme (Topoisomerase 2) which is necessary for cancer cells to divide.
- 5-Fluorouracil: works by stopping the cells making and repairing DNA.

These two chemotherapeutic drugs were chosen based on the knowledge about the chemo-sensitivity of HepG2 towards them (Okamura et al., 2008, Xie et al., 2011).

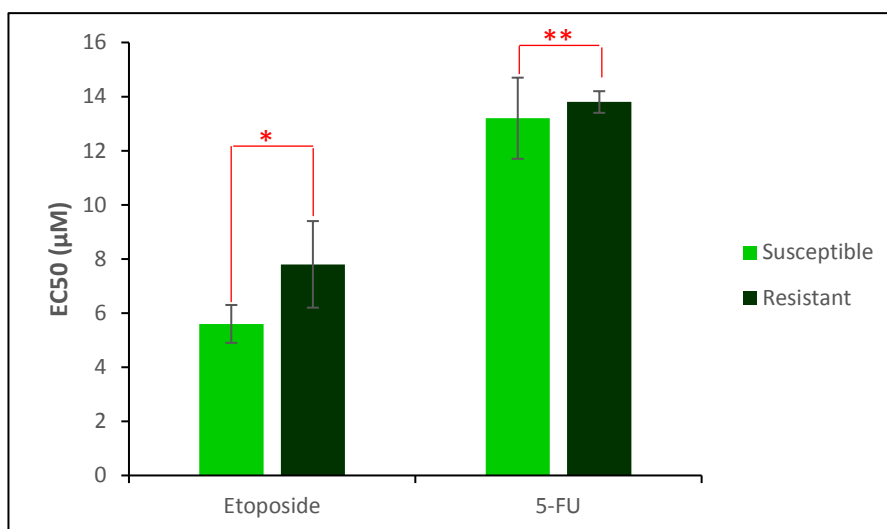


Figure 121: Assessment of the level of toxicity of Etoposide and 5-Fluorouracil (5-FU) against susceptible and resistant HepG2 cell lines.

HepG2 and HepG2R were seeded at the density of 5×10^4 cells/ml. The next day they were treated with different doses (0.5-80 μM) of Etoposide and 5-FU. 24 hours later, cell viability was measured using CellTiter-Blue assay. Ttest was used to calculate the p values: *p= 0.18 and **p= 0.25

No significant difference of the cytotoxic effect of both drugs was observed between the two cell lines indicating that the resistant HepG2 was not cross resistant to these two chemotherapeutic drugs.

Other drugs that were synthesized in the chemistry department of Sussex University by a PhD student (Fatai Afolabi) were also tested on both cell lines (figure 123). These drugs consists of acridine gold derivatives (figure 122).

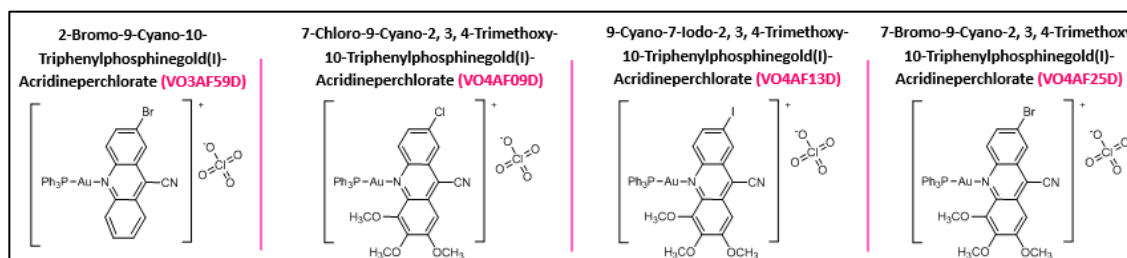


Figure 122: Different compounds that were used to assess the cross resistance phenotype in resistant HepG2 cell line

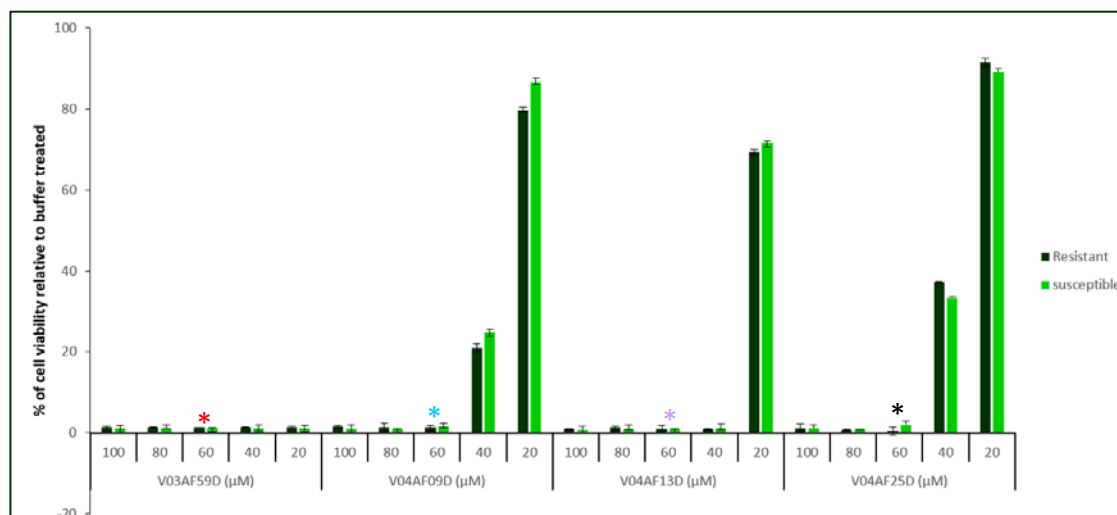


Figure 123: Assessment of the sensitivity of susceptible and resistant HepG2 cell lines to acridine gold derivatives. HepG2 and HepG2R were seeded at the density of 25×10^4 cells/ml. The next day they were treated of different concentrations of V03AF59D, V04AF09D, V04AF13D and V04AF25D. 24 hours later, cell viability was measured using CellTiter-Blue assay. Ttest: p values calculated for the 4 acridine compounds were $0.11 < p < 0.32$

According to our results, similar level of sensitivity of the susceptible and resistant HepG2 cell lines to these drugs was observed indicating that the generated resistant HepG2 was also not cross resistant to the acridine gold derivatives described above.

6.7 Assessment of membrane damage: Patch clamp analysis

Patch clamp is the most widely used experimental method allowing the measurement of ionic currents in excised patches as well as in intact membranes. Whole-cell recordings are used to assess ion channel activity of the entire cell membrane.

Whole cell patch clamping was then used to observe macroscopic current activity in HepG2 and HepG2R cells during exposure to PS-3. The cells were given to Barbara Domanska who carried out the electrophysiology experiments in collaboration with Prof Jean-Louis Schwartz in Montreal in 2016.

The recordings were obtained before toxin addition and every 5 minutes for 20 minutes after toxin treatment. A set of current /voltage relationships (I/V curve) of HepG2 and HepG2R cells exposed to T/C activated Cry41Aa was carried out in a time course experiments (Figures 124 and 125). Digitonin treated HepG2R cells served as a positive

control (Figure 127) while HepG2R cells exposed to Cry1Ca were tested as a negative control (Figure 126).

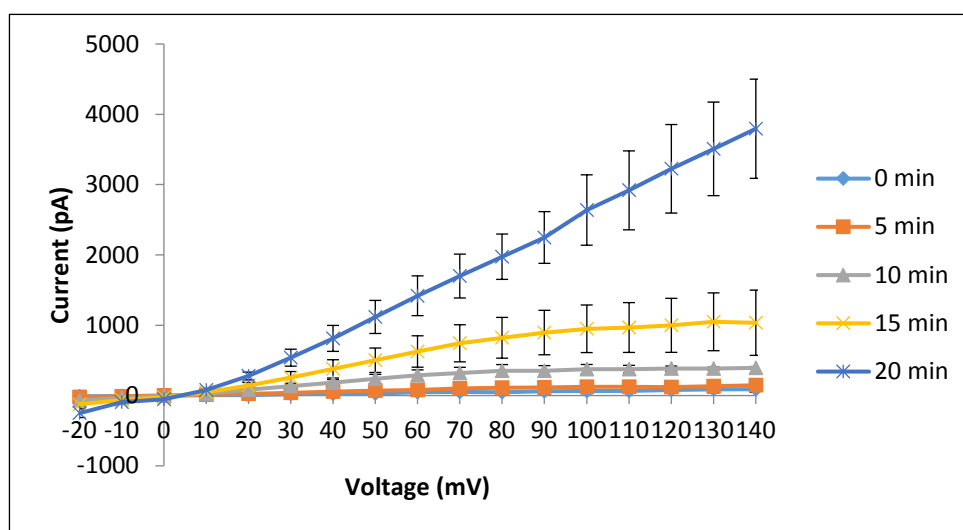


Figure 124: Whole cell patch clamp recordings from a time course experiment of HepG2 cells exposed to T/C activated Cry41Aa.

HepG2 cells were seeded at the density of 5×10^4 cells/ml on a glass coverslip inside a 35 mm petri dish. The next day whole cell patch clamp recordings from a single cell were reported at 0, 5, 10, 15, 20 minutes after Cry41Aa ($12 \mu\text{g/ml}$) addition to the bath containing NaCl solution. Currents were induced by a 1 second set of depolarizing potentials from -20 to 140 mV from a holding potential of -20 mV. Error bars indicate the standard error of the mean. The lines show the mean currents from three representative experiments from three different cells patched.

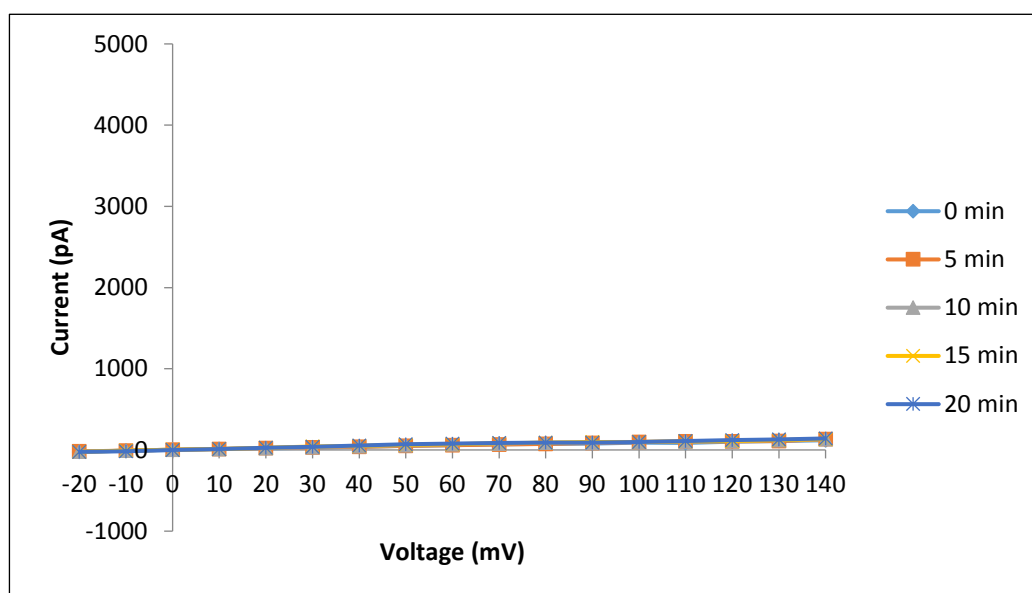


Figure 125: Whole cell patch clamp recordings from a time course experiment of HepG2R cells exposed to Cry41Aa.

HepG2R cells were seeded at the density of 5×10^4 cells/ml on a glass coverslip inside a 35 mm petri dish. The next day whole cell patch clamp recordings from a single cell were reported at 0, 5, 10, 15, 20 minutes after Cry41Aa ($20 \mu\text{g/ml}$) addition to the bath containing NaCl solution. Currents were induced by a 1 second set of depolarizing potentials from -20 to 140 mV from a holding potential of -20 mV. Error bars indicate the standard error of the mean. The lines show the mean currents from three representative experiments from three different cells patched.

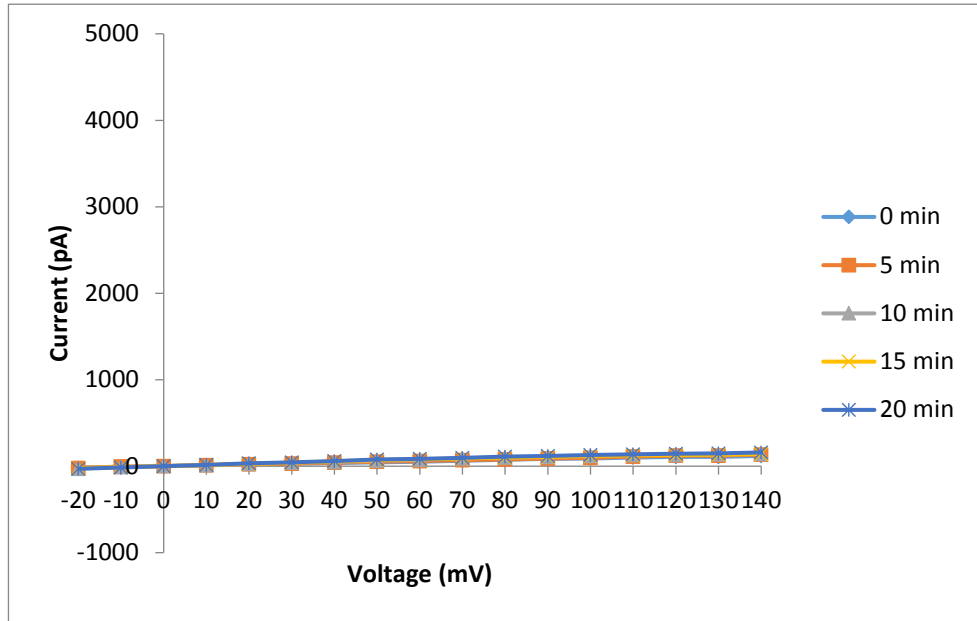


Figure 126: Whole cell patch clamp recordings from a time course experiment of HepG2R cells exposed to Cry1Ca. HepG2R cells were seeded at the density of 5×10^4 cells/ml on a glass coverslip inside a 35 mm petri dish. The next day whole cell patch clamp recordings from a single cell were reported at 0, 5, 10, 15, 20 minutes after Cry1Ca ($12 \mu\text{g/ml}$) addition to the bath containing NaCl solution. Currents were induced by a 1 second set of depolarizing potentials from -20 to 140 mV from a holding potential of -20 mV. Error bars indicate the standard error of the mean. The lines show the mean currents from three representative experiments from three different cells patched.

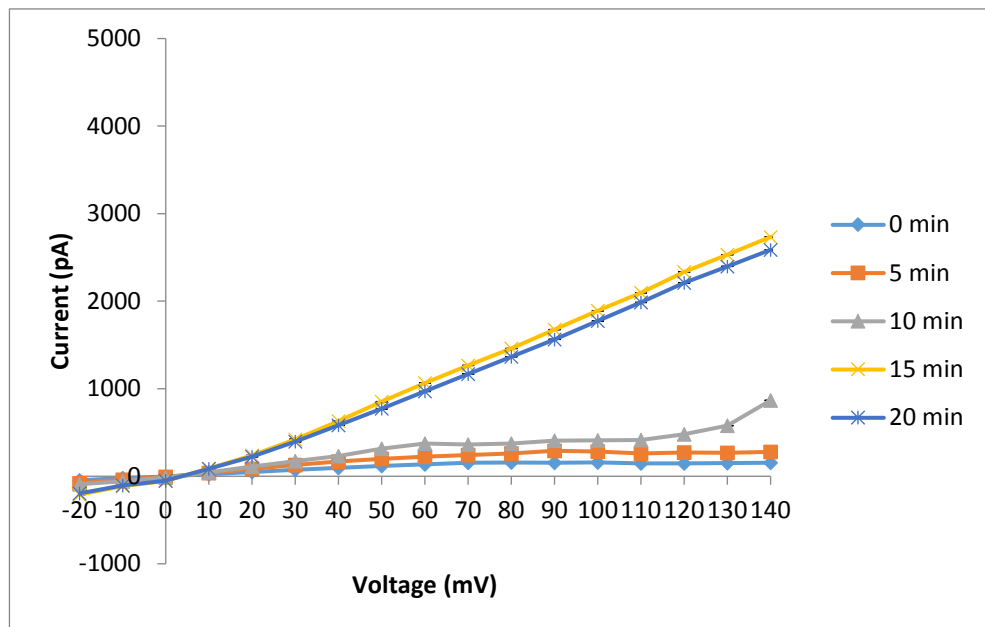


Figure 127: Whole cell patch clamp recordings from a time course experiment of HepG2R cells exposed to digitonin. HepG2R cells were seeded at the density of 5×10^4 cells/ml on a glass coverslip inside a 35 mm petri dish. The next day whole cell patch clamp recordings from a single cell were reported at 0, 5, 10, 15, 20 minutes after digitonin ($13 \mu\text{g/ml}$) addition to the bath containing NaCl solution. Data came from a single patch clamp experiment.

Whole cell patch clamp recordings showed that at a concentration of 12 $\mu\text{g/ml}$, T/C activated Cry41Aa induced large currents (which increased proportionally with increased voltage applied) in susceptible unlike in resistant HepG2 that were exposed to a higher dose of toxin (20 $\mu\text{g/ml}$).

Cry1Ca that was used as a negative control did not induce large currents while in digitonin treated cells at 20 minute time point currents increased proportionally with increased voltage applied.

6.8 Characterisation of HepG2R cell response to the toxin compared with the parental cell line

- **Activation of p38 MAP kinase pathway**

Knowing that Cry41Aa caused p38 phosphorylation in susceptible HepG2 (see chapter 5 section 5-2), it was interesting to investigate if this response was similar in the resistant line. Western blot technique was used to analyse the extracts of both cell lines that were exposed to toxin, sodium arsenite (potent p38 inducer), Cry1Ca and buffer (used as negative controls) (Figure 128).

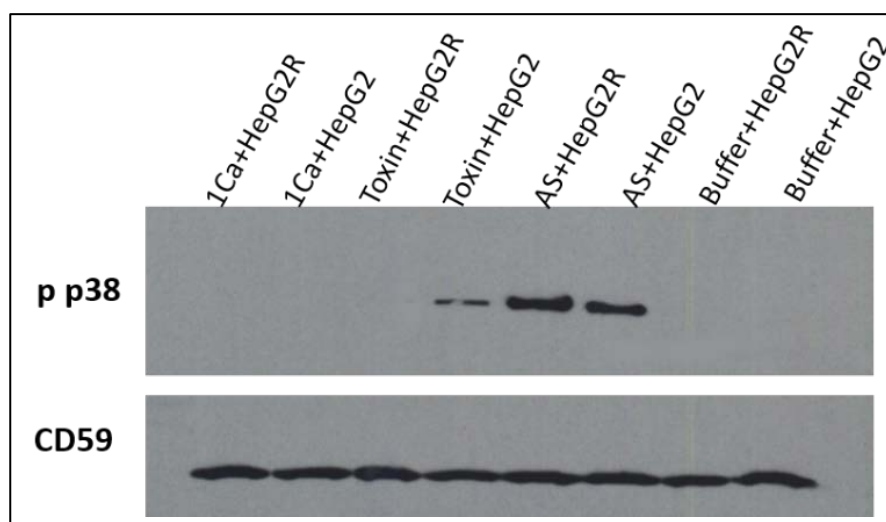


Figure 128: Assessment of p38 activation in toxin treated HepG2 and HepG2R cells.

HepG2 and HepG2R cells were treated with purified T/C activated Cry41Aa (12 $\mu\text{g/ml}$), buffer, sodium arsenite (0.5 mM), or Cry1Ca (12 $\mu\text{g/ml}$) for 30 minutes. Next, cells were lysed in RIPA buffer. 15 μg of protein from each sample were loaded in each lane and analysed by western blot for the presence of phosphorylated p38 (pp38). CD59 was used as the loading control.

p38 phosphorylation was elevated in sodium arsenite treated HepG2 and HepG2R. However T/C activated Cry41Aa at a concentration of 12 $\mu\text{g/ml}$ caused p38 phosphorylation in susceptible but not in resistant HepG2 cells and no signal was produced from the extracts of cells that were exposed to Cry1Ca.

In order to figure out if a higher dose of toxin would induce p38 phosphorylation in the resistant cell line, the cells were dosed with 120 $\mu\text{g/ml}$ of toxin and the extracts were analysed (Figure 129).

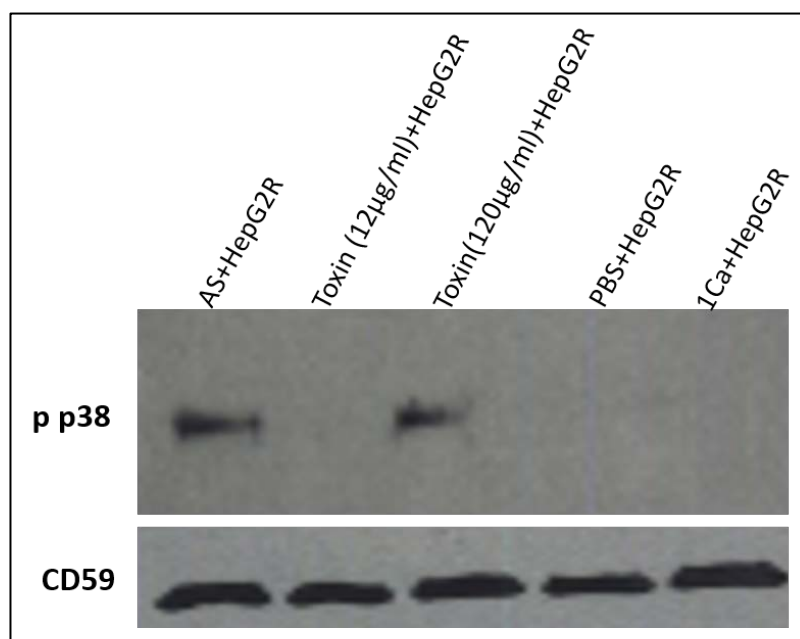


Figure 129: Assessment of p38 activation in toxin treated HepG2R cells.

HepG2R cells were treated with purified T/C activated Cry41Aa (120 $\mu\text{g/ml}$), buffer, sodium arsenite (0.5mM), or Cry1Ca (12 $\mu\text{g/ml}$) for 30 minutes. Next, cells were lysed in RIPA buffer. 20 μg of protein from each sample were loaded in each lane and analysed by western blot for the presence of phosphorylated p38. CD59 was used as the loading control.

Signal was produced from the extracts of cells exposed to sodium arsenite and T/C activated Cry41Aa at a concentration of 120 $\mu\text{g/ml}$ indicating that as with susceptible HepG2 (Domanska, 2016), toxin concentrations around the EC_{50} levels induced p38 phosphorylation in the resistant subline.

- **Assessment of EGTA effect on toxin action**

A detailed study on the effect of different metal ion chelators on Cry41Aa activity was carried out by Domanska in 2016 who had shown that EGTA inhibited the effect of

Cry41Aa on susceptible HepG2. We confirmed this finding (figure 130). The effect of this chelator on toxin activity in resistant HepG2 was then investigated (figure 131).

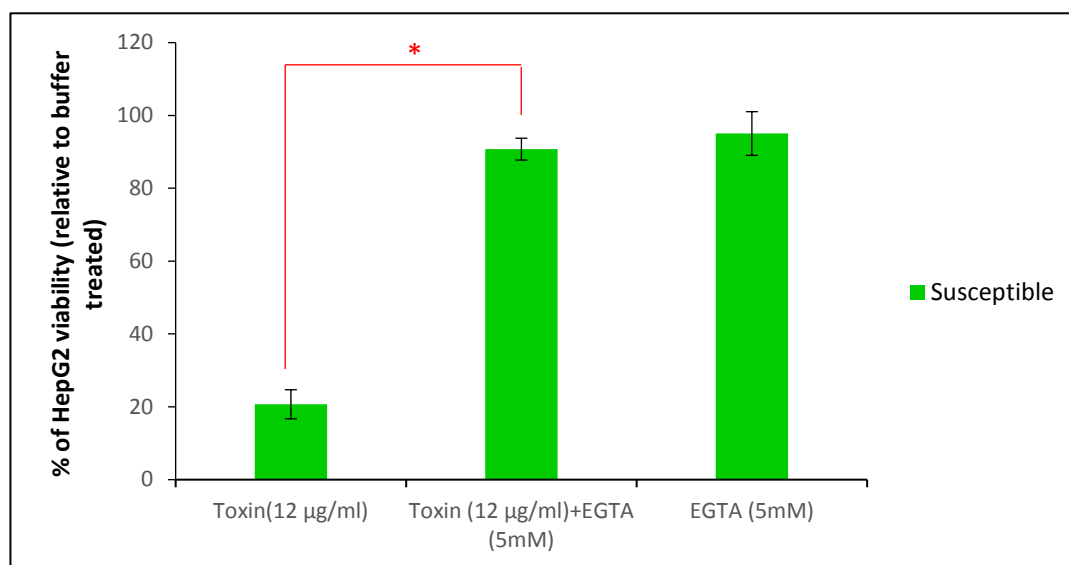


Figure 130: The effect of chelating agent (EGTA) on the viability of toxin treated HepG2 cells.

HepG2 cells were seeded at the density of 25×10^4 cells/ml. The next day cells were pre-incubated with 5 mM of EGTA or water (mock) for 30 min followed by the addition of toxin (12 µg/ml). The readings were taken 6 hours after toxin addition using CellTiter-Blue assay. Ttest was used to calculate the p value: * $p=0.0005$

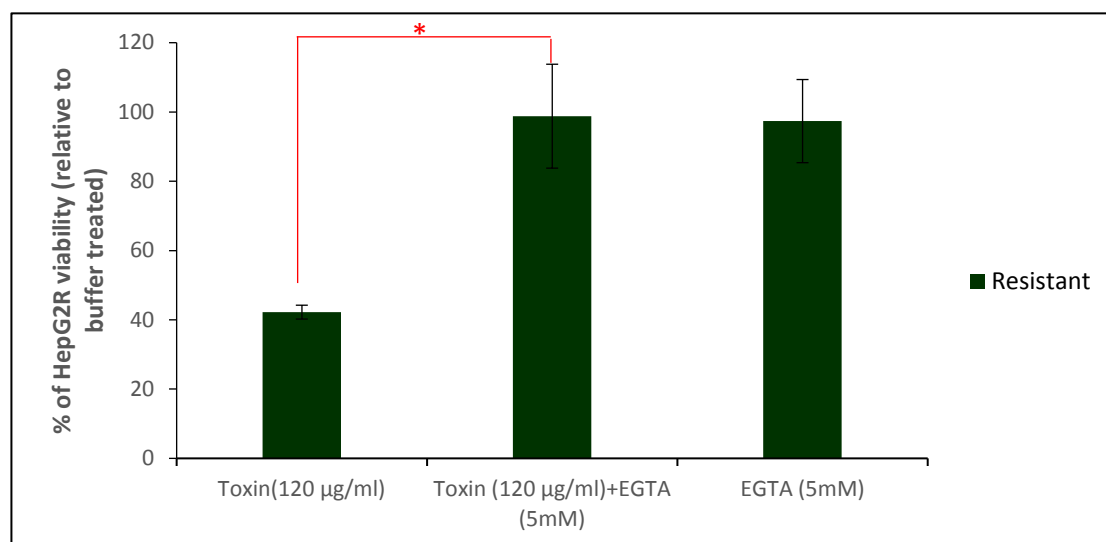


Figure 131: The effect of chelating agent (EGTA) on the viability of toxin treated HepG2R cells.

HepG2 cells were seeded at the density of 25×10^4 cells/ml. The next day cells were pre-incubated with 5 mM of EGTA or water (mock) for 30 min followed by the addition of toxin (120 µg/ml). The readings were taken 6 hours after toxin addition using CellTiter-Blue assay. Ttest was used to calculate the p value: * $p=0.0001$

According to our results EGTA significantly reduced the cytotoxicity of T/C activated Cry41Aa at a concentration of 12 and 120 $\mu\text{g}/\text{ml}$ in susceptible and resistant HepG2 cells respectively.

6.9 Stability of the resistance phenotype

In order to figure out the stability of the toxin-resistance phenotype in HepG2R cultured in the absence of the toxin, the selected cell line was cultured in DMEM only and the sensitivity to the toxin was monitored over time (Figure 132).

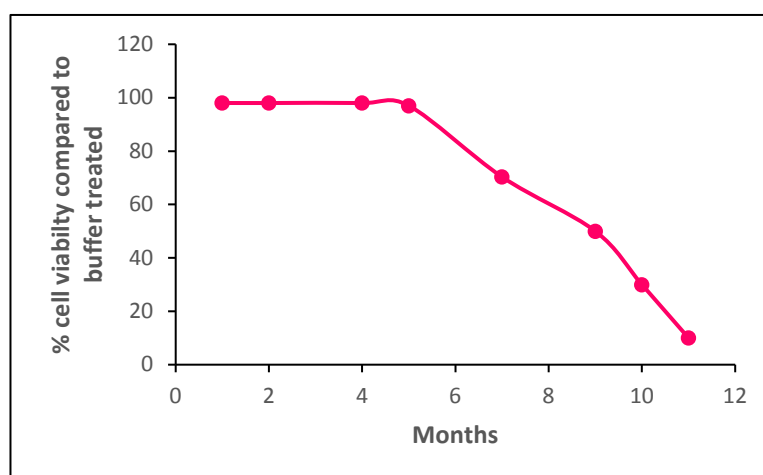


Figure 132: Assessment of the cytotoxic effect of T/C activated Cry41Aa on HepG2R cultured in medium free of toxin over time.

HepG2R at different time points during a period of 10 months were seeded at a density of 25×10^4 cells/ml. The next day the cells were treated with purified T/C activated Cry41Aa at a concentration of 20 $\mu\text{g}/\text{ml}$. 24 hours later, cell viability was measured using CellTiter-Blue assay.

According to figure 132, after 5 months of culturing the resistant HepG2 in medium free of T/C activated Cry41Aa, the level of toxin resistance started to decrease gradually over time. In fact, the treatment of cells with the toxin at a concentration of 20 $\mu\text{g}/\text{ml}$ had no cytotoxic effect at the beginning of the procedure. 5 months later, cell viability started to decrease gradually to reach 10% after 10 months.

The cytotoxicity level of T/C activated Cry41Aa was then assessed on both the reverted and the susceptible HepG2 cell lines (Figure 133).

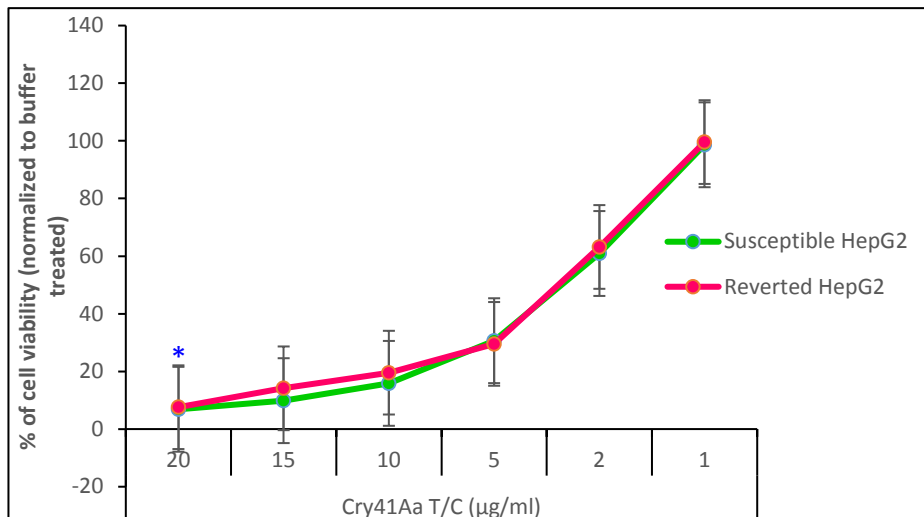


Figure 133: Comparison between the cytotoxic effect of the toxin on reverted and susceptible HepG2 cell lines.

Susceptible and reverted HepG2 cells were seeded at a density of 25×10^4 cells/ml. The next day they were treated with different concentrations of purified T/C activated Cry41Aa (20, 15, 10, 5, 2, 1 µg/ml). 24 hours later the cell viability was measured using CellTiter-Blue assay. Ttest was used to calculate the p value: *p=0.52 (p values for all other concentrations used were >0.05)

Our results indicated that the toxin exhibited the same level of cytotoxic effect on both cell lines suggesting that culturing resistant HepG2 in medium free of toxin during a period of around 10 months resulted in them reverting to a susceptible cell line.

In order to figure out if selective pressure was driving the reversion, the growth of HepG2 cell lines were monitored over time (Figure 134).

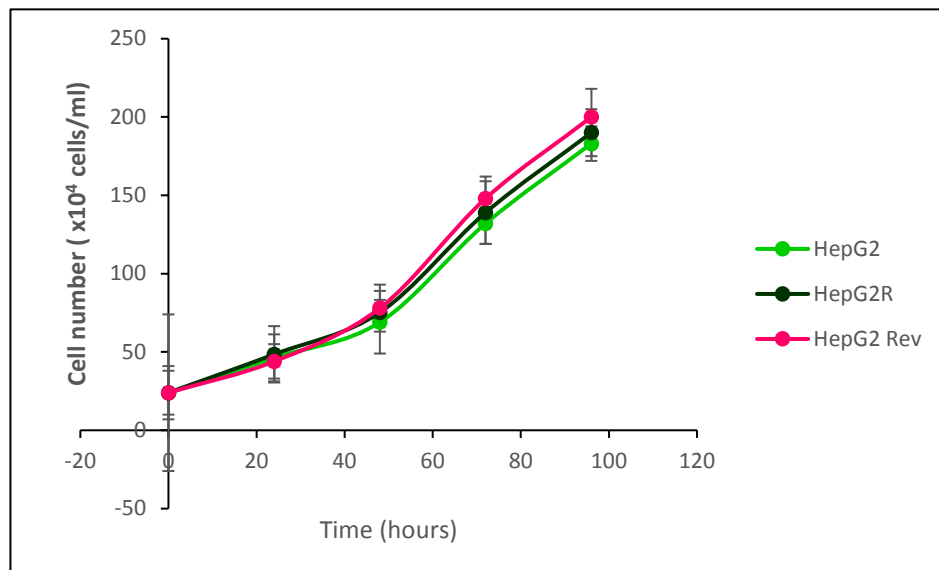


Figure 134: Growth curve comparison between susceptible, resistant and reverted HepG2 cell lines.

HepG2 cell lines were seeded at the same cell density (25×10^4 cells/ml). The growth of cells was monitored by counting cells using Trypan blue reagent and haemocytometer chamber. Three replicates were used for each determination and four cell counts for each replicate from each cell line were made every 24 hours for 5 days.

According to our results there was no selective pressure to drive HepG2R reversion as similar growth curves were observed in susceptible, reverted and resistant HepG2 cell lines. No selective pressure suggests no need to reverse a mutation. Therefore, perhaps an epigenetic effect might have influenced gene expression. RNA sequencing was a good approach to test this possibility.

Thus, transcriptome sequencing was used to unravel molecular processes potentially responsible for the resistance mechanism.

6.10 RNA isolation and sequencing

Total RNA was extracted from both susceptible and resistant HepG2 cell lines using RNeasy Kit (Qiagen) according to the manufacturer's instructions. The RNAs were eluted in 40 μ L of RNase/DNase-free water and stored at -80°C until analysis. Initially, concentration and purity of the RNA samples were measured using a NanoDrop ND-2000 spectrophotometer where A260/A280 ratios were in the range of 1.8 to 2.0 indicating the purity of the samples of interest. After being denatured, the RNAs were then run on agarose gel in order to check the presence of the desired bands (Figure 135).

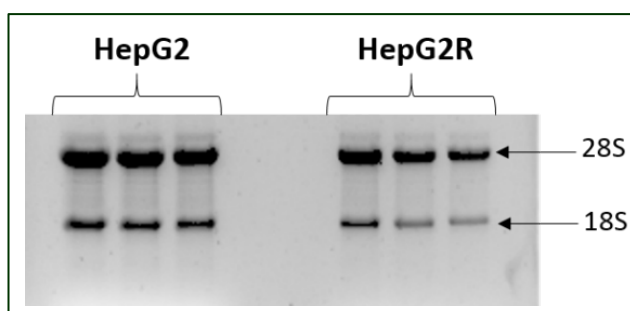


Figure 135: Agarose gel of total RNAs extracted from susceptible and resistant HepG2.

Total RNAs were extracted from HepG2 and HepG2R using RNeasy kit as per manufacturer's instructions. Three biological replicates for each cell line were then denatured using formaldehyde and heating then run on 1% agarose gel.

According to figure 135, the 28S and the 18S ribosomal RNAs were clearly visible. The absence of a smeary profile in the lanes suggested that the RNA samples were intact with no degradation observed.

The integrity of RNA samples was later assessed by microfluidic capillary electrophoresis using an Agilent 2100 Bioanalyzer and the RNA 6000 Nano Chip kit. Using electrophoretic separation on microfabricated chips, RNA samples were separated and subsequently detected via laser induced fluorescence detection. The Bioanalyzer software generated a gel-like image (figure 136) and electropherograms (figure 137) providing a detailed assessment of the quality of the RNA samples. In principle, by the mean of an Agilent Bioanalyser, the quality of RNA is determined based on an RNA Integrity Number (RIN) which varies between 1 and 10 with 10 being the highest quality samples showing the least degradation. Values of RIN that are greater than 8 were considered acceptable. In humans, 28S rRNA has around 5070 nucleotides, and 18S has 1869 nucleotides, which gives a 28S/18S ratio of around 2.7. A high 28S/18S ratio (usually greater than 2) is an indication that the purified RNA is intact and hasn't degraded.

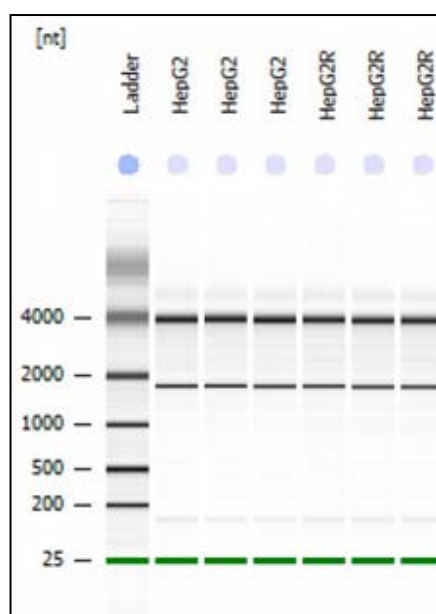


Figure 136: The computerised RNA gel generated by the BioAnalyser instrument.

Lane 1: ladder, 2-4 lanes: the three technical repeats of HepG2 and 5-7 lanes: the three technical repeats of HepG2R.

According to the banding profile, the presence of three distinct bands indicated high quality of RNA samples (Aranda et al., 2012). The top band represents 28S ribosomal RNA (rRNA) of around 4 kb, the middle band represents 18S rRNA of 1.9 kb and the third band represents 5.8S (154 nt) and 5S (117 nt) RNA. Transfer RNAs (73-93 nt) were not visible.

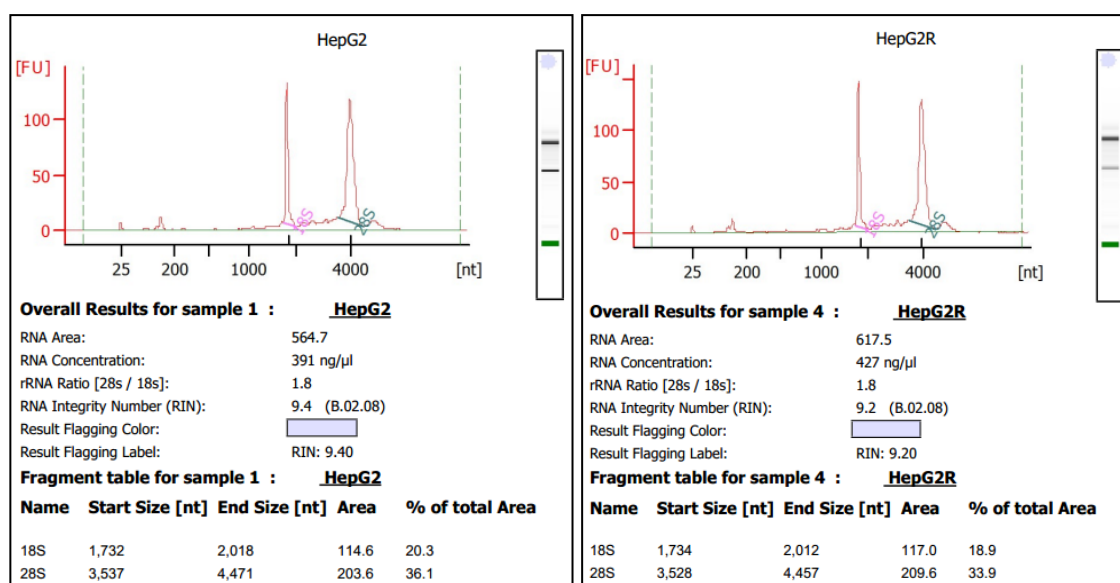


Figure 137: Electropherograms of extracted RNAs from susceptible and resistant HepG2 cell lines.

Electropherogram traces for approximately 400 ng of RNA target applied to an RNA Nano Chip were generated on the 2100 Bioanalyzer

According to the electropherograms, the RNA integrity number of resistant and susceptible HepG2 were 9.2 and 9.4 respectively, values that were considered within the range indicating high purity of the samples. 28S/18S ratio was 1.8 for both cell lines which was acceptable. The concentrations of RNA samples of susceptible and resistant HepG2 cell lines were 391 ng/μl and 427 ng/μl respectively which were satisfactory knowing that the concentration required for RNA sequencing technique was 1 μg per sample.

Thus, spectrophotometric measurements and molecular sizing with the 2100 Bioanalyzer have proven that the RNA samples were of a high quality.

Knowing that RNA sequencing analysis provides a comprehensive understanding of the complexity of eukaryotic transcriptome and in an attempt to better understand the mechanism of action of Cry41Aa against HepG2 cells, total RNAs of both susceptible and resistant HepG2 cell lines were sequenced by a third party-GATC biotech company.

The generated FASTQ files were analysed using bioinformatic tools (usegalaxy.org). The reads were aligned onto the UCSC reference genome (hg38) using TopHat. The aligned reads were assembled into transcripts using the Cufflinks software which computes normalized values termed FPKM (fragments per kilobase of exon per million fragments mapped), that reflect the mRNA expression levels. Statistical analysis of differentially expressed genes was performed using Cuffdiff, which is integrated into Cufflinks (figure 138).

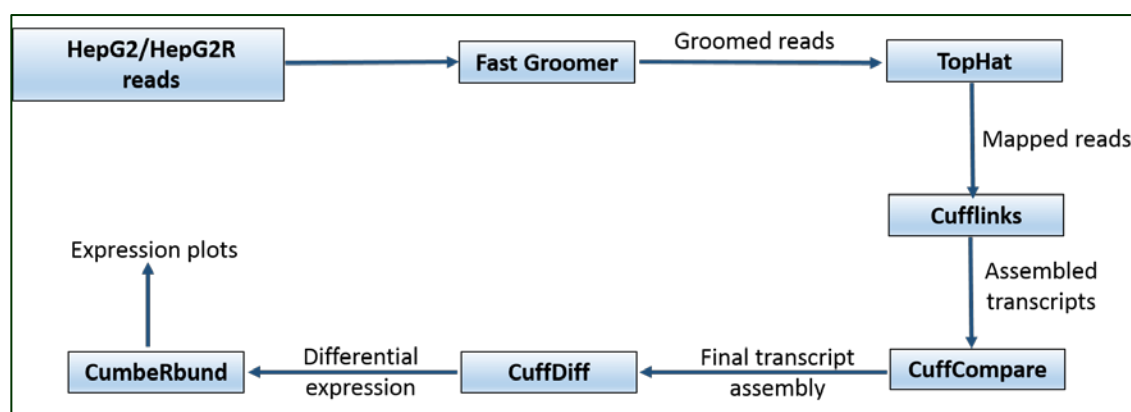


Figure 138: Steps followed in order to analyse the RNA-seq data.

Although around 22,000 protein-coding genes are present in the human genome, our data revealed 35123 differentially expressed transcripts between HepG2 and HepG2R. This could be explained by the fact that these would include a myriad of non-protein coding sequences.

Out of the 35123 differentially expressed transcripts, 56 were significantly dissimilar (table 6). Some of these transcripts were upregulated or downregulated, others were expressed in one cell line but not the other (table 7). Using the locus of each transcript, the gene name was determined using UCSC genome browser (genome.ucsc.edu/), although there were a few that could not be identified.

Table 6: List of differentially expressed genes between HepG2 and HepG2R (Data was altered from the differential gene expression file provide by 'Cuffdiff').

The test stat represents the value of the test statistic that is used to determine the significance of the observed expression levels. The p value shows the uncorrected probability value of the test statistic while the q value represents the false discovery rate corrected p-value. The significance level is determined by whether the p-value is greater than the false discovery rate after a number of computational corrections.

Gene Name	locus	sample 1	sample 2	value 1	value 2	log2(fold change)	test stat	p value	q value	Significant	
SERINC2	chr1:31413180-31434667	HepG2	HepG2R	12.0368	59.8681		2.31434	4.81204	5.00E-05	0.0317036	yes
LEPR	chr1:65525787-65635379	HepG2	HepG2R	0.751087	5.01881		2.74029	4.69117	5.00E-05	0.0317036	yes
FHAD1	chr1:15370337-15370949	HepG2	HepG2R	0	2.41222	inf	-nan	5.00E-05	0.0317036	yes	
SLC16A9	chr10:59650766-59664327	HepG2	HepG2R	0.424059	9.99457		4.55881	6.14033	5.00E-05	0.0317036	yes
AKR1C4	chr10:5218717-5219117	HepG2	HepG2R	0	4.0796	inf	-nan	5.00E-05	0.0317036	yes	
RTN4RL2	chr11:57460432-57477533	HepG2	HepG2R	2.57195	22.4577		3.12628	5.74333	5.00E-05	0.0317036	yes
PLEKHB1	chr11:73646725-73662876	HepG2	HepG2R	50.8047	12.9621		-1.97066	-4.14929	5.00E-05	0.0317036	yes
E2F8	chr11:19237852-19241648	HepG2	HepG2R	3.57194	0	inf	-nan	5.00E-05	0.0317036	yes	
HEPACAM	chr11:12491264-124936403	HepG2	HepG2R	27.558	3.74083		-2.88104	-5.10179	5.00E-05	0.0317036	yes
SLC22A25	chr11:63167014-63167793	HepG2	HepG2R	0	2.08587	inf	-nan	5.00E-05	0.0317036	yes	
ADGRD1	chr12:131005970-131141461	HepG2	HepG2R	0.738379	6.09474		3.04513	4.89252	5.00E-05	0.0317036	yes
HAL	chr12:95972623-95996375	HepG2	HepG2R	8.4644	181.61		4.42329	5.56081	5.00E-05	0.0317036	yes
KITLG	chr12:88494249-88495198	HepG2	HepG2R	1.60889	0	inf	-nan	5.00E-05	0.0317036	yes	
KITLG	chr12:88495343-88496180	HepG2	HepG2R	1.10846	0	inf	-nan	5.00E-05	0.0317036	yes	
unknown	chr12:132424517-132427268	HepG2	HepG2R	0.97553	6.77257		2.79545	4.49903	5.00E-05	0.0317036	yes
TNFRSF19	chr13:23570480-23676086	HepG2	HepG2R	69.1612	13.9083		-2.31401	-4.42069	5.00E-05	0.0317036	yes
SLC25A47	chr14:100323304-100330370	HepG2	HepG2R	0.994425	12.9667		3.70481	5.69909	5.00E-05	0.0317036	yes
GPX2	chr14:64939152-64942857	HepG2	HepG2R	368.142	97.3357		-1.91922	-4.13282	5.00E-05	0.0317036	yes
unknown	chr14:101325645-101326669	HepG2	HepG2R	0	1.01254	inf	-nan	5.00E-05	0.0317036	yes	
AQP9	chr15:5813837-58166800	HepG2	HepG2R	0	14.5351	inf	-nan	5.00E-05	0.0317036	yes	
unknown	chr15:85272646-85272811	HepG2	HepG2R	0	988.18	inf	-nan	5.00E-05	0.0317036	yes	
DPEP1	chr16:89622269-89638525	HepG2	HepG2R	16.9068	1.23833		-3.77114	-5.95789	5.00E-05	0.0317036	yes
COTL1	chr16:84565629-84618059	HepG2	HepG2R	27.5703	4.23102		-2.70404	-4.96356	5.00E-05	0.0317036	yes
GGPC	chr17:42900671-42916940	HepG2	HepG2R	5.29248	54.8682		3.37396	7.01461	5.00E-05	0.0317036	yes
unknown	chr17:40474400-40475470	HepG2	HepG2R	1.14776	0	inf	-nan	5.00E-05	0.0317036	yes	
OSBP1A	chr18:24171408-24178195	HepG2	HepG2R	0	5.03491	inf	-nan	5.00E-05	0.0317036	yes	
A1BG	chr19:58346739-58353630	HepG2	HepG2R	19.0802	95.8802		2.32916	4.96444	5.00E-05	0.0317036	yes
IL1RN	chr2:11312176-113134017	HepG2	HepG2R	25.6392	90.5076		1.81969	3.90344	5.00E-05	0.0317036	yes
EHD3	chr2:31266727-31267788	HepG2	HepG2R	1.46683	0	inf	-nan	5.00E-05	0.0317036	yes	
XIRP2	chr2:167258972-167259670	HepG2	HepG2R	0	2.36571	inf	-nan	5.00E-05	0.0317036	yes	
TMEFF2	chr2:192061439-192061974	HepG2	HepG2R	0	2.60188	inf	-nan	5.00E-05	0.0317036	yes	
PCK1	chr20:57561076-57571204	HepG2	HepG2R	5.29914	133.156		4.65121	5.26883	5.00E-05	0.0317036	yes
AGTR1	chr3:148697817-148743008	HepG2	HepG2R	1.37468	21.6965		3.9803	6.77748	5.00E-05	0.0317036	yes
unknown	chr3:64448099-64449152	HepG2	HepG2R	0	1.99212	inf	-nan	5.00E-05	0.0317036	yes	
SPP1	chr4:87975620-87983410	HepG2	HepG2R	328.811	4.99644		-6.04021	-11.1174	5.00E-05	0.0317036	yes
UGT2B11	chr4:69199719-69214737	HepG2	HepG2R	3.56954	27.5446		2.94796	5.43708	5.00E-05	0.0317036	yes
UGT2B4	chr4:69479485-69495896	HepG2	HepG2R	8.47553	126.444		3.89905	7.969	5.00E-05	0.0317036	yes
FAM13A	chr4:88726279-88823344	HepG2	HepG2R	4.59293	29.5521		2.68577	5.23934	5.00E-05	0.0317036	yes
VCAN	chr5:83483537-83493703	HepG2	HepG2R	2.30837	0	inf	-nan	5.00E-05	0.0317036	yes	
CPLX2	chr5:175871433-175884020	HepG2	HepG2R	13.451	1.51698		-3.14844	-5.94629	5.00E-05	0.0317036	yes
ARSI	chr5:150296343-150302935	HepG2	HepG2R	8.22685	0.770139		-3.41715	-5.08679	5.00E-05	0.0317036	yes
SPARC	chr5:151661848-151673217	HepG2	HepG2R	87.7454	16.4718		-2.41332	-5.20387	5.00E-05	0.0317036	yes
MEP1A	chr6:46793374-46839779	HepG2	HepG2R	0.810782	84.1934		6.69825	10.9076	5.00E-05	0.0317036	yes
ARFGF3	chr6:138307246-138344644	HepG2	HepG2R	2.61994	10.1529		1.95429	4.15221	5.00E-05	0.0317036	yes
PGC	chr6:41736702-41752240	HepG2	HepG2R	264.124	33.8331		-2.96471	-6.1292	5.00E-05	0.0317036	yes
FYN	chr6:111661184-111720065	HepG2	HepG2R	11.5528	0.908991		-3.66783	-5.69567	5.00E-05	0.0317036	yes
MTFR2	chr6:136249049-136250274	HepG2	HepG2R	4.84864	0	inf	-nan	5.00E-05	0.0317036	yes	
OGFR1	chr6:71302482-71303318	HepG2	HepG2R	1.38777	0	inf	-nan	5.00E-05	0.0317036	yes	
PLAGL1	chr6:143940517-143941399	HepG2	HepG2R	1.37984	0	inf	-nan	5.00E-05	0.0317036	yes	
PLEKHG1	chr6:150841641-150842203	HepG2	HepG2R	0	2.83515	inf	-nan	5.00E-05	0.0317036	yes	
unknown	chr8:57462705-57465767	HepG2	HepG2R	0	2.42493	inf	-nan	5.00E-05	0.0317036	yes	
ENPP2	chr8:119569200-119582595	HepG2	HepG2R	2.80991	0	inf	-nan	5.00E-05	0.0317036	yes	
unknown	chr8:88714119-88714813	HepG2	HepG2R	0	2.82437	inf	-nan	5.00E-05	0.0317036	yes	
ENPP2	chr8:119557130-119557683	HepG2	HepG2R	2.76483	0	inf	-nan	5.00E-05	0.0317036	yes	
GDA	chr9:72247399-72252207	HepG2	HepG2R	1.1682	11.7912		3.33535	4.97291	5.00E-05	0.0317036	yes

Table 7: Classification of differentially expressed genes between susceptible and resistant HepG2 cell lines.

Gene name	
Upregulated genes	SERINC2, LEPR, SLC16A9, RTN4RL2, ADGRD1, HAL, SLC25A47, G6PC, A1BG, IL1RN, PCK1, AGTR1, UGT2B11, UGT2B4, FAM13A, MEP1A, GDA
Downregulated genes	PLEKHB1, HEPACAM, TNFRSF19, GPX2, DPEP1, COTL1, SPP1, CPLX2, ARSI, SPARC, PGC, FYN
Transcripts present in HepG2R but not in HepG2	FHAD1, AKR1C4, SLC22A25, AQP9, OSBPL1A, XIRP2, TMEFF2, PLEKHG1
Transcripts present in HepG2 but not in HepG2R	E2F8, KITLG, EHD3, VCAN, MTRFR2, OGFRL1, PLAGL1, ENPP2,

The functions (table 8) as well as the pathway analysis (figure 139) of the differentially expressed genes were also determined using SPRING software.

Table 8: Functions of differentially expressed genes between susceptible and resistant HepG2 cell lines.

Gene	Gene function
AQP9	Forms a channel with a broad specificity. It allows passage of a broad range of non-charged solutes and also stimulates urea transport and osmotic water permeability. This protein may also facilitate the uptake of glycerol in hepatic tissue.
KITLG	KIT ligand: Ligand for the receptor-type protein-tyrosine kinase KIT. It plays an essential role in the regulation of cell survival and proliferation, hematopoiesis, stem cell maintenance, gametogenesis, mast cell development, migration and function, and in melanogenesis. KITLG/SCF binding can activate several signaling pathways. It promotes phosphorylation of PIK3R1 (the regulatory subunit of phosphatidylinositol 3-kinase) and subsequent activation of the kinase AKT1. KITLG/SCF and KIT also transmit signals via GRB2 and activation of RAS, RAF1 and the MAP kinases MAPK1/ERK2 and/or MAPK3/ERK.
MEP1A	Meprin A, alpha (PABA peptide hydrolase).
SPARC	cysteine-rich acidic matrix-associated protein. It appears to regulate cell growth through interactions with the extracellular matrix and cytokines. It binds calcium and copper, several types of collagen, albumin, thrombospondin, PDGF and cell membranes. It has been associated with

	tumor suppression but has also been correlated with metastasis based on changes to cell shape which can promote tumor cell invasion.
GDA	Guanine deaminase: Catalyzes the hydrolytic deamination of guanine, producing xanthine and ammonia.
E2F8	E2F transcription factor 8: participates in various processes such as angiogenesis and polyploidization of specialized cells. Mainly acts as a transcription repressor: it directly represses transcription of classical E2F transcription factors such as E2F1- component of a feedback loop in S phase by repressing the expression of E2F1, thereby preventing p53/TP53-dependent apoptosis.
G6PC	Glucose-6-phosphatase: catalytic subunit. It hydrolyzes glucose-6-phosphate to glucose in the endoplasmic reticulum and forms with the glucose-6-phosphate transporter (SLC37A4/G6PT) the complex responsible for glucose production through glycogenolysis and gluconeogenesis. It is then the key enzyme in homeostatic regulation of blood glucose levels.
IL1RN	Interleukin 1 receptor antagonist: It inhibits the activity of interleukin-1 by binding to receptor IL1R1 and preventing its association with the coreceptor IL1RAP for signaling.
ENPP2	Ectonucleotide pyrophosphatase/phosphodiesterase 2. The protein encoded by this gene functions as both a phosphodiesterase, which cleaves phosphodiester bonds at the 5' end of oligonucleotides, and a phospholipase, which catalyzes production of lysophosphatidic acid (LPA) in extracellular fluids. LPA evokes growth factor-like responses including stimulation of cell proliferation and chemotaxis. This gene product also stimulates the motility of tumor cells and has angiogenic properties and its expression is upregulated in several kinds of carcinomas.
HAL	Histidine ammonia-lyase. It is a cytosolic enzyme catalyzing the first reaction in histidine catabolism, the nonoxidative deamination of L-histidine to trans-urocanic acid.
DPEP1	The protein encoded by this gene is a kidney membrane enzyme involved in the metabolism of glutathione and other similar proteins by dipeptide hydrolysis. It is known to regulate leukotriene activity by catalyzing the conversion of leukotriene D4 to leukotriene E4. This protein uses zinc as a cofactor and acts as a disulfide-linked homodimer.
COTL1	Coactosin-like 1 (Dictyostelium): It binds to F-actin in a calcium-independent manner and acts as a chaperone for ALOX5 (5LO), influencing both its stability and activity in leukotrienes synthesis.
A1BG	alpha-1-B glycoprotein. The protein encoded by this gene is a plasma glycoprotein of unknown function. The protein shows sequence similarity to the variable regions of some immunoglobulin supergene family member proteins.
AKR1C4	Aldo-keto reductase family 1, member C4. It catalyzes the transformation of the potent androgen dihydrotestosterone (DHT) into the less active form, 5-alpha- androstan-3-alpha,17-beta-diol (3-alpha-diol). Also has some 20- alpha-hydroxysteroid dehydrogenase activity.

FAM13A	Family with sequence similarity 13, member A.
VCAN	This gene is a member of the aggrecan/versican proteoglycan family. It may play a role in intercellular signaling and in connecting cells with the extracellular matrix. It may also take part in the regulation of cell motility, growth and differentiation.
TMEFF2	Transmembrane protein with EGF-like and two follistatin-like domains 2. It may be a survival factor for hippocampal and mesencephalic neurons. The shedded form up-regulates cancer cell proliferation, probably by promoting ERK1/2 phosphorylation.
AGTR1	Angiotensin II receptor, type 1. Mediates its action by association with G proteins that activate a phosphatidylinositol- calcium second messenger system.
XIRP2	Xin actin-binding repeat containing 2. It acts by protecting actin filaments from depolymerisation.
HEPACAM	Hepatic and glial cell adhesion molecule. Involved in regulating cell motility and cell-matrix interactions. It may also inhibit cell growth through suppression of cell proliferation.
UGT2B4	UDP glucuronosyltransferase 2 family, polypeptide B4. UDPGTs are of major importance in the conjugation and subsequent elimination of potentially toxic xenobiotics and endogenous compounds. This isozyme is active on polyhydroxylated estrogens (such as estriol, 4-hydroxyestrone and 2-hydroxyestriol) and xenobiotics (such as 4-methylumbelliferone, 1-naphthol, 4- nitrophenol, 2-aminophenol, 4-hydroxybiphenyl and menthol).
SLC22A25	Solute carrier family 22, member 25.
PCK1	Phosphoenolpyruvate carboxykinase 1. It catalyzes the conversion of oxaloacetate (OAA) to phosphoenolpyruvate (PEP), the rate-limiting step in the metabolic pathway that produces glucose from lactate and other precursors derived from the citric acid cycle.
OSBPL1A	Oxysterol binding protein-like 1A. Binds phospholipids, 25-hydroxycholesterol and cholesterol, exhibits strong binding to phosphatidic acid and weak binding to phosphatidylinositol 3-phosphate. It stabilizes GTP-bound RAB7A on late endosomes/lysosomes and alters functional properties of late endocytic compartments via its interaction with RAB7A.
EHD3	EH-domain containing 3. It is an ATP- and membrane-binding protein that controls membrane reorganization/tubulation upon ATP hydrolysis. It plays a role in endocytic transport and in the formation of the ciliary vesicle, an early step in cilium biogenesis.
LEPR	Leptin receptor. On ligand binding, it mediates LEP central and peripheral effects through the activation of different signaling pathways such as JAK2/STAT3 and MAPK cascade/FOS. In the hypothalamus, LEP acts as an appetite-regulating factor that induces a decrease in food intake and an increase in energy consumption by inducing anorexigenic factors and suppressing orexigenic neuropeptides, also regulates bone mass and secretion of hypothalamo-pituitary-adrenal hormones (By similarity).

ARSI	Arylsulfatase family, member I. Displays arylsulfatase activity at neutral pH, when co- expressed with SUMF1.
RTN4RL2	Reticulon 4 receptor-like 2. It may play a role in regulating axonal regeneration and plasticity in the adult central nervous system.
PLEKHB1	Pleckstrin homology domain containing, family B (evectins) member 1. It is Required for proper localization of retinogeniculate projections but not for eye-specific segregation.
FYN	FYN oncogene related to SRC, FGR, YES. Non-receptor tyrosine-protein kinase that plays a role in many biological processes including regulation of cell growth and survival, cell adhesion, integrin-mediated signaling, cytoskeletal remodeling, cell motility, immune response and axon guidance. Inactive FYN is phosphorylated on its C-terminal tail within the catalytic domain. Following activation by PKA, the protein subsequently associates with PTK2/FAK1, allowing PTK2/FAK1 phosphorylation, activation and targeting to focal adhesions.
PLAGL1	Pleiomorphic adenoma gene-like 1. It exhibits weak transcriptional activatory activity. It is a transcriptional regulator of the type 1 receptor for pituitary adenylate cyclase-activating polypeptide.
PLEKHG1	Pleckstrin homology domain containing, family G (with RhoGef domain) member 1.
CPLX2	Complexin 2. It negatively regulates the formation of synaptic vesicle clustering at active zone to the presynaptic membrane in postmitotic neurons and it positively regulates a late step in exocytosis of various cytoplasmic vesicles, such as synaptic vesicles and other secretory vesicles. It is also involved in mast cell exocytosis (By similarity).
SLC25A47	Solute carrier family 25, member 47. This uncoupling protein may catalyze the physiological 'proton leak' in liver. Its overexpression induces the dissipation of mitochondrial membrane potential.
OGFRL1	Opioid growth factor receptor-like 1.
PGC	Progastricsin (pepsinogen C). It hydrolyzes a variety of proteins. The encoded protein is a digestive enzyme that is produced in the stomach and constitutes a major component of the gastric mucosa. It is secreted into the serum and synthesized as an inactive zymogen that includes a highly basic prosegment. This enzyme is converted into its active mature form at low pH by sequential cleavage of the prosegment that is carried out by the enzyme itself. Polymorphisms in this gene are associated with susceptibility to gastric cancers. Serum levels of this enzyme are used as a biomarker for certain gastric diseases including Helicobacter pylori related gastritis.
SERINC2	Serine incorporator 2.
FHAD1	Forkhead-associated (FHA) phosphopeptide binding domain 1.
TNFRSF19	Tumor necrosis factor receptor superfamily, member 19. It can mediate activation of JNK and NF-kappa-B and may promote caspase-independent cell death.
GPX2	Glutathione peroxidase 2 (gastrointestinal). Could play a major role in protecting mammals from the toxicity of ingested organic hydroperoxides.

SPP1	Secreted phosphoprotein 1. It binds tightly to hydroxyapatite and appears to form an integral part of the mineralized matrix. It may also be important to cell-matrix interaction.
SLC16A9	Solute carrier family 16, member 9 (monocarboxylic acid transporter 9). It is a proton-linked monocarboxylate transporter that catalyzes the rapid transport across the plasma membrane of many monocarboxylates (By similarity).
UGT2B11	UDP glucuronosyltransferase 2 family, polypeptide B11. UDPGT is of major importance in the conjugation and subsequent elimination of potentially toxic xenobiotics and endogenous compounds.
FAM54A	Family with sequence similarity 54, member A. It may play a role in mitochondrial aerobic respiration essentially in the testis and can also promote mitochondrial fission (By similarity).

Amongst the genes that were expressed in resistant but not in susceptible HepG2 cell line, *aqp9* was of interest. This gene belongs to the family of aquaporins that are water-selective membrane channels and shown biophysically to conduct water, glycerol, and a broad range of non-charged solutes.

The reason behind choosing *aqp9* was that aquaporins have been implicated in the mechanism of action of Cry1Aa against Sf9 cells expressing a *Bt* receptor (Endo et al., 2017).

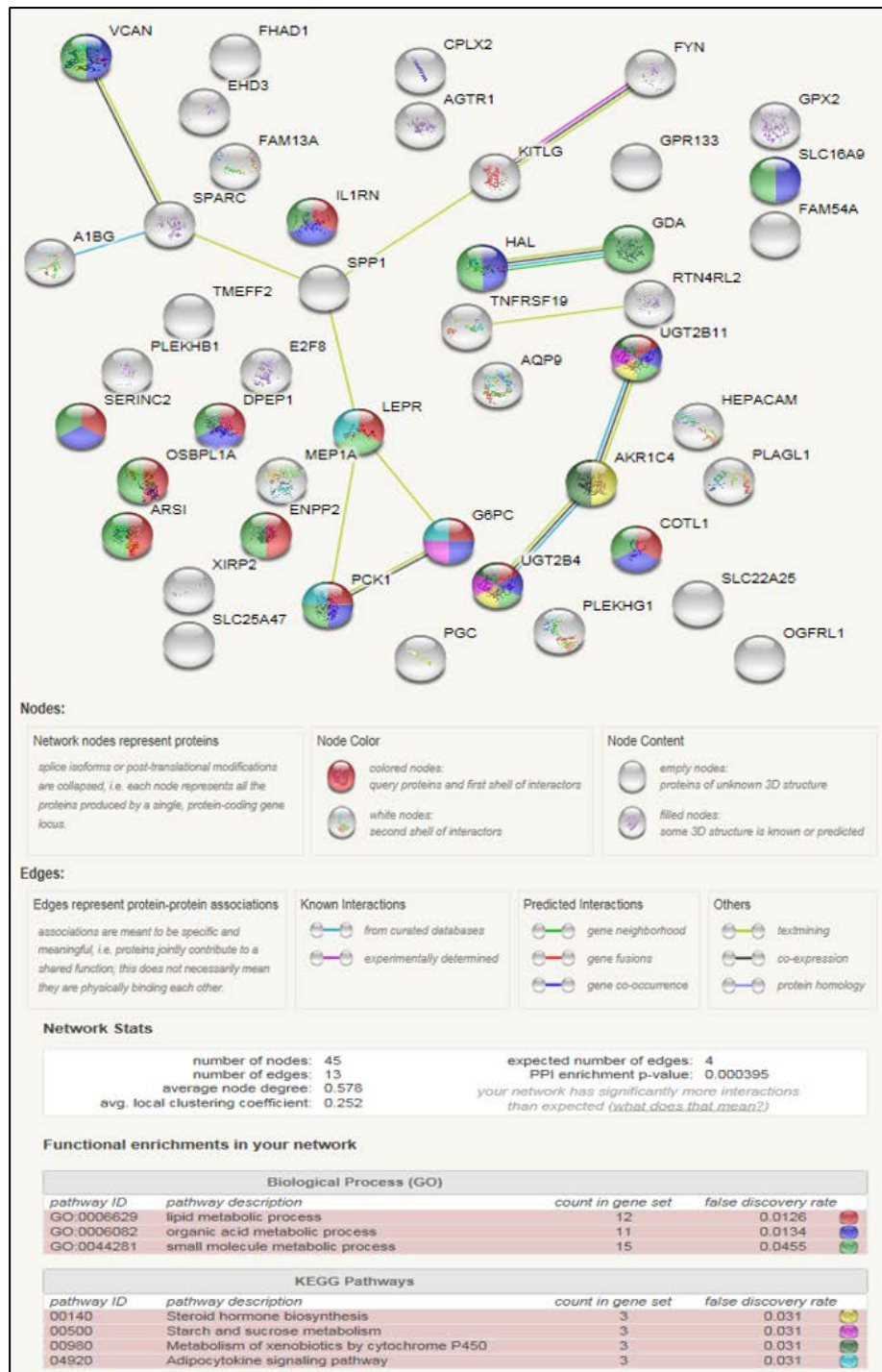


Figure 139: Pathway analysis/protein interaction network of differentially expressed genes between susceptible and resistant HepG2 cell lines.

According to figure 139, it appears that AQP9 does not have any interaction network with the other proteins therefore analysis were performed solely on AQP9.

6.10.1 Validation of *aqp9* expression level by RT-qPCR

Following the identification of AQP9 as this study's initial gene of interest, it became important to validate the gene expression levels obtained by the RNA-seq data. Total RNA from susceptible and resistant HepG2 cell lines was subjected to cDNA synthesis in a 10 μ L reaction using the high capacity cDNA reverse transcription kit (Applied Biosystems) according to the manufacturer's instructions. qPCR was performed on a Real-Time PCR System in a standard 96-well format in a 20 μ L reaction mixture using Power Syber Green PCR Master Mix (Applied Biosystems).

Forward and reverse Primers used for *aqp9* (figure 140) and for the housekeeping gene GAPDH (figure 141) were designed using NCBI/ Primer-BLAST program.



Figure 140: Schematic illustration of forward and reverse primers for *Aqp9*.

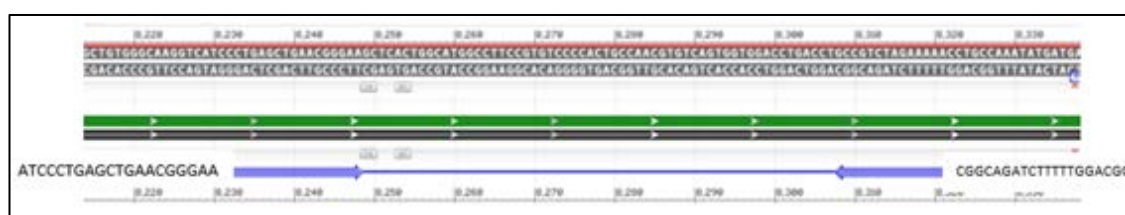


Figure 141: Schematic illustration of forward and reverse primers for *GAPDH*.

Three biological samples were used to investigate the level of expression of AQP9 in HepG2 and HepG2R cells. Genomic DNA and primer contamination assessments were carried out in all the RT-qPCR experiments showing no detection (data not shown). HepG2 (1) sample was used as the reference in this experiment (figure 142).

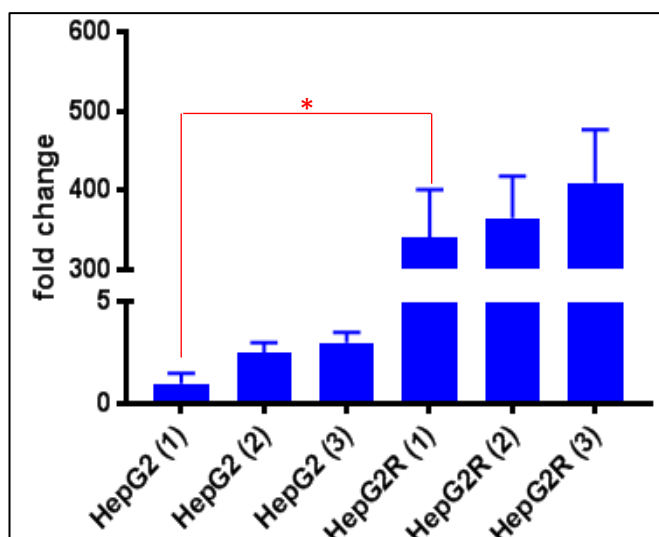


Figure 142: Graph showing RT- qPCR data for the level of AQP9 expression in three repeats of each HepG2R and HepG2.

Gene expression was analysed using the relative quantification (RQ) method. RQ estimates the difference at the level of gene expression against a calibrator (HepG2 drug sensitive line) (RQ of the calibrator = 1). The analysis was conducted employing the standard formula: $RQ = 2^{-\Delta\Delta Ct}$ (where $\Delta\Delta Ct = \Delta Ct$ for the sample (exp: HepG2 (2)) $-\Delta Ct$ for the calibrator (HepG2)). GAPDH was used as housekeeping gene. Error bars RQ min/max. Ttest: * $p=1.71E-06$

The mRNA level of *aqp9* was higher in resistant than in susceptible HepG2 cell line (around 100-fold difference) which confirmed the RNA-seq results. Quantities of RNA in each lane were normalized by GAPDH expression.

It was then worthwhile figuring out *aqp9* expression level in reverted HepG2. Therefore another RT-qPCR experiment was performed using susceptible (used as control), resistant and reverted cells (figure 143).

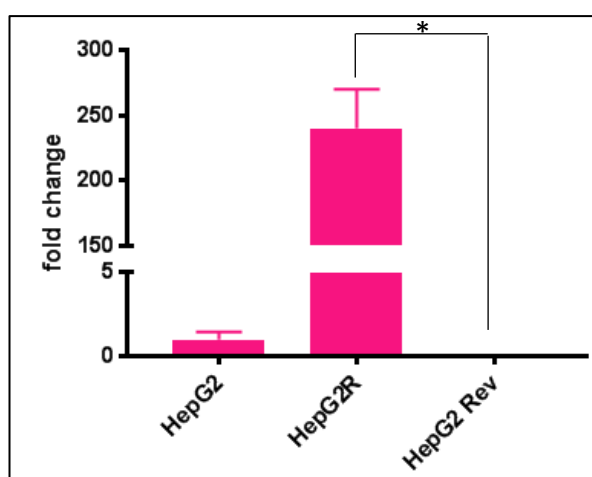


Figure 143: RT-qPCR analysis of AQP9 mRNA expression in HepG2 and HepG2R and HepG2 Rev cells.

Gene expression was analysed using the relative quantification (RQ) method. RQ estimates the difference at the level of gene expression against a calibrator (HepG2 drug sensitive line) (RQ of the calibrator = 1). The analysis was conducted employing the standard formula: $RQ = 2^{-\Delta\Delta Ct}$ (where $\Delta\Delta Ct = \Delta Ct$ for the sample (drug-resistant or reverted line) $-\Delta Ct$ for the calibrator (drug sensitive line)). GAPDH was used as housekeeping gene. Error bars RQ min/max. Ttest: * $p=1.22E-05$

The level of mRNA of *aqp9* dropped considerably in reverted HepG2 compared with the resistant cell line even reaching a lower value than that of the susceptible HepG2. This result suggested that upregulation of AQP9 may play a crucial role in the resistance mechanism.

The hypothesis adopted was that Cry41Aa induces AQP9 expression. This upregulation may have a role in maintaining homeostasis and in the resistant cell line it is constitutively upregulated. Therefore, we studied the expression level of AQP9 of susceptible HepG2 prior and post-treatment with the toxin (figure 144).

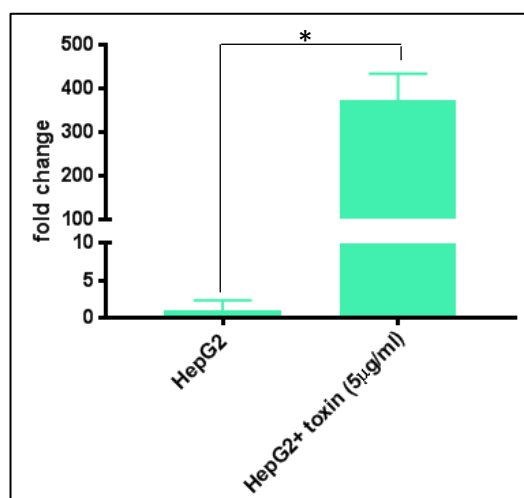


Figure 144: RT-qPCR analysis of AQP9 mRNA expression in HepG2 before and after toxin treatment.

Gene expression was analysed using the relative quantification (RQ) method. RQ estimates the difference at the level of gene expression against a calibrator (HepG2 drug sensitive line) (RQ of the calibrator = 1). The analysis was conducted employing the standard formula: $RQ = 2^{-\Delta\Delta Ct}$ (where $\Delta\Delta Ct = \Delta Ct$ for the sample (HepG2+toxin) $-\Delta Ct$ for the calibrator (drug sensitive line)). The qPCR data are presented as relative values normalized to those of the internal control (GAPDH). Error bars RQ min/max. Ttest: * $p=3.85E-05$

The level of mRNA of *aqp9* increased considerably (around 400-fold increase) in HepG2 cells upon treatment with the toxin. This result indicated that T/C activated Cry41Aa induced AQP9 expression. As a result of this finding we proposed a model of the role of AQP9 in the mechanism of action of Cry41Aa on HepG2.

The model suggests that when susceptible HepG2 are exposed to the toxin there will be creation of pores in the cell membrane through which water and other solutes will enter causing osmotic imbalance. AQP9, induced by this action, will try to retain the osmotic balance, however, if there is insufficient AQP9, the effect of toxin is too great causing

cell swelling leading to cell lysis and death. In HepG2R, pores are formed following exposure to the toxin which initiates swelling of the cell. This process activates the membrane protein AQP9 which begins to transport water, along with a number of other solutes out of the cell. The high expression of AQP9 in these cells plays a role in reducing the osmotic gradient and quickly restoring the cell to a healthy state, preventing lysis (figure 145).

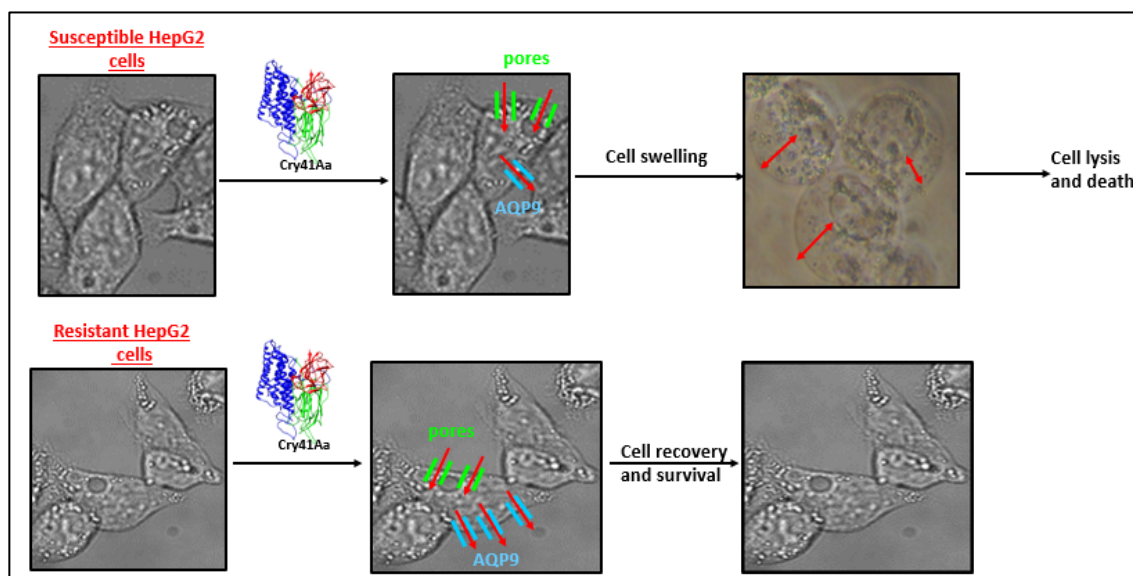


Figure 145: Proposed mode of action of Cry41Aa involving AQP9 protein.

6.10.2 Validation of AQP9 protein expression by western blot

Western blot experiment was carried out in order to figure out AQP9 protein expression levels in susceptible, resistant and reverted HepG2 cells +/- toxin. As sodium arsenite was shown to induce AQP9 expression (Torres-Avila et al., 2010), it was used as a positive control (figure 146).

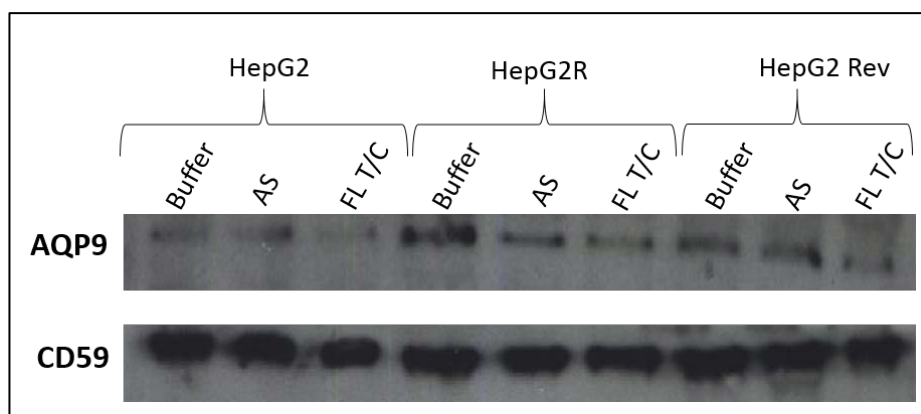


Figure 146: Western blot analysis of AQP9 expression in HepG2, HepG2R and HepG2 Rev extracts.

HepG2, HepG2R and HepG2 Rev cells were treated with toxin at a concentration of 5, 5 and 100 $\mu\text{g/ml}$ respectively, sodium arsenite (5 mM) or PBS for 30 min before being lysed with RIPA. 25 μg of proteins were loaded per well and run on 12% SDS-PAGE gel. After transfer the membrane was incubated with anti-AQP9 overnight then secondary antibody followed by ECL detection. CD59 was used as the loading control.

Our results showed that the level of AQP9 was higher in resistant than in susceptible HepG2 which correlated well with the mRNA levels previously assessed (see figure 142). On the other hand, AQP9 level in reverted HepG2 treated with buffer only, was higher than that of susceptible cell line in which case no correlation was observed between protein and mRNA level. At a protein level, Cry41Aa T/C (FL T/C) did not induce AQP9 expression in any of these cell lines following 30 min exposure. Perhaps 30 min exposure to the toxin might not have been enough to induce AQP9 expression or other biological/technical factors might have affected mRNA-protein correlation (see discussion).

In order to test the hypothesis that exposure time was not enough to induce AQP9 expression, susceptible HepG2 was exposed to a sub-lethal dose of toxin (1.5 $\mu\text{g/ml}$) and mRNA and protein levels were assessed at different time points (figure 147 and 148).

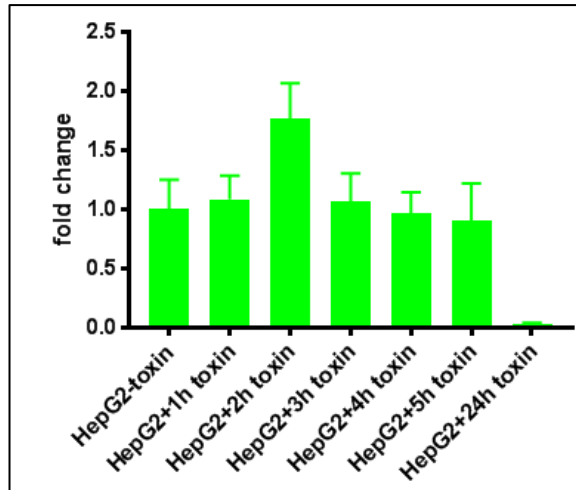


Figure 147: RT-qPCR data showing the mRNA level of *aqp9* in susceptible HepG2 +/- toxin

Gene expression was analysed using the relative quantification (RQ) method. RQ estimates the difference at the level of gene expression against a calibrator (HepG2-toxin) (RQ of the calibrator = 1). The analysis was conducted employing the standard formula: $RQ = 2^{-\Delta\Delta Ct}$ (where $\Delta\Delta Ct = \Delta Ct$ for the sample (HepG2+toxin) $-\Delta Ct$ for the calibrator (HepG2-toxin)). GAPDH used as housekeeping gene. Error bars RQ min/max.

After 2 hours of exposure to the toxin, AQP9 mRNA reached its maximal level. Western blot technique was next carried out to study any correlation of this result with AQP9 protein levels (figure 148).

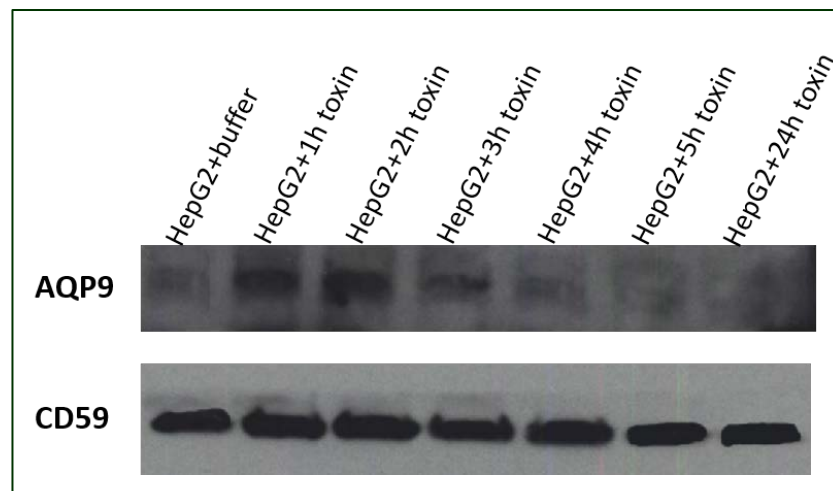


Figure 148: Western blot analysis of extracts from HepG2 cells that were treated with or without toxin at different time points.

HepG2 cells were treated with buffer or with toxin (1.5 $\mu\text{g}/\text{ml}$) at different time points (1, 2, 3, 4, 5, 24 hours) before being lysed with RIPA. 20 μg of proteins were loaded per well and run on 12% SDS-PAGE gel. After transfer the membrane was incubated with anti-AQP9 overnight then secondary antibody followed by ECL detection. CD59 was used as the loading control.

According to figure 148, the highest signal was produced after 2 hours of exposure to the toxin then dropped gradually to reach a similar level to the cells treated with buffer only after 24 hours. AQP9 protein levels correlated perfectly with the mRNA levels. We then investigated the cytotoxic effect of the toxin at these different time points in order to figure out any correlation between AQP9 level and cell viability. For this purpose CellTiter-Glo assay was carried out (figure 149).

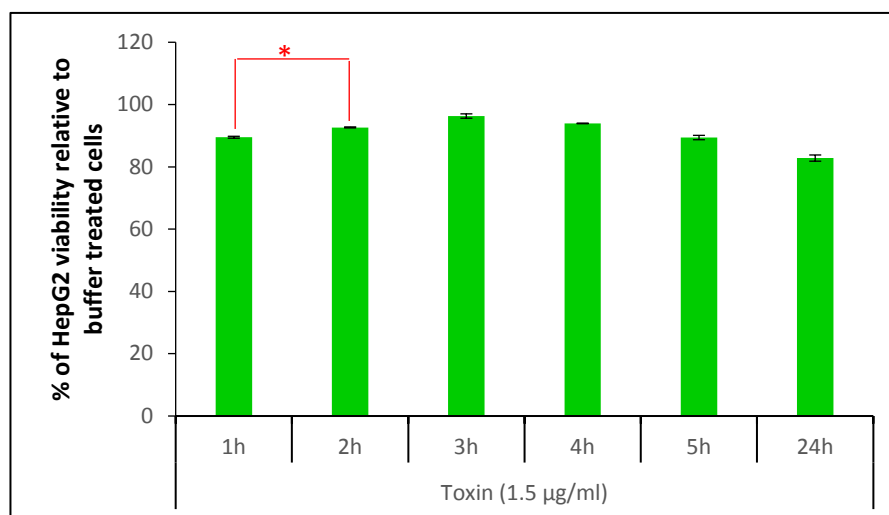


Figure 149: Assessment of ATP levels in susceptible HepG2 cells after exposure to T/C activated Cry41Aa at different time points.

HepG2 cells were seeded at the density of 25×10^4 cells/ml, in a white wall 96-well plate. The next day cells were dosed with of T/C activated Cry41Aa (1.5 $\mu\text{g/ml}$) or buffer. Luminescence was measured at different time points (1, 2, 3, 4, 5, 24 hours) using CellTiter-Glo. Ttest: * $p=0.12$ (p values for all other concentrations used were >0.05)

According to our results, no significant difference in ATP levels was observed at different time points of exposure to the toxin. Therefore the transient increase in AQP9 seemed to have no effect on Cry41Aa susceptibility.

Because incubation with the toxin for two hours increased AQP9 expression, based on our hypothesis that AQP9 has a role in cell defence, HepG2 cells were incubated with toxin (1.5 $\mu\text{g/ml}$) for 2 hours, the medium was then removed, the cells were washed with PBS and more toxin was added. Cell viability was later evaluated in order to see whether the cells had acquired immunity to the toxin, due to AQP9 expression, which would result in a decrease of the susceptibility level (figure 150).

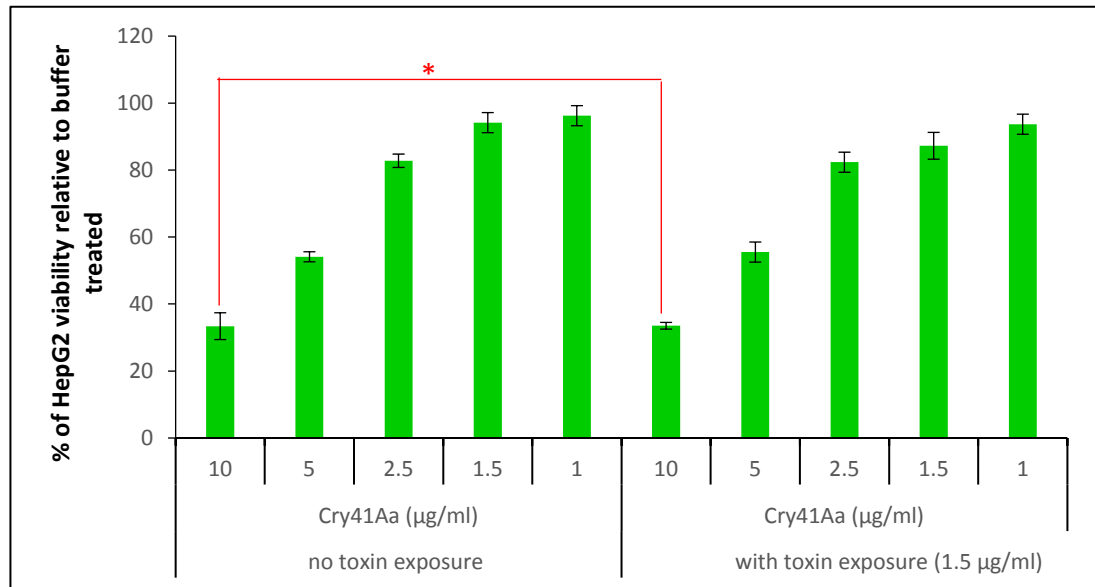


Figure 150: Assessment of the level of toxicity of T/C activated Cry41Aa on susceptible HepG2 pre-exposed to toxin. HepG2 cells were seeded at the density of 25×10^4 cells/ml. The next day a set of cells was treated with a dose of 1.5 µg/ml of T/C activated Cry41Aa. After 2 hours of incubation with the toxin, the cells were washed with PBS, fresh medium was added then both sets of cells were dosed with different concentrations of toxin (10, 5, 2.5, 1.5, 1 µg/ml). 24 hours later, cell viability was measured. Ttest: * $p=0.49$ (p values for all other concentrations used were >0.05)

According to the cell viability assay, the sensitivity to the toxin was similar between the cells pre-exposed to a sub-lethal dose of toxin and the cells that were not pre-exposed to the toxin. This result indicated that after two hours of incubation, HepG2 cells have not acquired immunity to the toxin. Therefore, AQP9 levels don't correlate with Cry41Aa susceptibility.

The same process was followed for the resistant HepG2 cell line in order to establish any relationship between AQP9 and resistance to the toxin. Initially the cells were exposed to a sub-lethal dose of toxin. Although we tried to use an equivalent dose to that of the susceptible cell line, it was difficult to figure out the exact dose. The mRNA (figure 151) as well as the protein levels (figure 152) of AQP9 were assessed at different time points.

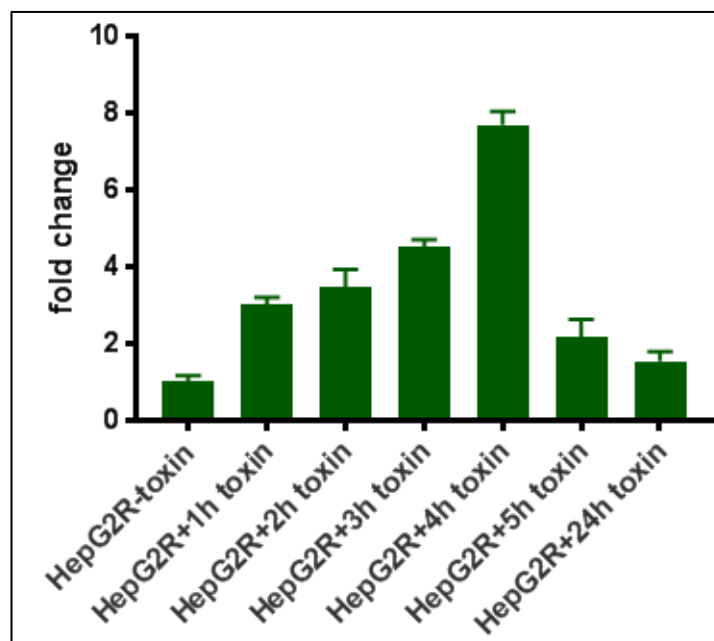


Figure 151: RT-qPCR data showing the mRNA level of aqp9 in resistant HepG2 +/- toxin at different time points
Gene expression was analysed using the relative quantification (RQ) method. RQ estimates the difference at the level of gene expression against a calibrator (HepG2R-toxin) (RQ of the calibrator = 1). The analysis was conducted employing the standard formula: $RQ = 2^{-\Delta\Delta Ct}$ (where $\Delta\Delta Ct = \Delta Ct$ for the sample (drug-resistant line+toxin) $-\Delta Ct$ for the calibrator (HepG2R-toxin)). GAPDH used as housekeeping gene. Error bars RQ min/max.

According to our results, the mRNA level of AQP9 increased gradually over time following the exposure of cells to the toxin (110 $\mu\text{g}/\text{ml}$). This level reached its maximum after 4 hours then decreased to reach approximately the same level as that of the cells treated with buffer only after 24 hours.

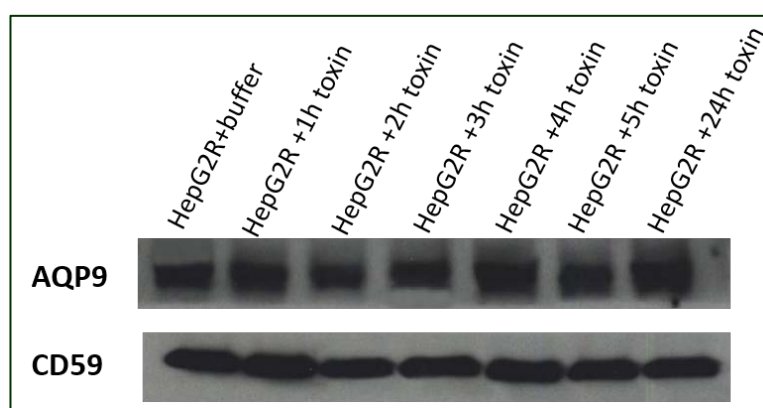


Figure 152: Western blot analysis of extracts from HepG2R cells that were treated with or without toxin at different time points.

HepG2R cells were treated with buffer or with toxin (110 $\mu\text{g}/\text{ml}$) at different time points (1, 2, 3, 4, 5, 24 hours) before being lysed with RIPA. 20 μg of proteins were loaded per well and run on 12% SDS-PAGE gel. After transfer the membrane was incubated with anti-AQP9 overnight then secondary antibody followed by ECL detection. CD59 was used as the loading control.

Our results showed that AQP9 protein level increased gradually in cells that were exposed to the toxin over time to reach its maximum after 4 hours, however, this level remained high after 24 hours.

As with the susceptible cell line, we investigated the cytotoxic effect of the toxin at these different time points in order to figure out any correlation between AQP9 level and cell viability. For this purpose CellTiter-Glo assay was carried out (figure 153).

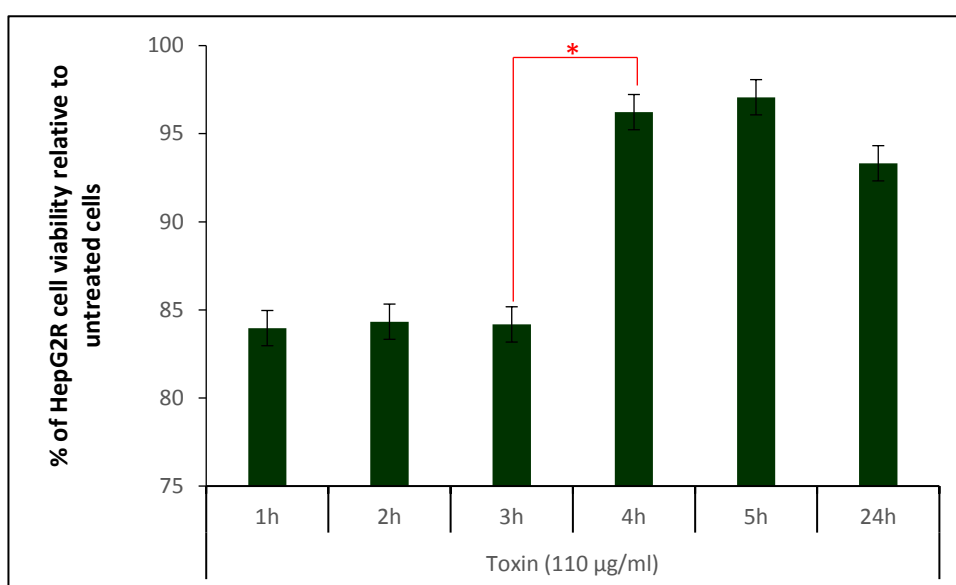


Figure 153: Assessment of ATP levels in resistant HepG2 cells after exposure to T/C activated Cry41Aa over time. HepG2R cells were seeded at the density of 25×10^4 cells/ml, in a white wall 96-well plate. The next day cells were dosed with of purified T/C activated Cry41Aa (110 μ g/ml) or buffer. Luminescence was measured at different time points (1, 2, 3, 4, 5, 24 hours) using CellTiter-Glo. Ttest: *p= 0.12

According to our results, upon 4 hours of treatment with the toxin which corresponded to the maximum level of AQP9, there was a slight increase in HepG2R viability (around 10%) suggesting that at that time point a small percentage of cells may have undergone a recovery process.

Microscopic observations were also carried out at different time points (1, 2, 3, 4, 5, 24 hours) following exposure of susceptible (figure 154) and resistant (figure 155) HepG2 cell lines to a concentration of 1.5 and 110 μ g/ml of toxin respectively. This was in order to assess any morphological response (+/- swelling) of the cells to the toxin over time.

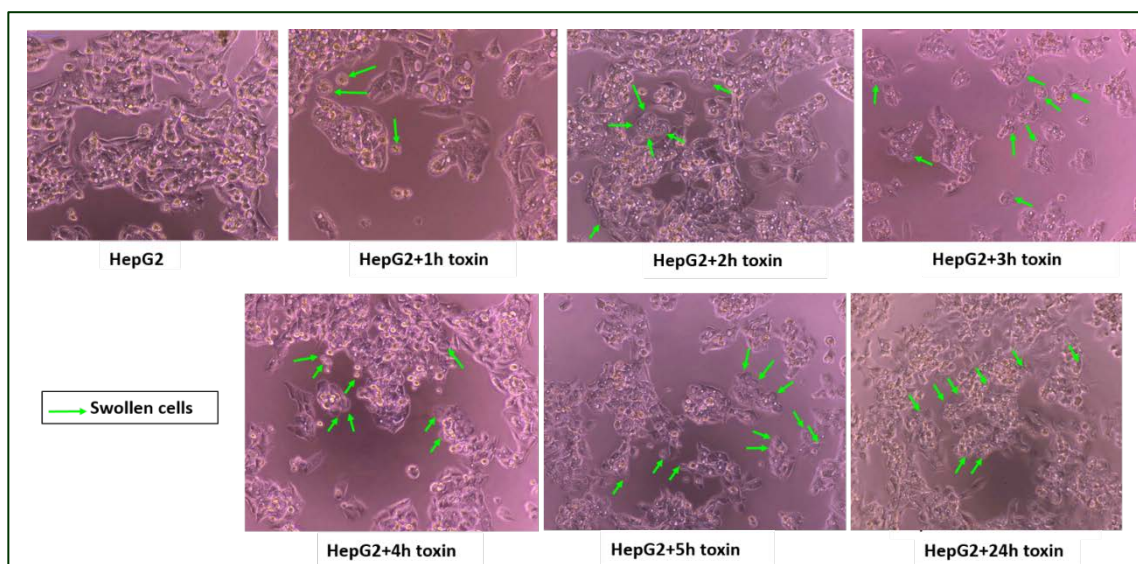


Figure 154: Microscopic observation of morphological changes in HepG2 exposed to the toxin over time.

HepG2 cells were seeded at the density of 25×10^4 cells/ml, in 6 well plates. The next day cells were dosed with T/C activated Cry41Aa ($1.5 \mu\text{g/ml}$) or buffer. Morphological changes were visualised using EVOS FL imaging system 10X objective over time.

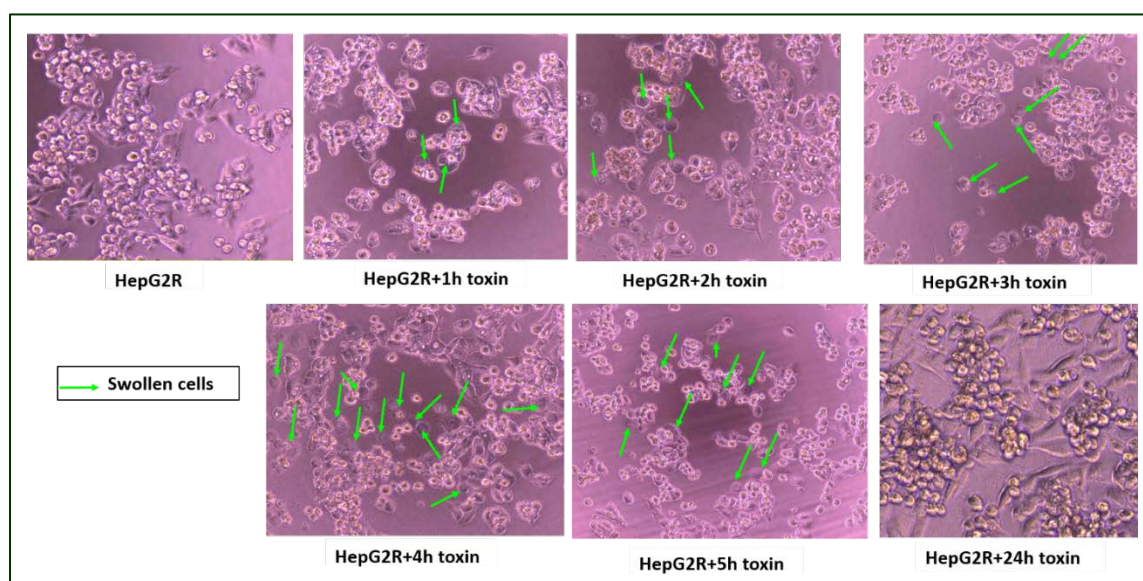


Figure 155: Microscopic observation of morphological changes in resistant HepG2 exposed to the toxin over time

HepG2R cells were seeded at the density of 25×10^4 cells/ml, in 6 well plates. The next day cells were dosed with of T/C activated Cry41Aa ($110 \mu\text{g/ml}$) or buffer. Morphological changes were visualised using EVOS FL imaging system 10x objective over time.

By comparing the morphology of the two cell lines following treatment with the toxin over time, it was obvious that the toxin induced swelling in both cell lines during the first 5 hours. However, after 24 hours, in case of susceptible HepG2 the swollen cells lysed

and died while they recovered and survived in case of resistant HepG2. These morphological facts observed in the two cell lines were consistent with the proposed model of action of Cry41Aa that was previously described. These findings also suggested that the toxin binds to the susceptible as well as the resistant HepG2 cell lines. For confirmation a ligand blot technique was used to study the binding of Δ R-HAP40 (figure 156) that, as with the non-tagged toxin, was shown to have a slight effect at high doses on HepG2R (data not shown). Same procedure as carried out for HepG2, HL-60 and HeLa in the previous chapter was performed.

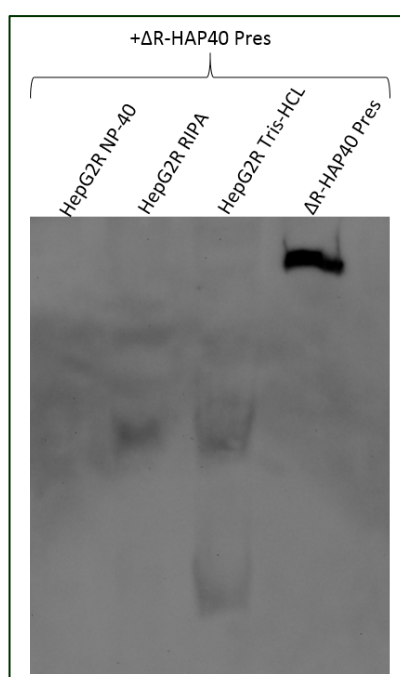


Figure 156: Ligand blot analysis of extracts from HepG2R cells.

20 μ g of extracts from HepG2R cells were loaded into 12% SDS-PAGE. 4 μ g of Δ R-HAP40 was loaded as a control. After transfer the membrane was blocked with 5% milk and was incubated with Δ R-HAP40 in PBS (20 μ g/ml) over night at 4°C. The next day the membrane was washed, incubated with anti-HA antibody and signal was detected with ECL.

As for HepG2, HL-60 and HeLa cell lines, our results indicated that toxin bound to the resistant HepG2 cell line. The two bands of around 46 and 30 kDa were again detected in this case. This result reinforced the hypothesis of the binding being not correlated to the susceptibility and also was with a good agreement with the model proposed that stressed the importance of a recovery phase.

To further investigate the possible involvement of AQP9 in this process, inhibition of AQP9 in the resistant HepG2 cell line was considered.

6.10.3 Inhibition of AQP9 using MMTS inhibitor

S-methylmethanethiosulfonate (MMTS) which is a relatively highly specific inhibitor of the water transport activity of aquaporins (Endo et al., 2017), was used to inhibit AQP9. Initially, two sets of cells were incubated with the inhibitor for 30 or 60 min. Then one set of cells was washed with PBS, resuspended in fresh medium and was exposed to different concentrations of toxin, while in the other set, no wash was carried out and the toxin was added immediately after incubation with MMTS (figure 157). Microscopic observations were carried out before and after treatment with the inhibitor and the toxin and the time point of measurement of cell viability was determined based on morphological changes of the cells (the initiation of swelling).

Incubation with MMTS for 60 min resulted in a significant decrease in cell viability (data not shown), therefore 30 min incubation time was considered (figure 157). If AQP9 exhibits a crucial role in resistance mechanism, an increase of susceptibility to the toxin in HepG2R cells should be observed.

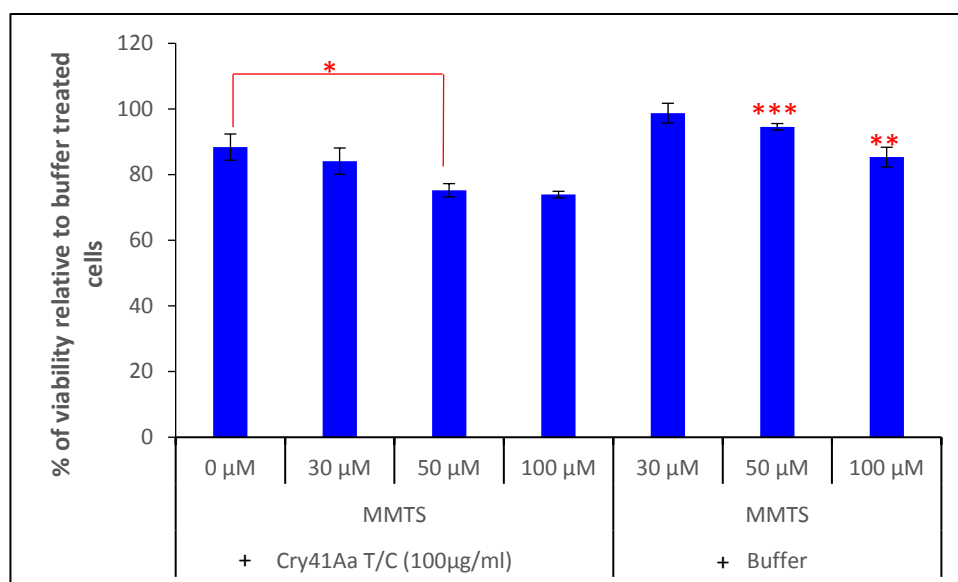


Figure 157: Role of AQP9 inhibition in Cry41Aa susceptibility in resistant HepG2.

HepG2R were seeded at the density of 25×10^4 cell/ml. The next day the cells were treated without or with different concentrations of MMTS (30, 50, 100 µM). 30 min later, the toxin (100 µg/ml) was added. 1h later, cell viability was measured using CellTiter-blue assay. Ttest: * $p=0.08$, ** $p=0.06$ and *** $p=0.15$

According to our results, the increase of the sensitivity to the toxin was due to the inhibitor being toxic to the cells rather than the effect of the inhibition of AQP9. This was indicated by the decrease in viability of cells exposed to the inhibitor in the absence of toxin. This decrease was shown to be a dose dependent.

Same results were shown for the cells that were washed after treatment with MMTS and for the cells that were treated with the inhibitor and the toxin at the same time (data not shown).

Since MMTS was toxic to the cells and because using CellTiter-blue assay, the cells need to be incubated with the dye for another two hours prior to the measurement of viability, CellTiter-Glo Luminescence was considered since only 10 min incubation is required prior the reading (figure 158). This was in order to reduce the exposure time to the inhibitor.

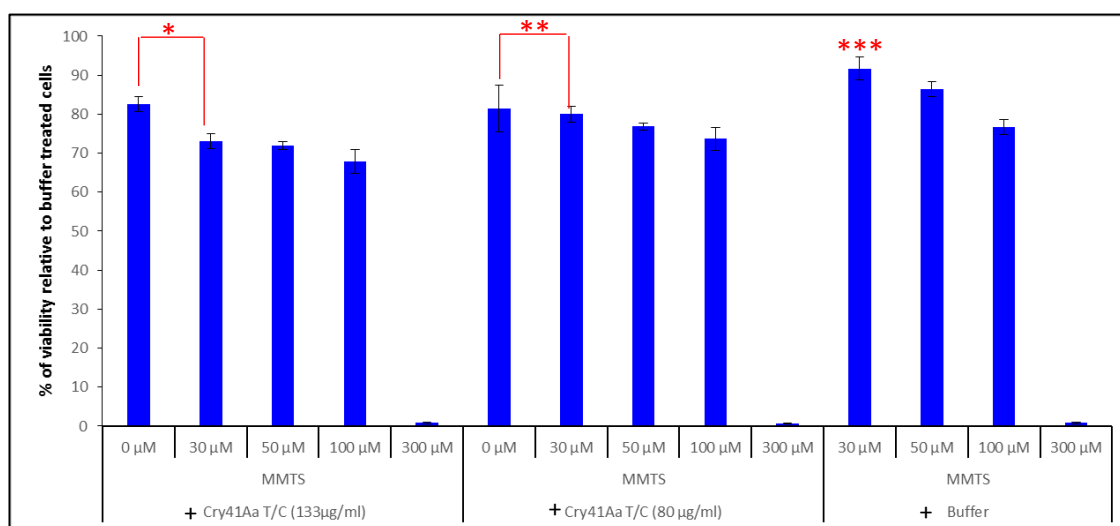


Figure 158: Role of AQP9 inhibition in Cry41Aa susceptibility in resistant HepG2.

HepG2R cells were seeded at the density of 25×10^4 cells/ml, in a white wall 96-well plate. The next day cells were dosed without or with different concentrations of MMTS (30, 50, 100, 300 µM) for 30min. T/C activated Cry41Aa (133, 80 µg/ml) or buffer were then added to the cells. 1 hour later, ATP levels were measured using CellTiter-Glo assay. Ttest: * $p=0.18$, ** $p=0.44$ and *** $p=0.14$

Despite the decrease in exposure time to MMTS, the inhibitor still exhibited a toxic effect towards the resistant HepG2 cells. Therefore AQP9 knockdown was considered as an alternative approach.

6.10.4 AQP9 knock down using small interfering RNA

In order to investigate the role of AQP9 in the resistance mechanism, RNA interference was utilized for knock down expression in HepG2R.

Many attempts were carried out in order to optimise different parameters for successful AQP9 silencing including the type of transfection (forward, reverse), the type and concentration of transfection reagent (hyperfect, lipofectamine, FuGene), incubation time, cell density and concentration of siRNA.

Following successful optimisation of the procedure, the cells were transfected with GeneSolution *aqp9* siRNA according to the manufacturer's instructions for a different periods of time (12, 24, 48 hours) then the knock down efficiency was assessed using RT-qPCR (figure 159) and western blot analysis (figure 160).

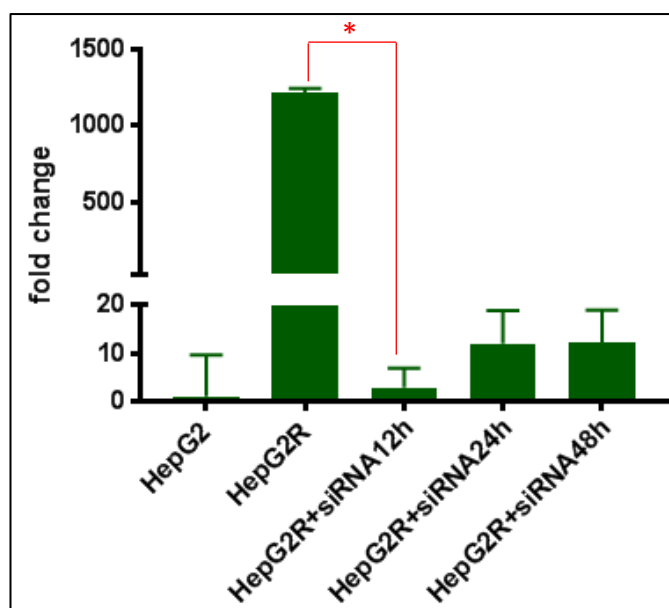


Figure 159: Assessment of AQP9 mRNA levels prior and post knock down in HepG2R.

Gene expression was analysed using the relative quantification (RQ) method. RQ estimates the difference at the level of gene expression against a calibrator (HepG2) (RQ of the calibrator = 1). The analysis was conducted employing the standard formula: $RQ = 2^{-\Delta\Delta Ct}$ (where $\Delta\Delta Ct = \Delta Ct$ for the sample (HepG2R) - ΔCt for the calibrator (HepG2)). GAPDH used as housekeeping gene. Error bars RQ min/max. Ttest: $p=2.08E-08$

According to our results, the mRNA level of AQP9 in resistant HepG2 transfected with siRNA for a period of 12, 24 and 48 hours showed a considerable decrease of up to 600-fold, 110-fold and 111-fold respectively compared with the mock (HepG2R). These

results indicated that AQP9 knockdown was optimal when cells were transfected with siRNA for 12h.

Next, the expression of AQP9 at the protein level was investigated using a western blot (figure 160).

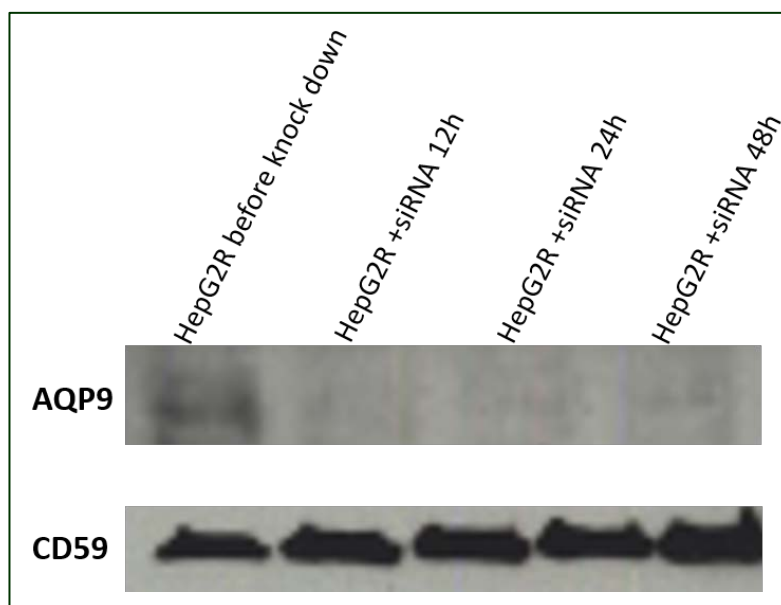


Figure 160: Western blot analysis of extracts from HepG2R +/- siRNA.

HepG2R cells were transfected with siRNA for different time points (12, 24, 48 hours) before being lysed with RIPA. 20 μ g of proteins were loaded per well and run on 4-20% precast gel (Bio-Rad). After transfer the membrane was incubated with anti-AQP9 overnight then secondary antibody followed by ECL detection. Non transfected HepG2 cell line was used as the positive control.

According to our results, a high signal was detected in non-transfected resistant HepG2 cell line while only negligible signal was detected in the extracts of transfected cells. These results indicated that the expression of AQP9 was successfully silenced.

The assessment of susceptibility of the transfected resistant cells to the toxin was then needed in order to confirm the role, if any, of AQP9 in resistance mechanism.

The cells were initially transfected with siRNA for 12h, then toxin was added at different concentrations and cell viability was measured using CellTiter-blue assay (figure 161). Assuming that AQP9 is important in the resistance mechanism, an increase in susceptibility to the toxin should be observed.

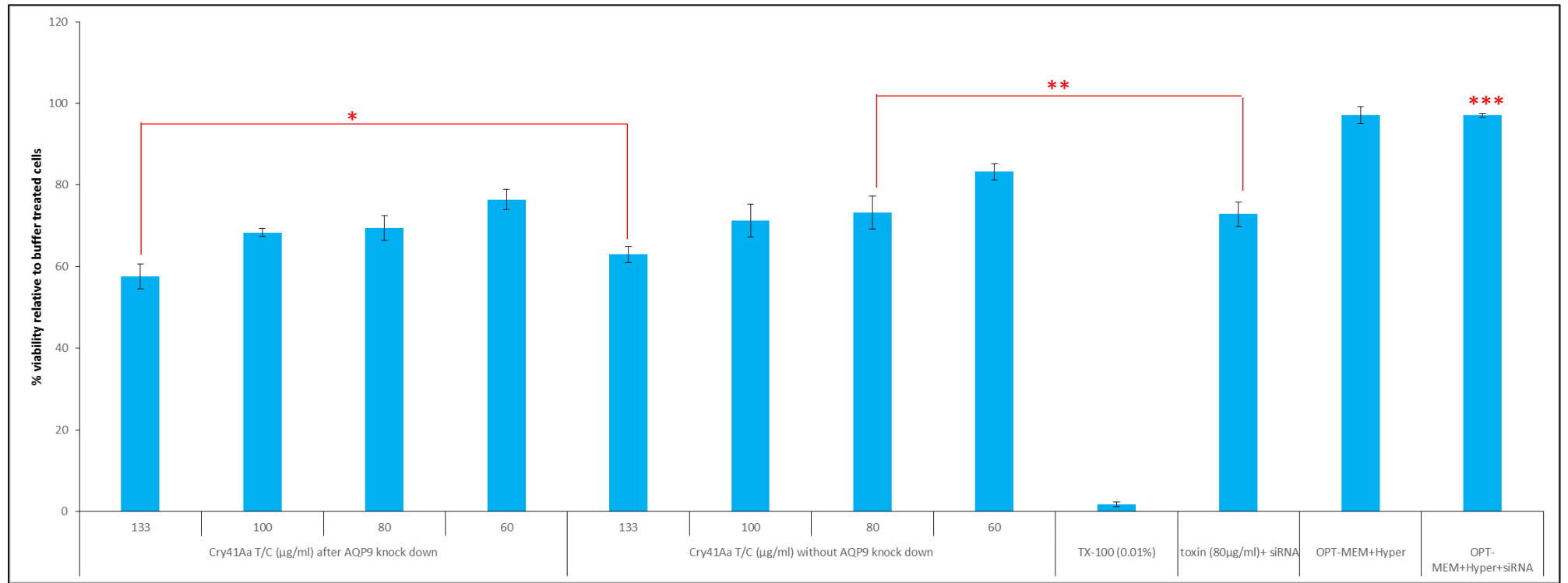


Figure 161: Role of AQP9 in resistance mechanism of HepG2 cells.

HepG2R cells were seeded at the density of 8×10^4 cells/ml and the transfection solution was added. 12 hours later, non-transfected and transfected HepG2R were treated with different concentrations of toxin (133, 100, 80, 60 µg/ml). 6 hours later, cell viability was measured using CellTiter-blue assay. The controls used were OPT-MEM+hyperfect, OPT-MEM+hyperfect+siRNA and siRNA+toxin. Ttest: * $p=0.08$, ** $p=0.46$ and *** $p=0.19$

According to our results, the same level of the toxic effect of T/C activated Cry41Aa against transfected and non-transfected cells was observed indicating that the knock down of AQP9 in resistant HepG2 cell line did not affect the resistance to the toxin. The controls used proved that there was no effect of transfection solution on cells and siRNA did not interfere with toxin activity.

In parallel to the cell assay the level of expression of AQP9 was monitored at each step for consistency. Two biological replicates were used for this purpose (figure 162).

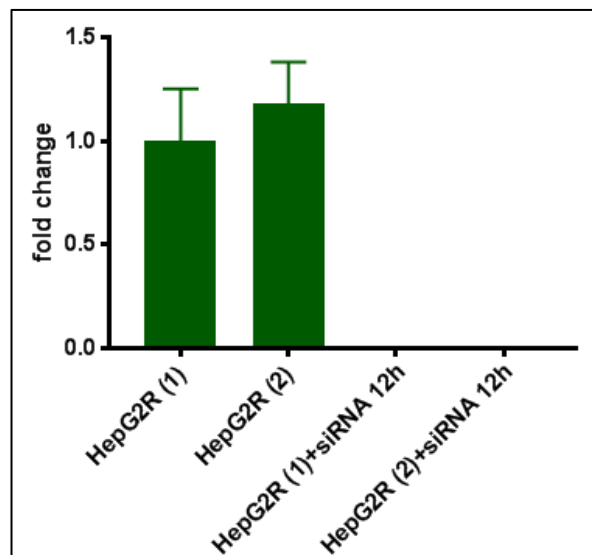


Figure 162: Confirmation of AQP9 knock down by RT-qPCR.

Gene expression was analysed using the relative quantification (RQ) method. RQ estimates the difference at the level of gene expression against a calibrator (HepG2R (1)) (RQ of the calibrator = 1). The analysis was conducted employing the standard formula: $RQ = 2^{-\Delta\Delta Ct}$ (where $\Delta\Delta Ct = \Delta Ct$ for the sample (HepG2R+siRNA 12h) - ΔCt for the calibrator (HepG2R (1))). GAPDH used as housekeeping gene. Error bars RQ min/max.

According to figure 162, the mRNA level of AQP9 was not detected in transfected cells indicating that AQP9 knock down was successful. AQP9 protein levels were also assessed at different stages of the cell assay experiment (figure 163).

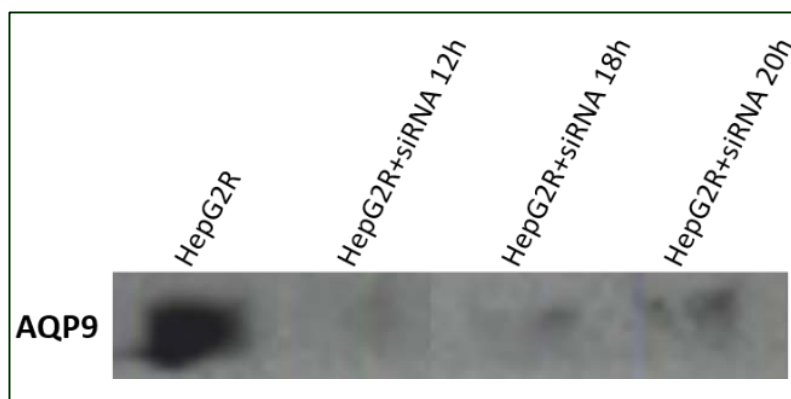


Figure 163: Western blot analysis of the level of expression of AQP9 over time

HepG2R cells were seeded at the density of 8×10^4 cells/ml and the transfection solution was added. 12 hours later, non-transfected and transfected HepG2R were treated with the toxin at a concentration of $133 \mu\text{g/ml}$ for 6 hours. At different time points, the cells were lysed using RIPA and the proteins were extracted. $20 \mu\text{g}$ of proteins were loaded per well and run on 4-20% precast gel. After transfer the membrane was incubated with anti-AQP9 overnight then secondary antibody followed by ECL detection. Non transfected HepG2R cell line was used as the negative control.

According to our results, a significant decrease in the level of AQP9 expression was observed over time. In fact, at 12 hours post transfection a negligible signal was detected indicating successful AQP9 knockdown. This signal slightly increased after incubation of the cells with toxin for a further 6 hours (HepG2R+siRNA 18h) and at the time point when cell viability was measured (HepG2R+siRNA 20h).

Although the increase in AQP9 expression was not significant upon treatment with the toxin, this increase could play a role in the defence/recovery process. In order to eliminate or confirm this possibility, AQP9 knock out should be considered in future work.

6.11 Discussion

The development of drug resistance during chemotherapy treatment is one of the major clinical obstacles. In order to clarify this phenomenon, drug-resistant cell line models were considered. In our study the method utilized to generate resistant HepG2 cell line to T/C activated Cry41Aa was continuous exposure of cells to increased doses of toxin over time. This method as well as the pulse treatment strategy were previously

approached leading to successful establishment of resistant HepG2 cell line to particular drug(s):

- Pulse treatment: where parental HepG2 were treated in pulse at the IC₅₀ of the drugs in question (Cisplatin (CDDP) or 5-Fluorouracil (5-FU)) for 4 hours. After 6 complete cycles of induction and after reaching certain confluency (70-80%), the survived cells were selected and used for further analysis (Odii and Coussons, 2012).
- Treatment of cells with step wise increases in the toxic agent: Where the development of resistant HepG2 to doxorubicin was successful through continuous exposure of the parental cell line to increasing concentrations (0.1mM to 100mM) of doxorubicin (Chan et al., 2000). Zhai et al in 2006 generated Adriamycin resistant HepG2 using the same technique by adding the drug to cells in stepwise increasing concentrations (0.001 mg/L to 1.0 mg/L). The remaining viable cells were identified as the resistant cell subline (HepG2/ADM) (Zhai et al., 2006).

In insect models, selection of resistant strain of *H. amigera* to Cry1Ac was conducted by incorporation of the protoxin in the diet with progressively increasing concentrations (from 1 to 60µg of protoxin per g of diet) over time (Xiao et al., 2016).

The length of the period of selection can vary from few weeks to several months. In our case, the successful establishment of resistant HepG2 to Cry41Aa took around 8 months. It appeared that using the second method mostly takes several months. In fact, adriamycin (ADM)-resistant variants of the human lung cancer cell lines were produced in a period of 7-9 months that included a period of drug-free growth (Twentyman et al., 1986). In addition, Oxaliplatin and SN-38 resistant colorectal carcinoma line variants were generated by continuous exposure to increasing concentrations of the toxic agents over a period of 8-10 and 6-9 months respectively (Jensen et al., 2015, Petitprez et al., 2013).

The success of the procedure sometimes depends on the method used. In fact, the pulse treatment method failed in making two human ovarian tumour cells resistant to CDDP. While culturing these cells in the continuous presence of stepwise increasing CDDP

concentrations led to the generation of resistant subline to the drug in question after about 7 months. (Kuppen et al., 1988).

Our results showed that the resistance profile reached a very high level. In fact the resistance index ((EC₅₀ of resistant cell line)/(EC₅₀ of the parental cell line)) was equal to 41. This value appeared to be reasonably high compared with other generated drug resistant cell lines. The resistant HepG2 to CDDP presented a resistance index which was around 13.76 (Zhou et al., 2010) while it was around 42 for those resistant to doxorubicin (Chan et al., 2000). The resistance index value was around 7.9 for the resistant ovarian cell line to CDDP drug (Kuppen et al., 1988). In case of insects, the laboratory selected strain of *Helicoverpa armigera* showed >1000-fold resistance to *Bt* toxin Cry1Ac (Xiao et al., 2016).

Morphological changes were visualised during the selection process. The cells appeared to acquire an elongated phenotype when cultured in toxin. These elongations were suggested to be filopodia since they were previously shown to be induced by AQP9 (Loitto et al., 2007) which was shown, in our study, to be induced by the toxin itself. Similar observation was shown in previous work where two established resistant sublines of a human ovarian cancer cell line (SKOV3) presented significant morphological changes showing a neuron-like shape, with some pseudopodia (Yan et al., 2007).

However, when the cells are cultured in medium free of toxin, there was no obvious morphological changes between the parental and resistant HepG2 cell lines.

According to previous studies, alterations in morphological features of the malignant cells during the development of the drug resistance phenotype could be present or absent. In fact, when compared to the parental line, the doxorubicin resistant breast cancer cells were larger with less defined irregular rounded shape and contained multiple nuclei in the cytoplasm (AbuHammad and Zihlif, 2013). Hudson et al in 2014 spotted tumour morphology changes in mesothelioma cell line with the acquisition of chemoresistance (Hudson et al., 2014). In contrast, microscopic observations of resistant human hepatoma cell line to CDDP revealed that the generated cell line adopted a shape that is similar to that of the parent cells (Zhou et al., 2010).

The acquisition of resistance to multiple anticancer drugs by human cells results in a serious problem in chemotherapy. Our results showed that the Cry41Aa resistant HepG2 was not cross resistant to other drugs such as Etoposide, 5-FU and acridine gold derivatives although most drug-resistant cell lines that were generated in previous work have developed multidrug resistant phenotype. In fact, Chan et al in 2000, who developed a resistant HepG2 line to doxorubicin, found that these cells were not only resistant to doxorubicin but also to multiple anticancer drugs among them Vincristine and methotrexate. In addition, the established chemo-resistant mesothelioma cell lines showed cross-resistance to other classes of anti-cancer agents (Hudson et al., 2014). In insect models, the laboratory selected resistant strains of pink bollworm (*Pectinophora gossypiella*) to Cry2Ab also developed cross-resistance to Cry1Ac and Cry2Aa (Tabashnik et al., 2009). Cross-resistance to Cry2Ab was observed in selected strain of *H. armigera* resistant to Cry1Ac (Wei et al., 2015). But most Cry1 resistant insects are not cross-resistant to Cry2Ab.

The stability of the resistance phenotype was monitored over time showing that it was stable after 5 months of growth in medium free of toxin however it became unstable after that time point with the resistance decreasing gradually to be completely lost after 10 months.

The stability of the resistance phenotype was previously examined in resistant cell line models and showed that it could be stable in some resistant sublines and completely lost in others. Jensen et al in 2015 showed that the evolved resistant colorectal cancer cell line to oxaliplatin and SN-38 drugs presented a stable phenotype when cultured in drug-free medium for up to five weeks (Jensen et al., 2015). Coussons et al in 2000 have found that the resistant HepG2 to CDDP and 5-FU presented a constant IC₅₀ after months of maintenance in drug-free medium indicating a very stable resistance phenotype. On the other hand, some reports showed that drug-resistant cell lines needed to grow in drug-containing medium in order to retain the stability of drug resistance. In fact, Kuppen et al in 1988 showed that to maintain resistance, the ovarian tumour cells were grown at a CDDP concentration of 3.3 mM. In addition, Zhai et al in 2006 who generated Adriamycin resistant HepG2, maintained them in a culture medium

containing 1000 µg/L ADM. Chan et al in 2000 maintained multidrug resistance by culturing HepG2 in 1.2mM of doxorubicin.

The instability of the resistance to *Bt* toxin in *Plutella xyostella* was previously studied showing that during selection with toxin, the LC50 of NO-Q larvae was 2800 times greater than the LC50 of the susceptible strain while after 13 generations without selection, the LC50 of both strains were similar. In this report, the rapid reversal of resistance in the absence of *Bt* was shown to be associated with a difference in biotic fitness (Tabashnik et al., 1994).

Previous work had studied closely the instability of drug resistance in cancer chemotherapy where it showed that the drug resistance clones from neuroblastoma cells upon extended growth in drug-free medium showed very unstable resistance phenotype that varies from completely stable clones to losing completely the resistance phenotype in a short period of time (8 weeks). They correlated the unstable resistant phase to the presence of amplified DHFR genes which are associated with small paired chromosomal elements called “double minute chromosomes” that are acentromeric and do not participate in equal segregation at mitosis. They concluded that in unstable cell variants a good percentage of these genes are extrachromosomal resulting in unequal distribution at mitosis leading to possible complete loss in subsequent generation (Baskin et al., 1981).

Previous studies have shown that acquired drug resistance, particularly in the case of prolonged drug exposure, can be due to prolonged generation doubling time, which in turn could have a profound impact on cancer cell sensitivity to antitumor agents such as 5-fluorouracil since it is an S-phase selective agent (Petitprez et al., 2013). We compared the growth rates of our parental and drug resistant cell line variants in drug-free growth medium. However, in our case the growth rate between susceptible, resistant and reverted HepG2 was similar.

Another important approach that was extensively used in previous work following the development of resistant cell line models was RNA sequencing in order to understand the molecular mechanisms associated with the resistance to the drugs. To elucidate the altered molecular processes responsible for emergence of doxorubicin resistance by

U87 glioblastoma cells, transcriptome sequencing was carried out (Han et al., 2016). This technique was also used by Fang et al in 2017 which helped in revealing key pathways and identifying genes associated with Cisplatin resistance in lung adenocarcinoma A549 cells (Fang et al., 2017). The use of RNA-seq and the identification of differentially expressed genes indicated the importance of actin cytoskeletal proteins in erythroleukemia cells (Fernandez-Calleja et al., 2017). Identification of resistance-related genes in insects was also carried out by the mean of RNA-seq technology. For example, transcriptome-seq analysis revealed candidate genes involved in Asian corn borer *Bt* resistance (Xu et al., 2015b).

In our study, we used this approach where the RNAs were initially extracted from susceptible and resistant HepG2 cell lines. The determination of the concentrations as well as the confirmation of the quality of the samples were carried out by the mean of Agilent Bioanalyser 2100 which is considered as a robust and reliable system that provides a high performance in analysis of RNA integrity compared with other standard techniques like agarose gel electrophoresis (Masotti and Preckel, 2006). Our results showed a high quality of the RNA samples presenting RIN values of 9.4.

Using bioinformatics tools we managed to extract the desired information from the raw data produced by the transcriptome sequencing. In fact it was possible to identify the differentially expressed genes where only the 56 significantly different ones were found. AQP9 that was only expressed in resistant HepG2 cell line, was one such gene that was flagged up knowing that it has been implicated in the mechanism of action of Cry1Aa against Sf9 cells expressing a *Bt* receptor (Endo et al., 2017).

Our RT-qPCR results were consistent with the RNA-seq data where the AQP9 mRNA level was shown to be significantly higher in the resistant compared with the susceptible cell line. In addition, the significant drop of this expression in reverted HepG2 reinforced the idea that this gene may play an important role in the resistance mechanism. Together with the fact that the toxin was shown to induce AQP9 expression made us produce a model of action of Cry41Aa where AQP9 was suggested to be involved in the recovery process of intoxicated cells through regulation of the osmotic imbalance and maintaining their homeostasis.

This model was produced based on the knowledge that 3-domain Cry toxins were shown to form nonselective channels where the influx of water resulted in cell swelling followed by lysis and death (Knowles and Ellar, 1987). In addition aquaporins were shown to be involved in cellular volume regulation following cell swelling or shrinkage. AQP9 being a water membrane channel was suggested to play a role in maintaining water balance via transcellular water flow in the glia limitans and into the antrum of the ovarian follicle which is a key aspect of folliculogenesis (Day et al., 2014). Moreover, the possible implication of AQP9 in the immune response of neutrophils to chemokines via water transport where it was shown that impaired migration and water transport were induced by chemokines in AQP9^{-/-} neutrophils reinforced the idea (Moniaga et al., 2015).

Our results showed that as well as the mRNA, the protein level of AQP9 was higher in resistant than in susceptible cell line. In addition, we demonstrated that toxin induced AQP9 expression in both parental and resistant cell lines. However, a pre-treatment of susceptible HepG2 cell line with a sub-lethal dose of toxin (1.5 µg/ml) that was shown to induce AQP9 expression after 2 hours of incubation, did not induce immunity to the toxin in these cells.

The absence of correlation between mRNA and protein abundances in the case of toxin inducing AQP9 expression, could be due to several biological parameters. These involve *cis*-acting and *trans*-acting mechanisms that generate systems able to enhance or repress the synthesis of proteins from a certain copy number of mRNA molecules. Amongst these parameters, ribosomal density and occupancy, RNA secondary structure, regulatory proteins acting as translational modulators and half-life of proteins which is considered as the major post-translational factor influencing this correlation (Maier et al., 2009).

Microscopic observation of both HepG2 cell lines exposed to sub-lethal doses of toxin showed swelling in both cell lines that continued in case of susceptible HepG2 leading to their lysis and death while disappeared in resistant cells that recovered and survived after 24 hours of exposure. These results were consistent with the model proposed and were fortified by the fact that binding of the toxin to the selected and parental HepG2 cell lines was observed.

The recovery process of epithelial cells in response to pore forming toxins was observed in previous work. It was also demonstrated that the osmotic stress produced after formation of pores by different PFTs in the target cells, induce a MAPK p38-phosphorylation-response that is crucial to prevent bacterial infection (Ratner et al., 2006b). This fact might explain the absence of pore formation in whole cell patch clamp experiment that was carried out on resistant HepG2 exposed to 20 μ g/ml of toxin which is consistent with absence of p38 activation using a low dose of toxin (12 μ g/ml) yet his activation was observed using a high dose of toxin that presumably led to formation of pores in cell membrane. However, although we showed that Cry41Aa caused p38 phosphorylation in both susceptible and resistant cell line, inhibition of p38 pathway did not result in the recovery of susceptible HepG2 cell line (Barbara Domanska, 2016).

All the data gathered to this point were heading towards the importance of AQP9 in the recovery process in response to the toxin action. Therefore in order to verify this hypothesis, MMTS which is an aquaporin inhibitor, shown by H. Endo et al in 2017 to efficiently inhibit AQP9 expression, was used. However, this compound appeared to have no effect at low doses while being highly toxic to cells at high doses. As an alternative, AQP9 knock down using siRNA was used. Using this technique, AQP9 knock down in HepG2 cells was shown to be successful as in previous work (Huang et al., 2016).

After 12 hours of cell transfection with siRNA, the AQP9 knock down was optimal at both mRNA and protein levels. However, the effect of toxin was similar between transfected and non-transfected HepG2R suggesting that there was no correlation between AQP9 expression and susceptibility to the toxin.

Looking at the western blot experiment where the expression of AQP9 was monitored over time during the cytotoxicity assay, it appeared that after AQP9 knock down, the expression was again induced after toxin exposure. Therefore, to eliminate the possible role of this protein, knock out of AQP9 in addition to the use of electrophysiology to study the channel activity should be considered in future work to help in identifying the role, if any, of AQP9.

Conclusions

- 1- Culturing HepG2 cells in step wise increases in the concentration of T/C activated Cry41Aa during a period of 8 months makes them resistant to the toxin with a resistance index equal to 41. The resistance levels is lost after 10 months of culture in the absence of the toxic agent.
- 2- Cross resistant study showed that the established resistant cell line is not cross resistant to other chemotherapeutic drugs such as etoposide and 5-Fluorouracil neither to some acriditine gold derivatives.
- 3- EGTA inhibits the toxin action in susceptible as well as in resistant HepG2.
- 4- P38 was shown to be activated in HepG2 and HepG2R cells following exposure to the toxin.
- 5- Transcriptome analysis revealed that 56 genes were differentially expressed between susceptible and resistant cell lines. *aqp9* that has been implicated in the mechanism of action of Cry1Aa against Sf9 cells expressing a *Bt* receptor is upregulated in the resistant cell line but has no obvious role in Cry41Aa mechanism of action.
- 6- Cry41Aa appeared to bind to resistant HepG2 similarly to the susceptible line. This binding appeared to initiate swelling followed by a recovery phase solely observed in the resistant cells.

7 The role of signal transduction in the mode of action of Cry41Aa

7.1 Introduction

The general mode of action of pore forming toxins (PFTs) consists of an initial interaction with the target membrane through receptor recognition, activation with proteases and conformational changes leading to membrane insertion and subsequent perforation. PFTs could have additional effects during their interaction with their host cells including intra-cellular signaling or transport of other enzymatic components reviewed by Cancino-Rodezno et al in 2010 (Cancino-Rodezno et al., 2010b).

Different models explaining the mode of action of *Bt* toxins have been proposed (see chapter 1). These included the pore formation as well as the Zhang model which showed an intracellular cascade response involving protein G, adenylate cyclase (AC) and protein kinase A (PKA) following interaction with the membrane receptor. Zhang et al showed that specific binding of the Cry1Ab toxin to cadherin receptor (BT-R1) stimulated G protein and adenylate cyclase causing the accumulation of cAMP and activation of PKA. These events were shown to disturb both structural and functional integrity of the host cell leading to its death (Zhang et al., 2006). These findings were demonstrated following an initial examination of the effect of divalent cations EGTA and EDTA on Cry1Ab toxicity which led to the assumption that this toxicity may be associated with a Mg²⁺-dependent signaling pathway resulting in cell death.

Previous work which studied in detail the effect of EGTA on Cry41Aa activity showed that this metalloprotease inhibitor inhibited the effect of toxin by means of metal ion chelation. It was demonstrated that EGTA acted by preventing stable interaction with the membrane and subsequent steps of membrane damage and P38 phosphorylation. The protective effect was shown to be established through chelating cations such as

Ca²⁺, Mn²⁺ and Zn²⁺ which were bound to membrane components. It is worthwhile mentioning that Ca²⁺ and Zn²⁺ were shown to have an important role in the structural integrity of *Bt* receptors (Pigott and Ellar, 2007). These findings were also in a good agreement with previous work showing a similar effect of EDTA and EGTA that were able to chelate divalent cations which could exhibit a critical role in the stability of the toxin's receptors or in the pore formation activity (Kirouac et al., 2006).

In this study we tried to test the connection between the Zhang model and Cry41Aa mode of action through investigating the effect of the toxin on several of the proteins/pathways mentioned in the model.

7.2 Investigating the connection between Zhang model and Cry41Aa mode of action

- **EGTA effect on toxin action on HepG2 and HL-60**

The effect of EGTA on toxin action against HepG2 and HL-60 was investigated (figures 164 and 165). PK and T/C activated Cry41Aa were used in this experiment.

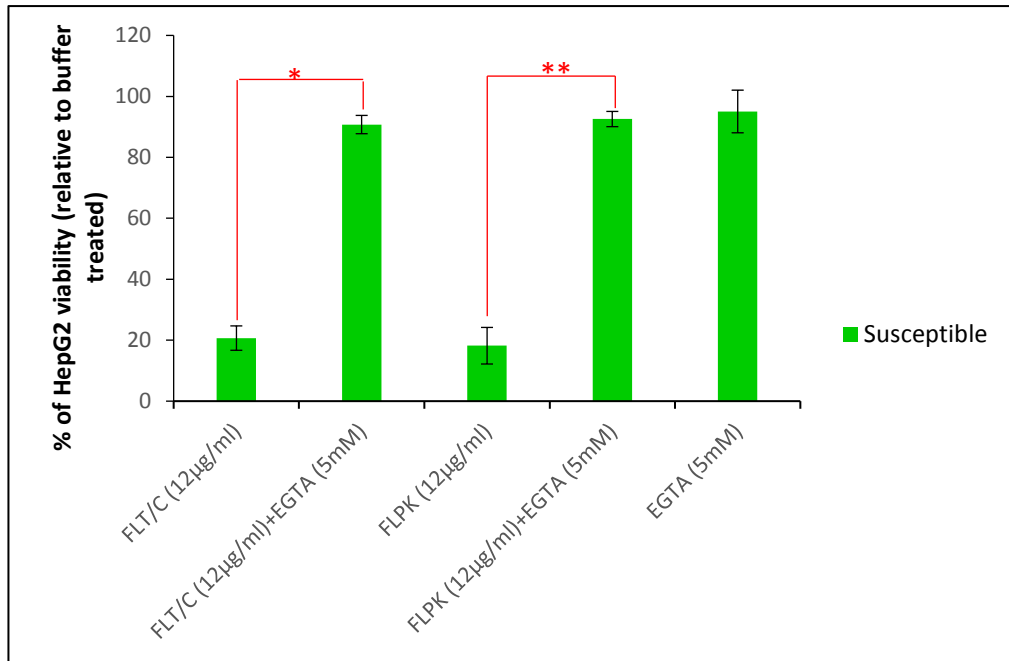


Figure 164: The effect of chelating agent (EGTA) on viability of HepG2 cells exposed to toxin.

HepG2 cells were seeded at the density of 25×10^4 cells/ml. The next day they were pre-incubated with 5 mM of EGTA or water (mock) for 30 min followed by the addition of T/C or PK activated Cry41Aa (12 µg/ml). Cell viability assessed 6 hours later using CellTiter-Blue assay. Ttest: * $p=0.0008$ and ** $p=6.16E-05$

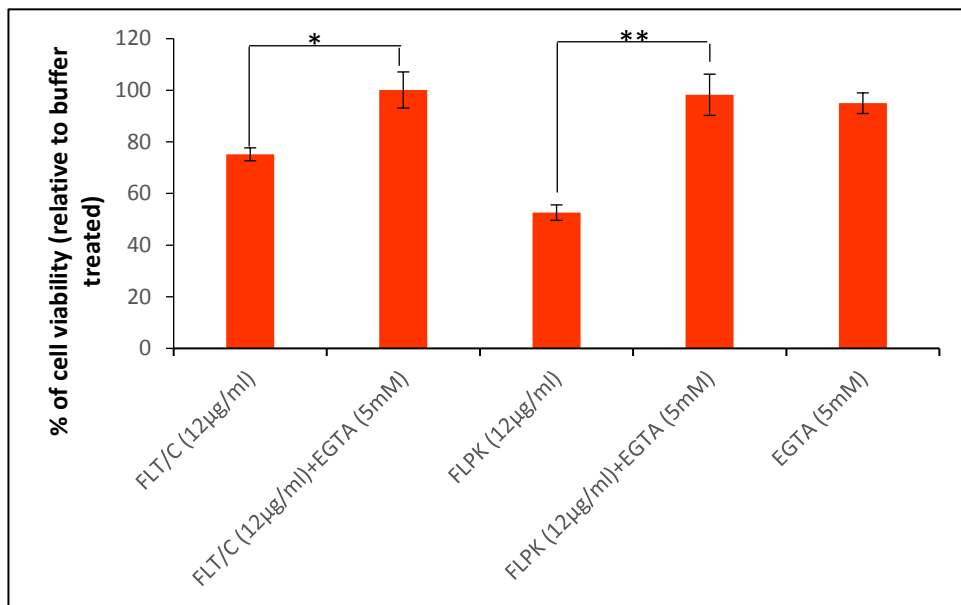


Figure 165: The effect of chelating agent (EGTA) on viability of HL-60 cells exposed to toxin.

HL-60 cells were seeded at the density of 25×10^4 cells/ml. The next day cells were pre-incubated with 5 mM of EGTA or water (mock) for 30 min followed by the addition of T/C or PK activated Cry41Aa (12 µg/ml). Cell viability assessed 6 hours later using CellTiter-Blue assay. Ttest: * $p=0.001$ and ** $p=0.0008$

According to our results, at a concentration of 5 mM EGTA considerably reduced the cytotoxic effect of both PK and T/C activated Cry41Aa on both HepG2 and HL-60 cell lines.

Therefore, regardless of the cell type and the protease used to activate the toxin, EGTA exhibited the same inhibitory effect.

- **Assessment of PKA activation following toxin treatment**

The cyclic adenosine monophosphate cAMP-related signal transduction pathways can either promote cell death or protect cells from death, depending on the cell type and the triggering stimulus (Taskén and Aandahl, 2004). The most common downstream effector of cAMP is PKA (Skalhegg and Tasken, 1997). PKA was considered as the key element in the cell death pathway proposed by Zhang et al in 2006 who showed that pre-treatment of S5 cells with inhibitors of PKA protected the cells from Cry1Ab toxin action (Zhang et al., 2006).

Assessment of the involvement of PKA in the mode of action of Cry41Aa was carried out through investigating the effect of PKA inhibitors (PKI 14-22 amide (PKI) and H-89) on the toxic effect of different activated forms of Cry41Aa on HepG2 as well as on HL-60 cell lines (Figures 166 and 167).

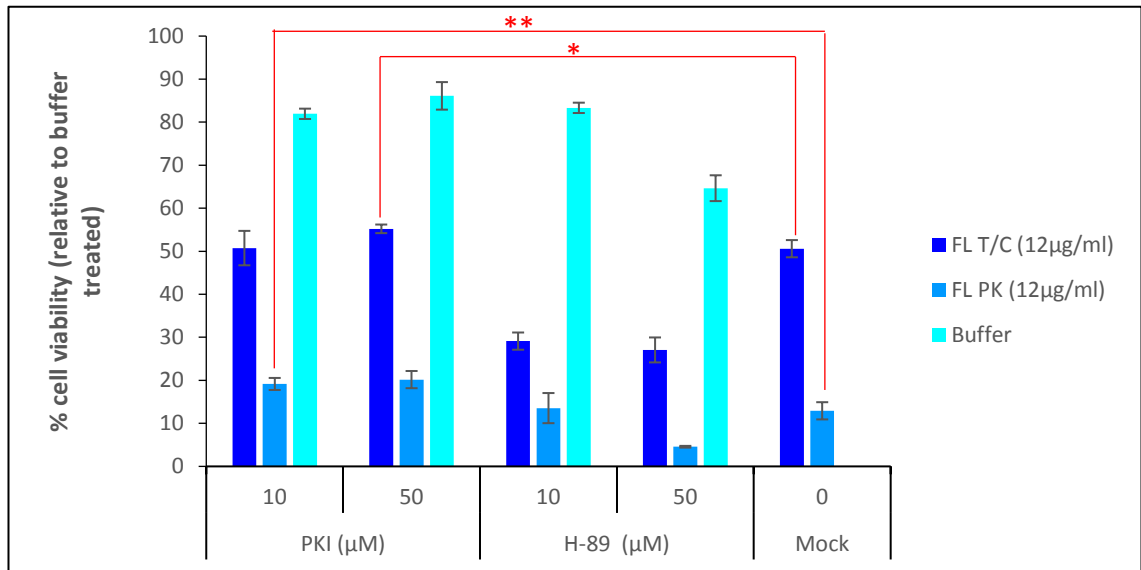


Figure 166: The effect of PKA inhibitors on Cry41Aa cytotoxicity against HepG2 cell line.

HepG2 cells were seeded at the density of 25×10^4 cells/ml. The next day cells were pre-treated with H-89 (10 or 50 μ M) or PKI (10 or 50 μ M) for 30 minutes. Next, PK or T/C activated toxin was added (12 μ g/ml) and cell viability was measured 6 hours later using CellTiter-Blue. Ttest: * $p=0.09$ and ** $p=0.06$

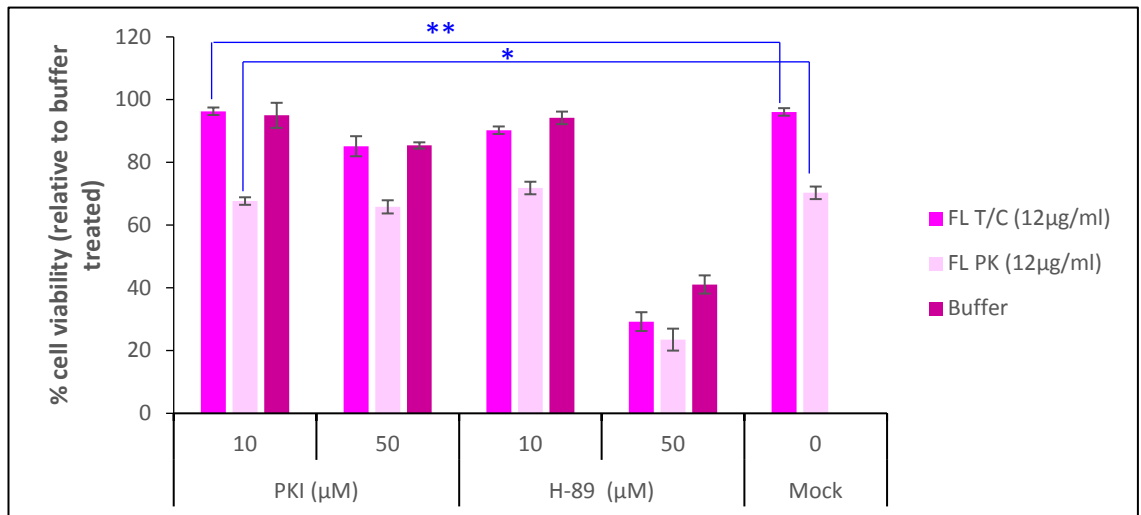


Figure 167: The effect of PKA inhibitors on Cry41Aa cytotoxicity against HL-60 cell line.

HL-60 cells were seeded at the density of 25×10^4 cells/ml. The next day cells were pre-treated with H-89 (10 or 50 μ M) or PKI (10 or 50 μ M) for 30 minutes. Next, PK or T/C activated toxin was added (12 μ g/ml) and cell viability was measured 6 hours later using CellTiter-Blue. Ttest: * $p=0.21$ and ** $p=0.43$

Our results indicated that PKA inhibitors did not prevent toxin activity. In fact, viability was decreased even in cells pre-exposed to PKI and H-89 before toxin addition. The latter inhibitor caused a significant decrease in both cell lines' viability at a concentration of 50 μ M in the absence of toxin revealing its toxicity towards these two cell lines.

In order to support these findings, the involvement of PKA in toxin activity was again investigated through CREB phosphorylation analysis. This was based on the knowledge that when activated, PKA phosphorylates this cAMP-response element binding protein (Rosenberg et al., 2002). Western blot technique was then performed on both HepG2 and HL-60 cell lines in order to detect phosphorylated CREB where 8-bromo-cAMP (8-br-cAMP), a cAMP analogue and as activator of PKA, was used as a positive control and the functionality of the previously used PKA inhibitors was also assessed (figures 168 and 169).

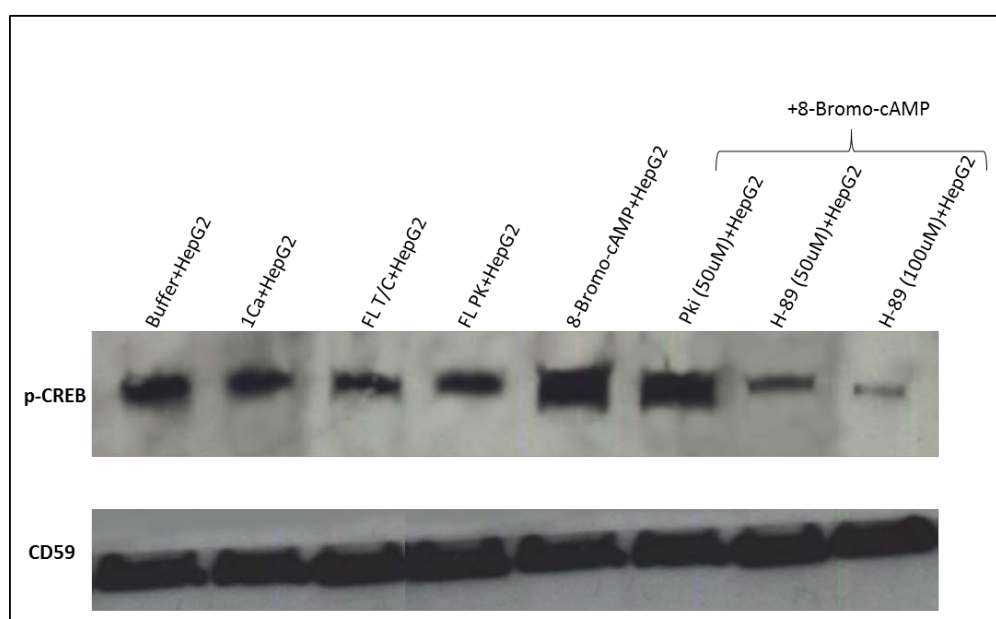


Figure 168: Analysis of CREB activation in toxin treated HepG2 cells.

HepG2 cells were treated with either PKi (50 μ M), H-89 (100 μ M) or water for 30 minutes. Next, 8-br-cAMP (0.5 mM) was added and cells were incubated for another 30 minutes, before cell lysis in RIPA. Another set of cells were treated with either PS-3 (12 μ g/ml), Cry1Ca (12 μ g/ml) or buffer for 15 minutes, before cell lysis in RIPA. 25 μ g of protein from each sample were loaded in each lane and analysed by western blot for the presence of phosphorylated CREB (p CREB). CD59 was used as the loading control.

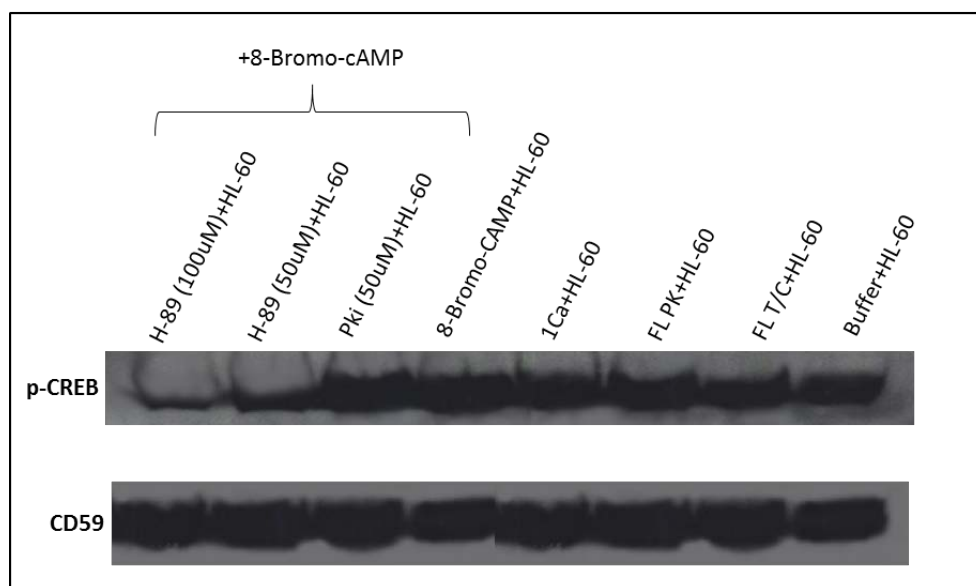


Figure 169: Analysis of CREB activation in toxin treated HL-60 cells.

HL-60 cells were treated with either PKi (50 μ M), H-89 (100 μ M) or water for 30 minutes. Next, 8-br-cAMP (0.5 mM) was added and cells were incubated for another 30 minutes, before cell lysis in RIPA. Another set of cells were treated with either PS-3 (12 μ g/ml), Cry1Ca (12 μ g/ml) or buffer for 15 minutes, before cell lysis in RIPA. 25 μ g of protein from each sample were loaded in each lane and analysed by western blot for the presence of phosphorylated CREB (p CREB) or CD59 (loading control).

Our results showed a high level of phosphorylated CREB in both HepG2 and HL-60 cell lines treated with buffer only. No significant increase, however, was observed in cells exposed to toxin. 8-br-cAMP, which was used as a positive control, significantly induced CREB phosphorylation in both cell lines. H-89 inhibited the effect of 8-br-cAMP resulting in a significant decrease in CREB phosphorylation, yet, PKi had no obvious effect.

Knowing that PKA was considered as the key component of the cell death pathway proposed by Zhang et al in 2006, and based on our results showing that this protein kinase is not activated following toxin treatment, therefore suggested that the mode of action of Cry41Aa does not correlate with the Zhang model.

7.3 Involvement of mitogen-activated protein kinases: assessment of activation of ERK1/2 pathway

The classic MAP kinase family consists of three subfamilies: extracellular signal-regulated kinase (ERK), c-Jun N-terminal kinase (JNK), and p38-MAP kinase (Lu and Xu,

2006). Previous studies have shown that the two mitogen-activated protein kinase (MAPK) pathways: p38 and c-Jun N-terminal kinase (JNK)-like were up-regulated in *Caenorhabditis elegans* in response to Cry5B toxin. Both of these MAPK pathways provided a significant cellular defense against the toxin and this defense was shown to be conserved in mammalian cells attacked by a PFT (Huffman et al., 2004). We have provided data showing that p38 is activated in HepG2, HepG2R and in HL-60 cell lines (see chapters 5 and 6) however according to Domanska et al. inhibition of this MAPK protein did not lead to cell survival (Domanska, 2016).

ERK1/2, another important subfamily of mitogen-activated protein kinases, controls a broad range of cellular activities and physiological processes. Activation of ERK1/2 generally promotes cell survival but can have pro-apoptotic functions in response to a large number of extracellular stimuli (Lu and Xu, 2006).

Assessment of ERK 1/2 activation was also carried out in this study on both HepG2 and HL-60 cell lines upon treatment with PK and T/C activated Cry41Aa by western blotting using antibodies detecting individually-, dually- or non-phosphorylated forms of ERK 1 and ERK 2 (figures 170 and 171).

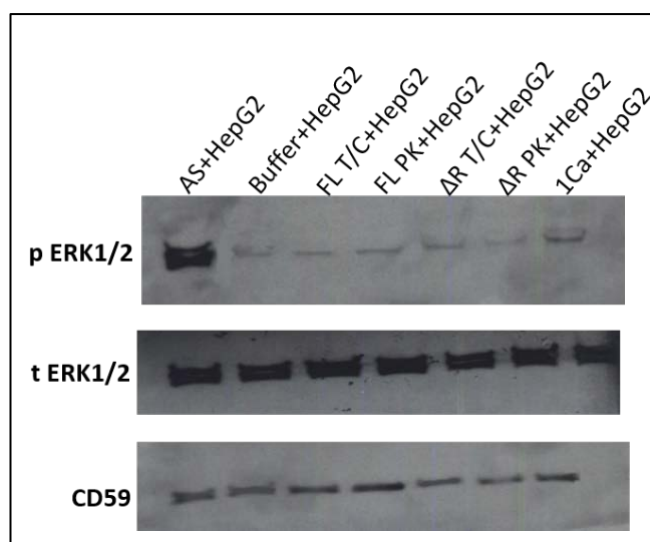


Figure 170: Assessment of ERK 1/2 phosphorylation in HepG2 cells exposed to toxin.

HepG2 cells were treated with T/C or PK activated Cry41Aa (12 $\mu\text{g}/\text{ml}$), buffer, sodium arsenite (0.5 mM), or Cry1Ca (12 $\mu\text{g}/\text{ml}$) for 15 minutes. Next, cells were lysed in RIPA. 10 μg of proteins from each sample were loaded in each lane and analysed by western blot for the presence of total (t ERK) or phosphorylated (p ERK) ERK 1/2. CD59 was used as the loading control.

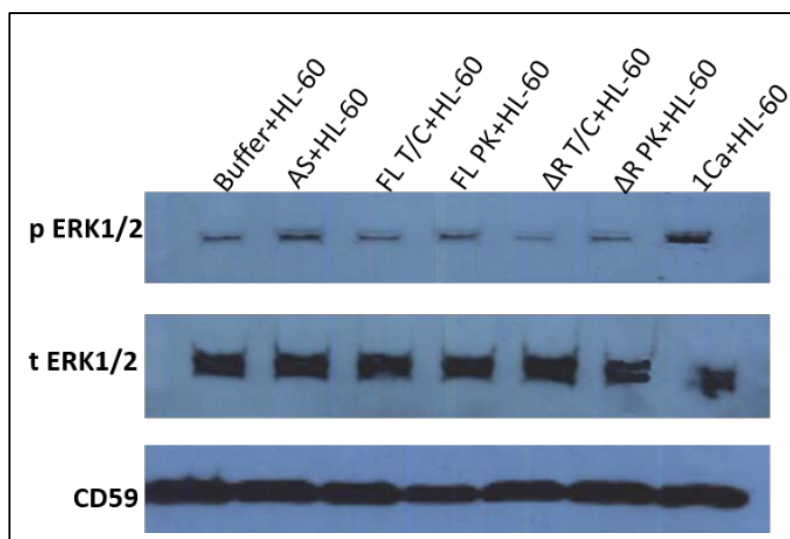


Figure 171: Analysis of ERK 1/2 phosphorylation in toxin treated HL-60 cells.

HL-60 cells were treated with PS-3 (12 $\mu\text{g/ml}$), buffer, sodium arsenite (0.5 mM), or Cry1Ca (12 $\mu\text{g/ml}$) for 15 minutes. Next, cells were lysed in RIPA. 15 μg of proteins from each sample were loaded in each lane and analysed by western blot for the presence of total (t ERK) or phosphorylated (p ERK) ERK 1/2.

According to our results, in toxin treated cells there was no activation of ERK1/2 regardless of the protease used for activation. Only a slight activation of ERK1/2 was observed in HL-60 cells treated with sodium arsenite while a high signal was produced from sodium arsenite treated HepG2.

7.4 Discussion

According to our study, regardless of the cell type (HepG2 vs HL-60), the level of susceptibility (HepG2 vs HepG2R), and the protease (T/C or PK) used to activate the toxin, it appeared that EGTA abolished the cytotoxic effect of Cry41Aa. Domanska in 2006 showed that addition of Ca^{2+} , Mn^{2+} or Zn^{2+} could restore toxin activity. This inhibitory effect was previously observed in insect models where Zhang et al in 2005 showed that in the presence of EDTA and EGTA chelators, the binding of the toxin (Cry1Ab) to the receptor (BT-R1) still occurred however only EDTA prevented subsequent cell death. Addition of Mg^{2+} to susceptible cells pre-exposed to EDTA restored cytotoxicity of Cry1Ab and microscopic observations showed that removal of this cation prevented the susceptible cells from swelling. These findings proposed that

Cry1Ab binding to BT-R1 and subsequent cell death were linked to an Mg^{2+} -dependent signaling pathway (Zhang et al., 2005).

The phosphorylation cascade of ERK1/2 has been extensively studied in human cells and its role was analysed through its involvement in phosphorylation of various substrates in different cellular compartments. The accumulation of stimulated ERK1/2 in the nucleus was suggested to play a role in cell proliferation (Porta et al., 2011). Phosphorylation of ERK1/2 was also shown to induce apoptosis in cancer cells following treatment with apoptotic stimuli. This was demonstrated in case of PS2Aa1 which induced an increase of ERK1/2 phosphorylation in prostate cancer cells (PC3). This activation was suggested to be required for the induction of apoptosis (Brasseur et al., 2015a). Although no evidence of toxicity has been shown for Cry1Ac proteins in mammalian cells, Rubio-Infante et al in 2018 showed that Cry1Ac protoxin was able to activate MAPKs including ERK1/2 in macrophages. The possibility that this effect could be seen in other mammalian cell types was then postulated (Rubio-Infante et al., 2018). According to our results, Cry41Aa did not induce ERK1/2 phosphorylation although it should be noted that only one time point was used. For validation, signalling events which are linked to the activation of this pathway and experiments with ERK inhibitors should be investigated.

PKA, the cAMP dependent protein kinase, was proposed to play a key role in the mode of action of Cry1Ab. Its involvement in the mechanism of action of Cry41Aa was initially investigated through the use of inhibitors (PKi and H-89). Protein kinase inhibitor peptide (PKi) specifically prevents the phosphorylation of PKA and was previously used to examine the role of PKA in various cellular processes however, despite the inhibitory effect of H-89 on PKA, this compound was also shown to have non-specific effects on other protein kinases, signaling molecules and basic cellular functions reviewed by Murray in 2008 (Murray, 2008).

Our results indicated that neither PKi nor H-89 prevented Cry41Aa toxicity.

Knowing that PKA has been previously implicated in various cellular processes including the regulation of transcription and that phosphorylation of CREB is one of the transcriptional responses induced upon activation of various kinases including PKA (Wu

et al., 2005), the involvement of PKA in Cry41Aa mode of action was also examined through the analysis of CREB phosphorylation. Western blot results showed no obvious effect of Cry41Aa on CREB phosphorylation. The endogenous levels of pCREB was high in both HepG2 and HL-60 treated with buffer only. This signal was not affected by PKi inhibitor yet it was significantly decreased by H-89. Due to the non-specific effect of this compound, we can conclude that the pCREB endogenous level was the result of kinase(s) activity other than PKA. These results all indicate that PKA does not play a role in Cry41Aa mode of action.

In insect models, Zhang et al in 2006 hypothesized that PKA plays an important role in Cry1Ab-induced signalling in S5 cells (originated from ovarian cells of the cabbage looper that express BT-R1 receptor) through the use of H-89 and myristoylated amide 14-22 (PKAI 14-22-amide) inhibitors that were shown to prevent membrane damage and cytotoxicity. On the other hand, previous work showed that signal transduction involving PKA, AC and cAMP was not activated upon Cry1Ab or Cry1Ac treatment, which induced apoptosis in CF1 cells. It was suggested that cell death response in these cells was stimulated by pore formation activity of the toxins (Portugal et al., 2017).

Conclusions

- 1- Despite the fact that EGTA inhibits Cry41Aa action and its protective effect was previously shown to be established through chelating cations, a fact that was observed by Zhang et al when studying the mode of action of Cry1Ab, it seemed that Cry41Aa does not act through a Mg^{2+} -dependent signaling pathway, a model that was proposed by Zhang et al in 2006.
- 2- Amongst the MAP kinase subfamilies, P38 but not ERK1/2 is activated following exposure of cancer cells (susceptible/non susceptible HepG2 and HL-60) to Cry41Aa.

8 General discussion

Safety concerns relating to the use of *Bt* based pesticides, that have been successfully used for more than 60 years have recently been raised. These are based on findings that some Cry toxins like Cry1Ab were shown to have an impact on mammals (Gab-Alla et al., 2012). On the other hand, parasporins, a group of *Bt* toxins, were shown to preferentially kill human cancer cells making PS proteins possible candidates for anticancer agents of medical use. Understanding the mechanism of action as well as the nature of specificity of Cry toxins against human/mammalian cells was then needed. Parasporin-3 (Cry41Aa) which most closely resembles the commercially used insecticidal toxins exhibits the narrowest activity spectrum against human cancer cells. In this research study the mode of action of this toxin was further investigated.

It has been previously shown that N-terminal cleavage is essential for *Bt* toxin action. The results of the experiments performed in this study showed that Cry41Aa could not be pre-activated by deletion of 23 aa at the N-terminal region however the deletion of the N-terminal 40 aa led to the production of a toxic core. Yet, this deletion was shown to affect the expression of the protein which was weak and was lost completely when 60 aa were deleted. This result was consistent with previous findings where the N-terminus was shown to play an important role in expression/crystallization of *Bt* Cry toxins (Oppert, 1999, Martens et al., 1995).

Although N-terminal cleavage was shown to be essential in *Bt* toxin action, certain Cry toxins needed a cleavage at the C-terminus to be activated therefore we investigated whether N or C-terminal cleavage(s) are important in Cry41Aa toxicity. Our results indicated that N-terminal cleavage alone can activate Cry41Aa toxin but that either C-terminal cleavage or the precise position of N-terminal cleavage may affect toxin activity.

Comparison between the N-terminal sequences of trypsin lab-grade vs trypsin MS-grade activated Cry41Aa as well as their toxic effect on HepG2 cell line revealed that the protein cannot be activated by MS-grade trypsin but can be presumably by contaminating chymotrypsin in some stocks.

Our results also showed that differential proteolysis of Cry41Aa can affect its toxicity. In fact, by comparing the cytopathic effect of proteinase K activated Cry41Aa to that of the trypsin/chymotrypsin activated protein against HepG2 and HL-60 cell lines, we showed that the effect of PK activated toxin is significantly higher to that of the T/C activated protein.

In addition, by comparing the protein banding profiles of both activated forms of the toxin, our results showed similarities revealing the production of two bands of around 75 and 65 kDa. Using anion exchange chromatography, the purification of the upper band (75 kDa) was successful and the assessment of its cytotoxic level towards HepG2 and HL-60 indicated that this protein is sufficient for toxicity. N-terminal sequencing of this protein, after proteolytic activation with PK, revealed that cleavage occurs at the 60th aa and that the N-terminal sequence of the toxic moiety is: DVRDA. This result in addition to Yamashita et al finding in 2005 indicated that the difference between the two fragments yielded after proteolytic digestion of Cry41Aa with PK resides in the C-terminal cleavage. On the other hand N-terminal sequencing of the T/C activated protein revealed that cleavage occurs at the 58th aa and the N-terminal sequence of the toxic moiety is: SADVRDA.

Examination of the predicted 3-D structure of Cry41Aa gave us a hint that possibly the N-terminal region of the protein is partially obscuring the DVRDA motif and that the removal of Ser and Ala residues would result in a great exposure of this motif speculated to be important in binding and therefore explaining the higher toxic effect of PK compared with T/C activated Cry41Aa. Creation of substitutions at this position and assessment of the toxic effect of the mutants created were not very helpful which made us move on to study the binding of the mutants as well as the wild type on susceptible and non-susceptible cell lines.

Many attempts have been previously carried out to study the binding of Cry41Aa on HepG2 cells, however they were unsuccessful due to many problems encountered, one of them being instability of a C-terminal tag (Domanska, 2016). In this study we managed to resolve this problem by the creation of a mutant Δ R-HAP40 that exhibits cytotoxic effect (after being activated with PreScission protease) against HepG2 cells and whose C-terminal HA tag was stable even after proteolytic activation.

Preliminary work carried out on binding of Cry41Aa to susceptible HepG2, less susceptible HL-60 and non-susceptible HeLa cell lines showed that there was lack of correlation between susceptibility and binding. This has been observed in previous work carried out on insecticidal Cry toxins showing that non-toxic Cry toxins can still bind to insect BBMV (Luo et al., 1999) and this phenomenon was also shown in resistant populations where post binding processes rather than binding were shown to play crucial role in toxicity (Masson et al., 1995b).

The development of resistant HepG2 to trypsin/chymotrypsin activated Cry41Aa was one of the approaches followed in this study to better understand the mechanism of action of the toxin. The generation of the resistant subline was successful using the stepwise increase of toxic agent method and this was achieved after a period of 8 months. The resistance index was equal to 41, this resistance phenotype, however, was shown to be unstable after 10 months of culture in medium free of toxin. A cross resistance study showed that this cell line was not cross resistant to other chemotherapeutic drugs like 5-Fluorouracil and etoposide. Microscopic observation (DIC) showed that there was no obvious changes in the morphological features between susceptible and resistant HepG2 cells.

Comparative transcriptome analysis on both susceptible and resistant HepG2 showed that there was around 56 genes that were differentially expressed between the two cell lines. AQP9 that was previously implicated in the mechanism of action of Cry1Aa against sf9 cell (Endo et al., 2017) was present in resistant but not in susceptible HepG2. Based on the known function of aquaporins as water-selective membrane channels, a mode of action model of Cry41Aa involving this protein was then proposed where it was suggested that the high expression of AQP9 in resistant HepG2 cells plays an important role in reducing the osmotic gradient and restoring the cell to a healthy state following exposure to the toxin. However, knock down of this protein by the mean of siRNA did not reduce the resistance level suggesting no crucial role of AQP9 in the resistance mechanism.

Microscopic observation of resistant HepG2 exposed to toxin showed initial swelling followed by recovery and survival, an aspect that was also observed in non-susceptible HeLa cells. This finding in addition to the binding results, where binding of Cry41Aa was

detected in resistant and non-susceptible HeLa cells, were consistent with the hypothesis that recovery determines specificity. This result has also been observed in an insect system where resistance of *Heliothis virescens* to Cry1Ac intoxication was correlated with enhanced repair of damaged gut epithelium (Forcada et al., 1999).

Knowing that p38 MAPK was previously shown to play an important role in the recovery mechanism by activating a cellular defense response following exposure to PFTs, assessment of the activation of this pathway was carried out. Our results indicated that Cry41Aa activates p38 in susceptible and resistant HepG2 as well as in HL-60 cells. However in a recent study, it was shown that inhibition of P38 did not rescue cell viability (Domanska, 2016) which may indicate that p38 pathway is not involved in the recovery of cells exposed to Cry41Aa.

In this study we also showed that the inhibitory effect of EGTA on Cry41Aa was observed in susceptible and resistant HepG2 as well as in HL-60 cells. In a recent study this inhibition was shown to be due to metal ion chelation which prevented stable interaction of the toxin with the cell membrane (Domanska, 2016). These findings in addition to the Zhang model which showed involvement of Mg^{2+} cell signaling pathway in the mechanism of action of Cry1Ab against *M. sexta* led us to test the involvement of a few of the signaling pathways reported to be involved in the mode of action of PFT. Our results showed that neither PKA nor ERK 1/2 play role in Cry41Aa mode of action.

Future work should involve:

- Investigation of the hypothesis that the toxin forms transient channels in other/all human cells using electrophysiology. This technique would also allow us to perform a comparison study of channel activity in susceptible and non-susceptible cell lines following toxin exposure in addition to confirm the role of channels (in particular AQP9) in the susceptibility of target cells to Cry41Aa.
- Further investigate binding and ideally identify cell binding protein(s) to test whether or not they are functional receptors. The use of a Green Fluorescent Protein (GFP) coupling technique could be considered in order to visualise the

localization of the toxin on the target cell membrane using different conditions eg. in presence/absence of the chelating agent EGTA.

- Investigate pathway(s) responsible for cell recovery that may be missing in susceptible cells.

9 References

- ABUHAMMAD, S. & ZIHLIF, M. 2013. Gene expression alterations in doxorubicin resistant MCF7 breast cancer cell line. *Genomics*, 101, 213-220.
- ADANG, M. J., CRICKMORE, N. & JURAT-FUENTES, J. L. 2014. Diversity of *Bacillus thuringiensis* Crystal Toxins and Mechanism of Action. In: DHADIALLA, T. S. & GILL, S. S. (eds.) *Insect Midgut and Insecticidal Proteins*.
- ADANG, M. J., STAVER, M. J., ROCHELEAU, T. A., LEIGHTON, J., BARKER, R. F. & THOMPSON, D. V. 1985. CHARACTERIZED FULL-LENGTH AND TRUNCATED PLASMID CLONES OF THE CRYSTAL PROTEIN OF *BACILLUS-THURINGIENSIS* SUBSP *KURSTAKI* HD-73 AND THEIR TOXICITY TO *MANDUCA-SEXTA*. *Gene*, 36, 289-300.
- AKIBA, T., ICHIMATSU, T., KATAYAMA, H., AKAO, T., NAKAMURA, O., MIZUKI, E., OHBA, M. & HARATA, K. 2005. *Structure of parasporin-1, a novel bacterial cytotoxin against human cancer cells*.
- AKIBA, T. & OKUMURA, S. 2017. Parasporins 1 and 2: Their structure and activity. *Journal of Invertebrate Pathology*, 142, 44-49.
- AKIRA, S., UEMATSU, S. & TAKEUCHI, O. 2006. Pathogen Recognition and Innate Immunity. *Cell*, 124, 783-801.
- ANGST, B. D., MARCOZZI, C. & MAGEE, A. I. 2001. The cadherin superfamily: diversity in form and function. *Journal of Cell Science*, 114, 629-641.
- ARANDA, P. S., LAJOIE, D. M. & JORCYK, C. L. 2012. Bleach gel: A simple agarose gel for analyzing RNA quality. *Electrophoresis*, 33, 366-369.
- AROIAN, R. & VAN DER GOOT, F. G. 2007. Pore-forming toxins and cellular non-immune defenses (CNiDs). *Current Opinion in Microbiology*, 10, 57-61.
- ATSUMI, S., MIYAMOTO, K., YAMAMOTO, K., NARUKAWA, J., KAWAI, S., SEZUTSU, H., KOBAYASHI, I., UCHINO, K., TAMURA, T., MITA, K., KADONO-OKUDA, K., WADA, S., KANDA, K., GOLDSMITH, M. R. & NODA, H. 2012. Single amino acid mutation in an ATP-binding cassette transporter gene causes resistance to Bt toxin Cry1Ab in the silkworm, *Bombyx mori*. *Proceedings of the National Academy of Sciences of the United States of America*, 109, E1591-E1598.
- AVISAR, D., SEGAL, M., SNEH, B. & ZILBERSTEIN, A. 2005. Cell-cycle-dependent resistance to *Bacillus thuringiensis* Cry1C toxin in Sf9 cells. *Journal of Cell Science*, 118, 3163-3171.
- BAH, A., VAN FRANKENHUYZEN, K., BROUSSEAU, R. & MASSON, L. 2004. The *Bacillus thuringiensis* Cry1Aa toxin: effects of trypsin and chymotrypsin site mutations on toxicity and stability. *Journal of Invertebrate Pathology*, 85, 120-127.
- BANKS, D. J., JURAT-FUENTES, J. L., DEAN, D. H. & ADANG, M. J. 2001. *Bacillus thuringiensis* Cry1Ac and Cry1Fa delta-endotoxin binding to a novel 110 kDa aminopeptidase in *Heliothis virescens* is not N-acetylgalactosamine mediated. *Insect Biochemistry and Molecular Biology*, 31, 909-918.
- BASKIN, F., ROSENBERG, R. N. & DEV, V. 1981. CORRELATION OF DOUBLE-MINUTE CHROMOSOMES WITH UNSTABLE MULTIDRUG CROSS-RESISTANCE IN UPTAKE MUTANTS OF NEURO-BLASTOMA CELLS. *Proceedings of the National Academy of Sciences of the United States of America-Biological Sciences*, 78, 3654-3658.
- BERRY, C. 2012. The bacterium, *Lysinibacillus sphaericus*, as an insect pathogen. *Journal of Invertebrate Pathology*, 109, 1-10.
- BISCHOF, L. J., KAO, C.-Y., LOS, F. C. O., GONZALEZ, M. R., SHEN, Z., BRIGGS, S. P., VAN DER GOOT, F. G. & AROIAN, R. V. 2008. Activation of the Unfolded Protein Response Is Required for Defenses against Bacterial Pore-Forming Toxin In Vivo. *Plos Pathogens*, 4, e1000176.

- BOKORI-BROWN, M., SAVVA, C. G., DA COSTA, S. P. F., NAYLOR, C. E., BASAK, A. K. & TITBALL, R. W. 2011. Molecular basis of toxicity of *Clostridium perfringens* epsilon toxin. *Febs Journal*, 278, 4589-4601.
- BOONSERM, P., DAVIS, P., ELLAR, D. J. & LI, J. 2005. Crystal Structure of the Mosquito-larvicidal Toxin Cry4Ba and Its Biological Implications. *Journal of Molecular Biology*, 348, 363-382.
- BOONSERM, P., MO, M., ANGSUTHANASOMBAT, C. & LESCAR, J. 2006. Structure of the Functional Form of the Mosquito Larvicidal Cry4Aa Toxin from *Bacillus thuringiensis* at a 2.8-Angstrom Resolution. *Journal of Bacteriology*, 188, 3391-3401.
- BRASSEUR, K., AUGER, P., ASSELIN, E., PARENT, S., COTE, J.-C. & SIROIS, M. 2015a. Parasporin-2 from a New *Bacillus thuringiensis* 4R2 Strain Induces Caspases Activation and Apoptosis in Human Cancer Cells. *Plos One*, 10.
- BRASSEUR, K., AUGER, P., ASSELIN, E., PARENT, S., COTE, J. C. & SIROIS, M. 2015b. Parasporin-2 from a New *Bacillus thuringiensis* 4R2 Strain Induces Caspases Activation and Apoptosis in Human Cancer Cells. *Plos One*, 10.
- BRAVO, A., GILL, S. S. & SOBERON, M. 2007. Mode of action of *Bacillus thuringiensis* Cry and Cyt toxins and their potential for insect control. *Toxicon*, 49, 423-435.
- BRAVO, A., GOMEZ, I., CONDE, J., MUNOZ-GARAY, C., SANCHEZ, J., MIRANDA, R., ZHUANG, M., GILL, S. S. & SOBERON, M. 2004. Oligomerization triggers binding of a *Bacillus thuringiensis* Cry1Ab pore-forming toxin to aminopeptidase N receptor leading to insertion into membrane microdomains. *Biochimica Et Biophysica Acta-Biomembranes*, 1667, 38-46.
- BRAVO, A., SANCHEZ, J., KOUSKOURA, T. & CRICKMORE, N. 2002. N-terminal activation is an essential early step in the mechanism of action of the *Bacillus thuringiensis* Cry1Ac insecticidal toxin. *Journal of Biological Chemistry*, 277, 23985-23987.
- BRAVO, R., PARRA, V., GATICA, D., RODRIGUEZ, A. E., TORREALBA, N., PAREDES, F., WANG, Z. V., ZORZANO, A., HILL, J. A., JAIMOVICH, E., QUEST, A. F. G. & LAVANDERO, S. 2013. Endoplasmic Reticulum and the Unfolded Protein Response: Dynamics and Metabolic Integration. *International review of cell and molecular biology*, 301, 215-290.
- BRETSCHNEIDER, A., HECKEL, D. G. & PAUCHET, Y. 2016. Three toxins, two receptors, one mechanism: Mode of action of Cry1A toxins from *Bacillus thuringiensis* in *Heliothis virescens*. *Insect Biochemistry and Molecular Biology*, 76, 109-117.
- BUTKO, P. 2003. Cytolytic toxin Cyt1A and its mechanism of membrane damage: Data and hypotheses. *Applied and Environmental Microbiology*, 69, 2415-2422.
- BUZDIN, A. A., REVINA, L. P., KOSTINA, L. I., ZALUNIN, I. A. & CHESTUKHINA, G. G. 2002. Interaction of 65- and 62-kD proteins from the apical membranes of the *Aedes aegypti* larvae midgut epithelium with Cry4B and Cry11A endotoxins of *Bacillus thuringiensis*. *Biochemistry-Moscow*, 67, 540-546.
- CACCIA, S., HERNANDEZ-RODRIGUEZ, C. S., MAHON, R. J., DOWNES, S., JAMES, W., BAUTSOENS, N., VAN RIE, J. & FERRE, J. 2010. Binding Site Alteration Is Responsible for Field-Isolated Resistance to *Bacillus thuringiensis* Cry2A Insecticidal Proteins in Two *Helicoverpa* Species. *Plos One*, 5.
- CANCINO-RODEZNO, A., ALEXANDER, C., VILLASENOR, R., PACHECO, S., PORTA, H., PAUCHET, Y., SOBERON, M., GILL, S. S. & BRAVO, A. 2010a. The mitogen-activated protein kinase p38 is involved in insect defense against Cry toxins from *Bacillus thuringiensis*. *Insect Biochemistry and Molecular Biology*, 40, 58-63.
- CANCINO-RODEZNO, A., PORTA, H., SOBERON, M. & BRAVO, A. 2010b. Defense and death responses to pore forming toxins. In: HARDING, S. E. & TOMBS, M. P. (eds.) *Biotechnology and Genetic Engineering Reviews*, Vol 26.
- CASTAGNOLA, A. & JURAT-FUENTES, J. L. 2016. Intestinal regeneration as an insect resistance mechanism to entomopathogenic bacteria. *Current opinion in insect science*, 15, 104-110.

- CHAKROUN, M., BANYULS, N., BEL, Y., ESCRICHE, B. & FERRE, J. 2016. Bacterial Vegetative Insecticidal Proteins (Vip) from Entomopathogenic Bacteria. *Microbiology and Molecular Biology Reviews*, 80, 329-350.
- CHAN, J. Y. W., CHU, A. C. Y. & FUNG, K. P. 2000. Inhibition of P-glycoprotein expression and reversal of drug resistance of human hepatoma HepG2 cells by multidrug resistance gene (mdr1) antisense RNA. *Life Sciences*, 67, 2117-2124.
- CHEN, J., AIMANOVA, K. G., FERNANDEZ, L. E., BRAVO, A., SOBERON, M. & GILL, S. S. 2009. Aedes aegypti cadherin serves as a putative receptor of the Cry11Aa toxin from Bacillus thuringiensis subsp israelensis. *Biochemical Journal*, 424, 191-200.
- COATES, B. S. & SIEGFRIED, B. D. 2015. Linkage of an ABC transporter to a single QTL that controls Ostrinia nubilalis larval resistance to the Bacillus thuringiensis Cry1Fa toxin. *Insect Biochemistry and Molecular Biology*, 63, 86-96.
- COHEN, S., ALBECK, S., BEN-DOV, E., CAHAN, R., FIRER, M., ZARITSKY, A. & DYM, O. 2011. Cyt1Aa Toxin: Crystal Structure Reveals Implications for Its Membrane-Perforating Function. *Journal of Molecular Biology*, 413, 804-814.
- COHEN, S., DYM, O., ALBECK, S., BEN-DOV, E., CAHAN, R., FIRER, M. & ZARITSKY, A. 2008. High-resolution crystal structure of activated Cyt2Ba monomer from Bacillus thuringiensis subsp israelensis. *Journal of Molecular Biology*, 380, 820-827.
- COLLETIER, J.-P., SAWAYA, M. R., GINGERY, M., RODRIGUEZ, J. A., CASCIO, D., BREWSTER, A. S., MICHELS-CLARK, T., HICE, R. H., COUELLE, N., BOUTET, S., WILLIAMS, G. J., MESSERSCHMIDT, M., DEPONTE, D. P., SIERRA, R. G., LAKSMONO, H., KOGLIN, J. E., HUNTER, M. S., PARK, H.-W., UERVIROJNANGKOORN, M., BIDESHI, D. K., BRUNGER, A. T., FEDERICI, B. A., SAUTER, N. K. & EISENBERG, D. S. 2016. De novo phasing with X-ray laser reveals mosquito larvicide BinAB structure. *Nature*, 539, 43.
- CONTRERAS, E., SCHOPPEMEIER, M., REAL, M. D. & RAUSELL, C. 2013. Sodium Solute Symporter and Cadherin Proteins Act as Bacillus thuringiensis Cry3Ba Toxin Functional Receptors in Tribolium castaneum. *The Journal of Biological Chemistry*, 288, 18013-18021.
- CRICKMORE, N., BAUM, J., BRAVO, A., LERECLUS, D., NARVA, K., SAMPSON, K., SCHNEPF, E., SUN, M. AND ZEIGLER, D.R. 2016. *Bacillus thuringiensis toxin nomenclature* [Online]. Available: <http://www.btnomenclature.info/> [Accessed].
- CRICKMORE, N., ZEIGLER, D. R., FEITELSON, J., SCHNEPF, E., VAN RIE, J., LERECLUS, D., BAUM, J. & DEAN, D. H. 1998. Revision of the nomenclature for the Bacillus thuringiensis pesticidal crystal proteins. *Microbiology and Molecular Biology Reviews*, 62, 807-+.
- DAY, R. E., KITCHEN, P., OWEN, D. S., BLAND, C., MARSHALL, L., CONNER, A. C., BILL, R. M. & CONNER, M. T. 2014. Human aquaporins: Regulators of transcellular water flow. *Biochimica Et Biophysica Acta-General Subjects*, 1840, 1492-1506.
- DE MAAGD, R. A., BRAVO, A. & CRICKMORE, N. 2001. How Bacillus thuringiensis has evolved specific toxins to colonize the insect world. *Trends in Genetics*, 17, 193-199.
- DEIST, B. R., RAUSCH, M. A., FERNANDEZ-LUNA, M. T., ADANG, M. J. & BONNING, B. C. 2014. Bt Toxin Modification for Enhanced Efficacy. *Toxins*, 6, 3005-3027.
- DENHOLM, I., DEVINE, G. J. & WILLIAMSON, M. S. 2002. Evolutionary genetics - Insecticide resistance on the move. *Science*, 297, 2222-2223.
- DERBYSHIRE, D. J., ELLAR, D. J. & LI, J. 2001. Crystallization of the Bacillus thuringiensis toxin Cry1Ac and its complex with the receptor ligand N-acetyl-d-galactosamine. *Acta Crystallographica Section D*, 57, 1938-1944.
- DERETIC, V. 2006. Autophagy as an immune defense mechanism. *Current Opinion in Immunology*, 18, 375-382.
- DOMANSKA, B. 2016. *Mode of action of a human cancer cell active toxin (Parasporin-3) from Bacillus thuringiensis*. PhD Doctoral thesis, University of Sussex.
- DORSCH, J. A., CANDAS, M., GRIKO, N. B., MAATY, W. S. A., MIDBOE, E. G., VADLAMUDI, R. K. & BULLA, L. A. 2002. Cry1A toxins of Bacillus thuringiensis bind specifically to a region adjacent to the membrane-proximal extracellular domain of BT-R1 in Manduca sexta::

- involvement of a cadherin in the entomopathogenicity of *Bacillus thuringiensis*. *Insect Biochemistry and Molecular Biology*, 32, 1025-1036.
- EKINO, K., OKUMURA, S., ISHIKAWA, T., KITADA, S., SAITOH, H., AKAO, T., OKA, T., NOMURA, Y., OHBA, M., SHIN, T. & MIZUKI, E. 2014. Cloning and Characterization of a Unique Cytotoxic Protein Parasporin-5 Produced by *Bacillus thuringiensis* A1100 Strain. *Toxins*, 6, 1882-1895.
- ENDO, H., AZUMA, M., ADEGAWA, S., KIKUTA, S. & SATO, R. 2017. Water influx via aquaporin directly determines necrotic cell death induced by the *Bacillus thuringiensis* Cry toxin. *Febs Letters*, 591, 56-64.
- FANG, Y. N., ZHANG, C., WU, T., WANG, Q., LIU, J. H. & DAI, P. G. 2017. Transcriptome Sequencing Reveals Key Pathways and Genes Associated with Cisplatin Resistance in Lung Adenocarcinoma A549 Cells. *Plos One*, 12.
- FERNANDES-ALNEMRI, T., WU, J., YU, J. W., DATTA, P., MILLER, B., JANKOWSKI, W., ROSENBERG, S., ZHANG, J. & ALNEMRI, E. S. 2007. The pyroptosome: a supramolecular assembly of ASC dimers mediating inflammatory cell death via caspase-1 activation. *Cell Death and Differentiation*, 14, 1590-1604.
- FERNANDEZ-CALLEJA, V., HERNANDEZ, P., SCHVARTZMAN, J. B., DE LACOPA, M. G. & KRIMER, D. B. 2017. Differential gene expression analysis by RNA-seq reveals the importance of actin cytoskeletal proteins in erythroleukemia cells. *Peerj*, 5.
- FERNANDEZ, L. E., AIMANOVA, K. G., GILL, S. S., BRAVO, A. & SOBERON, M. 2006. A GPI-anchored alkaline phosphatase is a functional midgut receptor of Cry11Aa toxin in *Aedes aegypti* larvae. *Biochemical Journal*, 394, 77-84.
- FERRÉ, J. & VAN RIE, J. 2002. BIOCHEMISTRY AND GENETICS OF INSECT RESISTANCE TO *BACILLUS THURINGIENSIS*. *Annual Review of Entomology*, 47, 501-533.
- FINK, S. L. & COOKSON, B. T. 2005. Apoptosis, Pyroptosis, and Necrosis: Mechanistic Description of Dead and Dying Eukaryotic Cells. *Infection and Immunity*, 73, 1907-1916.
- FIUZA, L. M., KNAAK, N., DA SILVA, R. F. P. & HENRIQUES, J. A. P. 2013. Receptors and Lethal Effect of *Bacillus thuringiensis* Insecticidal Crystal Proteins to the *Anticarsia gemmatalis* (Lepidoptera, Noctuidae). *ISRN microbiology*, 2013, 940284-940284.
- FIUZA, L. M., POLANCZYK, R. A. & CRICKMORE, N. 2017. *Bacillus thuringiensis* and *Lysinibacillus sphaericus* : characterization and use in the field of biocontrol [Online]. Available: <http://public.ebib.com/choice/publicfullrecord.aspx?p=4875285> [Accessed].
- FORCADA, C., ALCACER, E., GARCERA, M. D., TATO, A. & MARTINEZ, R. 1999. Resistance to *Bacillus thuringiensis* Cry1Ac toxin in three strains of *Heliothis virescens*: Proteolytic and SEM study of the larval midgut. *Archives of Insect Biochemistry and Physiology*, 42, 51-63.
- GAB-ALLA, EL-SHAMEI, SHATTA, A., MOUSSA & RAYAN, A. 2012. *Morphological and Biochemical Changes in Male Rats Fed on Genetically Modified Corn (Ajeeb YG)*.
- GABRIEL GUTIERREZ, M., SAKA, H. A., CHINEN, I., ZOPPINO, F. C. M., YOSHIMORI, T., BOCCO, J. L. & COLOMBO, M. I. 2007. Protective role of autophagy against *Vibrio cholerae* cytolysin, a pore-forming toxin from *V. cholerae*. *Proceedings of the National Academy of Sciences of the United States of America*, 104, 1829-1834.
- GAHAN, L. J., GOULD, F. & HECKEL, D. G. 2001. Identification of a gene associated with bit resistance in *Heliothis virescens*. *Science*, 293, 857-860.
- GALITSKY, N., CODY, V., WOJTCZAK, A., GHOSH, D., LUFT, J. R., PANGBORN, W. & ENGLISH, L. 2001. Structure of the insecticidal bacterial [delta]-endotoxin Cry3Bb1 of *Bacillus thuringiensis*. *Acta Crystallographica Section D*, 57, 1101-1109.
- GOMEZ, I., SANCHEZ, J., MIRANDA, R., BRAVO, A. & SOBERON, M. 2002. Cadherin-like receptor binding facilitates proteolytic cleavage of helix alpha-1 in domain I and oligomer pre-pore formation of *Bacillus thuringiensis* Cry1Ab toxin. *Febs Letters*, 513, 242-246.

- GRIFFITTS, J. S., HASLAM, S. M., YANG, T. L., GARCZYNSKI, S. F., MULLOY, B., MORRIS, H., CREMER, P. S., DELL, A., ADANG, M. J. & AROIAN, R. V. 2005. Glycolipids as receptors for *Bacillus thuringiensis* crystal toxin. *Science*, 307, 922-925.
- GRIFFITTS, J. S., HUFFMAN, D. L., WHITACRE, J. L., BARROWS, B. D., MARROQUIN, L. D., MULLER, R., BROWN, J. R., HENNET, T., ESKO, J. D. & AROIAN, R. V. 2003. Resistance to a bacterial toxin is mediated by removal of a conserved glycosylation pathway required for toxin-host interactions. *Journal of Biological Chemistry*, 278, 45594-45602.
- GRIFFITTS, J. S., WHITACRE, J. L., STEVENS, D. E. & AROIAN, R. V. 2001. Bt toxin resistance from loss of a putative carbohydrate-modifying enzyme. *Science*, 293, 860-864.
- GRINGORTEN, J. L., SOHI, S. S. & MASSON, L. 1999. Activity spectra of *Bacillus thuringiensis* delta-endotoxins against eight insect cell lines. *In Vitro Cellular & Developmental Biology-Animal*, 35, 299-303.
- GROCHULSKI, P., MASSON, L., BORISOVA, S., PUSZTAI-CAREY, M., SCHWARTZ, J.-L., BROUSSEAU, R. & CYGLER, M. 1995. *Bacillus thuringiensis* CryIA(a) Insecticidal Toxin: Crystal Structure and Channel Formation. *Journal of Molecular Biology*, 254, 447-464.
- GUIHARD, G., VACHON, V., LAPRADE, R. & SCHWARTZ, J. L. 2000. Kinetic properties of the channels formed by the *Bacillus thuringiensis* insecticidal crystal protein Cry1C in the plasma membrane of Sf9 cells. *Journal of Membrane Biology*, 175, 115-122.
- GUNNING, R. V., DANG, H. T., KEMP, F. C., NICHOLSON, I. C. & MOORES, G. D. 2005. New resistance mechanism in *Helicoverpa armigera* threatens transgenic crops expressing *Bacillus thuringiensis* Cry1Ac toxin. *Applied and Environmental Microbiology*, 71, 2558-2563.
- GUO, S., YE, S., LIU, Y., WEI, L., XUE, J., WU, H., SONG, F., ZHANG, J., WU, X., HUANG, D. & RAO, Z. 2009. Crystal structure of *Bacillus thuringiensis* Cry8Ea1: An insecticidal toxin toxic to underground pests, the larvae of *Holotrichia parallela*. *Journal of Structural Biology*, 168, 259-266.
- GURCEL, L., ABRAMI, L., GIRARDIN, S., TSCHOPP, J. & VAN DER GOOT, F. G. 2006. Caspase-1 Activation of Lipid Metabolic Pathways in Response to Bacterial Pore-Forming Toxins Promotes Cell Survival. *Cell*, 126, 1135-1145.
- HAIDER, M. Z., KNOWLES, B. H. & ELLAR, D. J. 1986. SPECIFICITY OF BACILLUS-THURINGIENSIS VAR COLMERI INSECTICIDAL DELTA-ENDOTOXIN IS DETERMINED BY DIFFERENTIAL PROTEOLYTIC PROCESSING OF THE PROTOXIN BY LARVAL GUT PROTEASES. *European Journal of Biochemistry*, 156, 531-540.
- HAKIM, R. S., BALDWIN, K. & SMAGGHE, G. 2009. Regulation of Midgut Growth, Development, and Metamorphosis. *Annual Review of Entomology*, 55, 593-608.
- HAN, J., JUN, Y., KIM, S. H., HOANG, H. H., JUNG, Y., KIM, S., KIM, J., AUSTIN, R. H., LEE, S. & PARK, S. 2016. Rapid emergence and mechanisms of resistance by U87 glioblastoma cells to doxorubicin in an in vitro tumor microfluidic ecology. *Proceedings of the National Academy of Sciences of the United States of America*, 113, 14283-14288.
- HECKEL, D. G. 2012. Learning the ABCs of Bt: ABC transporters and insect resistance to *Bacillus thuringiensis* provide clues to a crucial step in toxin mode of action. *Pesticide Biochemistry and Physiology*, 104, 103-110.
- HECKEL, D. G., GAHAN, L. J., BAXTER, S. W., ZHAO, J.-Z., SHELTON, A. M., GOULD, F. & TABASHNIK, B. E. 2007. The diversity of Bt resistance genes in species of Lepidoptera. *Journal of Invertebrate Pathology*, 95, 192-197.
- HERNÁNDEZ-MARTÍNEZ, P., NAVARRO-CERRILLO, G., CACCIA, S., DE MAAGD, R. A., MOAR, W. J., FERRÉ, J., ESCRICHE, B. & HERRERO, S. 2010. Constitutive Activation of the Midgut Response to *Bacillus thuringiensis* in Bt-Resistant *Spodoptera exigua*. *Plos One*, 5, e12795.
- HERNÁNDEZ-RODRÍGUEZ, C. S., FERRÉ, J. & HERRERO, S. 2008. Genomic structure and promoter analysis of pathogen-induced repeat genes from *Spodoptera exigua*. *Insect Molecular Biology*, 18, 77-85.

- HERRERO, S., ANSEMS, M., VAN OERS, M. M., VLAK, J. M., BAKKER, P. L. & DE MAAGD, R. A. 2007. REPAT, a new family of proteins induced by bacterial toxins and baculovirus infection in *Spodoptera exigua*. *Insect Biochemistry and Molecular Biology*, 37, 1109-1118.
- HOFMANN, C., LUTHY, P., HUTTER, R. & PLISKA, V. 1988a. BINDING OF THE DELTA ENDOTOXIN FROM *BACILLUS-THURINGIENSIS* TO BRUSH-BORDER MEMBRANE-VESICLES OF THE CABBAGE BUTTERFLY (*PIERIS-BRASSICAE*). *European Journal of Biochemistry*, 173, 85-91.
- HOFMANN, C., VANDERBRUGGEN, H., HOFTE, H., VANRIE, J., JANSSENS, S. & VANMELLAERT, H. 1988b. SPECIFICITY OF *BACILLUS-THURINGIENSIS* SIGMA-ENDOTOXINS IS CORRELATED WITH THE PRESENCE OF HIGH-AFFINITY BINDING-SITES IN THE BRUSH-BORDER MEMBRANE OF TARGET INSECT MIDGUTS. *Proceedings of the National Academy of Sciences of the United States of America*, 85, 7844-7848.
- HÖFTE, H. & WHITELEY, H. R. 1989. Insecticidal crystal proteins of *Bacillus thuringiensis*. *Microbiological Reviews*, 53, 242-255.
- HOSSAIN, D. M., SHITOMI, Y., MORIYAMA, K., HIGUCHI, M., HAYAKAWA, T., MITSUI, T., SATO, R. & HORI, H. 2004. Characterization of a novel plasma membrane protein, expressed in the midgut epithelia of *Bombyx mori*, that binds to Cry1A toxins. *Applied and Environmental Microbiology*, 70, 4604-4612.
- HUA, G., JURAT-FUENTES, J. L. & ADANG, M. J. 2004. Fluorescent-based assays establish *Manduca sexta* Bt-R-1a cadherin as a receptor for multiple *Bacillus thuringiensis* Cry1A toxins in *Drosophila* S2 cells. *Insect Biochemistry and Molecular Biology*, 34, 193-202.
- HUA, G., ZHANG, R., ABDULLAH, M. A. F. & ADANG, M. J. 2008. *Anopheles gambiae* cadherin AgCad1 binds the Cry4Ba toxin of *Bacillus thuringiensis israelensis* and a fragment of AgCad1 synergizes toxicity. *Biochemistry*, 47, 5101-5110.
- HUA, G., ZHANG, R., BAYYAREDDY, K. & ADANG, M. J. 2009. *Anopheles gambiae* Alkaline Phosphatase Is a Functional Receptor of *Bacillus thuringiensis* jegathesan Cry11Ba Toxin. *Biochemistry*, 48, 9785-9793.
- HUANG, R., JIANG, L., DING, Z., JIA, Z., ZHANG, K., LU, Y., HE, R. & ZHANG, W. 2016. Aquaporin 9 related to carcinogenic in hepatocellular carcinoma through regulating glucose metabolism. *International Journal of Clinical and Experimental Pathology*, 9, 4901-4908.
- HUDSON, A. L., WEIR, C., MOON, E., HARVIE, R., KLEBE, S., CLARKE, S. J., PAVLAKIS, N. & HOWELL, V. M. 2014. Establishing a panel of chemo-resistant mesothelioma models for investigating chemo-resistance and identifying new treatments for mesothelioma. *Scientific Reports*, 4.
- HUFFMAN, D. L., ABRAMI, L., SASIK, R., CORBEIL, J., VAN DER GOOT, F. G. & AROIAN, R. V. 2004. Mitogen-activated protein kinase pathways defend against bacterial pore-forming toxins. *Proceedings of the National Academy of Sciences of the United States of America*, 101, 10995.
- HUSMANN, M., DERSCH, K., BOBKIEWICZ, W., BECKMANN, E., VEERACHATO, G. & BHAKDI, S. 2006. Differential role of p38 mitogen activated protein kinase for cellular recovery from attack by pore-forming *S. aureus* α -toxin or streptolysin O. *Biochemical and Biophysical Research Communications*, 344, 1128-1134.
- IBRAHIM, M. A., GRIKO, N., JUNKER, M. & BULLA, L. A. 2010. *Bacillus thuringiensis*: a genomics and proteomics perspective. *Bioengineered bugs*, 1, 31-50.
- IBRAHIM, M. A., GRIKO, N. B. & BULLA, L. A., JR. 2013. Cytotoxicity of the *Bacillus thuringiensis* Cry4B toxin is mediated by the cadherin receptor BT-R-3 of *Anopheles gambiae*. *Experimental Biology and Medicine*, 238, 755-764.
- IDONE, V., TAM, C., GOSS, J. W., TOOMRE, D., PYPAERT, M. & ANDREWS, N. W. 2008. Repair of injured plasma membrane by rapid Ca(2+)-dependent endocytosis. *The Journal of Cell Biology*, 180, 905-914.
- IGARASHI, A. 1978. ISOLATION OF A SINGHS AEDES-ALBOPICTUS CELL CLONE SENSITIVE TO DENGUE AND CHIKUNGUNYA VIRUSES. *Journal of General Virology*, 40, 531-544.

- ITO, A., SASAGURI, Y., KITADA, S., KUSAKA, Y., KUWANO, K., MASUTOMI, K., MIZUKI, E., AKAO, T. & OHBA, M. 2004. A *Bacillus thuringiensis* crystal protein with selective cytotoxic action to human cells. *Journal of Biological Chemistry*, 279, 21282-21286.
- JENSEN, N. F., STENVANG, J., BECK, M. K., HANAKOVA, B., BELLING, K. C., DO, K. N., VIUFF, B., NYGARD, S. B., GUPTA, R., RASMUSSEN, M. H., TARPGAARD, L. S., HANSEN, T. P., BUDINSKA, E., PFEIFFER, P., BOSMAN, F., TEJPAR, S., ROTH, A., DELORENZI, M., ANDERSEN, C. L., ROMER, M. U., BRUNNER, N. & MOREIRA, J. M. A. 2015. Establishment and characterization of models of chemotherapy resistance in colorectal cancer: Towards a predictive signature of chemoresistance. *Molecular Oncology*, 9, 1169-1185.
- JIMENEZ-JUAREZ, N., MUNOZ-GARAY, C., GOMEZ, I., SAAB-RINCON, G., DAMIAN-ALMAZO, J. Y., GILL, S. S., SOBERON, M. & BRAVO, A. 2007. *Bacillus thuringiensis* Cry1Ab mutants affecting oligomer formation are non-toxic to *Manduca sexta* larvae. *Journal of Biological Chemistry*, 282, 21222-21229.
- JIMENEZ-JUAREZ, N., MUNOZ-GARAY, C., GOMEZ, I., SAAB-RINCON, G., DAMIAN-ALMAZO, J. Y., GILL, S. S., SOBERON, M. & BRAVO, A. 2013. *Bacillus thuringiensis* Cry1Ab mutants affecting oligomer formation are non-toxic to *Manduca sexta* larvae (vol 282, pg 21222, 2007). *Journal of Biological Chemistry*, 288, 8560-8560.
- JOHNSON, D. E. 1994. CELLULAR TOXICITIES AND MEMBRANE-BINDING CHARACTERISTICS OF INSECTICIDAL CRYSTAL PROTEINS FROM *BACILLUS-THURINGIENSIS* TOWARD CULTURED INSECT CELLS. *Journal of Invertebrate Pathology*, 63, 123-129.
- JUNG, Y. C., MIZUKI, E., AKAO, T. & COTE, J. C. 2007. Isolation and characterization of a novel *Bacillus thuringiensis* strain expressing a novel crystal protein with cytotoxic activity against human cancer cells. *Journal of Applied Microbiology*, 103, 65-79.
- JURAT-FUENTES, J. L. & ADANG, M. J. 2004. Characterization of a Cry1Ac-receptor alkaline phosphatase in susceptible and resistant *Heliothis virescens* larvae. *European Journal of Biochemistry*, 271, 3127-3135.
- JURAT-FUENTES, J. L. & ADANG, M. J. 2006. Cry toxin mode of action in susceptible and resistant *Heliothis virescens* larvae. *Journal of Invertebrate Pathology*, 92, 166-171.
- JURAT-FUENTES, J. L. & CRICKMORE, N. 2017. Specificity determinants for Cry insecticidal proteins: Insights from their mode of action. *Journal of Invertebrate Pathology*, 142, 5-10.
- KATAYAMA, H., KUSAKA, Y., YOKOTA, H., AKAO, T., KOJIMA, M., NAKAMURA, O., MEKADA, E. & MIZUKI, E. 2007. Parasporin-1, a novel cytotoxic protein from *Bacillus thuringiensis*, induces Ca²⁺ influx and a sustained elevation of the cytoplasmic Ca²⁺ concentration in toxin-sensitive cells. *Journal of Biological Chemistry*, 282, 7742-7752.
- KATAYAMA, H., KUSAKA, Y. & MIZUKI, E. 2011. Parasporin-1 receptor and use thereof *Google Patents*.
- KIROUAC, M., VACHON, V., QUIEVY, D., SCHWARTZ, J. L. & LAPRADE, R. 2006. Protease inhibitors fail to prevent pore formation by the activated *Bacillus thuringiensis* toxin Cry1Aa in insect brush border membrane vesicles. *Applied and Environmental Microbiology*, 72, 506-515.
- KITADA, S., ABE, Y., MAEDA, T. & SHIMADA, H. 2009. Parasporin-2 requires GPI-anchored proteins for the efficient cytotoxic action to human hepatoma cells. *Toxicology*, 264, 80-88.
- KITADA, S., ABE, Y., SHIMADA, H., KUSAKA, Y., MATSUO, Y., KATAYAMA, H., OKUMURA, S., AKAO, T., MIZUKI, E., KUGE, O., SASAGURI, Y., OHBA, M. & ITO, A. 2006. Cytotoxic actions of parasporin-2, an anti-tumor crystal toxin from *Bacillus thuringiensis*. *Journal of Biological Chemistry*, 281, 26350-26360.
- KLETER, G. A., BHULA, R., BODNARUK, K., CARAZO, E., FELSOT, A. S., HARRIS, C. A., KATAYAMA, A., KUIPER, H. A., RACKE, K. D., RUBIN, B., SHEVAH, Y., STEPHENSON, G. R., TANAKA, K., UNSWORTH, J., WAUCHOPE, R. D. & WONG, S.-S. 2007. Altered pesticide use on

- transgenic crops and the associated general impact from an environmental perspective. *Pest Management Science*, 63, 1107-1115.
- KNIGHT, P. J. K., CRICKMORE, N. & ELLAR, D. J. 1994. THE RECEPTOR FOR BACILLUS-THURINGIENSIS CRYLA(C) DELTA-ENDOTOXIN IN THE BRUSH-BORDER MEMBRANE OF THE LEPIDOPTERAN MANDUCA-SEXTA IS AMINOPEPTIDASE-N. *Molecular Microbiology*, 11, 429-436.
- KNOWLES, B. H. & ELLAR, D. J. 1987. COLLOID-OSMOTIC LYSIS IS A GENERAL FEATURE OF THE MECHANISM OF ACTION OF BACILLUS-THURINGIENSIS DELTA-ENDOTOXINS WITH DIFFERENT INSECT SPECIFICITY. *Biochimica Et Biophysica Acta*, 924, 509-518.
- KRISHNAMOORTHY, M., JURAT-FUENTES, J. L., MCNALL, R. J., ANDACHT, T. & ADANG, M. J. 2007. Identification of novel CryIaC binding proteins in midgut membranes from *Heliothis virescens* using proteomic analyses. *Insect Biochemistry and Molecular Biology*, 37, 189-201.
- KRISHNAN, K., KER, J. E. A., MOHAMMED, S. M. & NADARAJAH, V. D. 2010. Identification of Glyceraldehyde-3-phosphate dehydrogenase (GAPDH) as a binding protein for a 68-kDa *Bacillus thuringiensis* parasporal protein cytotoxic against leukaemic cells. *Journal of Biomedical Science*, 17.
- KRISHNAN, V., DOMANSKA, B., ELHIGAZI, A., AFOLABI, F., WEST, M. J. & CRICKMORE, N. 2017. The human cancer cell active toxin Cry41Aa from *Bacillus thuringiensis* acts like its insecticidal counterparts. *Biochemical Journal*, 474, 1591-1602.
- KUKURBA, K. R. & MONTGOMERY, S. B. 2015. RNA Sequencing and Analysis. *Cold Spring Harbor protocols*, 2015, 951-969.
- KUPPEN, P. J. K., SCHUITEMAKER, H., VANTVEER, L. J., VANOOSTEROM, A. T., SCHRIER, P. I. & DEBRUIJN, E. A. 1988. CIS-DIAMMINEDICHLOROPLATINUM(II)-RESISTANT SUBLINES DERIVED FROM 2 HUMAN OVARIAN TUMOR-CELL LINES. *Pharmaceutisch Weekblad-Scientific Edition*, 10, 296-296.
- KWA, M. S. G., DE MAAGD, R. A., STIEKEMA, W. J., VLAK, J. M. & BOSCH, D. 1998. Toxicity and binding properties of the *Bacillus thuringiensis* delta-endotoxin Cry1C to cultured insect cells. *Journal of Invertebrate Pathology*, 71, 121-127.
- LEE, M. K., RAJAMOCHAN, F., JENKINS, J. L., CURTISS, A. S. & DEAN, D. H. 2000. Role of two arginine residues in domain II, loop 2 of Cry1Ab and Cry1Ac *Bacillus thuringiensis* delta-endotoxin in toxicity and binding to *Manduca sexta* and *Lymantria dispar* aminopeptidase N. *Molecular Microbiology*, 38, 289-298.
- LI, J., CARROLL, J. & ELLAR, D. J. 1991. Crystal structure of insecticidal δ -endotoxin from *Bacillus thuringiensis* at 2.5 Å resolution. *Nature*, 353, 815.
- LI, J., KONI, P. A. & ELLAR, D. J. 1996. Structure of the mosquitocidal delta-endotoxin CytB from *Bacillus thuringiensis* sp *kyushuensis* and implications for membrane pore formation. *Journal of Molecular Biology*, 257, 129-152.
- LIANG, Y., PATEL, S. S. & DEAN, D. H. 1995. Irreversible Binding Kinetics of *Bacillus thuringiensis* CryIA δ -Endotoxins to Gypsy Moth Brush Border Membrane Vesicles Is Directly Correlated to Toxicity. *Journal of Biological Chemistry*, 270, 24719-24724.
- LILIEN, J. & BALSAMO, J. 2005. The regulation of cadherin-mediated adhesion by tyrosine phosphorylation/dephosphorylation of beta-catenin. *Current Opinion in Cell Biology*, 17, 459-465.
- LIU, C., XIAO, Y., LI, X., OPPERT, B., TABASHNIK, B. E. & WU, K. 2014. Cis-mediated down-regulation of a trypsin gene associated with Bt resistance in cotton bollworm. *Scientific Reports*, 4, 7219.
- LIU, K. Y., ZHENG, B. L., HONG, H. Z., JIANG, C. F., PENG, R., PENG, J. X., YU, Z. H., ZHENG, J. & YANG, H. 2004. Characterization of cultured insect cells selected by *Bacillus thuringiensis* crystal toxin. *In Vitro Cellular & Developmental Biology-Animal*, 40, 312-317.

- LIU, Y., WANG, Y., SHU, C., LIN, K., SONG, F., BRAVO, A., SOBERON, M. & ZHANG, J. 2018. Cry64Ba and Cry64Ca, Two ETX/MTX2-Type *Bacillus thuringiensis* Insecticidal Proteins Active against Hemipteran Pests. *Applied and Environmental Microbiology*, 84.
- LIU, Y. B., TABASHNIK, B. E., MEYER, S. K. & CRICKMORE, N. 2001. Cross-resistance and stability of resistance to *Bacillus thuringiensis* toxin Cry1C in diamondback moth. *Applied and Environmental Microbiology*, 67, 3216-3219.
- LOEB, M. J., HAKIM, R. S., MARTIN, P., NARANG, N., GOTO, S. & TAKEDA, M. 2000. Apoptosis in cultured midgut cells from *Heliothis virescens* larvae exposed to various conditions. *Archives of Insect Biochemistry and Physiology*, 45, 12-23.
- LOITTO, V. M., HUANG, C., SIGAL, Y. J. & JACOBSON, K. 2007. Filopodia are induced by aquaporin-9 expression. *Experimental Cell Research*, 313, 1295-1306.
- LOS, F. C. O., RANDIS, T. M., AROIAN, R. V. & RATNER, A. J. 2013. Role of Pore-Forming Toxins in Bacterial Infectious Diseases. *Microbiology and Molecular Biology Reviews : MMBR*, 77, 173-207.
- LU, Z. & XU, S. 2006. ERK1/2 MAP kinases in cell survival and apoptosis. *Life*, 58, 621-631.
- LUO, K., BANKS, D. & ADANG, M. J. 1999. Toxicity, binding, and permeability analyses of four *Bacillus thuringiensis* Cry1 delta-endotoxins using brush border membrane vesicles of *Spodoptera exigua* and *Spodoptera frugiperda*. *Applied and Environmental Microbiology*, 65, 457-464.
- LUO, K., SANGADALA, S., MASSON, L., MAZZA, A., BROUSSEAU, R. & ADANG, M. J. 1997. The *Heliothis virescens* 170kDa aminopeptidase functions as "receptor A" by mediating specific *Bacillus thuringiensis* Cry1A delta-endotoxin binding and pore formation. *Insect Biochemistry and Molecular Biology*, 27, 735-743.
- LUQMANI, Y. A. 2005. Mechanisms of Drug Resistance in Cancer Chemotherapy. *Medical Principles and Practice*, 14(suppl 1), 35-48.
- MA, G., ROBERTS, H., SARJAN, M., FEATHERSTONE, N., LAHNSTEIN, J., AKHURST, R. & SCHMIDT, O. 2005a. Is the mature endotoxin Cry1Ac from *Bacillus thuringiensis* inactivated by a coagulation reaction in the gut lumen of resistant *Helicoverpa armigera* larvae? *Insect Biochemistry and Molecular Biology*, 35, 729-739.
- MA, G., ROBERTS, H., SARJAN, M., FEATHERSTONE, N., LAHNSTEIN, J., AKHURST, R. & SCHMIDT, O. 2005b. Is the mature endotoxin Cry1Ac from *Bacillus thuringiensis* inactivated by a coagulation reaction in the gut lumen of resistant, *Helicoverpa armigera* larvae? *Insect Biochemistry and Molecular Biology*, 35, 729-739.
- MAIER, T., GÜELL, M. & SERRANO, L. 2009. Correlation of mRNA and protein in complex biological samples. *FEBS Letters*, 583, 3966-3973.
- MANDAL, C. C., GAYEN, S., BASU, A., GHOSH, K. S., DASGUPTA, S., MAITI, M. K. & SEN, S. K. 2007. Prediction-based protein engineering of domain I of Cry2A entomocidal toxin of *Bacillus thuringiensis* for the enhancement of toxicity against lepidopteran insects. *Protein Engineering Design & Selection*, 20, 599-606.
- MARTENS, J. W. M., KNOESTER, M., WEIJTS, F., GROFFEN, S. J. A., HU, Z. H., BOSCH, D. & VLAK, J. M. 1995. CHARACTERIZATION OF BACULOVIRUS INSECTICIDES EXPRESSING TAILORED BACILLUS-THURINGIENSIS CRYIA(B) CRYSTAL PROTEINS. *Journal of Invertebrate Pathology*, 66, 249-257.
- MASOTTI, A. & PRECKEL, T. 2006. Analysis of small RNAs with the Agilent 2100 Bioanalyzer. *Nature Methods*, 3.
- MASSON, L., LUN, Y. J., MAZZA, A., BROUSSEAU, R. & ADANG, M. J. 1995a. THE CRYIA(C) RECEPTOR PURIFIED FROM MANDUCA-SEXTA DISPLAYS MULTIPLE SPECIFICITIES. *Journal of Biological Chemistry*, 270, 20309-20315.
- MASSON, L., MAZZA, A., BROUSSEAU, R. & TABASHNIK, B. 1995b. KINETICS OF BACILLUS-THURINGIENSIS TOXIN BINDING WITH BRUSH-BORDER MEMBRANE-VESELLES FROM SUSCEPTIBLE AND RESISTANT LARVAE OF PLUTELLA-XYLOSTELLA. *Journal of Biological Chemistry*, 270, 11887-11896.

- MCCLANE, B. A. & CHAKRABARTI, G. 2004. New insights into the cytotoxic mechanisms of *Clostridium perfringens* enterotoxin. *Anaerobe*, 10, 107-114.
- MCNALL, R. J. & ADANG, M. J. 2003. Identification of novel *Bacillus thuringiensis* Cry1Ac binding proteins in *Manduca sexta* midgut through proteomic analysis. *Insect Biochemistry and Molecular Biology*, 33, 999-1010.
- MIRANDA, R., ZAMUDIO, F. Z. & BRAVO, A. 2001. Processing of Cry1Ab delta-endotoxin from *Bacillus thuringiensis* by *Manduca sexta* and *Spodoptera frugiperda* midgut proteases: role in protoxin activation and toxin inactivation. *Insect Biochemistry and Molecular Biology*, 31, 1155-1163.
- MIZUKI, E., OHBA, M., AKAO, T., YAMASHITA, S., SAITOH, H. & PARK, Y. S. 1999. Unique activity associated with non-insecticidal *Bacillus thuringiensis* parasporal inclusions: in vitro cell-killing action on human cancer cells. *Journal of Applied Microbiology*, 86, 477-486.
- MIZUKI, E., PARK, Y. S., SAITOH, H., YAMASHITA, S., AKAO, T., HIGUCHI, K. & OHBA, M. 2000. Parasporin, a human leukemic cell-recognizing parasporal protein of *Bacillus thuringiensis*. *Clinical and Diagnostic Laboratory Immunology*, 7, 625-634.
- MONIAGA, C. S., WATANABE, S., HONDA, T., NIELSEN, S. & HARA-CHIKUMA, M. 2015. Aquaporin-9-expressing neutrophils are required for the establishment of contact hypersensitivity. *Scientific Reports*, 5.
- MORSE, R. J., YAMAMOTO, T. & STROUD, R. M. 2001. Structure of Cry2Aa Suggests an Unexpected Receptor Binding Epitope. *Structure*, 9, 409-417.
- MURRAY, A. J. 2008. Pharmacological PKA Inhibition: All May Not Be What It Seems. *Science Signaling*, 1, re4-re4.
- NAGAMATSU, Y., OKAMURA, S., SAITOU, H., AKAO, T. & MIZUKI, E. 2010. Three Cry Toxins in Two Types from *Bacillus thuringiensis* Strain M019 Preferentially Kill Human Hepatocyte Cancer and Uterus Cervix Cancer Cells. *Bioscience Biotechnology and Biochemistry*, 74, 494-498.
- NAIMOV, S., VALKOVA, R., DUKIANDJIEV, S., MINKOV, I. & DE MAAGD, R. A. 2011. Carboxy-terminal extension effects on crystal formation and insecticidal properties of Cry15Aa. *Journal of Invertebrate Pathology*, 108, 56-58.
- NELSON, K. L., BRODSKY, R. A. & BUCKLEY, J. T. 1999. Channels formed by subnanomolar concentrations of the toxin aerolysin trigger apoptosis of T lymphomas. *Cellular Microbiology*, 1, 69-74.
- OCELOTL, J., SANCHEZ, J., ARROYO, R., GARCIA-GOMEZ, B. I., GOMEZ, I., UNNITHAN, G. C., TABASHNIK, B. E., BRAVO, A. & SOBERON, M. 2015. Binding and Oligomerization of Modified and Native Bt Toxins in Resistant and Susceptible Pink Bollworm. *Plos One*, 10.
- ODII, B. O. & COUSSONS, P. 2012. Pharmacological Isolation of Experimental Models of Drug-resistant Hepatocellular Carcinoma Cell Line. *Journal of Cancer Therapy*, Vol.03No.04, 6.
- OHBA, M. & AIZAWA, K. 1986. INSECT TOXICITY OF BACILLUS-THURINGIENSIS ISOLATED FROM SOILS OF JAPAN. *Journal of Invertebrate Pathology*, 47, 12-20.
- OHBA, M., MIZUKI, E. & UEMORI, A. 2008. PARASPORIN, A NEW ANTICANCER PROTEIN GROUP FROM BACILLUS THURINGIENSIS. *Anticancer Research*, 28, 3426-3426.
- OHBA, M., MIZUKI, E. & UEMORI, A. 2009. Parasporin, a New Anticancer Protein Group from *Bacillus thuringiensis*. *Anticancer Research*, 29, 427-433.
- OKAMURA, M., SHIMADA, J. & SAKAGAMI, H. 2008. Comparative analysis of cell death induction by cisplatin and 5-FU in human oral squamous and hepatocellular carcinoma cell lines. *Anticancer Research*, 28, 253-259.
- OKASSOV, A., NERSESYAN, A., KITADA, S. & ILIN, A. 2015. Parasporins as new natural anticancer agents: a review. *Journal of Buon*, 20, 5-16.
- OKUMURA, S., SAITOH, H., ISHIKAWA, T., INOUE, K. & MIZUKI, E. 2011. Mode of action of parasporin-4, a cytotoxic protein from *Bacillus thuringiensis*. *Biochimica Et Biophysica Acta-Biomembranes*, 1808, 1476-1482.

- OKUMURA, S., SAITOH, H., ISHIKAWA, T., WASANO, N., YAMASHITA, S., KUSUMOTO, K., AKAO, T., MIZUKI, E., OHBA, M. & INOUE, K. 2005. Identification of a novel cytotoxic protein, Cry45Aa, from *Bacillus thuringiensis* A1470 and its selective cytotoxic activity against various mammalian cell lines. *Journal of Agricultural and Food Chemistry*, 53, 6313-6318.
- OPPERT, B. 1999. Protease interactions with *Bacillus thuringiensis* insecticidal toxins. *Archives of Insect Biochemistry and Physiology*, 42, 1-12.
- OPPERT, B., KRAMER, K. J., BEEMAN, R. W., JOHNSON, D. & MCGAUGHEY, W. H. 1997. Proteinase-mediated insect resistance to *Bacillus thuringiensis* toxins. *Journal of Biological Chemistry*, 272, 23473-23476.
- PACHECO, S., GOMEZ, I., ARENAS, I., SAAB-RINCON, G., RODRIGUEZ-ALMAZAN, C., GILL, S. S., BRAVO, A. & SOBERON, M. 2009. Domain II Loop 3 of *Bacillus thuringiensis* Cry1Ab Toxin Is Involved in a "Ping Pong" Binding Mechanism with *Manduca sexta* Aminopeptidase-N and Cadherin Receptors. *Journal of Biological Chemistry*, 284, 32750-32757.
- PADILLA, C., PARDO-LOPEZ, L., DE LA RIVA, G., GOMEZ, I., SANCHEZ, J., HERNANDEZ, G., NUNEZ, M. E., CAREY, M. P., DEAN, D. H., ALZATE, O., SOBERON, M. & BRAVO, A. 2006. Role of tryptophan residues in toxicity of Cry1Ab toxin from *Bacillus thuringiensis*. *Applied and Environmental Microbiology*, 72, 901-907.
- PALMA, L., MUNOZ, D., BERRY, C., MURILLO, J. & CABALLERO, P. 2014. *Bacillus thuringiensis* Toxins: An Overview of Their Biocidal Activity. *Toxins*, 6, 3296-3325.
- PANG, Y., FRUTOS, R. & FEDERICI, B. A. 1992. SYNTHESIS AND TOXICITY OF FULL-LENGTH AND TRUNCATED BACTERIAL CRYIVD MOSQUITOCIDAL PROTEINS EXPRESSED IN LEPIDOPTERAN CELLS USING A BACULOVIRUS VECTOR. *Journal of General Virology*, 73, 89-101.
- PARDO-LOPEZ, L., SOBERON, M. & BRAVO, A. 2013. *Bacillus thuringiensis* insecticidal three-domain Cry toxins: mode of action, insect resistance and consequences for crop protection. *Fems Microbiology Reviews*, 37, 3-22.
- PARKER, M. W. & FEIL, S. C. 2005. Pore-forming protein toxins: from structure to function. *Progress in Biophysics & Molecular Biology*, 88, 91-142.
- PETERSON, B., BEZUIDENHOUT, C. C. & VAN DEN BERG, J. 2017. An Overview of Mechanisms of Cry Toxin Resistance in Lepidopteran Insects. *Journal of Economic Entomology*, 110, 362-377.
- PETITPREZ, A., POINDESSOUS, V., OUARET, D., REGAIRAZ, M., BASTIAN, G., GUERIN, E., ESCARGUEIL, A. E. & LARSEN, A. K. 2013. Acquired irinotecan resistance is accompanied by stable modifications of cell cycle dynamics independent of MSI status. *International Journal of Oncology*, 42, 1644-1653.
- PIGOTT, C. R. & ELLAR, D. J. 2007. Role of receptors in *Bacillus thuringiensis* crystal toxin activity. *Microbiology and Molecular Biology Reviews*, 71, 255-+.
- PORTA, H., CANCINO-RODEZNO, A., SOBERON, M. & BRAVO, A. 2011. Role of MAPK p38 in the cellular responses to pore-forming toxins. *Peptides*, 32, 601-606.
- PORTUGAL, L., GRINGORTEN, J. L., CAPUTO, G. F., SOBERON, M., MUNOZ-GARAY, C. & BRAVO, A. 2014. Toxicity and mode of action of insecticidal Cry1A proteins from *Bacillus thuringiensis* in an insect cell line, CF-1. *Peptides*, 53, 292-299.
- PORTUGAL, L., MUÑOZ-GARAY, C., MARTÍNEZ DE CASTRO, D. L., SOBERÓN, M. & BRAVO, A. 2017. Toxicity of Cry1A toxins from *Bacillus thuringiensis* to CF1 cells does not involve activation of adenylate cyclase/PKA signaling pathway. *Insect Biochemistry and Molecular Biology*, 80, 21-31.
- POTVIN, L., LAPRADE, R. & SCHWARTZ, J. L. 1998. Cry1Ac, a *Bacillus thuringiensis* toxin, triggers extracellular Ca²⁺ influx and Ca²⁺ release from intracellular stores in Cf1 cells (*Choristoneura fumiferana*, Lepidoptera). *Journal of Experimental Biology*, 201, 1851-1858.

- PROMDONKOY, B. & ELLAR, D. J. 2003. Investigation of the pore-forming mechanism of a cytolytic delta-endotoxin from *Bacillus thuringiensis*. *Biochemical Journal*, 374, 255-259.
- QIU, L., HOU, L., ZHANG, B., LIU, L., LI, B., DENG, P., MA, W., WANG, X., FABRICK, J. A., CHEN, L. & LEI, C. 2015. Cadherin is involved in the action of *Bacillus thuringiensis* toxins Cry1Ac and Cry2Aa in the beet armyworm, *Spodoptera exigua*. *Journal of Invertebrate Pathology*, 127, 47-53.
- RAHMAN, M. M., ROBERTS, H. L. S., SARJAN, M., ASGARI, S. & SCHMIDT, O. 2004. Induction and transmission of *Bacillus thuringiensis* tolerance in the flour moth *Ephestia kuehniella*. *Proceedings of the National Academy of Sciences of the United States of America*, 101, 2696-2699.
- RAHMAN, M. M., ROBERTS, H. L. S. & SCHMIDT, O. 2007. Tolerance to *Bacillus thuringiensis* endotoxin in immune-suppressed larvae of the flour moth *Ephestia kuehniella*. *Journal of Invertebrate Pathology*, 96, 125-132.
- RAJAGOPAL, R., SIVAKUMAR, S., AGRAWAL, N., MALHOTRA, P. & BHATNAGAR, R. K. 2002a. Silencing of midgut aminopeptidase N of *Spodoptera litura* by double-stranded RNA establishes its role as *Bacillus thuringiensis* toxin receptor. *Journal of Biological Chemistry*, 277, 46849-46851.
- RAJAGOPAL, R., SIVAKUMAR, S., AGRAWAL, N., MALHOTRA, P. & BHATNAGAR, R. K. 2002b. Silencing of Midgut Aminopeptidase N of *Spodoptera litura* by Double-stranded RNA Establishes Its Role as *Bacillus thuringiensis* Toxin Receptor. *Journal of Biological Chemistry*, 277, 46849-46851.
- RATNER, A. J., HIPPE, K. R., AGUILAR, J. L., BENDER, M. H., NELSON, A. L. & WEISER, J. N. 2006a. EPITHELIAL CELLS ARE SENSITIVE DETECTORS OF BACTERIAL PORE-FORMING TOXINS. *The Journal of Biological Chemistry*, 281, 12994-12998.
- RATNER, A. J., HIPPE, K. R., AGUILAR, J. L., BENDER, M. H., NELSON, A. L. & WEISER, J. N. 2006b. Epithelial cells are sensitive detectors of bacterial pore-forming toxins. *Journal of Biological Chemistry*, 281, 12994-12998.
- RAUSELL, C., GARCIA-ROBLES, I., SANCHEZ, J., MUNOZ-GARAY, C., MARTINEZ-RAMIREZ, A. C., REAL, M. D. & BRAVO, A. 2004a. Role of toxin activation on binding and pore formation activity of the *Bacillus thuringiensis* Cry3 toxins in membranes of *Leptinotarsa decemlineata* (Say). *Biochimica Et Biophysica Acta-Biomembranes*, 1660, 99-105.
- RAUSELL, C., MUNOZ-GARAY, C., MIRANDA-CASSOLUENGO, R., GOMEZ, I., RUDINO-PINERA, E., SOBERON, M. & BRAVO, A. 2004b. Tryptophan spectroscopy studies and black lipid bilayer analysis indicate that the oligomeric structure of Cry1Ab toxin from *Bacillus thuringiensis* is the membrane-insertion intermediate. *Biochemistry*, 43, 166-174.
- RODRIGUEZ-ALMAZAN, C., RUIZ DE ESCUDERO, I., EMILIANO CANTÓN, P., MUÑOZ-GARAY, C., PÉREZ, C., GILL, S. S., SOBERÓN, M. & BRAVO, A. 2011. The amino- and carboxyl-terminal fragments of the *Bacillus thuringiensis* Cyt1Aa toxin have differential roles on toxin oligomerization and pore formation. *Biochemistry*, 50, 388-396.
- ROSENBERG, D., GROUSSIN, L., JULLIAN, E., PERLEMOINE, K., BERTAGNA, X. & BERTHERAT, J. 2002. Role of the PKA-regulated transcription factor CREB in development and tumorigenesis of endocrine tissues. In: STRATAKIS, C. A. & CHOCHUNG, Y. S. (eds.) *Protein Kinase a and Human Disease*.
- RUBIO-INFANTE, N., ILHUICATZI-ALVARADO, D., TORRES-MARTINEZ, M., PABLO REYES-GRAJEDA, J., NAVA-ACOSTA, R., GONZALEZ-GONZALEZ, E. & MORENO-FIERROS, L. 2018. The Macrophage Activation Induced by *Bacillus thuringiensis* Cry1Ac Protoxin Involves ERK1/2 and p38 Pathways and the Interaction with Cell-Surface-HSP70. *Journal of Cellular Biochemistry*, 119, 580-598.
- SAKAI, H., HOWLADER, M. T. H., ISHIDA, Y., NAKAGUCHI, A., OKA, K., OHBAYASHI, K., YAMAGIWA, M. & HAYAKAWA, T. 2007. Flexibility and strictness in functional replacement of domain III of cry insecticidal proteins from *Bacillus thuringiensis*. *Journal of Bioscience and Bioengineering*, 103, 381-383.

- SANAHUJA, G., BANAKAR, R., TWYMAN, R. M., CAPELL, T. & CHRISTOU, P. 2011. *Bacillus thuringiensis*: a century of research, development and commercial applications. *Plant Biotechnology Journal*, 9, 283-300.
- SANZ, Y. 2007. Aminopeptidases. In: POLAINA, J. & MACCABE, A. P. (eds.) *Industrial Enzymes: Structure, Function and Applications*. Dordrecht: Springer Netherlands.
- SAYYED, A. H., GATSI, R., KOUSKOURA, T., WRIGHT, D. J. & CRICKMORE, N. 2001. Susceptibility of a Field-Derived, *Bacillus thuringiensis*-Resistant Strain of Diamondback Moth to In Vitro-Activated Cry1Ac Toxin. *Applied and Environmental Microbiology*, 67, 4372-4373.
- SAYYED ALI, H. & WRIGHT DENIS, J. 2001. Cross-resistance and inheritance of resistance to *Bacillus thuringiensis* toxin Cry1Ac in diamondback moth (*Plutella xylostella* L) from lowland Malaysia. *Pest Management Science*, 57, 413-421.
- SCHNEPF, E., CRICKMORE, N., VAN RIE, J., LERECLUS, D., BAUM, J., FEITELSON, J., ZEIGLER, D. R. & DEAN, D. H. 1998. *Bacillus thuringiensis* and its pesticidal crystal proteins. *Microbiology and Molecular Biology Reviews*, 62, 775-+.
- SCHNEPF, H. E. & WHITELEY, H. R. 1985. DELINEATION OF A TOXIN-ENCODING SEGMENT OF A BACILLUS-THURINGIENSIS CRYSTAL PROTEIN GENE. *Journal of Biological Chemistry*, 260, 6273-6280.
- SHOMA, S., TSUCHIYA, K., KAWAMURA, I., NOMURA, T., HARA, H., UCHIYAMA, R., DAIM, S. & MITSUYAMA, M. 2008. Critical Involvement of Pneumolysin in Production of Interleukin-1 α and Caspase-1-Dependent Cytokines in Infection with *Streptococcus pneumoniae* In Vitro: a Novel Function of Pneumolysin in Caspase-1 Activation. *Infection and Immunity*, 76, 1547-1557.
- SIMPSON, R. M. & NEWCOMB, R. D. 2000. Binding of *Bacillus thuringiensis* delta-endotoxins Cry1Ac and Cry1Ba to a 120-kDa aminopeptidase-N of *Epiphyas postvittana* purified from both brush border membrane vesicles and baculovirus-infected Sf9 cells. *Insect Biochemistry and Molecular Biology*, 30, 1069-1078.
- SIVAKUMAR, S., RAJAGOPAL, R., VENKATESH, G. R., SRIVASTAVA, A. & BHATNAGAR, R. K. 2007. Knockdown of Aminopeptidase-N from *Helicoverpa armigera* Larvae and in Transfected Sf21 Cells by RNA Interference Reveals Its Functional Interaction with *Bacillus thuringiensis* Insecticidal Protein Cry1Ac. *Journal of Biological Chemistry*, 282, 7312-7319.
- SKALHEGG, B. S. & TASKEN, K. 1997. Specificity in the cAMP/PKA signaling pathway: Differential expression, regulation, and subcellular localization of subunits of PKA. *Frontiers in Bioscience (online)*, 2, D331-342.
- SMAGGHE, G. 2007. Insect Cell Lines as Tools in Insecticide Mode of Action Research. In: ISHAAYA, I., HOROWITZ, A. R. & NAUEN, R. (eds.) *Insecticides Design Using Advanced Technologies*. Berlin, Heidelberg: Springer Berlin Heidelberg.
- SMOUSE, D. & NISHIURA, J. 1997. A *Bacillus thuringiensis* delta-endotoxin induces programmed cell death in mosquito larvae. *Cell Death and Differentiation*, 4, 560-569.
- SOBERON, M., GILL, S. S. & BRAVO, A. 2009. Signaling versus punching hole: How do *Bacillus thuringiensis* toxins kill insect midgut cells? *Cellular and Molecular Life Sciences*, 66, 1337-1349.
- SOBERON, M., LOPEZ-DIAZ, J. A. & BRAVO, A. 2013. Cyt toxins produced by *Bacillus thuringiensis*: A protein fold conserved in several pathogenic microorganisms. *Peptides*, 41, 87-93.
- SOBERON, M., PARDO-LOPEZ, L., LOPEZ, I., GOMEZ, I., TABASHNIK, B. E. & BRAVO, A. 2007. Engineering modified Bt toxins to counter insect resistance. *Science*, 318, 1640-1642.
- SOBERÓN, M., PORTUGAL, L., GARCIA-GÓMEZ, B.-I., SÁNCHEZ, J., ONOFRE, J., GÓMEZ, I., PACHECO, S. & BRAVO, A. 2018. Cell lines as models for the study of Cry toxins from *Bacillus thuringiensis*. *Insect Biochemistry and Molecular Biology*, 93, 66-78.
- SPEICHER, K. D., GORMAN, N. & SPEICHER, D. W. 2009. N-terminal sequence analysis of proteins and peptides. *Current protocols in protein science*, Chapter 11, Unit11.10-Unit11.10.

- SUMMERS, M. D. & SMITH, G. E. 1987. A MANUAL OF METHODS FOR BACULOVIRUS VECTORS AND INSECT CELL-CULTURE PROCEDURES. *Texas Agricultural Experiment Station Bulletin*, 1-56.
- TABASHNIK, B. E. 2001. Breaking the code of resistance. *Nature Biotechnology*, 19, 922-924.
- TABASHNIK, B. E., FINSON, N., GROETERS, F. R., MOAR, W. J., JOHNSON, M. W., LUO, K. & ADANG, M. J. 1994. REVERSAL OF RESISTANCE TO BACILLUS-THURINGIENSIS IN PLUTELLA-XYLOSTELLA. *Proceedings of the National Academy of Sciences of the United States of America*, 91, 4120-4124.
- TABASHNIK, B. E., UNNITHAN, G. C., MASSON, L., CROWDER, D. W., LI, X. & CARRIERE, Y. 2009. Asymmetrical cross-resistance between *Bacillus thuringiensis* toxins Cry1Ac and Cry2Ab in pink bollworm. *Proceedings of the National Academy of Sciences of the United States of America*, 106, 11889-11894.
- TASKÉN, K. & AANDAHL, E. M. 2004. Localized Effects of cAMP Mediated by Distinct Routes of Protein Kinase A. *Physiological Reviews*, 84, 137-167.
- TAY, W. T., MAHON, R. J., HECKEL, D. G., WALSH, T. K., DOWNES, S., JAMES, W. J., LEE, S.-F., REINEKE, A., WILLIAMS, A. K. & GORDON, K. H. J. 2015. Insect Resistance to *Bacillus thuringiensis* Toxin Cry2Ab Is Conferred by Mutations in an ABC Transporter Subfamily A Protein. *Plos Genetics*, 11.
- TEIXEIRA CORREA, R. F., ARDISSON-ARAUJO, D. M. P., MONNERAT, R. G. & RIBEIRO, B. M. 2012. Cytotoxicity analysis of three *Bacillus thuringiensis* subsp. israelensis delta-endotoxins towards insect and mammalian cells. *Plos One*, 7, e46121-e46121.
- THEODOULOU, FREDERICA L. & KERR, IAN D. 2015. ABC transporter research: going strong 40 years on. *Biochemical Society Transactions*, 43, 1033-1040.
- THOMAS, W. E. & ELLAR, D. J. 1983a. BACILLUS-THURINGIENSIS-VAR-ISRAELENIS CRYSTAL DELTA-ENDOTOXIN - EFFECTS ON INSECT AND MAMMALIAN-CELLS INVITRO AND INVIVO. *Journal of Cell Science*, 60, 181-197.
- THOMAS, W. E. & ELLAR, D. J. 1983b. MECHANISM OF ACTION OF BACILLUS-THURINGIENSIS-VAR-ISRAELENIS INSECTICIDAL DELTA-ENDOTOXIN. *Febs Letters*, 154, 362-368.
- TIEWSIRI, K. & WANG, P. 2011. Differential alteration of two aminopeptidases N associated with resistance to *Bacillus thuringiensis* toxin Cry1Ac in cabbage looper. *Proceedings of the National Academy of Sciences of the United States of America*, 108, 14037-14042.
- TORRES-AVILA, M., LEAL-GALICIA, P., SANCHEZ-PENA, L. C., DEL RAZO, L. M. & GONSEBATT, M. E. 2010. Arsenite induces aquaglyceroporin 9 expression in murine livers. *Environmental Research*, 110, 443-447.
- TRUMP, B. F. & BEREZESKY, I. K. 1994. Cellular and molecular pathobiology of reversible and irreversible injury. In: TYSON, C. A. & FRAZIER, J. M. (eds.) *Methods in Toxicology; In-vitro toxicity indicators*.
- TSUZUKI, K., KIMURA, K., FUJII, N., YOKOSAWA, N., INDOH, T., MURAKAMI, T. & OGUMA, K. 1990. Cloning and complete nucleotide sequence of the gene for the main component of hemagglutinin produced by *Clostridium botulinum* type C. *Infect. Immun.*, 58, 3173-3177.
- TWENTYMAN, P. R., FOX, N. E., WRIGHT, K. A. & BLEEHEN, N. M. 1986. DERIVATION AND PRELIMINARY CHARACTERIZATION OF ADRIAMYCIN RESISTANT LINES OF HUMAN-LUNG CANCER-CELLS. *British Journal of Cancer*, 53, 529-537.
- VACHON, V., PARADIS, M. J., MARSOLAIS, M., SCHWARTZ, J. L. & LAPRADE, R. 1995. IONIC PERMEABILITIES INDUCED BY BACILLUS-THURINGIENSIS IN SF9 CELLS. *Journal of Membrane Biology*, 148, 57-63.
- VALAITIS, A. P., JENKINS, J. L., LEE, M. K., DEAN, D. H. & GARNER, K. J. 2001. Isolation and partial characterization of gypsy moth BTR-270, an anionic brush border membrane glycoconjugate that binds *Bacillus thuringiensis* Cry1A toxins with high affinity. *Archives of Insect Biochemistry and Physiology*, 46, 186-200.

- VAN RIE, J., MCGAUGHEY, W. H., JOHNSON, D. E., BARNETT, B. D. & VAN MELLAERT, H. 1990. MECHANISM OF INSECT RESISTANCE TO THE MICROBIAL INSECTICIDE BACILLUS-THURINGIENSIS. *Science (Washington D C)*, 247, 72-74.
- VAUGHN, J. L., GOODWIN, R. H., TOMPKINS, G. J. & MCCAWLEY, P. 1977. ESTABLISHMENT OF 2 CELL LINES FROM INSECT SPODOPTERA-FRUGIPERDA (LEPIDOPTERA-NOCTUIDAE). *In Vitro-Journal of the Tissue Culture Association*, 13, 213-217.
- WALTERS, F. S., STACY, C. M., LEE, M. K., PALEKAR, N. & CHEN, J. S. 2008a. An Engineered Chymotrypsin/Cathepsin G Site in Domain I Renders Bacillus thuringiensis Cry3A Active against Western Corn Rootworm Larvae. *Applied and Environmental Microbiology*, 74, 367-374.
- WALTERS, F. S., STACY, C. M., LEE, M. K., PALEKAR, N. & CHEN, J. S. 2008b. An engineered chymotrypsin/cathepsin site in domain I renders Bacillus thuringiensis Cry3A active against western corn rootworm larvae. *Applied and Environmental Microbiology*, 74, 367-374.
- WANG, P., ZHANG, X. & ZHANG, J. 2005. Molecular characterization of four midgut aminopeptidase N isozymes from the cabbage looper, *Trichoplusia ni*. *Insect Biochemistry and Molecular Biology*, 35, 611-620.
- WANG, P., ZHAO, J. Z., RODRIGO-SIMON, A., KAIN, W., JANMAAT, A. F., SHELTON, A. M., FERRE, J. & MYERS, J. 2007. Mechanism of resistance to Bacillus thuringiensis toxin Cry1Ac in a greenhouse population of the cabbage looper, *Trichoplusia ni*. *Applied and Environmental Microbiology*, 73, 1199-1207.
- WANG, Y., WANG, Y., WANG, Z., BRAVO, A., SOBERON, M. & HE, K. 2016. Genetic Basis of Cry1F-Resistance in a Laboratory Selected Asian Corn Borer Strain and Its Cross-Resistance to Other Bacillus thuringiensis Toxins. *Plos One*, 11.
- WEI, J., GUO, Y., LIANG, G., WU, K., ZHANG, J., TABASHNIK, B. E. & LI, X. 2015. Cross-resistance and interactions between Bt toxins Cry1Ac and Cry2Ab against the cotton bollworm. *Scientific Reports*, 5.
- WEI, J., ZHANG, M., LIANG, G., WU, K., GUO, Y., NI, X. & LI, X. 2016. APN1 is a functional receptor of Cry1Ac but not Cry2Ab in *Helicoverpa zea*. *Scientific Reports*, 6, 19179.
- WICKHAM, T. J., DAVIS, T., GRANADOS, R. R., SHULER, M. L. & WOOD, H. A. 1992. SCREENING OF INSECT CELL-LINES FOR THE PRODUCTION OF RECOMBINANT PROTEINS AND INFECTIOUS VIRUS IN THE BACULOVIRUS EXPRESSION SYSTEM. *Biotechnology Progress*, 8, 391-396.
- WOLFERSBERGER, M. G. 1990. The toxicity of two Bacillus thuringiensis delta-endotoxins to gypsy moth larvae is inversely related to the affinity of binding sites on midgut brush border membranes for the toxins. *Experientia*, 46, 475-7.
- WU, J., SU, G., MA, L., ZHANG, X., LEI, Y., LI, J., LIN, Q. & FANG, L. 2005. Protein kinases mediate increment of the phosphorylation of cyclic AMP-responsive element binding protein in spinal cord of rats following capsaicin injection. *Molecular Pain*, 1.
- WU, Y. D. 2014. Detection and Mechanisms of Resistance Evolved in Insects to Cry Toxins from Bacillus thuringiensis. In: DHADIALLA, T. S. & GILL, S. S. (eds.) *Insect Midgut and Insecticidal Proteins*.
- XIAO, Y., LIU, K., ZHANG, D., GONG, L., HE, F., SOBERON, M., BRAVO, A., TABASHNIK, B. E. & WU, K. 2016. Resistance to Bacillus thuringiensis Mediated by an ABC Transporter Mutation Increases Susceptibility to Toxins from Other Bacteria in an Invasive Insect. *Plos Pathogens*, 12.
- XIE, B. S., ZHAO, H. C., YAO, S. K., ZHUO, D. X., JIN, B., LV, D. C., WU, C. L., MA, D. L., GAO, C., SHU, X. M. & AI, Z. L. 2011. Autophagy inhibition enhances etoposide-induced cell death in human hepatoma G2 cells. *International Journal of Molecular Medicine*, 27, 599-606.
- XU, C., CHINTE, U., CHEN, L., YAO, Q., MENG, Y., ZHOU, D., BI, L.-J., ROSE, J., ADANG, M. J., WANG, B.-C., YU, Z. & SUN, M. 2015a. Crystal structure of Cry51Aa1: A potential novel

- insecticidal aerolysin-type β -pore-forming toxin from *Bacillus thuringiensis*. *Biochemical and Biophysical Research Communications*, 462, 184-189.
- XU, L.-N., WANG, Y.-Q., WANG, Z.-Y., HU, B.-J., LING, Y.-H. & HE, K.-L. 2015b. Transcriptome differences between Cry1Ab resistant and susceptible strains of Asian corn borer. *Bmc Genomics*, 16.
- YAMASHITA, S., AKAO, T., MIZUKI, E., SAITOH, H., HIGUCHI, K., PARK, Y. S., KIM, H. S. & OHBA, M. 2000. Characterization of the anti-cancer-cell parasporal proteins of a *Bacillus thuringiensis* isolate. *Canadian Journal of Microbiology*, 46, 913-919.
- YAMASHITA, S., KATAYAMA, H., SAITOH, H., AKAO, T., PARK, Y. S., MIZUKI, E., OHBA, M. & ITO, A. 2005. Typical three-domain cry proteins of *Bacillus thuringiensis* strain A1462 exhibit cytotoxic activity on limited human cancer cells. *Journal of Biochemistry*, 138, 663-672.
- YAN, X. D., LI, M., YUAN, Y., MAO, N. & PAN, L. Y. 2007. Biological comparison of ovarian cancer resistant cell lines to cisplatin and Taxol by two different administrations. *Oncology Reports*, 17, 1163-1169.
- YASUNORI, N., TAKASHI, K., KAZUHIRO, S., AKIHIRO, Y. & YASUO, F. 1999. The cadherin-like protein is essential to specificity determination and cytotoxic action of the *Bacillus thuringiensis* insecticidal CryIAa toxin. *Febs Letters*, 460, 385-390.
- ZHAI, B. J., SHAO, Z. Y., ZHAO, C. L., HU, K. & WU, F. 2006. Development and characterization of multidrug resistant human hepatocarcinoma cell line in nude mice. *World Journal of Gastroenterology*, 12, 6614-6619.
- ZHANG, R., HUA, G., ANDACHT, T. M. & ADANG, M. J. 2008. A 106-kDa aminopeptidase is a putative receptor for *Bacillus thuringiensis* Cry11Ba toxin in the mosquito *Anopheles gambiae*. *Biochemistry*, 47, 11263-11272.
- ZHANG, X., CANDAS, M., GRIKO, N. B., ROSE-YOUNG, L. & BULLA, L. A. 2005. Cytotoxicity of *Bacillus thuringiensis* Cry1Ab toxin depends on specific binding of the toxin to the cadherin receptor BT-R-1 expressed in insect cells. *Cell Death and Differentiation*, 12, 1407-1416.
- ZHANG, X., CANDAS, M., GRIKO, N. B., TAUSSIG, R. & BULLA, L. A., JR. 2006. A mechanism of cell death involving an adenylyl cyclase/PKA signaling pathway is induced by the Cry1Ab toxin of *Bacillus thuringiensis*. *Proceedings of the National Academy of Sciences of the United States of America*, 103, 9897-9902.
- ZHAO, W. & MERESSE, S. 2015. A Method to Introduce an Internal Tag Sequence into a *Salmonella* Chromosomal Gene. In: SCHATTEN, H. & EISENSTARK, A. (eds.) *Salmonella: Methods and Protocols, 2nd Edition*.
- ZHOU, Y., LING, X. L., LI, S. W., LI, X. Q. & YAN, B. 2010. Establishment of a human hepatoma multidrug resistant cell line in vitro. *World Journal of Gastroenterology*, 16, 2291-2297.
- ZHOU, Z.-S., LIN, H.-Y., LI, Y., SHU, C.-L., SONG, F.-P. & ZHANG, J. 2014. The Minimal Active Fragment of the Cry1Ai Toxin is Located Between 36(I) and 605(I). *Journal of Integrative Agriculture*, 13, 1036-1042.
- ZHUANG, M. B., OLTEAN, D. I., GOMEZ, I., PULLIKUTH, A. K., SOBERON, M., BRAVO, A. & GILL, S. S. 2002. *Heliothis virescens* and *Manduca sexta* lipid rafts are involved in Cry1A toxin binding to the midgut epithelium and subsequent pore formation. *Journal of Biological Chemistry*, 277, 13863-13872.